RUSSIAN ACADEMY OF SCIENCES
URALS BRANCH
INSTITUTE OF MINERALOGY
INTERNATIONAL ASSOCIATION ON THE GENESIS OF ORE DEPOSITS
RUSSIAN FOUNDATION FOR BASIC RESEARCH
NATIONAL RESEARCH SOUTH URAL STATE UNIVERSITY

ORE GENESIS

ABSTRACTS OF THE INTERNATIONAL CONFERENCE (AUGUST 7-9, 2013)

Miass
2013

UDK 553

Oregenesis. Proceeding papers of the international conference (August 7–9, 2013) / Edited by V.V. Maslennikov, N.R. Ayupova., I.Yu. Melekestseva, E.V. Belogub. Miass: Institute of Mineralogy UB RAS, 2013. 125 p.

ISBN 978-5-696-04448-4

Recent models of ore genesis related to massive sulfide, iron, manganese, and gold deposits are considered in the papers. The papers include last data on comparative ore facies and mineralogical-geochemical analysis of modern and ancient hydrothermal sulfide systems. Numerous papers are dedicated to reconstructions of ore forming conditions. The information about biomineralization in metalliferous sediments and massive sulfide deposits is given. Some papers display results of modern methods of mineral and chemical research of explored ore deposits, host rocks, and environmental geology.

The conference is supported by projects of the Urals Branch of RAS (12-П-5-1003, 12-С-5-1010, 13-5-012-NEDRA), Russian Foundation for Basic Research (13-05-06052), and International Association on the genesis of ore deposits.

УДК 553

Рудогенез. Материалы международной конференции (7–9 августа 2013) / Под ред. В.В. Масленникова, Н.Р. Аюповой, И.Ю. Мелекесцевой, Е.В. Белогуб. Миасс: Институт минералогии УрО РАН, 2013. 125 с.

ISBN 978-5-696-04448-4

В сборнике представлены последние модели рудогенеза колчеданных, железорудных, марганцевых и золоторудных месторождений. Рассмотрены новейшие данные по сравнению рудных фаций и минералого-геохимическому анализу современных и древних гидротермальных сульфидных систем. Множество статей посвящено реконструкции рудообразующих процессов. Представлены материалы по биоминерализации металлоносных отложений и колчеданных руд. Некоторые статьи содержат результаты использования современных методов минералогического и геохимического изучения разрабатываемых месторождений полезных ископаемых, вмещающих пород и экологических систем.

Administrative address:
Miass, Chelyabinsk district, Russia, 456317
Institute of Mineralogy UB RAS
Phone +7-3513-573562
Fax +7-3513-570286
Email: oregenesis@mineralogy.ru

Miass, Chelyabinsk district, Russia, 456318,
National Research South Ural State University (Miass Branch)
Oktyabrya ave., 16
Phone +7-3513-531173
Fax +7-3513-546033

http://baseserv.ilmeny.ac.ru/files/BIBLIO/BOOKS/19789.pdf

V.V. Maslennikov
Institute of Mineralogy UB RAS, Miass, Russia
National Research South Ural State University, Chelyabinsk, Russia

AN INTRODUCTION: NEW GENETIC MODELS AS A BACKGROUND FOR PROSPECTING OF ORE DEPOSITS

Рассмотрены новые модели формирования колчеданных, железорудных, марганцеворудных и золоторудных месторождений. В частности, установлено, что колчеданные месторождения черносланцевой ассоциации, также как и месторождения яшмовой ассоциации, формировались по модели «черных курильщиков» в противовес модели «рассольных бассейнов». Предлагается гальмиролитическая модель формирования железорудных и марганцеворудных месторождений. Рассмотрены последние достижения в развитии мультистадийной модели формирования месторождений золота черносланцевой ассоциации. На этой основе предлагаются новые критерии прогнозирования рудных месторождений.

Last time, several models of ore genesis are developed in the Institute of Mineralogy UB RAS in collaboration with CODES (University of Tasmania). These models are related to massive sulfide, iron, manganese, and gold deposits.

In theory of massive sulfide deposits, the “brine-pools” theory is seems to be not in opposition with “black smoker” model of ore precipitation. Several criteria have been elaborated for distinguishing brine-pool-type from black smoker-type sulfide deposition [Solomon et al., 2004]. Brine pool massive sulfide deposits associated with volcanic carbonaceous sedimentary rocks have: (1) potentially very large size, and high aspect ratio; (2) higher Zn/Cu and Fe/Cu values (3) no evidence of chimneys; (4) relative abundant framboidal pyrite and primary mineral banding; (5) reduced mineral assemblages (pyrite-arsenopyrite/pyrrhotite), and minor or rare barite in massive sulfide; (6) associated stratiform and/or vein carbonates; (7) relative unimportant zone refining; (8) lack of vertical variation in sphalerite and sulfur isotopic composition; (9) evidence of local bacterial sulfate reduction [Solomon et al., 2004]. These criteria are unlikely to be completely accepted because of their convergence. In the Urals, large size of VMS deposits (>2Mt up to 6.5 Mt Cu+Zn) associated with jasper (Gai, Sibay, Octyabr’skoye, Uchaly, Uzelga) contain abundant fragments of the chimneys. A lot of chimney fragments have been found in sulfide breccias at black shale hosted VMS deposits (Saf’yanovka in the Central Urals, Nikolayevskoye, Artem’yevskoye, Zarechenskoye in Rudnyi Altai). Some of those have high aspect ratio of sulfide lenses (Zarechenskoye, Artem’yevskoye). Aspect ratio depends on the degree of sulfide mound destruction, and therefore are a function of volcanism intensity and duration of common sedimentation [Maslennikov, 2012]. The chimneys revealed in black shale hosted VMS deposits may be considered as a key argument against brine-pool model, because chimney growth include first stage of anhydrite shell formation [Haymon, 1983]. The development brine-pool model needs other, than suggest for black smokers, mechanism of chimneys growth.

Origin of banded sulfides is a key question in discussion of “black smokers” versus “fallout chemical precipitation” and versus “replacement” mechanism of VMS deposits formation. Sulfide-rich exhalites can be signature of both models. Hydrothermal sedimentary origin of banded sulfides is difficult to prove because of commonly plentiful replacement textures. The most of studied banded sulfides have been recognized as intercalation of altered clastic sulfide turbidites by “load cast” signatures. Strongly altered clastic sulfides are located out of feeder zones in the distal flanks of ore bodies and are alternated with unaltered jasper, chert, calcareous, carbonaceous, chloritic shale and hyaloclastic sedimentary rocks. Diverse relic primary hydrothermal sulphide fragments, secondary sulfide seg-

regations and pseudomorphs in many ancient and modern clastic sulfide deposits are distinguished in the banded sulfide ores. The ore fragments show open space growth features were transformed to replacement, recrystallization and nodular growth textures. Colloform and dendritic pyrite, pyrrhotite crystals were replaced by coarse grained pyrite agregates. The replacement of colloform and crystalline pyrite fragments by chalcopyrite and sphalerite is the rare case of inheriting of the primary texture. Fragmental subhedral chalcopyrite and ISS lattice textures were modified to aggregates of twinned crystals. Chalcopyrite deseased radial-concentric sphalerite and euhedral wurtzite were adjusted to twinned Fe-pure sphalerite with mixture of fahlores. The replacement and coeval recrystallization masked the primary clastic origins of sulfides. Seafloor or early diagenetic nature of most alterations is testified by asymmetry in mineral zoning of sulfide rhythms [Safina, Maslennikov, 2008]. The styles of mineral and chemical evolution of fragmental massive sulfide ores at VMS deposits depends on the primary composition of sulfide clasts and impurity of adjacent sediments. In calcareous and serpentitite-rich clastic sulfide sediments, pyrite nodules are commonly the products of diagenesis. All sulfides can be replaced by oxyhydroxides and then were transformed to hematite and magnetite in later metamorphic stages. In carbonaceous clastic sulfide sediments, diagenesis results in nodular as well as framboidal pyrite. In the metamorphic stage, the diagenetic pyrites are replaced by pyrrhotite, arsenopyrite and euhedral pyrite. Barite is one of the unstable mineral in carbonaceous sedimens as was calculated using SELECTOR program based on GIBBS free energy minimization [Maslennikov, Tret'yakov, 2010] Therefore, framboidal pyrite and pyrrhotite-rich reduced assemblages may be products of clastic sulfide alteration, as well and can not be exclusively related to brine pool models of VMS deposits. Moreover, these reduced mineral assemblages are typical for chimneys and sulfide mounds of jasper-volcanic hosted VMS deposits.

A lot of studied VMS deposits at the Urals, Pontides, and Cyprus, including black shale hosted Saf'yanovka VMS deposit, yield abundant vent fauna species. This is in contradiction with brine-pool model, because vent fauna need oxygen in seawater. In other VMS deposits, no vent fauna was found because of high state of primary hydrothermal fluid oxidation, and high degree of sulfide mound destruction with formation of altered sulfide turbidite.

In general, preference of either brine-pool or black smoker model will influence on criteria of prospecting of VMS deposits. Brine-pool model suggests wide expansion of ore deposition in depression, that leads to using of regional lithostratigrafic criteria of prospecting. In contrary, black smoker model pay attention to local ore facies and lithofacies criteria using clastic sulfides and their products of diagenetic alteration (diagenites) and seafloor oxidation (halmyrolysites) in volcano-sedimentary horizon as the direct signature of VMS deposits halo. This rocks display specific mineral and chemical feature reflecting VMS deposits formation. This rock can be useful in addition to exhalites. Pyrite nodules can be new interesting subject for trace element research, as possible indicator of VMS deposits. F.e. the pyrite nodules collected in ore black shales from Saf'yanovka VMS deposits display unusually high grades of Te, Bi, Au, Ag, Pb and high Au/Ag values.

In the Urals and other VMS deposits, ferruginous and manganiferous sedimentary rocks are widespread. These rocks have been subdivided into jasperites, gossanites and umbers [Maslennikov et al., 2012]. Some of these rocks may be interpreted as exhalites as is commonly accepted without strong evidence. However, most of these rocks display signatures of seafloor replacement of volcanic glasses, clastic sulfides and carbonate by hematite-quartz aggregates with apearence variable contents of authigenic manganese minerals. The process of seafloor replacement is considered as halmyrolysis [Maslennikov et al., 2012]. The replacement textures are background for new models of iron and manganese ore deposits formation. In some variant of the halmyrolysis models, the subtraction of Al, Si, Ti, and REE from hyaloclastic material mixed with organic matter and carbonate have been proved. This substraction is accompanied by concentration of Fe and/or Mn followed by formation of Fe- and Mn- halmyrolysistes which may be considered as analogues of some Fe and Mn ore deposits. Relic bacterial filaments in ferruginous sediments are reminded in numerous publication. The halmyrolysis can be improved by bacterial activity [Aupova, Maslennikov, 2013]. This data confirms the halmyrolysis model suggested by Hummel [1922] for hematite ore in Germany. Many other iron deposits including BIF, hematite exhalites and magnetite "scarn" types display the features of volcanic glasses halmyrolysis. The halmyrolysis models merits a further research. Therefore, possible new criteria for iron deposit prospecting is finding and exploration of submarine calcareous hyaloclastic inits with features of halmyrolysis.

A number of unresolved questions remains the models for orogenic and Carlin-type gold deposits. The models declare three current views related to orogenic gold deposits: gold-rich fluids are derived from deep metamorphic processes or from crustal granites; (2) organic-rich sediments are traps for gold; (3) gold is introduced late, i.e. syn- or posttectonic. Some recent investigation sought to determine whether, or not, carbonaceous sedimentary rocks could have been important for source for gold in orogenic and Carlin-type gold deposits [Large et al., 2007, 2009, 2011; Meffre et al., 2008; Chang et al., 2008; Thomas et al., 2011]. This research that gold is sourced in the sedimentary basin, organic-rich sediments are excellent source rocks for gold and variety of other elements (As, Zn, V, Mo, Ag, Ni, Se, Te) and (3) gold is introduced early (syndiagenetic) and remobilized and concentrated locally during syntectonic and/or sinmagmatic fluid flow. The most important process for gold remobilization is replacement of gold-rich pyrite by pyrrhotite. The last signature can be used in prospecting exploration of gold deposits in carbonaceous sedimentary units.

This research was supported by the projects of UB RAS (no. 12-IT-5-1003, no. 12-C-5-1010, 13-5-012-NEDRA), and CODES Visiting Program of Tasmania University (Australia).

References

Ayupova, N.R., Maslennikov, V.V. Biomineralisation in ferruginous-siliceous sediments of massive sulfide deposits of the Urals // Doklady Earth Sciences, RAS, 2012. Vol. 442. P. 193–195.

Chang, Z., Large, R.R., Maslennikov, V.V. Sulfur isotopes in sediment-hosted orogenic gold deposits: Evidence for an early timing and a seawater sulfur source // Geology, 2008. Vol. 36. Issue 12. P. 971–974.

Haymon, R.M. Growth history of hydrothermal black smoker // Nature, 1983. Vol. 301. P. 695–698.

Hummel, K. Die Einstehung eitheneicher Gestein durch Halmyrose (submarine Gesteinrsetzung). Geol. Rundsh. 1922;13:40–81 (in Germany).

Large, R.R., Bull, S.W., Maslennikov, V.V. A carbonaceous sedimentary source-rock model for Carlin-type and orogenic gold deposits // Economic Geology, 2011. Vol. 106. C. 331–358.

Large, R.R., Bull, S.W., Maslennikov, V.V., Thomas, H.V. The controversy of gold source in orogenic and Carlin style deposits // Economic Geology Research Unit, 2009. Townswelle. Vol. 1. P. 366–369.

Large, R.R., Danyushevsky, L., Hillit, H., Maslennikov, V., Meffere, S., Gilbert, S., Bull, S., Scott, R., Emsbo, P., Thomas, H., Singh, B., Foster, J. Gold and trace element zonation in pyrite using a laser imaging technique: implications for the timing of gold in orogenic and Carlin-style sediment-hosted deposits // Economic Geology, 2009. Vol. 104. P. 635–668.

Large, R.R., Maslennikov, V.V., Robert, F., Danyushevsky, L.V., Chang, Z. Multistage sedimentary and metamorphic origin of pyrite and gold in the giant Sukhoi Log deposit, Lena gold province, Russia // Economic Geology, 2007. Vol. 102. P. 1233–1267.

Maslennikov, V.V. Morphogenetic types of massive sulfide deposits as reflection of volcanic regim// Lithosphera, 2012. № 5. P. 96 – 113.

Maslennikov, V.V., Ayupova, N.R., Herrington, R.J., Danyushevskiy, L.V., Large, R.R. Ferruginous and manganiferous haloes around massive sulphide deposits of the Urals // Ore Geology Reviews, 2012. Vol. 47. P. 5–41.

Maslennikov, V.V., Tret'yakov, G.A. Physico-chemical modeling of mineralization succession in submarine hypergenesis of Uralian and Kuroko types of massive sulfide deposits // Ural mineralogical collection. Miass-Yekaterinburg, UB RAS, 2010. No. 15. P. 9–16.

Meffre, S., Large, R.R., Scott, R., Woodhead, J., Chang, Z., Gilbert, S.E., Danyushevsky, L.V., Maslennikov, V.V., Hergt, J.M. Age and pyrite Pb isotopic composition of the Giant Sukhoi Log Sediment-hosted gold deposit, Russia // Geochimica et Cosmochimica Acta, 2008. Vol. 72. P. 2377–2391.

Safina, NP, Maslennikov, V.V. Lithological and mineralogical zonation of sulfide cyclites Yaman-Kasy and Saf'yanovskoye massive sulfide deposits (the Urals) / / Doklady Earth Sciences, RAS, 2008. Vol. 419. No. 6. P. 804–806.

Solomon, M., Tornos, F., Large, R.R., Badham, J.N.P., Both, R.A., Kin, Zaw. Zn-Pb-Cu volcanic-hosted massive sulfide deposits criteria for distinguishing brine pool-type from black-smoker type sulfide deposition // Ore geology reviews, 2004. Vol. 25. P. 259–283.

Thomas, H.V., Large, R.R., Bull, S.W., Maslennikov, V.V., Berry, R.F., Fraser, R., Froud, S., Moye, R. Pyrite and pyrrhotite textures and composition in sediments, laminated quartz veins, and reefs at Bendigo gold mine, Australia: Insights for ore genesis // Economic Geology, 2011. Vol. 106. P. 1–31.

K. Adomako-Ansah[1], T. Mizuta[1], D. Ishiyama[1],
N.Q. Hammond[2], M. Yamamoto[1]
[1] Akita University, Akita, Japan, adomako@gipc.akita-u.ac.jp
[2]Council for Geoscience, Pretoria, South Africa

ARCHEAN BANDED IRON FORMATION GOLD-HOSTED DEPOSIT IN THE AMALIA GREENSTONE BELT, SOUTH AFRICA: ORE TEXTURES AND GEOCHEMICAL FEATURES OF MINERALIZATION

На основании изучения минералогических и структурных особенностей и изотопного состава C, O, Sr месторождения Блю Дот, локализованного в формации железистых кварцитов зеленокаменного пояса Амалия, обсуждаются механизмы рудообразования и источники флюидов. Основные типы изменений, наложенные на железистые кварциты – карбонатизация, хлоритизация, развитие сульфидов. Золото-сульфидное оруденение связано с контактами наложенных кварц-карбонатных жил и железистых кварцитов. По составу арсенопирита температура образования продуктивной ассоциации оценивается ниже 300–350 °C. На основании изотопных данных в качестве источника флюида предполагаются син- и пост-тектонические гранитоиды.

Introduction

This study investigates the mineralogical, textural and C-O-Sr-isotopic characteristics of gold mineralization and discusses their implication(s) for the ore-forming mechanism and source of ore fluids in the Archean banded iron formation (BIF)-hosted Blue Dot gold deposit of South Africa.

Regional Geology

The Blue Dot gold deposit is located in the Archean Amalia Greenstone Belt (AGB), which forms part of the Amalia-Kraaipan terrane of N-S trending greenstone belts, situated in the western Kaapvaal craton (Fig.1). It is approximately 4~5 km wide and 55 km long. Banded iron formation is the only distinct outcrop in the studied area [Jones and Anhaeusser, 1993]. The highly deformed, subvertically inclined volcano-sedimentary rock units of the AGB are generally fault-bounded and partially engulfed by abundant intrusive syn- to post-deformational granitoids [Schmitz et al., 2004]. Three episodic granitic intrusions have been recorded in the belt: (1) tonalite-trondjemite-granodioritic gneiss (TTGs) dated at 3.08 Ga and represents reworking of older basement granitic rocks, (2) syntectonic granodioritic plutons of the Kraaipan group dated at 2.93 Ga and, (3) post-tectonic Schweizer-Reneke K-rich quartz monzonites dated ca. 2.88 Ga, believed by many researchers to have played a major role in controlling gold mineralization in the region [Anhaeusser & Walraven, 1999].

Ore deposit geology

Three discrete BIF-hosted gold orebodies namely; Bothmasrust, Abelskop and Goudplaats, have been recognized at the Blue Dot gold deposit. The BIF units are flanked by mafic schist and muscovite-carbonate-chlorite-quartz schist in the footwall (F/W), and chlorite schists in the hanging wall (H/W). The Amalia BIF is subdivided into two units: (i) jasper-rich BIF and (ii) jasper-free BIF. The jasper-free variety is the common BIF type in the Amalia greenstone belt. However, it is the veined jasper-rich BIF that is commonly sulfidized and mineralized. Quartz, chlorite and carbonate (i.e. siderite, ankerite, dolomite and minor calcite) constitute the main gangue mineral assemblage in the BIF with minor amounts of muscovite. In less-altered, undeformed BIF units, platy magnetite occurs as fine-grained, unaltered layers, while chert is partly intergrown with siderite and chlorite. In highly deformed units, the magnetite is re-crystallized into coarse grains and undergoes pseudomor phic replacement by hematite. This hematitic alteration is prominent in portions where the quartz-carbonate veins crosscut the BIF layerings. In this study, the term mineralized BIF is used to represent sulfidized altered/bleached jasper-rich or jasper-free BIF units that are related to crosscutting quartz-carbonate veins, whiles non-mineralized BIF represents the non-sulfidized, less altered BIF units that are not veined.

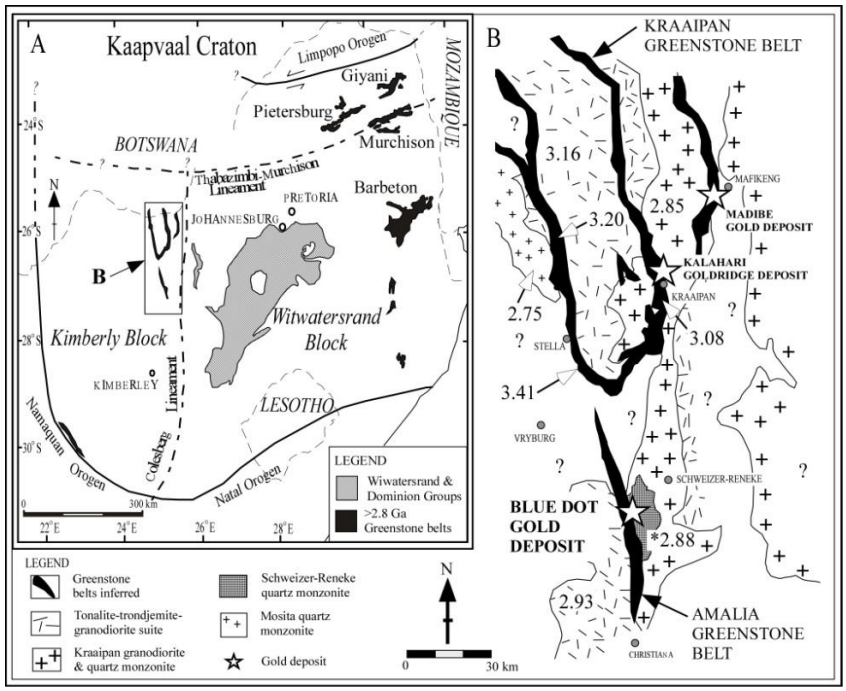

Fig. 1. Location of the Blue Dot gold deposit in Amalia Greenstone belt.

Hydrothermal alteration and ore precipitation mechanism

The crosscutting, vein-related gold mineralization and hydrothermal alteration show some relationship with the lithologies present at Amalia. The main alteration processes associated with the mineralization include carbonatization, which is characterized by the replacement of magnetite and hematite by carbonates such as siderite in BIF and replacement of quartz by ankerite-dolomite series, chloritization (characterized by chlorite replacement of magnetite and quartz in BIF and, quartz, carbonate and albite in schists), hematization (characterized by alteration of magnetite to hematite), sulfide precipitation (characterized by pyrite ± chalcopy-rite ± arsenopyrite precipitation in the BIF) and rare potassium metasomatism (characterized by sericitic replacement of albite, quartz and chlorite). Sulfide precipitation and associated gold mineralization is restricted to the proximity of contacts between BIF and quartz-carbonate veins [Kiefer, 2004; Adomako-Ansah et al., 2013]. Pyrite (with minor chalcopyrite and arsenopyrite; Fig. 2a, b) is the dominant sulfide mineral [Adomako-Ansah et al., 2013] and restricted to the zones of sulfide precipitation in the mineralized BIF. Gold occurs as rounded to irregular-shaped inclusions and as fracture fills in pyrite (Fig. 2c). Previous authors proposed pyrite-gold precipitation by sulfidation of magnetite±hematite in the BIF [Kiefer, 2004] or hematization of pyrite [Vearncombe, 1986]. However, petrographic investigation by Adomako-Ansah et al. [2013] shows non-replacement textures between hydrothermal pyrite and coexisting recrystallized magnetite±hematite minerals and does not suggest sulfidation of the Fe-oxides. Rather, it suggests conditions of contemporaneous sulfide-gold precipitation with magnetite-hematite recrystallization. Also, in the BIFs, most of the sulfide-gold mineral assemblages are petrographically observed within quartz-carbonate layers rather than magnetite-hematite layers (Fig. 2).

Mineral chemistry of ores and temperature for gold mineralization

A simplified paragenetic sequence for the principal minerals occurring in the Blue Dot gold deposit is illustrated in Fig. 3. Arsenopyrite grains show a general composition from 28.6 to 30.8 at. % As with negligible base metal contents. Less or no variation in rim-to-core compositions, absence of zoning and the negligible base metal contents in arsenopyrite from the various analyzed samples suggest that conditions of crystallization were fairly stable (i.e. the sulfide precipitation, and consequent gold mineralization, probably occurred during one hydrothermal event). Temperature estimated by using the arsenopyrite-pyrite geothermometer of Scott [1983] for associated gold mineralization, based on the As contents of arsenopyrite, is < 300–350 °C (Fig. 4). Native gold grains from both mineralized BIF and veins, indicate an average value of Au 0.92 Ag 0.08 and a high relative fineness of 952±5, which is consistent with the observed range for most Archean lode gold deposits [Adomako-Ansah et al., 2013]. C-O-Sr isotopic signatures on ore fluid source and formation environment.

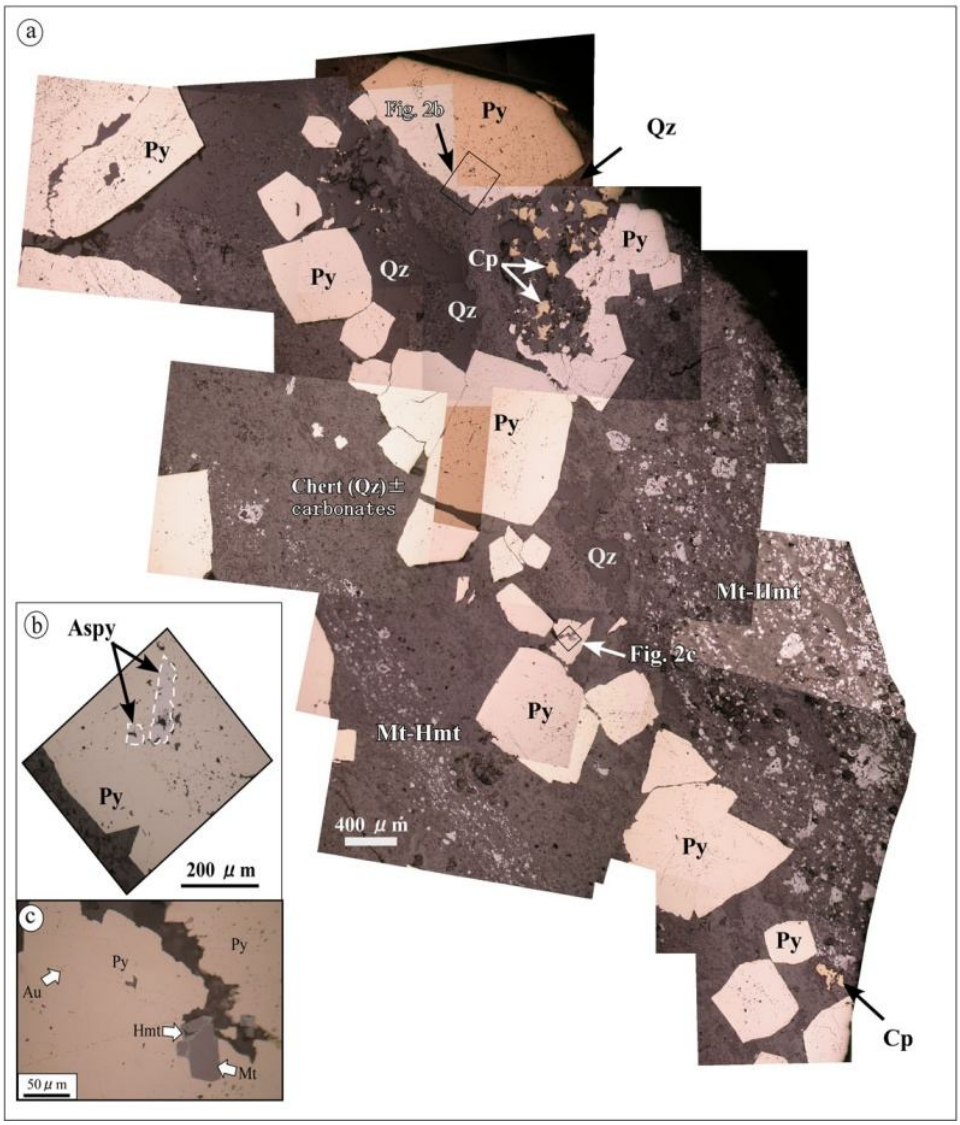

Fig. 2. Ore minerals and textures of mineralization.

Geochemical data from C, O and Sr isotopes of carbonates and O isotopes of quartz (summarized in Table; this study) suggest that the hydrothermal ore fluid responsible for the associated gold mineralization in the Amalia BIF was sourced from magmatic fluids that are temporally and spatially represented by the syn-to-post tectonic granitoids in the studied area. Tight clustering of S-isotope data of +1.8 to +2.5 per mil for the S in the ore fluid at the Blue Dot deposit [Adomako-Ansah et al., 2013] also indicates a probable magmatic or mantle origin according to Ohmoto [1986] for a cluster of –3 to 3 per mil S-isotopic data. Geochemical studies on the surrounding granitoids by Kiefer [2004] indicated that the Schwiezer-Reneke quartzmonzonite, largely tipped to be the potential source for the exolved ore fluids, formed from mixing of magmas derived from partial melting of depleted mantle-wedge and TTG sources.

C-O-Sr isotopic signatures on ore fluid source and formation environment

Geochemical data from C, O and Sr isotopes of carbonates and O isotopes of quartz (summarized in Table 1; this study) suggest that the hydrothermal ore fluid responsible for the associated gold mineralization in the Amalia BIF was deep-sourced, and likely from magmatic fluids that are temporally and spatially represented by the syn-to-post tectonic granitoids in the studied area. Tight clustering of S-isotope data of +1.8 to +2.5 per mil for the S in the ore fluid at the Blue Dot deposit (Adomako-Ansah et al., 2013) also indicates a probable magmatic or mantle origin according to Ohmoto (1986) for a cluster of -3 to 3 per mil S-isotopic data. Geochemical studies on the surrounding granitoids by Kiefer (2004) indicated that the Schwiezer-Reneke quartzmonzonite, largely tipped to be the potential source for the exolved ore fluids, formed from mixing of magmas derived from partial melting of depleted mantle-wedge and TTG sources.

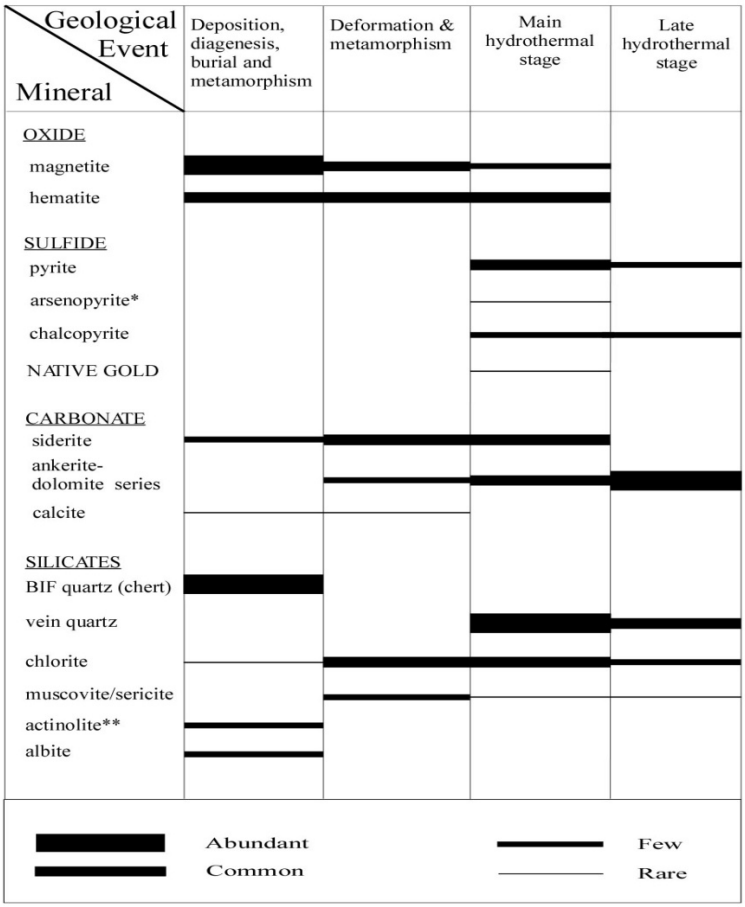

Fig. 3. Paragenetic sequence of principal minerals in the Blue Dot gold deposit

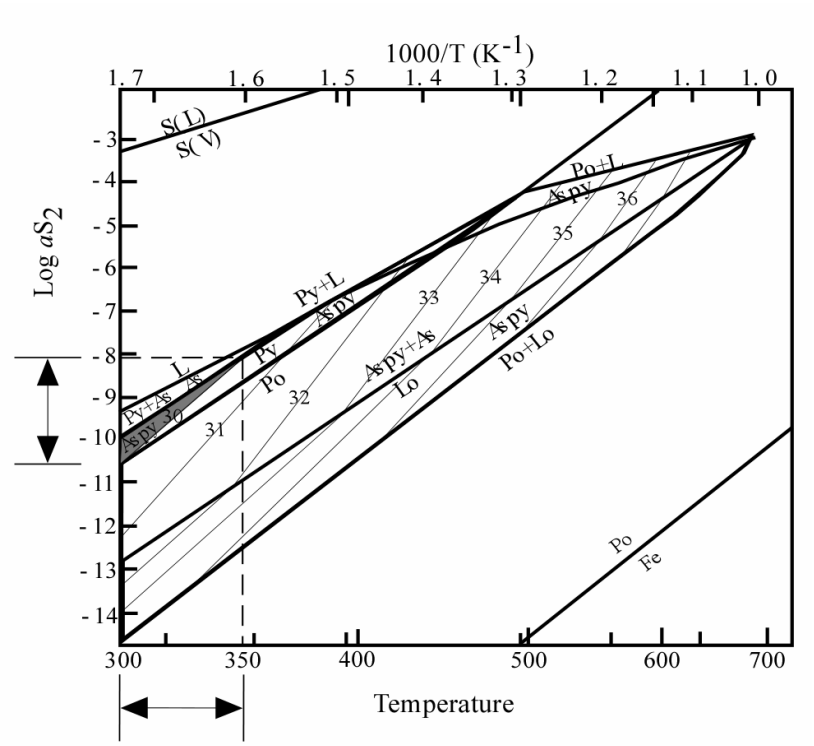

Fig. 4. Arsenopyrite geo-thermometer. Shaded regioin is the ore-forming condition for gold mineralization at the Blue Dot gold deposit

Table

$\delta^{13}C$ of carbonates and $\delta^{18}O$ of quartz of gold mineralization in the Amalia BIF

Sample	Host lithology	Carbonate	Remark	$\delta^{13}C_{PDB}$ (‰)	$\delta^{18}O_{smow}$ (‰)
C17-20	Vein in mineralized BIF	ankerite	Q-C vein	-3.2	17.2
C11-5A-3	-»-	Fe-dolomite	–»–	-3.7	16.3
C17-15B	-»-	ankerite	–»–	-4.8	13.5
C17-23B	-»-	ankerite	–»–	-3.1	16.3
C17-6	Vein in hanging wall schist (non mineralized)	Fe-dolomite	–»–	-3.8	16.3
V8-3	Mineralized BIF	Fe-dolomite	whole rock	-3.4	15.0
V8-10PIb	-»-	siderite	–»–	-5.0	13.5
V8-12PII	Cherty band from mineralized BIF	siderite	–»–	-4.8	13.8
AB22-15A	Mineralized BIF	siderite	–»–	-3.4	13.6
V8-26(b)	Mineralized BIF	Fe-dolomite	–»–	-4.2	14.4

Acknowledgement

This study is a collaborative program between Akita University, Japan and Council for Geoscience, South Africa (Project No. ST-2009-1057). The first part of the program, which resulted in a doctoral thesis (D. Eng.) for the first author, was made possible with financial support to the first author from the Japanese Govt (Monbusho scholarship) and Society of Resource Geology (Overseas travel grant). Continued financial support through a postdoctoral fellowship from Akita University's Leading program and the Center for Geo-Environmental Science to the first author enabled the C-O isotopic and ICP-MS analyses on carbonates. Prof. Emeritus O. Matsubaya is gratefully thanked for help in conducting the C-O isotope experiments.

References

Adomako-Ansah, K., Mizuta, T., Hammond, N.Q., Ishiyama, D., Ogata, T and Chiba, H. Gold mineralization in banded iron formation in the Amalia Greenstone belt, South Africa: a min-eralogical and sulfur isotope study // Resource Geol., 2013. Vol. 63. P. 119–140.

Anhaeusser, C. R. and Walraven, F. Episodic granitoid emplacement in the western Kaapvaal Craton: evidence from the Archean-Kraaipan granite-greenstone terrane, South Africa // J. Afr. Earth Sci., 1999. Vol. 28. P. 289–309.

Jones, I.M. and Anhaeusser, C.R. Accretionary lapilli associated with Achaean banded iron formations of the Kraaipan Group, Amalia greenstone belt, South Africa // Precambrian Res., 1993. Vol. 61. P. 117–136.

Schmitz, M.D., Bowring, S.A., Maarten, J. de W. and Gartz, V. Subduction and terrane collision stabilize the western Kaapval craton tectosphere 2.9 billion years ago // Earth Planet. Sci. Lett., 2004. Vol. 222. P. 363–376.

Scott, S.D. Chemical behavior of sphalerite and arsenopyrite in hydrothermal and metamorphic environments // Mineral. Magazine, 1983. Vol. 47. P. 427–435.

Vearncombe, J.R. Structure of veins in a gold-pyrite deposit in banded iron-formation, Amalia Greenstone Belt, South Africa // Geological Magazine, 1986. Vol. 123. P. 601–609.

V.N. Anfilogov[1,2], Y.V. Khachay[3]

[1]Institute of Mineralogy UB RAS, Miass, Russia

[2]National Research South Ural State University, Chelyabinsk, Russia

[3]Institute of Geophysics UB RAS, Yekaterinburg, Russia

FORMATION OF THE EARTH'S CORE AND SILICATE LAYERS

Предложена принципиально новая модель гетерогенной аккумуляции Земли. Она позволяет объяснить механизм образования частично расплавленного железо-никелевого ядра на начальном этапе формирования Земли и обосновывает новый механизм дифференциации вещества в процессе аккумуляции Земли. Процесс аккумуляции завершается отложением на поверхности Земли материала углистых хондритов. Из этого материала будет сформирована внешняя твердая оболочка Земли.

The composition of the Earth's core and silicate layers depends on the way of the Earth's accumulation and later differentiation. The modern hypotheses assume that protoplanetary material had gone through two consecutive stages of (i) solid phase condensation from the gas and (ii) solid particle agglomeration in a gas-dust cloud [Dorofeeva, Makalkin, 2004] resulted in the planet formation [Vitiazev et al., 1990]. The currently available data of the cooling of the protoplanetary cloud (10^4–10^5 years) [Dorofeeva, Makalkin, 2004] shows that these processes cannot be separated by time and by distance from the Sun. It is beyond reason to exclude the possibility of the concurrent occurrence of these two stages. This allows us to use the sequence of the solid phase condensation, which was founded in laboratory experiment on mechanism of the planet formation [Ringwood, 1979].

The assumption that the solid particle agglomeration began after the primary gas condensation was completed and had gone in the cold cloud allows only homogenous Earth's accretion. This scenario leads to the primary homogenous cold planet. The portioning of the homogenous planet material on the iron core and silicate mantle is conceivable at the final stages of its formation, which could occur only after the secondary warming-up of the upper planet strata. The problem is an energy contributor to the start-up of the primary homogenous Earth differentiation. The radioactive decay was able to warm-up the Earth two billion years only after its formation. The suggestion that the warming-up of the Earth was caused by the impact of the Mars-sized space body is speculative and will not be the subject of our discussion. Moreover, the homogenous accretion models contradict the isotopic data, which indicate that the core and mantle reservoirs were separated at the initial stage of the Earth's formation [Harper, Jacobsen, 1996].

The heterogeneous accretion is an alternative hypothesis in contrast to the homogenous one. It proposes that the composition of material for the Earth's formation was inconstant and varied as the Earth's size increases. This idea was supported by many researchers [Anderson et al., 1972; Harper, Jacobsen, 1996]. The most radical point of view was stated by Anderson et al. [1972], who proposed that the inner core was built up from the early condensates, which were condensed before iron. The

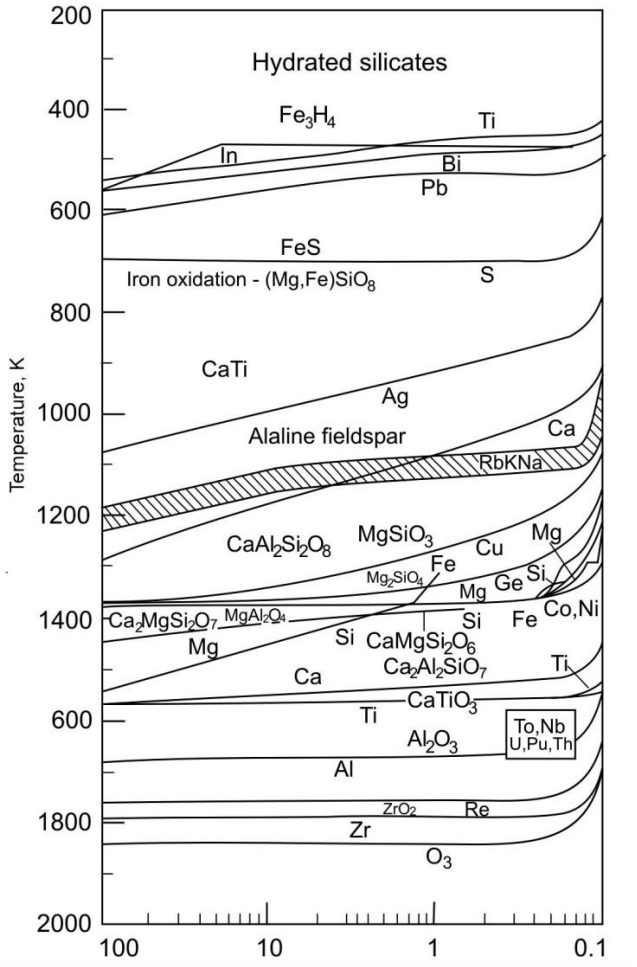

Fig.1. The condensed element fraction.

possible composition of the Earth's layers and their evolution are discussed on the basis of the two stage model of the Earth's formation in the given work.

Simultaneous condensation and solid particle agglomeration allows proposition that the composition of the central part of the planets at the first stage of the planet formation was close to CAI – white inclusions in the Allende meteorite [Anfilogov, Khachay, 2005]. They are most high temperature and ancient condensates in the Solar system [Brearley, Jones, 1998]. As the embryos grow and the protoplanetry cloud cools, the composition of the condensate changes (Fig. 1) and the iron and iron-silicate fractions will precipitate on the embryo surface owing to the high temperature. The planet embryos, which size is the first hundred kilometers, will be formed as a result of the impacts and partially integration of the planetesimales. The structure of these embryos is shown in the Fig. 2.

The warming-up of the embryos as a result of the short-live radioactive decay occurs during the growth. ^{26}Al is the major short-live isotope with half decay period of 7.38?10^5 years. The ^{26}Al/^{27}Al ratio in the protoplanetary material is 5?10^{-5} [Merk et al., 2002]. The temperature in the embryo center may be as much as 1850–2200 K at this ^{26}Al content if the embryo size is 200 km [Anfilogov, Khachay, 2005]. It is large enough for the partial melting of Al-Si mixture in the central part of the embryo and for complete melting of the Fe-Ni mixture in its intermediate layer. The outer layer complicated by olivine-pyroxene chondrite material remains solid at this time (Fig. 2).

The further evolution of the planet goes in the following manner. In accordance with the Safronov's model of the planet accumulation [Robie et al., 1978], the amount of embryos, which are formed at initial stage of agglomeration, is high and they often impact each other. The impact of two embryos with similar size partially smelts the core and medium iron layer and makes hard the outer silicate layer, terminating the failure. The intermediate smelt iron layers will coalesce after the impact and form a new embryo complicated from Fe-Ni molten alloy. The material of Al-Si cores will be pressed out from the inner part of the primary embryos and thrown out partially beyond the new embryo. The outer solid layers will be destroyed and a part of their fragments goes out the growing planet. The impact of two primary embryos is schematically shown in Fig. 3.

According to the dynamic estimations [Khachay, Anfilogov, 2007], the duration of the first stage is >10^6 years that is in agreement with period of formation of chemical reservoirs of the Earth's core and mantle separation [Harper, Jacobsen, 1996].

The integration of the iron layers after the impact of the primary embryos gives rise to the second embryo generation, the most part of which represents the Fe-Ni molten core. Two problems may be solved this way: the core formation at initial stage of the Earth's formation and possibility of MHD dynamic start-up and geomagnetic field formation, which are inducted in the smelt iron core by the outer magnetic field [Khachay, Anfilogov, 2007]. The dynamics of further process of the Earth's formation is described by the Safonov's model. When the Fe-Ni core reaches the most part of its modern mass, it becomes able to hold and form a silicate layer around itself.

The two stage model of the Earth's formation discussed above represents the heterogeneous accretion scenario. Contrary to the scenarios suggested before [Ringwood, 1978], it proposes the real mechanism of the smelt iron core formation at initial stage of the Earth's formation, removal of the primary light Al-Si material from the center of the embryo and explains the origin of high temperature in the growing Earth.

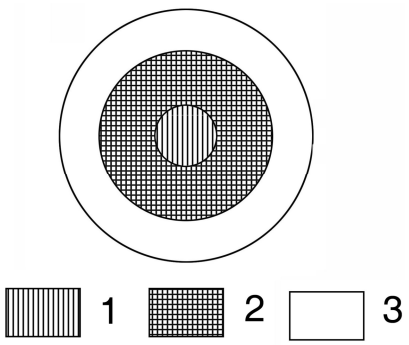

Fig. 2. The schematic structure of the primary Earth embryo. 1– the high aluminum core; 2 – the smelt iron envelope; 3 – the outer hard envelope.

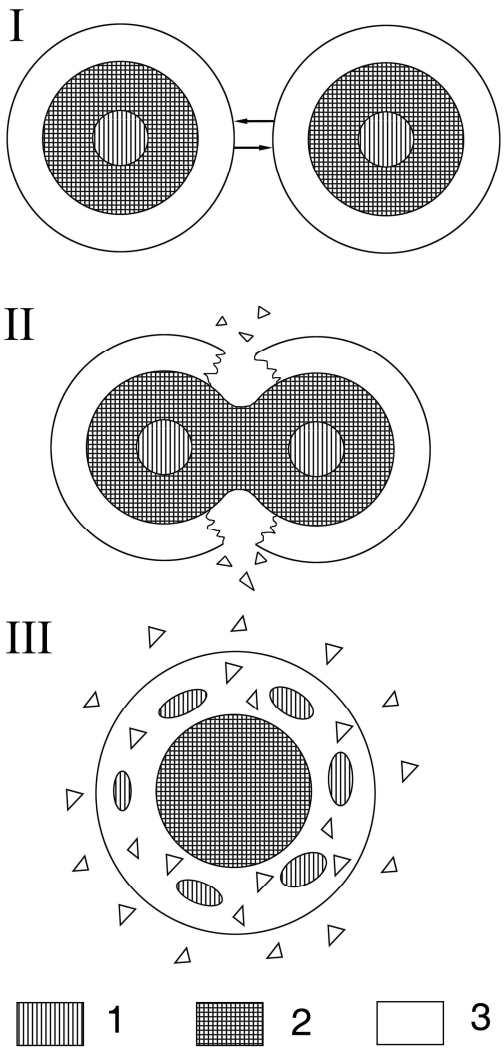

Fig. 3. Scheme of the new Earth embryo formation as a result of the two primary embryos collision. 1 – high aluminum material; 2 – smelt iron material; 3– ordinary chondritic material.

The two stage mechanism allows proposition of the Moon formation along with the Earth and explanation of the absence of metallic iron in the Moon and high primary temperature in the Moon interior. The Moon was mostly formed from the fragments resulted from the primary Earth's embryo destruction and went out from the feeding area of the growing Earth. Because the main part of iron is concentrated in the Earth's core, the Moon lacks material for the formation. In addition to iron, the Moon material accessible for investigation was depleted of potassium. In line with condensation sequence (Fig. 1), it allows us to exclude the alkali fieldspars and other solid phases, which are condensed at temperature lower than 1100 K. This suggests that the Moon was separated from the Earth before the accretion of the Earth was completed. In this case, the most part of potassium should accumulate by the Earth at the last stage of its formation and is concentrated in the upper mantle.

Let us consider the possible composition of the Earth's silicate layers. The meteoritic material is a primary information source about mantle composition. The iron meteorites give the data on the core composition and the stone meteorites considered to be a possible material for the Earth's silicate layers have rather different composition, thus the problem of the meteorite type necessary for the mantle composition is ambiguous. The problem is complicated, because some part of meteorites are the fragments knocked from the Moon and nearest planets [Shukolyukov, 2003] and cannot serve the material for the Earth's formation. A similar statement is true for meteorites, which age is younger than that of the Earth [Marakushev, 1991].

A.E. Ringwood has analyzed the complex of physical and mineralogical criterions (the distribution of seismic waves velocities, springiness, density, mineralogical composition, and phase transformation of minerals at high pressure) and drawn a conclusion that two alternative models can be con-

sidered [Dorofeeva, Makalkin, 2004]: (i) the lower mantle is pyrolitic and its density excess is conditioned by phase transitions and (ii) the lower mantle is enriched in FeO and, possibly, SiO_2.

We believe that these scenarios are not alternative. First, it is not evident that the composition of the material for the Earth's formation was constant during the whole period of its accumulation and it corresponded to carbonaceous chondrites. Second, the phase transformations of the mantle minerals are studied experimentally and it is impossible to build up the correct model of the lower mantle without account of these transformations.

Based on the sequence of solid phase condensation (Fig 1), it is most likely that the lower mantle correspond to olivine-pyroxene chondrites in composition. These chondrites are distinct from carbonaceous chondrites by the absence of water and presence of large amount of iron and troilite (Table).

Similarly, the base of the mantle is expected to correspond to the composition of H-chondrites with high content of iron. As the Earth's mass increases, the composition of the H-chondrite varied to L- and LL-chondrite. The proposed chondritic lower mantle has no strong difference from the pyrolitic one. As seen from Table, the intermediate composition of chondrites devoid of Fe and FeS is close to pyrolite. It differs from pyrolite by high FeO lower MgO contents. It well to bear in mind, that its initial composition was formed during the Earth's growing process. As the temperature and pressure increased, the lower mantle differentiated and Fe and FeS moved to the core. The part of iron oxide disproportionated and transformed into magnetite and metallic iron: $4FeO = Fe_3O_4 + \alpha Fe$. Then, it moved to the core too [Ringwood, 1978]. The final composition of the lower mantle became pyrolitic.

The pyrolitic model of the upper mantle put forward by A.E. Ringwood [1978] was generally accepted. The model is based on the correlation of composition of carbonaceous chondrites, alpine ultramafic rocks, and deep-seated xenoliths in kimberlites and alkali basalts. In spite of general acceptance, the pyrolitic model has some contradictions. It is agreed that the Earth's material corresponds to the intermediate meteorite. However, no meteorites, except for the Allende and rare ureilites, have high MgO and low FeO contents as pyrolite. Thus, the question arises, where is the excess of FeO and what is the source of the MgO excess in the mantle? By this is meant that models of pyrolitic and other mantle composition are approximate.

Let us consider the origin of the Archean crust, which is made up of mafic volcanic and acid igneous and metamorphic rocks [Salop, 1982]. V.E. Khain and N.A Boshko [1988] advocated that grey gneisses quantitatively dominate among the Archean rocks and could be formed by partial melting of the primary mantle with the specific toward Archean active constraint of water only.

The sequence of solid phase condensation, which is used by two stage model of the Earth's formation, suggests that water and carbon appear at the final stage of this process. Absence of carbon in the early condensates is caused by CO_2 generation, which remains in the gaseous phase of the protoplanetary cloud: $C + O_2 = CO_2$ ($\Delta G_{1400K} = -396.17$ kJ/mol [Robie et al., 1978]).

An iron is oxidized simultaneously with CO_2 production, the free energy of this process changed at 1400 K is –180.44 kJ/mol [Robie et al., 1978], and the oxidation of Fe is noncompetitive with CO_2 production.

Carbon, H_2O and organic compounds appear in the protoplanetary material and meteorites as temperature decreases, hydrogen concentration increase, and carbon is reduced: $CO_2 + H_2 + C + 2H_2O$ ($\Delta G_{600\,K} = -95.70$ kJ/mol [Robie et al., 1978]).

Table

Composition of chondrites and the Ringwood's pyrolite

Component	Type H [Mason, 1962] (53)	Type L [Mason, 1962] (79)	Type LL [Marakushev,1991] (17)	Pyrolite [Ringwood, 1979]
SiO_2	47. 0	45.2	42.8	45.1
Al_2O_3	3.0	2.9	2.7	3.3
FeO	12.9	17.7	21.5	8.0
MgO	30.1	28.6	27.8	38.1
CaO	2.5	2.2	2.0	3.1
Na_2O	1.1	1.0	0.9	0.4
FeS	5.6	5.8	5.3	
Fe	17.3	6.7	1.3	

It follows that the Earth's formation is finished by the formation of the outer layer enriched in water and carbon with chondritic composition of its silicate component. Two processes may occur in this layer at high temperature: (i) degassing of the outer layer, which gave rise to the atmosphere and ocean formation and (ii) production of the large volume of dioritic and granitic melt, which are able to be formed at the presence of water.

All stated above allows us to propose the hypothesis of the entire and upper mantle composition. The average mantle composition is most likely consistent with composition of olivine-pyroxene chondrites without metallic Fe and FeS. Compared to the Ringwood's pyrolite, it is enriched in FeO and depleted in MgO. The material of carbonaceous chondrites exists in the upper mantle. Three types of geochemical reservoirs may occur in the outer part of the upper mantle: primitive mantle consistent with average mantle composition, partially depleted mantle consistent with the Ringwood's pyrolite, and depleted mantle. The latter composition is formed after basaltic magma smelted from the pyrolite.

Thus, the smelt iron core is formed at initial stage of the Earth's formation by integration of the smelt iron layers and collision of the primary embryos. The overwhelming bulk of the mantle made up of chondrites, which composition is changed from H- to LL-chondrite. The carbonaceous chondrite was involved only during formation of the outer part of the upper mantle. The activity of the water during the differentiation produces the large volume of acid igneous rocks, which are known as Archean grey gneisses.

The work is supported by Russian Foundation for Basic Research (project no. 07-05-00395).

References

Anderson, D.L., Sammis, C., Jordan, T. Composition of the mantle and core // E.C. Robertson (ed.). The nature of the solid Earth. McGraw-Hill. New York, 1972. P. 41–66.

Anfilogov, V.N., Khachay, Y.V. A possible scenario of material differentiation at the initial stage of the Earth's formation // Dokl. Earth Sci., 2005. Vol. 403. P. 954–957.

Brearley, A.J, Jones, R.H. Chondrite meteorites // Rev. Min., 1998. Vol. 36. P. 3–1 to 3–398.

Cameron, A.G.W. Accumulation processes in the primitive solar nebula // Icarus, 1973. Vol. 18. P. 407–450.

Dorofeeva, V.A., Makalkin, A.B. The evolution of the early solar system. The cosmochemical and physical aspects. Moscow: UPSS, 2004. 264 p. [in Russian].

Khain, V.E., Bozhko, H.A. Historical geotectoniks. Pre-Cambrian. Moscow, Nedra, 1988. 382 p. [in Russian].

Harper, C, Jacobsen, S. Evidence for ^{182}Hf in early Solar system and constraints the timescale for terrestrial accretion and core formation // Geochim. Cosmochim. Acta, 1996. Vol. 60. No. 7. P. 1131–1153.

Khachay, U.V., Anfilogov, V.N. Conditions and process of the Earth's formation at the early stage of its accumulation // The Fundamental Problems of Geotectonic. Moscow, 2007. Vol. II. P. 330–333 [in Russian].

Marakushev, A.A. The early Earth's crust based on meteorite composition research // The early crust: the composition and edge. Moscow, Nauka, 1991. P. 27–38 [in Russian].

Merk, R., Breuer, D., Spohn, T. Numerical modeling of ^{26}Al – Induced radioactive melting of asteroids concerning accretion, Icarus, 2002. Vol. 159. P. 183–191.

Ringwood, A.E. Origin of the Earth and Moon. Springer-Verlag. 1979. 295 p.

Robie, R.A, Hemingway, B.S., Fisher, J.R. Thermodynamic properties of minerals and related substances at 298.15 K and 1 bar (10^5 Pascals) pressure and at high temperatures // Geol. Surv. Bull., 1978. No. 1452. 456 p.

Salop, L.I. The geological development of the Earth in Pre-Cambrian. Leningrad, Nedra, 1982. 343 p. [in Russian].

Shukolyukov, U.A. An isotope-cosmochemical evidence of the native material transport between terrestrial planets // Geochem. Intern., 2003. No 11. P. 1139–1171 [in Russian].

Vitiazev, A.V., Pechernikova, G.V., Safronov, V.S. The terrestrial planets. Moscow, Nauka, 1990. 296 p. [in Russian].

Voitkevich, G.V. The foundation of the Earth's origin theory. Moscow, Nedra, 1973. 116 p. [in Russian].

O. Apukhtina[1], V.S. Kamenetsky[1], K. Ehrig[2]
[1] ARC Centre of Excellence in Ore Deposit Research, University of Tasmania, Hobart, Australia
olgaa@utas.edu.au
[2] BHP-Billiton, Adelaide, Australia

GEOLOGY AND MINERALISATION OF THE IOCG-TYPE OLYMPIC DAM DEPOSIT (SOUTH AUSTRALIA)

Рассмотрено геологическое строение и минеральный состав руд крупнейшего месторождения золота и меди Олимпик Дам (Австралия). Руды месторождения преимущественно прожилковые и состоят из флюорита, гематита, серицита, хлорита, барита, сидерита, доломита, кварца и сульфидов меди. Обсуждаются модели формирования и источники рудных компонентов, включая мантийные и седиментогенные.

The supergiant polymetallic Olympic Dam (OD) deposit is the world's largest uranium deposit, and fourth largest gold and copper deposit with significant Ag quantities and a total resource of about 9 Mt [BHP Billiton Annual Report, 2012].

The OD is located in South Australia and represents the type locality for Iron-Oxide-Copper-Gold (IOCG) deposits [Hitzman et al., 1992]. It is hosted by the Olympic Dam Breccia Complex (ODBC) that is situated within a Mesoproterozoic Roxby Downs Granite. This granite was intruded by numerous ultramafic and mafic dykes [Johnson & McCulloch, 1995; Ehrig et al. 2013]. The ODBC is covered by undeformed Late Proterozoic and Cambrian sedimentary rocks of the Stuart Shelf [Johnson & McCulloch, 1995].

According to Reeve et al. [1990], there are many types of different veins and veinlets in the deposit. They can contain fluorite, hematite, sericite, chlorite, barite, siderite, dolomite, quartz that may incorporate pitchblende and diverse copper sulphides. Some veins were precipitated within the fault zones and show multiple phases of brecciation. The paragenetic sequence though is very complex and multistage.

Geologists have been studying the genesis of the supergiant IOCG Olympic Dam deposit for more than 30 years, including numerous analyses such as radiogenic isotopes (U-Pb, Pb-Pb, Sm-Nd, Re-Os and Rb-Sr isotopes in various gangue and ore minerals), stable isotopes (C-O isotopes in siderite, O isotopes in magnetite, hematite, quartz and whole rock samples), fluid inclusion studies (siderite, quartz, fluorite), chemical composition (including REE) of some minerals and whole rock samples etc. However, there still exist many issues regarding its formation and especially sources of elements like U, Fe, Cu, REE, S and C. In addition, the ages of the multiple mineralisation events at the OD are still enigma. The proposed models for formation of the ODBC range from the maar-diatreme setting with a fluid mixing and mantle contribution to the mineralisation [e.g. Oreskes & Enaudi, 1992] to sedimentary-dominated [e.g. McPhie et al., 2011].

References

Reeve, J.S., Cross, K.C., Smith, R.N., Oreskes, N. Olympic Dam copper-uranium-gold-silver deposit. Geology of the Mineral Deposits of Australia and Papua New Guinea, 1990. P. 1009–1035.

Hitzman, M.W., Oreskes, N., Einaudi, M.T. Geological characteristics and tectonic setting of Proterozoic iron oxides (Cu–U–Au–REE) deposits. Precambrian Res., 1992. Vol. 58. P. 241–287.

Oreskes, N., Einaudi, M.T. Origin of hydrothermal fluids at Olympic Dam: preliminary results from fluid inclusions and stable isotopes. Econ. Geology, 1992. Vol. 87. P. 64–90.

Johnson, J.P., McCulloch, M.T. Sources of mineralising fluids for the Olympic Dam deposit (South Australia): Sm-Nd isotopic constraints. Chem. Geology, 1995. Vol. 121. P. 177–199.

McPhie, J., Kamenetsky, V., Chamberfort, I., Ehrig K., Green, N. Origin of the supergiant Olympic Dam Cu–U–Au–Ag deposit, South Australia: was a sedimentary basin involved? Geology, 2011. Vol. 39. P. 795–798.

BHP Billiton Annual Report, 2012 // http://www.bhpbilliton.com

Ehrig, K., McPhie, J., Kamenetsky, V. Geology and mineralogical zonation of the Olympic Dam Iron Oxide Cu-U-Au-Ag deposit, South Australia // In: Hedenquist J.W., Harris M., and Camus F., eds., Special Publication 16. Geology and Genesis of Major Copper Deposits and Districts of the World: A Tribute to Richard H. Sillitoe, Society of Economic Geologists, Inc., 2013. P. 237–268.

N.R. Ayupova[1, 2], I.G. Zhukov[1, 2]

[1] Institute of Mineralogy, Urals Branch of RAS, Miass, Russia, aupova@mineralogy.ru
[2] National Research South Ural State University, Chelyabinsk, Russia

DEVONIAN Fe-Mn NODULES OF THE URALS PALEOOCEAN

На марганцевых месторождениях Урала изучены Fe-Mn конкреции разной формы и величины, характеризующиеся присутствием структур роста и облекания, наличием реликтовой слоистости в законсервированной внутренней части и повышенными содержаниями Cu (46–325 г/т), Ni (47–144 г/т), Co (36–184 г/т), Ba (37–6467 г/т), U (0.2–2.78 г/т), сопоставимые с железомарганцевыми конкрециями современных океанов. Реликты вулканокластики и биоморфных структур в конкрециях свидетельствуют о важной роли литогенного и биогенного фактора в их формировании. Низкие содержания РЗЭ, небольшие вариации в аномалиях Ce (от –2.7 to +0.28) и появление небольшой положительной Eu аномалии в спектре РЗЭ конкреций отражают трансформации, происходившие в диагенетических процессах.

Introduction

Several metallogenic zones, including Sakmara, Magnitogorsk, and East Uralian zones, are distinguished in the Urals foldbelt. They are considered to be the paleogeodynamic sectors, corresponding to the marginal sea, island arc system, and uplift, respectively [Prokin, Buslaev, 1999]. Manganiferous rocks in the Southern Urals are hosted in the basalt-rich volcano-sedimentary complex of the Magnitogorsk paleoisland arc system, which consists of the West and East Magnitogorsk island arcs and Sibai inter-arc basin [Gavrilov, 1972]. The manganiferous mineralization occurs in association with the Middle Devonian stratabound hematite-quartz rocks and bedded red jaspers localized on the foot or hanging walls of massive sulfide deposits [Maslennikov et al., 2012]. Fe-Mn nodules are widespread in the jasper horizons, which occur at the flanks of manganese deposits. We have studied Fe-Mn nodules from the Faizulino and Yanzigitovo Mn-deposits, which were formed in the Sibai inter-arc basin, and compared them with well known Fe-Mn nodules from the modern oceans.

Methods

Identification of Fe-Mn nodules was based on their superficial color, external morphology and size. Selected samples were cut vertically in two parts with respect to their position on the seafloor. Individual nodules of special interest for mineralogical and geochemical determinations were first thoroughly examined in reflected light and by SEM microscopy. The internal structure was described, outlined and photographed. The chemical composition was analyzed with atomic absorption (AAS) using a Perkin Elmer 3110. The trace elements and REE concentrations were determined using induced coupled plasma mass spectrometry on a Agilent Technologies 7500 cx in the Center for Geo-Environmental Science, Faculty of Engineering and Resource Science, Akita University.

Faizulino deposit

Manganese nodules 1.5 ? 2 cm in size and less occur in the top of the jasper horizon and are hosted in the fine hyaloclastic siliceous rocks. Most of them have oval, lenticular, lens, and mushroom-shaped morphology with columnar structure of prominent sinters and thin-laminate external layers. The well visible outer layering is caused by stratification of separate Mn and Fe layers with thickness up to 1 mm. The layers differ by reflection resulted from enrichment in Mn or Fe. The nodular cores have complicate structure with relict lamination in the internal part. The non-opaque fine volcanic glass is scattered inside the manganese minerals. All varieties of the nodules contain abundant microfossil molds and silica filaments (Fig. a).

The Mn layers are composed of fine-grained K-psilomelane, which replaces jacobsite. The composition of K-psilomelane is as follows (wt %): MnO* 71.70–89.44, FeO* 1.20–13.27, SiO_2 0.83–2.00, Al_2O_3 0.44–3.52, TiO_2, 0.42–0.59, K_2O 0.96–1.22, CaO 0.89–1.17.

Jacobsite has gray color with a specific olive shade in the matrix of ferruginous layers. Its composition varies relative to stoichiometric species (wt %): MnO* 48.51–58.88, FeO* 25.49–37.99, SiO_2 0.75–2.08, Al_2O_3 1.81–2.87, TiO_2 0.40–0.42, K_2O 0.64–0.77, CaO 0.62–1.07.

Numerous magnetite crystals with a good facet occur in the core and Fe-rich layers of the nodules. Magnetite is enriched in MnO* (up to 3.73 wt %) and TiO_2 (up to 3.69 wt %) and, locally, it has extraordinary high Mn and Ti contents (wt %): MnO* 12.35–17.25, FeO* 57.80–70.12, SiO_2 0.58–1.87, Al_2O_3 1.08–2.09, TiO_2 15.20–21.09 (pyrophanite?). The elevated Mn and Ti contents in magnetite could possibly be related to the replacement of Ti-hematite. The replacement textures are observed in the nuclear part of the nodules, where ferruginous minerals predominate above the manganese ones. The cores of the nodules are enriched in volcanic glass identified by the higher Al, Mn, Fe, and K contents and sporadic pyrite inclusions.

Yanzigitovo deposit

Manganese nodules are localized at the contact of the hematite-quartz lens and hanging wall jaspers. Several horizons with manganese nodules indicate the discontinuous and periodical formation of nodules. Nodules have slightly asymmetric structure, rough surface, and sharp contacts with overlying rocks and are composed of Mn-oxides, clasts of felsic glass and microconcretions of Mn-biotite filaments overgrown by Mn-oxides. Ba-psilomelane is the major manganese mineral of the nodules (wt %: MnO* 76.73–78.33, BaO 12.57–14.69, K_2O 0.54–0.72, CaO 0.70–0.97). Numerous inclusions of radiolarian are widespread in the external layers of the nodules (Fig. b). Supergene processes formed veins and nests with late Mn-oxide.

Chemical composition of nodules

Manganese (5–40 wt %), iron (1–15 wt %), and silica (14–40 wt %) are the principal components of the nodules admixed with varying contents of (wt %) Al_2O_3 (2–5), MgO (0.4–1.3), Na_2O+K_2O (0.7–2.2), CaO (2–3), and P_2O_5 (0–0.07). The high concentrations of Zr, Ti, V and Al are probably related to the relict volcanic glass. The variations of concentration (ppm) of Cu (46–325), Ni (47–144), Co (36–184), Ba (37–6467), Sr (35–527), V (0.51–214), Zr (1–135) and U (0.2–2.78) are the specific features of nodules.

The nodules show low REE contents (up to 155 ppm) and Ce/La ratio (0.42–1.73) compared to the average content of the hydrogenous deep-seabed nodules from the oceanic areas and also exhibit a negative Ce anomaly. Magnitude of the Ce anomaly, ranging from –2.7 to +0.28, was calculated using the equation of log [3Ce/(2La+Nd)], where Ce, La, and Nd are the NASC normalized values [Elderfield et al., 1981]. The positive Eu anomaly indicates the presence of hyloclastic detritus and mineral precipitation from the fluids with a hydrothermal component under reduced conditions. The nodules are enriched in LREE that is evident from the La/Lu* ratio ($[La_{sample}/La_{shale})/(Lu_{sample}/Lu_{shale})]$) of 0.54–1.85.

Discussion and conclusions

Fe-Mn nodules, which were formed in the Devonian Urals paleoocean, could be compared with those from the modern oceans. Good preservation of delicate textures of the nodules is related to their fast overlapping by the fine-grained sediments. The morphology and columnar structure of the nodules are also typical of modern Fe-Mn nodules [Halbach et al., 1981; Baturin and Dubinchuk, 1989; Banerjee et al., 1999]. The nodules are diverse in shape and Fe and Mn contents. The external zones of the nodules have layered structure. The growth structures are most typical for nodules in contrast to the corrosion, excluding dissolution of volcanic glass and its replacement by manganese minerals

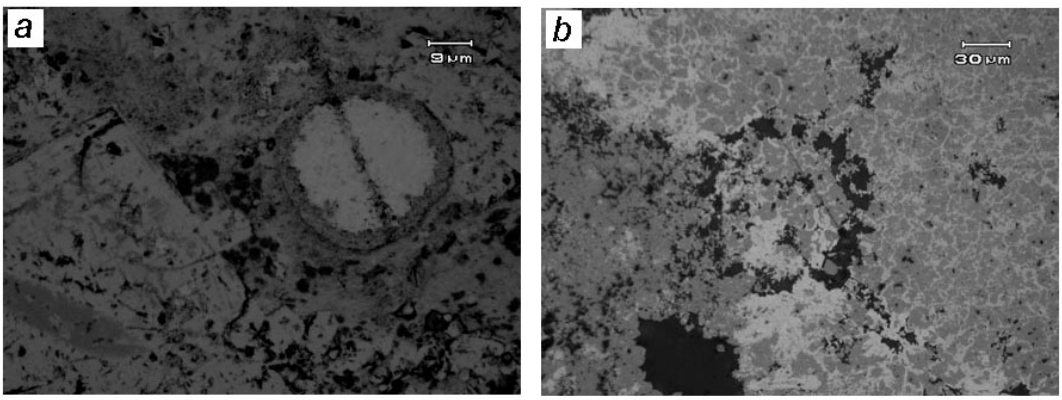

Fig. Microfossils in the Fe-Mn nodules: a – Faizulino, and b – Yanzigitovo deposits.

The common presence of radial cracks, cross-cutting the oxide layers, and the high porosity and permeability of the nodules are evidences of somewhat open formation conditions. The primary manganese minerals (probably, manganite and vernadite) of the nodules have not been found yet and the occurrence of jacobsite in the Faizulino deposit points to some degree of postsedimentary alteration.

It is suggested that the volcanic glass is one of the main source of Fe and Mn owing to their correlation with high Ti and Al content. The biogenic (mainly radiolarian, some individual filaments, and spheroidal microforms) relics in the nodules are thought to play a vital role in the variation of chemical composition (possibly including radionuclide) in the internal part of the nodules, since plankton is known to scavenge the trace metals during the life cycles similar to the modern Fe-Mn nodules [Ehrlich, 1980]. An accumulation of some amount of K^+ in the filaments may be also related to the organic matter [Harder and Dijkhuisen, 1983].

Thus, the studied nodules are comparable to the modern counterparts by high grades of Ni, Co, Ba, Cu, and elevated of Fe contents. The depletion in ΣREE in the nodules may reflect diagenetic processes. The formation of Fe-Mn nodules could represent a combination of hydrogenetic and diagenetic conditions under important role of biogenic factor.

The work is supported by the Russian Federal Program of Ministry of Science and Education (no. 14.740.11.1048) and the Joint Program of Uralian and Siberian Branches of Russian Academy of Science (no. 12-C-5-1010).

References

Baturin, G.N, and Dubinchuk, V.T. Microtexture of Fe-Mn nodules: atlas of microphotos. Moscow, 1989. 288 p. [in Russian].

Ehrlich, H.L. Different forms of microbial manganese oxidation and reduction and their environmental significance // Biogeochemistry of ancient and modern environment. Berlin, Springer, 1980. P. 327–332.

Gavrilov, A.A. Exhalative-sedimentary accumulation of manganese. Moscow, Nauka, 1972. 216 p. [in Russian].

Halbach, P., Scherhag, C., Hebisch, U., Marchig, V. Geochemical and mineralogical control of different genetic types of deep-sea nodules from the Pacific ocean // Ibid., 1981. Vol. 16. No 1. P. 59–84.

Banerjee, R., Roy, S., Dasgupta, S., Mukhopadhyay, S., Miura, H. Petrogenesis of ferromanganese nodules from east of the Chagos Archipelago, Central Indian Basin, Indian Ocean // Marine Geology, 1999. Vol. 157. P. 145–158.

Harder, W., Dijkhuisen, L. Physical responses to nutrient limitation. Annu. Rev. Microbiol., 1983. Vol. 37. P. 1–23.

Maslennikov, V.V., Ayupova, N.R., Herrington, R.J., Danyushevskiy, L.V., Large, R.R. Ferruginous and manganiferous haloes around massive sulphide deposits of the Urals // Ore geology reviews, 2012. Vol. 47. P. 5–41.

Prokin, V.A., Buslaev, F.P. Massive copper-zinc sulphide deposits in the Urals // Ore geology reviews, 1999. Vol. 14. P. 1–69.

Elderfield, H., Hawkesworth, C.J., Greaves, M.J., Calvert S.E. Rare earth element geochemistry of oceanic ferromanganese nodules and associated sediments // Geochim. Cosmochim. Acta, 1981. Vol. 45. P. 513–528.

N.R. Ayupova[1, 2], V.V. Maslennikov[1, 2], S.P. Maslennikova[1], S.A. Sadykov[1], L.V. Danyushevsky[3]

[1] Institute of Mineralogy UB RAS, Miass, Russia, aupova@mineralogy.ru
[2] National Research South Ural State University, Chelyabinsk, Russia
[3] CODES, University of Tasmania, Hobart, Australia

BIOMORPHIC SIGNATURES OF METALLIFEROUS FERRUGINOUS AND MANGANIFEROUS ROCKS FROM THE URALS VMS DEPOSITS

В оксидно-железистых и марганцевых продуктах придонных преобразований известково-висто-сульфидно-гиалокластитовых осадков колчеданных месторождений Урала обнаружены

бактериоморфные структуры, представленные нитчатыми и микротрубчатыми формами, и реликты микрофауны – трубчатых организмов, тентакулитов, радиолярий и фораминифер. В ассоциации с биогенными образованиями установлены аутигенные лейкоксен, титанит, рутил, хлорит, иллит, гематит, апатит и сульфидные минералы. Результаты ЛА-ИСП-МС анализов показывают, что в гематите биоморфоз наблюдается концентрация Mn (до 9393 г/т), Ti (до 528 г/т), As (до 1872 г/т), V (779 г/т), W (до 1091 г/т) и Mo (до 40 г/т), а также повышенные содержания Zn, Pb, Sb и U. Изотопный состав углерода $\delta^{13}C$ в карбонатах варьирует от –4 до –11 ‰ в отличие от $\delta^{13}C$ (от 0 до +2.64 ‰) надрудных известняков. Предполагается, что биологическая активность в совокупности с экстремальными условиями среды привели к ускоренной трансформации биогенного ОВ, создавая уникальные возможности для постседиментационных преобразований исходных компонентов осадка.

The brecciated proximal ferruginous and manganiferous rocks related to the Urals VMS deposits include jasperites, gossanites, and umbers, in addition to thin-bedded jaspers and cherts [Maslennikov et al., 2012]. An abundance of replacement textures of hyaloclastites and carbonates by hematite and silica is the most important feature of jasperites and umbers. The replacement of clastic sulfides by hematite and magnetite is characteristic of gossanites. These sedimentary rocks are accompanied by pseudomorphs of hematite and quartz after microplankton fossils and bacterial filaments [Maslennikov et al., 2012; Ayupova and Maslennikov, 2012].

In gossanites from the Talgan and Imeni XIX Parts'ezda deposits, widespread carbonate-hematite tube forms are hollow-centered or incrusted by concentric layers of microcrystalline hematite. Locally, the cavities of these worms are mineralized with sulfide minerals. The tube forms can be compared with the near vent tube worms discovered in the modern and ancient black smoker systems but of smaller diameter [Little et al., 1999]. Typical tentaculates from the Talgan, XIX Parts'ezd, Molodezhnoye, Alexandrinka, and Shemoor deposits have similar diameters of tube but are made up of calcite partly replaced by hematite. The authigenic leucoxene, titanite, chlorite, hematite, and apatite are often observed inside the shell of tentaculites. The spherical radiolarians of *Astroentactinia* 100–160 μm in size with a number of short thin outer needles are recognized in ferruginous and manganiferous rocks. Rare round or oval foraminifera shells are composed of quartz, albite, apatite, chlorite, and carbonate-cemented ferruginous material.

All varieties of ferruginous and manganiferous rocks from the Urals VMS deposits contain abundant silica-hematite filaments. Two types of filaments may be distinguished on the basis of their dimensions. The filaments of the larger diameter (6–16 μm) cross cut the clusters of filaments in calcareous gossanites from the Talgan VMS deposit. Much thinner (1–4 μm in diameter) filaments were found in hematite-chlorite gossanites from the Molodezhnoye and Alexandrinka deposits. The bulbous swelling is a common feature of the filaments. The numerous thick (20–30 μm) and thin (1–4 μm) filaments were revealed in jasperites from the hanging wall of the Saf'yanovka VMS deposit. Cylindrical to elliptical filaments are up to 500 μm long. They are coated by the red cryptocrystalline hematite and are filled with quartz. The network of numerous curved hematite filaments with a 1-μm axial hole is the most striking feature of jasperites from the Babaryk VMS deposit.

The inorganic self-organized processes may produce the patterns of silica and iron oxides that resemble bacterial filament structures [Hopkinson et al., 1998]. Notwithstanding, the studied filaments display no regular fractal or dendritic branches and may be found as a single fragment in the clastic matrix of ferruginous rocks. In comparison with fractal structures, the coating and infilling are common that is attributed to the near vent fauna fossilization [Little et al., 1999].

The diameters of the filaments are comparable with some varieties of hemoautotrophic bacteria found in the modern vent sites [Juniper and Fouquet, 1988]. More recent work on the ancient VMS deposits indicates an important role of similar biogenic processes in formation of silica-ferruginous rocks [Duhig et al., 1992; Greene, Slack, 2003; Little et al., 1999].

The carbon isotopic composition of limestones closely related to the sulfide orebodies at the Uzelga, Talgan, Yubileinoe, and Sibai VMS deposits varies from 0 up to + 2.64‰ [Maslennikov, 1999; Ayupova, Sadykov, 2013]. The $\delta^{13}C$ values of the authigenic carbonates from the metalliferous sediments are low (–4 to –11‰) and similar to those measured in gossanites, jasperites, and umbers [Ayupova, Sadykov, 2013]. In some cases, $\delta^{13}C$ values in carbonates from gossanites of the Molodezhnoye and jasperites of the Sibai deposits are extremely low (–19.5 and –13.0 ‰, respectively) [Maslennikov, 1999].

The average value is close to the $\delta^{13}C$ values of the vestimentiferas from the rift zones of the Pacific Ocean that in trophosome proved activity of chemoautotrophic bacterial-symbionts [Felbeck, 1983] and to the mean $\delta^{13}C$ value (–15.87 ‰ ± 4.96‰) determined for the organic constituents of the ferrihydrite samples from the Axial Volcano black-gray smoker hydrothermal field [Kennedy et al., 2010]. The direct relationship between the carbon isotopic values and presence of iron-oxidizing bacteria from natural and laboratory samples shows the ability of these microorganisms to fractionate the carbon [Kennedy et al., 2010; Konhaueser, 2006].

The results of LA-ICP-MS analyses show that the distribution of trace elements in hematite pseudomorphs after the tube worms is relatively uniform and stable. The hematite biomorphic structures concentrate Mn (up to 9393 ppm), Ti (up to 528 ppm), As (up to 1872 ppm), V (779 ppm), W (to 1091 ppm), and Mo (up to 40 ppm), indicating the biological mechanisms of accumulation and retention of these metals in the system. It should be emphasized that the elevated contents of these elements are typical of the modern vestimentiferas and polychaetes [Juniper et al., 1992; Demin et al, 2007], as well as mineralized fauna from the ancient hydrothermal systems [Maslennikov, 2006].

The finding of the filaments in the ferruginous and manganiferous sedimentary rocks suggests that they may be confirmed to the bacterial destruction of the volcanic glass [Thorseth et al., 1995] and/or the oxidation of previously formed sulfides [Konhauser, 2006]. It is likely that microbial activity, evidenced by the relic biomorphic textures, leads iron, manganese precipitation, and silica nucleation at sediment-water interface [Duhing et al., 1992]. Basically, bacteria and microorganisms create a local microenvironment as a result of their metabolic products. The bacterial activity in submarine transformations of initial sulfide, hyaloclastic, and carbonate sediments played a major role in the development of microfossils. The microbial alteration also results in formation of authigenic minerals and is accompanied by redistribution of elements. The chemical composition of biotic alteration products may strongly vary, indicating that different bacteria types should accumulate different elements. The mobility of elements during biotic alteration also seems to be significantly different relative to abiotic alteration. The accumulation of Mo, W, V, Mn, Ti and other elements and formation of titanite, hematite, chlorite, apatite, and illite are the early low-temperature process produced by microbial activity.

The work is supported by the Russian Federal Program of Ministry of Science and Education (no. 14.740.11.1048) and the Joint Program of the Urals and Siberian Branches of Russian Academy of Science (no. 12-C-5-1010).

References

Ayupova, N.R., Maslennikov, V.V. Biomineralisation in ferruginous-siliceous sediments of massive sulfide deposits of the Urals) // Doklady Earth Sciences, 2012. Vol. 442. P. 193–195.

Ayupova, N.R., Sadykov, C.A. Isotopic carbon composition of carbonates from oxide-ferriginous metalliferous rocks of the Uraks massive sulfide deposits // Metallogeny of ancient and modern oceans-2013. Miass, IMin UB RAS, 2013. P. 100–104 [in Russian].

Demin, L.L, Galkin, A.V, Lein, AY, Lisitsyn, A.P. First data on microelemental composition of benthic organisms from the 9°50′ N hydrothermal field, East Pacific Rise // Doklady Earth Sciences, 2007. Vol. 415. P. 528–531 .

Duhig, N.C, Stolz, J., Davidson, G.J., Large, R.R. Cambrian microbial and silica gel textures in silica iron exhalites from the Mount Windsor volcanic belt, Australia: their petrography, chemistry and origin // Economic Geology, 1992. Vol. 87. P. 764–784.

Felbeck, H. Chemoautotrophic potential of the hydrothermal vent tube worm Riftia pachyptila Jones (Vestimentifera) // Science, 1981. Vol. 213. P. 336–338.

Grenne, T., Slack, J.F. Bedded jaspers of the Ordovician Lokken ophiolite, Norway: seafloor deposition and diagenetic maturation of hydrothermal plume-derived silica-iron gels // Mineralium Deposita, 2003. Vol. 38. P. 625–639.

Hopkinson, L., Roberts, S., Herrington, R., Wilkinson, J. Self-organization of submarine hydrothermal siliceous deposits: evidence from the TAG hydrothermal mound 26? N Mid-Atlantic Ridge // Geology, 1998. Vol. 26. P. 347–350.

Juniper, S.K., Jonnasson, I.R., Tunnicliffe, V., Southward, A.J. Influence of tube building polychaete on hydrothermal chimney mineralization // Geology, 1992. Vol. 20. P. 895–898.

Juniper, SK, Fouquet, Y. Filamentous iron-silica deposits from modern and ancient hydrothermal sites // Canadian Mineralogist, 1988. Vol. 26. P. 859–869.

Kennedy, C.B., Gault, A.G., Fortin, D., Clark, I.D., Pedersen, K., Scott, S.D. et al. Carbon isotope fractionation by sircumneutral iron-oxidizing bacterias // Geology, 2010. Vol. 38. P. 1087–1090.

Konhauser K. Introduction to Geomicrobiology. Maldon, Oxford, Carlton: Blacklwell Publishing, 2006. 425 p.

Lein AY, Sedyh E.M, Starshinova NP et al. The distribution of metals in bacteria and worms of submarine hydrothermal fields // Geochemistry, 1989. no. 2. P. 297–303 [in Russian].

Little CTS, Maslennikov VV, Morris NJ, Gubanov AP. Two paleozoic hydrothermal vent communities from the southern Ural Mountains, Russia // Paleontology, 1999. Vol. 42. P. 1043–1078.

Maslennikov, V.V., Ayupova, N.R., Herrington R.J., Danyushevskiy, L.V., Large, R.R. Ferruginous and manganiferous haloes around massive sulphide deposits of the Urals // Ore geology reviews, 2012. Vol. 47. P. 5–41.

Maslennikov, V.V. Sedimentogenesis, halmyrolysis and ecology of the massive sulfide paleohydrothermal fields (after the example of the Southern Urals). The Scientific Edition. Miass: Geotur, 1999. 348 p. [in Russian].

Maslennikov, V.V. Lithological control of copper massive sulfide ores (after the example of Sibai and Oktyabrskoye deposits, Ural). Sverdlovsk, UB AN USSR, 1991. 139 p. [in Russian].

Thorseth, I.H., Torsvik, T., Furnes, H., Muehlenbachs, K. Microbes play an important role in the alteration of oceanic crust // Chemical Geology, 1995. Vol. 126. P. 137–146.

E.V. Belogub, K.A. Novoselov, E.E. Palenova, M.V. Zabotina, P.V. Khvorov
Institute of Mineralogy UB RAS, Miass, bel@mineralogy.ru

MINERALOGY OF OXIDIZED ORE OF IKRYANSKOYE GOLD DEPOSIT (SVERDLOVSK DISTRICT, RUSSIA)

Икрянское месторождения золота приурочено к зоне Егоршинского глубинного разлома и локализовано в рассланцованных метавулканитах и метаосадочных породах – эпидот-актинолит-хлоритовых, хлоритовых, кремнистых, глинисто-кремнистых и углеродисто-глинисто-кремнистых сланцах. Руды вкрапленные, прожилково-вкрапленные. Золото связано с пиритизацией, находится преимущественно в самородной форме, обычно содержит примесь ртути. Окисленные руды глинистые, при этом метавулканиты характеризуются высокими содержаниями хлорит-смектита, в то время как метаосадки обогащены слюдой и каолинитом. Наличие глинистых мирнералов с высокой сорбционной емкостью ухудшает технологические свойства руд, предполагаемых для гидрометаллургической переработки.

Due to the depletion of gravel and large gold deposits in the Urals in the last decade a small objects that are available for open-pit mining are involved to exploitation. As a rule, these deposits of oxidized ore with low grade of gold. Gold from ore is extracted by heap leaching cyanidation. The efficiency of this process is largely determined by the mineral composition of the ore: size and morphology of gold, clay content, the presence of fresh sulphides and copper minerals. The study of the mineral composition of oxidized ore was held in conjunction with the planned mining of the deposit ZAO Aurum. Currently Ikryanskoye deposit is excavated by shallow pit.

Ikryanskoye deposit is a part of larger Fevralskoye deposit, which belongs to submeridional Reft schist band of Sillurian–Lower Devonian volcanic-sedimantary rocks. Deposit locates in Yegorshinskiy regional fault. Ore zone is located within tectonic wedge, which contacts with Lower Carbon carbon-bearing sedimentary rock and limestone in East. In West direction schist band boardered with Low Carbon Reft gabbro-granite complex. Vein bodies of granite in schist band connect with this complex. There is regional weathering crust above deposit. Its thickness at the plane area is about 25–30 m. Linear weathering crust above tectonic zone spread deeper more, then 60 m [Koshkin et al., 2009].

Host rocks because of tectonic influence are schistose. There are metavolcanites (basalt with rare dacite), their clastic varieties, metasediments, and rare vein plagiogranite. Metavolcanic rocks were metamorphosed under epidote-amphibolite subfacie of green-schist facie. In ore zone they al-

tered to chlorite, epidote-chlorite, gauffering schists. Chert, quartz-sericite, clayey shists and rare black shales are metasediments in ore zone. Gold concentration is connected with metasomatical processes as disseminated pyrite and some quartz-carbonate veinlets [Sazonov et al., 1999].

Pyrite is the main ore mineral of fresh ore. Chalcopyrite, sphalerite, pyrrhotite, pentlandite are secondary. Alloclasite, galena, altaite, cinnabar (?), and native gold are rare. Nickel and cobalt enrichment of iron sulfides is typical for deposit. Main matrix minerals of metavolcanites are epidote group, chlorite, actinolite, albite, quartz. In metasediments there are quartz, albite, sericite, carbon matter.

Clayey eluvial weathering crust after schist with steep bedding is outcropped in open pit. The separation of wheathered metasediments and metavolcanites in open pit is very difficult. But some small lenses of black shale among brownish clayey oxidized chert and schist can be allocated in the central part of open pit.

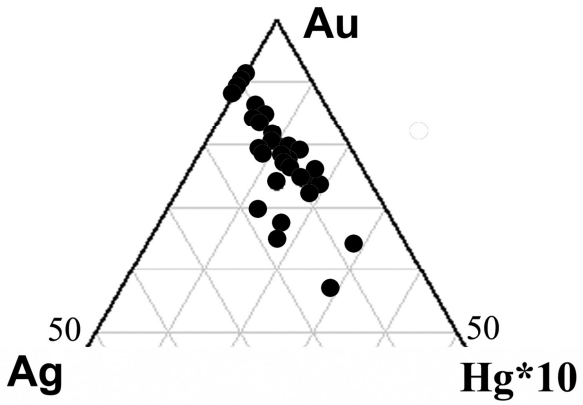

Fig. 1. Composition of gold (mas.%).

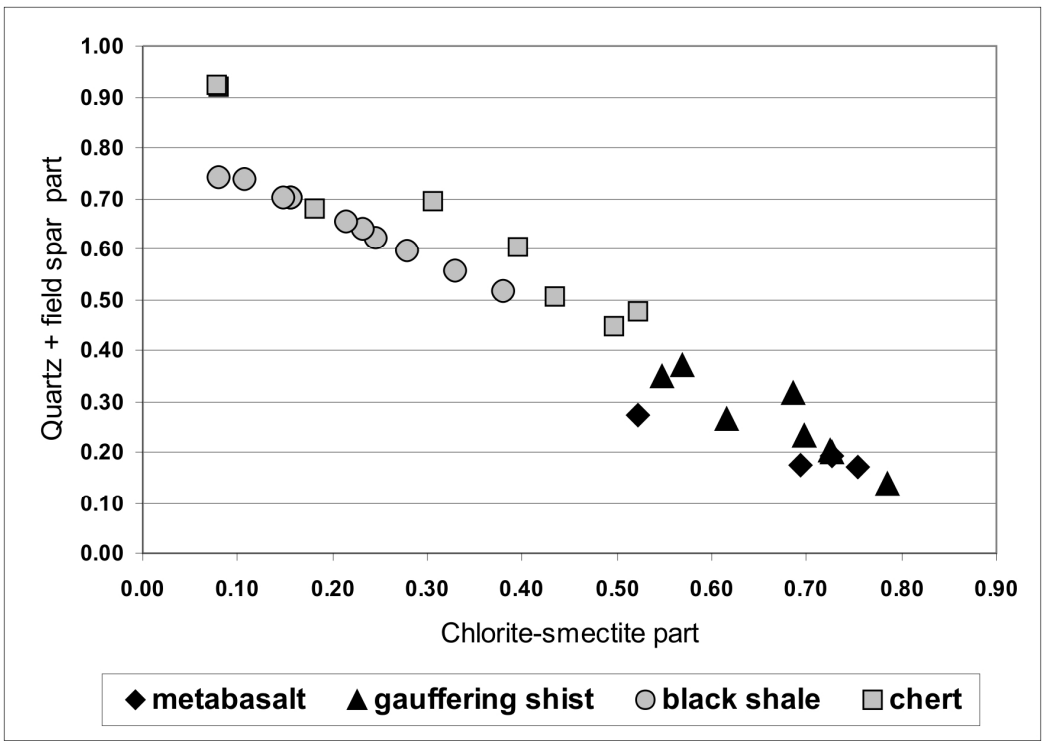

Fig 2. Quartz + field spar and smectite-chlorite + kaolinite in different weathered rock type plot.

Ore bodies can be isolated only by sampling. Oxidized ore is clayey, ocher-cleyey with relic schistosity. Gold content very varies, average 3.4 g/t with cut-off grade 1.4 g/t and reach more then 1 kg/t [Koshkin et al., 2009]. Au/Ag ratio also varies from 10 to 0.07, usually 1–3.

Goethite is prevailing ore mineral in heavy concentrate of ore independently of matrix. Rutile and semioxidized pyrite and chalcopyrite are occasional. Gold forms free particles with complex morphology up to 2 mm in size as well as micron-size inclusion in pyrite. Impurity of silver (10–20 mas. %) and mercury (up to 3.9 mas.%) is characterized for chemical composition of gold (fig.1). Impurity content is higher in free gold then inclusions.

Light fraction mineral composition depends of matrix. After XRD analysis (Shimadzu XRD-6000, Cu-Kα) it have been obtained that layer silicate part is higher in metavilcanites then metasediments. Oxidized and hydrated chlorite (chlorite-smectite) prevails in metavolcanites (fig. 2). Hydrated mica and kaolinite also presented in minor percentage. Layer silicates sum in this rock type is 60 % and more. Secondary minerals are quartz, albite, relics of actinolite and epidite. In general, metasediments consist of quartz and field spaar. The main layer silicate in chert is sericite and kaolinite. Carbon-bearing shale is enriched by sericite. But chlorite-smectite is in both rock type (fig. 2).

Degree of supergene change of chlorite depends after depth. At the 0–10(12) m chlorite is transformed into vermiculite-like mineral ("chlorite-smectite" with complete destroying of "brucite" layer and its replacing by smectite layer. These features are good identified using thermogravimetric analysis. After 10–12 m in depth the relics of chlorite structure became preserved. After 20 m chlorite are not changed practically.

These features of the mineral composition of oxidized ores are the base for planning of hydrometallurgical processing of Ikryanskoye deposit.

We are sincerely grateful to the ZAO Aurum administration for permission to work on deposit.

References

Sazonov, V.N., Ogorodnikov, V.N., Koroteev, V.A., Polenov, Yu.A. The gold deposits of Urals. Yekaterinburg: UGGA Publishing House 1999. 570 p. [in Russian].

Koshkin, V.A. et al. Report about results of the exploration work for ore gold, which were provided by OAO Aurum during 2006–2008 on the site of Reft Zone (Fevralskoye deposit) with reserve calculation of oxidized ore for 01.07.08 state. Sukhoy Log, 2009. 187 p. [in Russian].

I.A. Blinov
Institute of Mineralogy UB RAS, Miass, Russia, ivan_a_blinov@mail.ru

MINERALOGY OF THE OXIDIZED ORES FROM THE VERKHNYAYA ARSHA Pb-Zn DEPOSIT, SOUTH URALS

В работе представлены первые данные о минералах бурых железняков и полуокисленных руд стратиформного Верхне-Аршинского Pb-Zn месторождения. Набор минеральных видов схож с Амурским Zn-месторождением, представлен золотом, галогенидами серебра, галенитом, минералами семейства алунита и другими.

The Verkhnyaya Arsha deposit is located 1.5 km to north from the village of Verkhnyaya Arsha in the Republic of Bashkortostan. It belongs to the West Urals metallogenic zone and is hosted in the Riphean dolomites. The deposit was exploited before 1958. The ores include sulfide (Fe and Pb-Zn), semioxidized and oxidized types. The major minerals of the sulfide ores are pyrite, galena, and sphalerite [Rotar et al., 1976]. Anglesite, cerussite, jarosite, and Pb-jarosite were identified in the oxidized ores in addition to Fe-hydroxides [Shumikhin et al., 1956]. The technogene supergene mineralisation was previously described [Blinov et al., 2011].

The oxidized ores (or brown ore) are characterized by heterogeneous chemical composition and contain up to 0.7 % Zn and Pb and up to 0.3–1.5 % Ag in some samples. The brown ore with high amount of sulfides represent semioxidized ore with the higher Zn and Pb contents.

The objective of the abstract is a characteristic of supergene minerals in the oxidized and semioxidized ores from the Verkhnyaya Arsha deposit.

Native metals

Native *gold* was revealed in the massive geode part and in the brown ore with a box structure. Gold contains up to 2 wt % Cu and 0.2 wt % Ag. Some grains of the pure gold contain less than 0.1 wt % of admixtures.

One grain of native *zinc* 10 ?m in size was found in the brown ore at the contact of Fe-hydroxides and quartz. The ED-spectrum is characterized by Fe and Al peaks.

Sulfides

Acanthite in the brown ore forms aggregates 3–5 ?m in size, intergrowing with iodargyrite. In the semioxidized ores, acanthite grains up to 7 ?m in size were found as thin veinlets and rims around pyrite.

The supergene chemically pure *galena* in the brown ore occurs as grains up to 15 ?m in size in Fe-hydroxides. In semioxidized polymetallic ores, galena forms cubic and occasionally case-like crystals 30 ?m in size, microdruses, rare framboids or rims around pyrite or Fe-hydroxides. The primary and supergene galena in semioxidized polymetallic ores contains admixture of silver. In semioxidized pyrite ores, supergene galena forms crystals, microveins 10–20 ?m thick or rims around pyrite crystals. Some grains are also characterized by admixture of silver.

Oxides and hydroxides

Fe-hydroxides are widespread minerals of the brown ore and occur as massive, radial, box-like or gel-like aggregates. Fe-hydroxides are characterized by Zn content up to 1.4 wt %, which is mostly typical of box-like aggregates. Based on the correlation analysis of 35 SEM analyses of Fe-hydroxides, zinc has positive correlation with lead (0.7) and negative, with sulfur (–0.8). In semioxidized polymetallic ores, Fe-hydroxides form pseudomorphoses after sulfides or rims around them. The concentration of admixtures is as follows (wt %): Zn 3, S 5, SiO_2 4, Al_2O_3 0.5. In semioxidized pyrite ores, Fe-hydroxides contain 0.2–2 wt % Zn and traces of S, Si, Al.

Sulfates

The *jarosite group* minerals were previously described by Zhumikhin et al. (1958). We have found several grains of Ba-bearing mineral similar to Pb-jarosite in the brown ore.

Ag-bearing *anglesite* in semioxidized polymetallic ores forms the low-thick crusts.

Halogenides

Iodargyrite in the brown ore forms the crystals 20–30 ?m in size in geodes. Iodargyrite was also found in thin acanthite microveins in the semioxidized ores.

Conclusions

Thus, native zinc and gold, acanthite, iodargyrite and supergene galena were found for the first time in the oxidation zone of the Verkhnyaya Arsha deposit. The joint occurrence of native zinc, supergene galena and Fe-hydroxides indicates the repeatedly varieted conditions during formation of the oxidation zone at the deposit.

Author is grateful to E.V. Belogub, K.A. Novoselov, V.A. Kotlyarov, and I.Yu. Melekestseva for consultations and help during the work. This research is supported by Program of Presidium of the Russian Academy of Sciences (project no. 12–П–5–1003).

References

Blinov, I.A., Belogub, E.V., Novoselov, K.A., Fillipova, K.A. Technogene supergene mineralization of the Verkhnyaya Arsha Pb-Zn deposit, Bashkortostan // Bashkirian chemical journal, 2011. Vol. 14. No. 4. P. 136–144 [in Russian].

Rotar, A.F., Rotar, Z.M., Gulyaev, Yu.A., Tambovtsev, V.V. An unpublished report on geological study on a scale of 1 : 50000 at the Iremel area, plane-tables №-40-58-В и №-40-58-Г (western part) and searching of polymetallic ores on a scale of 1 : 50000 at the Avkyar area. Ufa, 1976. Vol. 1 [in Russian].

Shumikhin, E.A., Grunvald, V.P., Topko, I.P. An unpublished report on the works of the Verkhnyaya Arsha searching-prospecting party for lead conducted in the Beloretsk region of the Bashkirian ASSR in 1950–1956. Ufa, 1956 [in Russian].

B.I. Chuvashov, A.L. Anfimov, E.I. Soroka
Institute of Geology and Geochemistry UB RAS, Yekaterinburg, Russia

AGE AND FORMATION CONDITION OF ORE-HOSTING SEQUENCE OF THE SAF'YANOVKA DEPOSIT, CENTRAL URALS: DATA ON FORAMINIFERS

Раковины фораминифер эйфеля-живета *Parathurammina aff. tamarae* L. Petrova, 1981, *Parathurammina magna* и др. встречаются в породах рудовмещающей толщи Сафьяновского медноколчеданного месторождения (Средний Урал) в интервале глубин от 100 до 200 м. Хорошая сохранность фораминифер, нередкое обволакивание раковин пелитовым материалом, следы продавливания осадков указывают на захоронение раковин в мелководных морских условиях недалеко от места обитания. Видовое однообразие раковин фораминифер свидетельствует о неблагоприятных условиях обитания и мелководности бассейна осадконакопления. На основании этого можно сделать вывод, что породы рудовмещающей толщи формировались в эйфель-живетском мелководном морском бассейне при практически непрерывном привносе вулканогенного материала.

The Saf'yanovka massive sulfide deposit confined to the Eastern Uralian uplift is situated in the south of the Rezh lithotectonic zone. It is localized in the altered Middle Devonian volcanic (rhyolite-dacite) and volcano-sedimentary rocks [Korovko et al., 1991], which are exposed in the open pit (10 km northeast of the town of Rezh). The thickness of the ore-hosting sequence is about 400 m. The main body of massive sulfide ores is 400 m long and 140 m wide. The southern flank of the orebody is strongly pinched out and the northern orebody transits into a series of apophyses, which represent massive and stringer-disseminated sulfide ores. Massive chalcopyrite ores consist of pyrite, chalcopyrite, and sphalerite. Polymetallic ores present in subordinate amount include tennantite, tetrahedrite, digenite, enargite, galena and famatinite and rare marcasite, pyrrhotite, arsenopyrite, and gold. Copper-zinc ores contain high amounts of sphalerite and some galena [Yazeva et al., 1992]. The depth of the open pit now is 170 m. After the depth will attain 200 m, the deposit will be operated by the mines.

A layer of Carboniferous limestones exposed by the open pit in the upper section of the ore-hosting sequence (to a depth of 30 m) contains the Upper Tournaisian foraminifers identified in the core of the wells of P-4, 3030 [Chuvashov et al., 2012]. The Upper Eifellian–Givetian [Chuvashov et al., 2011] non-carbonate foraminifera shells of *Parathurammina aff. tamarae* L. Petrova, 1981 [Petrova, 1981] were found in the underlying carboniferous-siliceous sitly claystones (horizon of 187 m).

The members of carbonaceous-siliceous rocks 0.1 to 1.5 m thick are located at the depths of 187–100 m both in the upper horizons exposed by the open pit and at the deeper levels exposed by mines (southwest of the Saf'yanovka ore field, depth of 200 m). The rocks consist of quartz, plagioclase, chlorite, mica, kaolinite, barite, and pyrite. The organic matter is sapropelic of marine origin [Yaroslavtseva et al., 2012].

The *Parathurammina aff. tamarae* L. Petrova, 1981 foraminifera shells composed of quartz or apatite were found in several outcrops of the carbonaceous-siliceous rocks in the southeastern and southern part of the open pit (horizons 187–100 m) (Fig. 1) [Chuvashov et al., 2011]. The shells have three-layered wall, reduced size and mouths that may be attributed to unfavorable habitat conditions in a shallow marine basin, where carbonate sedimentation was significantly suppressed by additional supply of volcanic material.

An attachment disk found in one of the shell sections points to the attached way of life of foraminifers (Fig. 2). Good preservation of the foraminifera shells, frequent enveloping by clay material, and traces of punching precipitation indicate that the shells were buried in the shallow marine environments near the habitat.

The study of shells on a JSM-6390LV (JEOL) electron microscope equipped with an Inca Energy 450 EDS (Institute of Geology and Geochemistry UB RAS, Yekaterinburg, analyst S.P. Glavatskikh) has revealed that originally they were composed of aragonite, calcite, and organic matter (pseudochitin) and later were replaced by apatite and quartz.

The calcareous *Parathurammina magna* Antropov, 1950 foraminifera shells were found in mine in limestones on the southwest flank of the deposit in a fault zone at the contact with serpentinites (sample SH10/12) at a depth of 200 m (Fig. 3). They also inhabited the Middle-Late Devonian

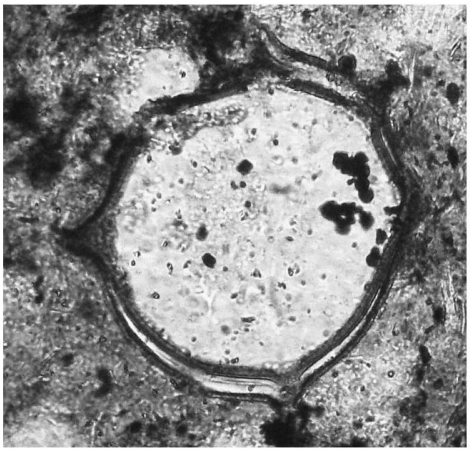

Fig. 1. Non-carbonate (apatite-silicon) shell of Foraminifera *Parathurammina aff. tamarae* L. Petrova of carbonaceous-siliceous rocks of ore-hosting strata of the Saf'yanovka deposit, horizon 187 m. One can clearly see wellhead elevation and three-layer wall of the shell. The Late Eiffelian-Givetian age. Thin section, transmitted light, magnification 140.

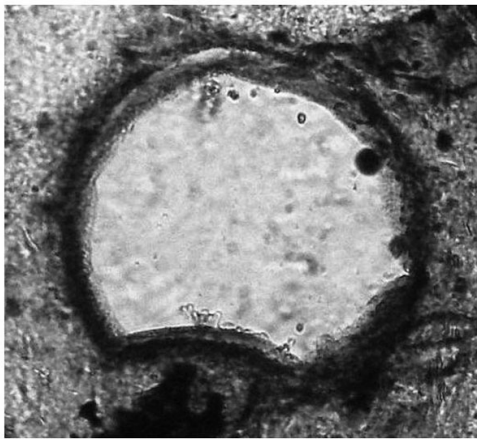

Fig. 2. Non-carbonate shell of Foraminifera *Parathurammina aff. tamarae* L. Petrova with attachment disc, proving that it belongs to the attached benthos. The Saf'yanovka deposit, horizon 187 m. Thin section, transmitted light, magnification 140.

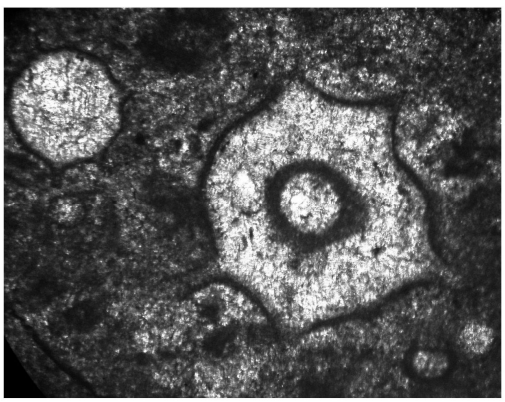

Fig. 3. Carbonate shells of Foraminifera *Parathurammina magna* Antropov with attachment disc in limestone, depth of 200 m, mine of the Saf'yanovka deposit. The Middle-Late Devonian age. Thin section, transmitted light, magnification 140.

shallow sea [Antropov, 1950]. Some specimens have an attachment disk (Fig. 3). Previously, the calcareous *Auroria delineate* L. Petr., *Tamarina corpulenta* L. Petr., *Parathurammina aff. tamarae* L. Petr. foraminifers [Korovko et al., 1999] were found in limestone lenses in wells (M-23, 2142) drilled through the serpentinite melange. The monotony of foraminifera species indicates unfavorable habitat and shallow water basin of sedimentation. The presence of volcanic material in limestones favors for its simultaneous formation with carbonaceous-siliceous rocks from the ore-hosting sequence.

Thus, the volcano-sedimentary rocks of the ore-hosting sequence of the Saf'yanovka deposit were formed in the Eifellian-Givetian shallow marine basin with almost continuous gain of volcanic material. The Eifelian-Givetian foraminifers were found in the ore-hosting rocks at a depth of 100 m to 200 m. According to [Korovko et al., 1999], the Late Lochkovian conodonts were found in the well 2149 at a depth of 298.5–335 m. Consequently, we may expect to find the boundaries between the Lochkovian, Pragian, Emsian, and Eifellian stages at the depths, ranging from 100 to 298.5 m, in case of undisturbed rock bedding.

The work is supported by the Urals Branch of Russian Academy of Sciences (project no. 12-C-1032).

References

Antropov, I.A. New species of the Upper Devonian foraminifera in some areas of the east of the Russian Platform // Proc. Kazan Branch USSR. Geol. Inst., 1950. No. 1. P. 20–28 [in Russian].

Chuvashov, B.I, Anfimov, A.L., Soroka, E.I., Yaroslavtseva, N.S. New data on the age of ore-hosting sequence of the Saf'yanovka deposit, Central Urals, based on foraminifers // Dokl. Earth Sci., 2011. Vol. 439. P. 1076–1078.

Chuvashov, B.I., Anfimov, A.L., Soroka, E.I., Yaroslavtseva, N.S. Devonian foraminifers with non-carbonate shell from the ore-hosting sequence of the Saf'yanovka deposit, Central Urals // Lithosphere, 2012. №. 5. P. 114–126 [in Russian].

Korovko, A.V., Dvoeglazov, D.A., Leshchev, N.V. et al. The Saf'yanovka copper-zinc sulfide deposit, Central Urals // In: Geodynamics and Metallogeny of the Urals. Sverdlovsk: UB AS USSR, 1991. P. 152–153 [in Russian].

Korovko, A.V., Postoyalko, M.V., Stepanova, T.I. et al. Stratigraphy and fauna of the Devonian and Carboniferous rocks from the Saf'yanovka ore field, Central Urals // In: Problems Stratig. Paleont. Urals. Yekaterinburg: Ministry of Natural Resources, Inc. UGSE, 1999. P. 136–141 [in Russian].

Petrova, L.G. Middle Devonian Foraminifera of the eastern slope of the Urals // In: Paleozoic West Siberian plain and its mountain frame. Novosibirsk, Nauka, 1981. P. 81–101 [in Russian].

Yazeva, R.G., Moloshag, V.P., Bochkarev, V.V. Geology of the Saf'yanovka sulfide deposit, Central Urals. Yekaterinburg: UB RAS, 1992. 71 p. [in Russian].

Yaroslavtseva, N.S., Maslennikov, V.V., Safina, N.P., Leshchev, N.V., Soroka, E.I. Carboniferous silty claystone from the Saf'yanovka copper-zinc sulfide deposit, Central Urals // Lithosphere, 2012. № 2. P. 106–123 [in Russian].

N. Fujioka[1], D. Ishiyama[2], V. Maslennikov[3, 4], K. Adomako-Ansah[2]
[1] Taiheiyo Cement Corporation, Tokyo, Japan
[2] Center for Geo-Environmental Science, Akita Univeristy, Akita
[3] Institute of Mineralogy UB RAS, Miass, Russia
[4] National Research South Ural State University, Chelyabinsk, Russia

CONTRASTING CHARACTERISTICS OF URAL- AND BAIMAK-TYPE VMS DEPOSITS IN THE URALS, RUSSIA

В статье приводится краткая характеристика геодинамической позиции, структуры, вмещающих пород, околорудных метасоматитов, геохимии руд и изотопного состава кислорода измененных вмещающих пород месторождений уральского и баймакского типа. Сделан вывод о том, что месторождения уральского типа с медно-цинковыми рудами, обогащенными кобальтом и теллуром, локализуются в бимодальных сериях с преобладанием вулканитов основного состава и формируются при температурах 220–320 °С. Месторождения баймакского типа со свинцово-медно-цинковыми рудами, обогащенными баритом, связаны с бимодальными вулканическими комплексами с преобладанием кислых вулканитов в задуговой обстановке и формируются при более низких температурах около 200 °С. Эта разница обусловлена различиями магматической активности и удаленностью от магматического источника.

Introduction

The geology of the area studied is composed of the Silurian oceanic arc complex in the Sakmara allochthon zone, Devonian oceanic arc complex in the Magnitogorsk zone and the East Uralian zone from west to east (Herrington et al., 2005). These areas host arc-related volcanogenic massive sulfide deposits (VMS deposits) of Ural, Baimak, Cyprus and Bessi types. The deposits examined in this study were Molodezhnoe deposit for Ural-type deposits and Alexandrinka and Saf'yanovka deposits for Baimak-type deposits (Fig. 1). The aim of this study was to clarify the geological and geochemical features of ore formation of these VMS deposits in the southern and central parts of the Urals based on geological and mineralogical data, hydrothermal alteration and oxygen isotopic ratios of host rocks.

Geology and mineralization

The geology of the Molodezhnoe deposit is dominated by middle Devonian basalt to basaltic andesite lava, altered massive dacite lava and massive basalt to basaltic andesite lava in ascending order. The dacite lava unit hosts a Cu-Zn-rich orebody. The geology of the Alexandrinka deposit consists of middle Devonian altered dacitic tuff and altered basalt to basaltic andesite lava in ascending

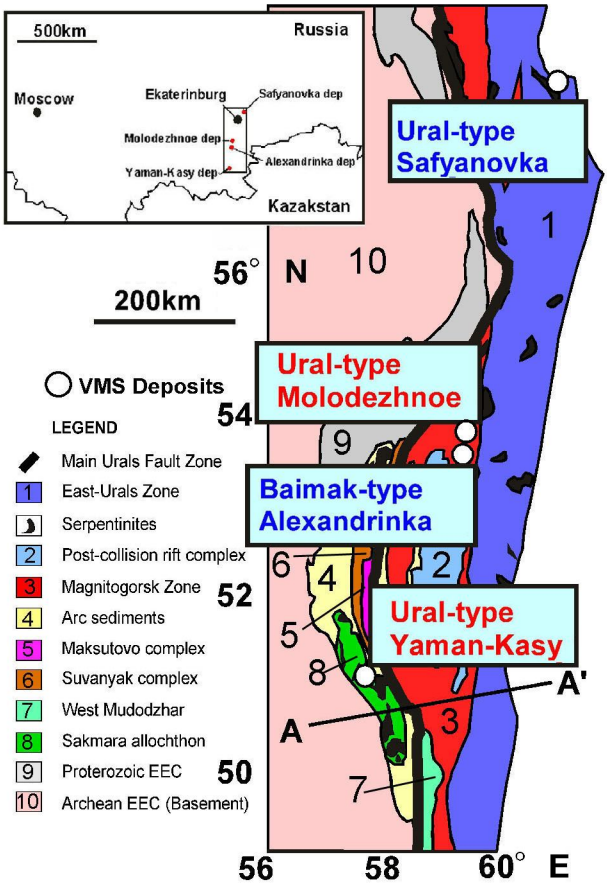

Fig. 1. Simplified geological map of South and Middle Urals (modified from Herrington et al., 2005).

order. A Cu-Zn-Pb-rich orebody occurs in the dacitic tuff. The geology of the Saf'yanovka deposit consists of late Devonian altered dacitic tuff and altered dacitic tuff in ascending order. A lenticular Cu-Zn-Pb-rich orebody of the Saf'yanovka deposit occurs between the dacitic tuff units.

Mineralogical characteristics of ores

The mineral assemblage of ores of Ural-type VMS deposits from Molodezhnoe deposit is characterized by large amounts of pyrite, chalcopyrite and sphalerite with trace amounts of galena and barite. On the other hand, the mineral assemblages of ores of Baimak-type deposits from the Alexandrinka and Saf'yanovka deposits are characterized by large amounts of sphalerite, galena, chalcopyrite and barite with lesser amounts of pyrite. The ores from Ural-type VMS deposits (Molodezhnoe deposit) are characterized by high Cu, Zn, Co and Te and contents low Pb and Ba contents (Fig. 2). The characteristics of ores from Ural-type VMS deposits are similar to those of ores from Cyprus- and Bessi-type VMS deposits, which are related to basaltic volcanic activity. On the other hand, the Baimak-type VMS deposits (Alexandrinka and Saf'yanovka deposits) are characterized by high Cu, Zn, Pb and Ba contents and low Co and Te contents in ores (Fig.2). Those characteristics are similar to those of ores from Kuroko-type VMS deposits associated with felsic volcanic activity. Based on the data of chemical compositions of heavy and rare metals in ores of the deposits examined, Ural-type and Baimak-type VMS deposits are thought to have had a genetic relation with basaltic and dacitic volcanic activities, respectively.

Hydrothermal alteration

Alteration of the Molodezhnoe deposit is divided into three types: quartz-illite-kaolinite, quartz-chlorite-illite and quartz-chlorite alterations. The quartz-illite-kaolinite alteration is recognized

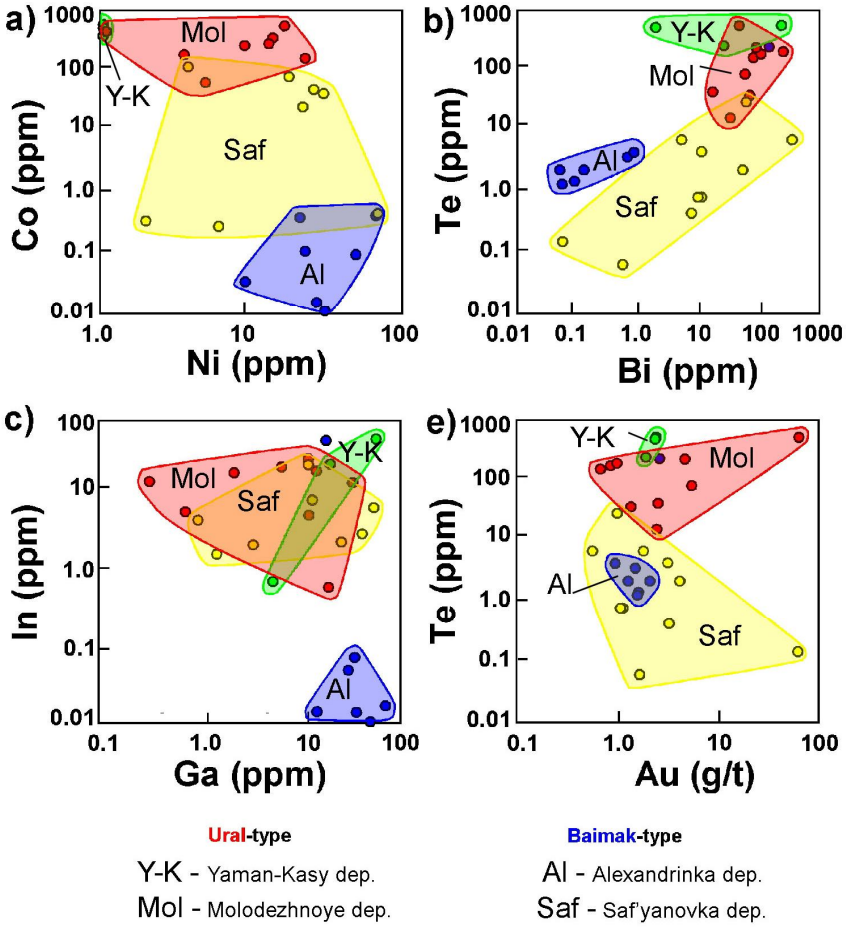

Fig. 2. Characteristics of Co, Ni, Te, Bi, In, Ga and Au contents in ores from the Yaman-Kasy, Molodezhnoe, Alexandrinka and Saf'yanovka deposits.

in a strongly altered zone located immediately below the orebody of the Molodezhnoe deposit. The quartz-chlorite-illite alteration zone surrounds the quartz-illite-kaolinite alteration zone. The quartz-chlorite alteration is the dominant alteration of the deposit and is widely distributed outside the quartz-illite-kaolinite alteration and quartz-chlorite-illite alteration zones. Based on the stability of clay minerals [Inoue, 1995], the Molodezhnoe deposit was formed at a temperature of 220–350 °C. Alteration of Alexandrinka deposit is divided into two types: quartz-illite/montmorillonite mixed layered mineral-chlorite and quartz-illite-chlorite alteration zones. The quartz-illite/montmorillonite mixed layered mineral-chlorite alteration is distributed in the footwall of the orebody of the deposit. Alteration of the Saf'yanovka deposit is divided into three types: quartz-illite-chlorite, quartz-illite-kaolinite and quartz-illite/montmorillonite mixed layered mineral alteration zones. The alteration zones of the Alexandrinka and Saf'yanovka deposits are thought to have been formed at 220–250 °C on the basis of thermal stability of clay minerals and the mineral assemblage.

Oxygen isotopes

The $\delta^{18}O$ values of footwall basalt, footwall dacite and hanging wall basalt of the Molodezhnoe deposit range from +3.8 to +7.5 ‰, +6.0 to +9.3 ‰ and +5.5 ‰, respectively (Fig. 3). Calculation based on an isotopic exchange model (Taylor, 1972) suggests that the Molodezhnoe deposit was formed at high temperatures of approximately 180–320 °C in seawater. The $\delta^{18}O$ values of footwall dacite of the Alexandrinka and Saf'yanovka deposits range from +8.9 to +12.1 ‰ and +8.8 to +12.9 ‰, respectively (Fig. 3). The Alexandrinka and Saf'yanovka deposits were formed of low temperatures of approximately 140–190 °C compared to the formation temperature of the Molodezhnoe deposit in seawater. The temperatures estimated from O-isotopes are generally consistent with those estimated from clay mineral stability for each deposit.

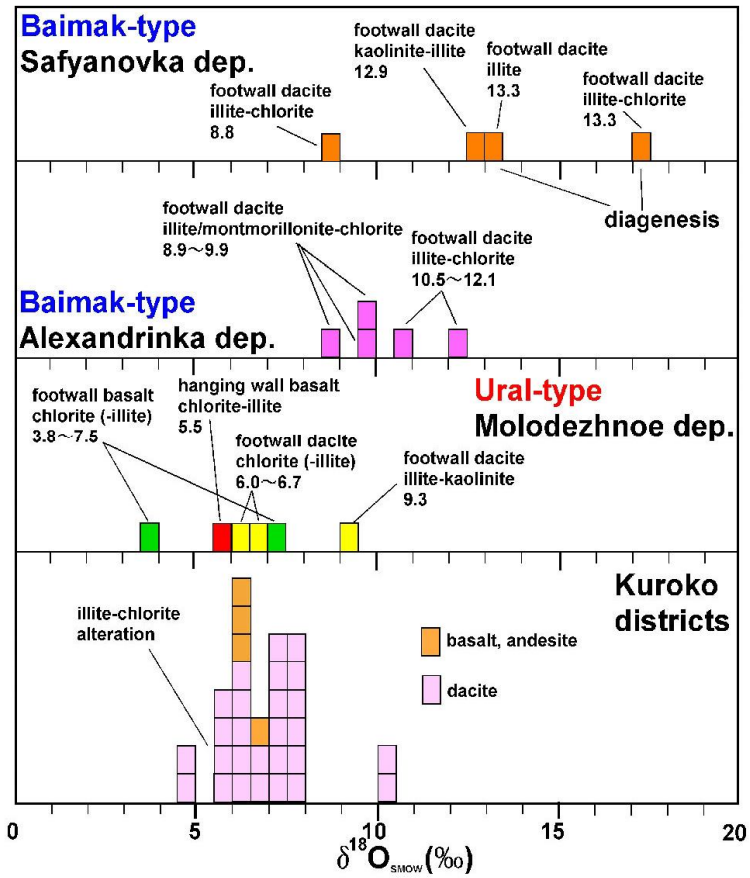

Fig. 3. δ ^{18}O values for volcanic rocks of Saf'yanovka, Alexandrina and Molodezhnoe VMS deposits (this study) compared with δ ^{18}O values of volcanic rocks for Kuroko VMS deposits [Green et al., 1983].

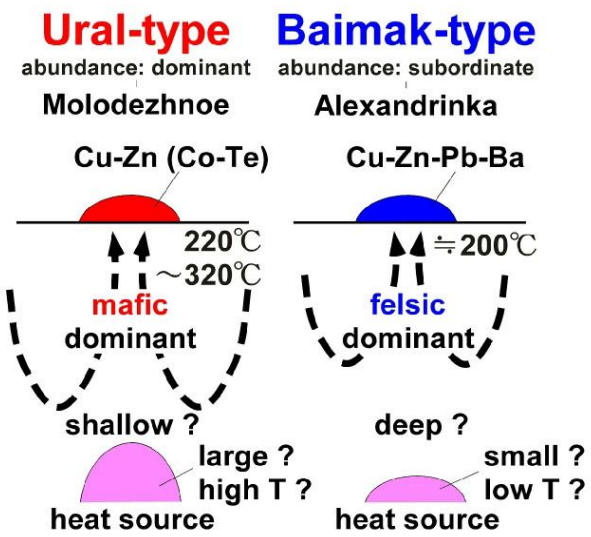

Fig. 4. Schematic model for the Ural- and Baimak-type VMS deposits in the Urals, Russia.

Summary

Fig. 4 illustrates the formation environment of Ural-type VMS deposits (Molodezhnoe deposit) and Baimak-type VMS deposits (Alexandrinka and Saf'yanovka deposits) as proposed in this study and is summarized as below.

The abundant Ural-type VMS deposits (e.g. Molodezhnoe) containing Cu and Zn (Co, Te)-rich ores were formed at relatively high temperatures of 220–320 °C associated with large mafic-

dominant bimodal volcanic activity close to the volcanic front of an oceanic volcanic arc setting. On the other hand, the surbodinate Baimak-type VMS deposits (e.g. Alexandrinka and Saf'yanovka) associated with Cu, Zn, Pb and Ba-rich ores were formed at relatively lower temperatures of approximately 200 °C associated with small felsic-dominant bimodal volcanic activity in a back arc environment of an oceanic volcanic arc setting. The difference between Ural- and Baimak-types is thought to be caused by differences in magma activity or distance between magma and these ore deposits.

References

Green, G.R., Ohmoto, H., Date, J., Takahashi, T. Whole-rock oxygen isotope distribution in the Fukazawa-Kosaka area, Hokuroku district, Japan, and its potential application to mineral exploration // Economic Geology. Monograph, 1983. Vol. 5. P. 395–411.

Herrington, R., Zaykov, V.V., Maslennikov, V.V., Brown, D., Puchkov V.N. Mineral Deposits of the Urals and Links to Geodynamic Evolution // Economic Geology., 2005. Vol. 100. P. 1069–1095.

Inoue, A. Formation of clay minerals in hydrothermal environments // In: Velde, B. (Ed.), Origin and mineral of clays, Springer, 1995. P. 268–329.

Taylor, H.P.Jr. Oxygen isotope evidence for large scale interaction between meteoric ground waters and Tertiary granodiorite intrusions, Western Cascade Range, Oregon // Jour. Geophy. Research, 1972. Vol. 76. P. 7855–7875.

Kaneto F.[1], Murzin V.V.[2], Hoshino K.[1]
[1]Department of Earth and Planetary Systems Science, Hiroshima University, Japan
[2]Institute of Geology and Geochemistry UB RAS, Ekaterinburg, Russia

GOLD-BEARING RODINGITES FROM THE KARABASH ALPINE-TYPE ULTRABASIC MASSIF, SOUTH URALS, RUSSIA

Обсуждаются вопросы состава и генезиса родингитов месторождения «Золотая гора» в Карабашском массиве альпинотипных серпентинитов. Изучены петрография, минералогия и геохимия родингитов по основным стадиям рудообразующего процесса. Особое внимание уделено вопросам анализа состава флюидных включений и зависимости солёности палеорастворов от температуры.

Rodingites occur as inclusions or dykes with serpentinite and are formed by Ca-rich metasomatizm with replacement of primary minerals by zoisite, epidote, diopside, grossularite and vesuvianite. Most rodingites worldwide are barren rocks, but high contents of noble metals, primarily, gold, were occasionally observed in them. Such dynamic transformations correspond generally to (150–450?C) and are now largely ascribed to the hydrothermal circuration taking place at oceanic spreading centers. The rodingite rocks have generally been thought to be derived from mafic igneous rocks. It was also reported that, although in rare cases, some rodingites were metasomatized from intermediate to acidic igneous rocks and even from sedimentary rocks. The geotectonic setting of rodingites occurrences may represent an ancient suture between an oceanic and a continental plate, lending support to the suggestion that serpentinization and rodingitization predate the uplifting of the ultramafic bodies and that they take place in the deeper oceanic crust.

Gold-bearing rodingites in the Karabash alpine-type ultrabasic massif have been mined at the Zolotaya Gora deposit in 1902–1946. Although a number of mineralogical and fluid inclusion studies of the area have been taken in the previous researches, a genesis and a formation condition of cupriferous gold characteristically observed in the deposit has not been clarified yet. In order to solve this problem, chemical compositions of rodingite, rodingite-forming minerals and a placer gold, and fluid inclusions in the rocks were analyzed in this study.

Geological setting the Karabash-alpine-type ultrabasic massif is located in the southern part of the Main Ural Fault Zone, which separates the paleocontinental and paleooceanic segments of the Urals. The massif is a part of a serpentinite diapir, which is confined to the central portion of the

fault zone and represents the extruded melanocratic basement of the Silurian-Devonian volcano-sedimentary complexes of the Magnitogorsk megasynclinorium. The detailed characteristic geological position of the massif and condition of ores localization is provided earlier [Murzin, Shanina, 2007].

Methods XRF qualitative analyses of elements and density measurements of the rodingite, chlorite zone and host serpentinite at the both outcrops were carried out to characterize the compositional changes during the rodingitization. Microscopic observations and EPMA analyses were carried out to identify mineralogical sequences and to determine the chemical compositions of minerals. Microthermometric examinations of fluid inclusions were carried out by using the LinkamL-600K and L-600PM programmable heating-cooling stage.

The rodingites in the Karabash massif consist of garnet, clinopyroxene, chlorite, apatite, sphene and calcite. Two types of diopside were recognized in back-scatter-electron images of the rodingite in the southern outcrop. One is a primary diopside showing a clear and unsystematic chemical zonation, while the other is a secondary one free of clear chemical zonation. Microscopic studies of the rodingite in the southern outcrop have revealed a mineralogical sequence as, from early to late, diopside-apatite-garnet-calcite. The chlorite zone is remarkably developed in the northern outcrop. The rocks contain chlorite, clinopyroxene (diopside) and a small amount of Cr-spinel and magnetite. A thin chlorite vein was also observed between the chlorite zone and the host serpentinite. The veins are presented only by chlorite. Chlorite in the chlorite zone has an unsystematic chemical zonation. An Fe-rich core and Fe-poor rim were observed in diopside in the chlorite zone. EPMA analyses revealed the presence of heazlewoodite (Ni_3S_2), native cupper, anilite (Cu_7S_4), geerite (Cu_8S_5) and covellite (CuS) in the chlorite zone. In the southern outcrops, a thin (1–3 cm) reaction zone composed of chlorite, diopside and calcite was observed between rodingite and the host serpentinite. Serpentinite in the northern outcrop is made up of serpentine, olivine, magnetite, chromite, Cr-spinel and small amount of heazlewoodite, while serpentinite in the southern outcrop consist of serpentine, chlorite, magnetite, chromite and Cr-spinel. EPMA analysis revealed the presence of Fe-rich Cr-spinel (picotite). Olivine crystals are rich in forsterite. EPMA data on the placer gold are shown in Fig. 1. There are two types of the placer gold, the first one contains Au and Ag, and the second one – Au, Ag, and Cu. Both types show chemical zonations, where the core consists of Au-Ag or Au-Ag-Cu alloy, while the rim is almost pure. It is known that Ag solubility in Cu-Au alloys is low due to limited miscibility of components in the Au-Ag-Cu system and increases only with rising temperature. Therefore, the chemical

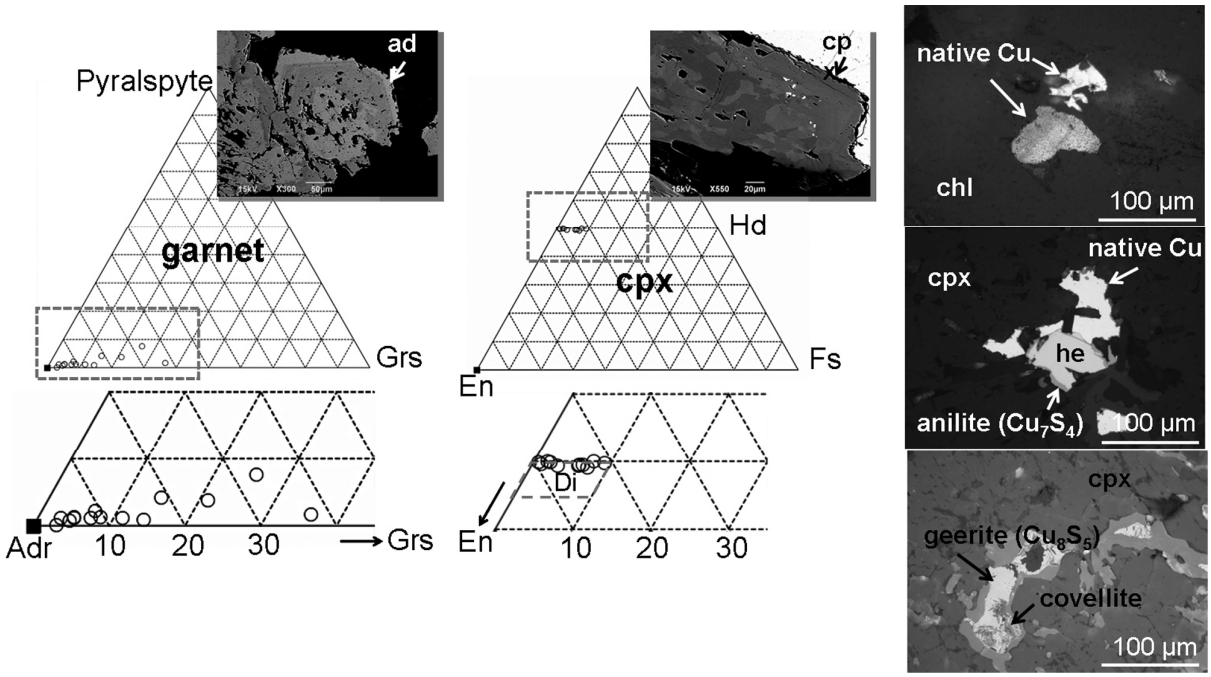

Fig. 1. EPMA analyses revealed the presence of heazlewoodite (Ni_3S_2), native Cu, anilite (Cu_7S_4), geerite (Cu_8S_5) and covellite (CuS) in the chlorite zone.

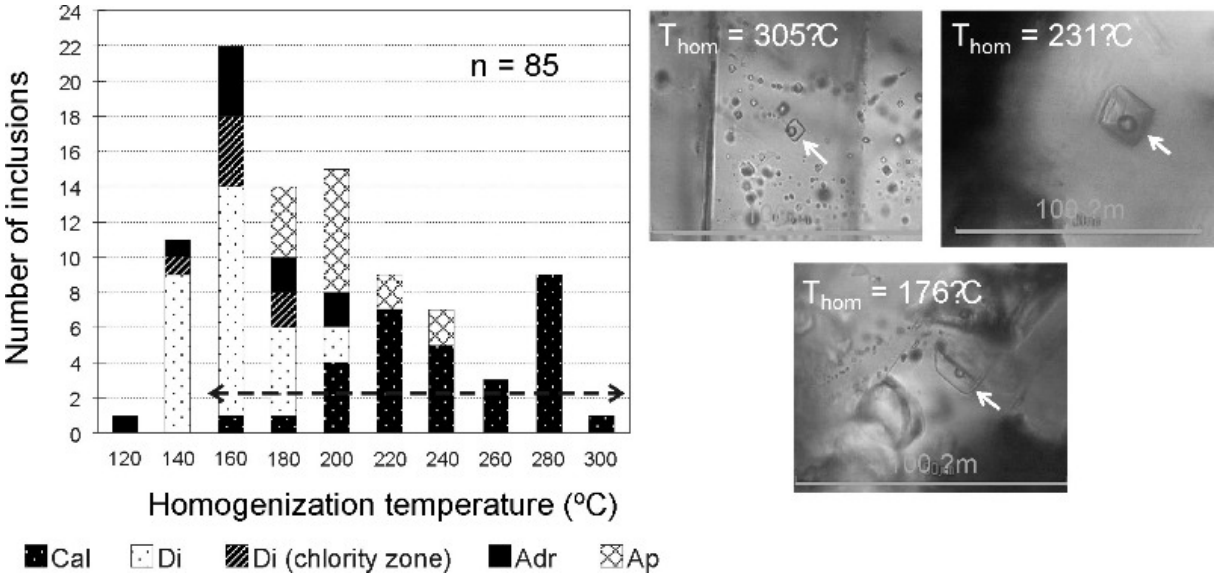

Fig.2. The homogenization temperatures of fluid inclusions in calcite.

composition of the Au-Ag-Cu alloys may serve as a geothermometer. In this study, however the estimation of the formation temperature of the alloys was impossible, because of the low Cu contents in the studied samples.

Most of the fluid inclusions are primary or pseudosecondary and their diameter was less than 35 ?m (Fig. 2). All fluid inclusions were composed of two phases. The primary inclusions in diopside sometimes are distributed along its growth planes. In calcite, several trails of the secondary inclusions cutting the crystals were observed. Most of the fluid inclusions in the minerals were homogenized at 140–200 ?C. The homogenization temperatures of fluid inclusions in calcite varied from 160 ?C to 290 ?C with a peak in the histogram at 270–290 ?C. It should be emphasized that since there is no evidence for leaking of the fluid inclusions in calcite, they may show the proper ones. The homogenization temperatures of fluid inclusions in apatite show slightly higher values than those in diopside and garnet. The ice melting temperatures of the fluid inclusions varied from –0.5 to –6.7 ?C, hence a salinity range was 0.8–10 wt. % NaCleq. The salinities of primary and pseudosecondary fluid inclusions in diopside varied from 2 to 10 wt. % NaCleq. The high-salinity (7–10 wt. % NaCleq.) inclusions occurred in cores of the primary diopside. On the other hand, the low-salinity (2–4 wt. % NaCleq.) inclusions occurred in the rims of the primary diopside and the secondary one. Some of the high-salinity inclusions occurred in Fe-rich part of the primary diopside.

The protolith of rodingite could not been clarified in this study. Conditions of formation of rodingites and fluid evolutions [Murzin, Shanina, 2007] estimated the pressure condition (2–3 kbar) of the early mineralization of rodingite. Considering the pressure condition, the low homogenization temperatures of the fluid inclusions in the early minerals may represent their high formation pressures. On the contrary, the high homogenization temperatures of the fluid inclusions in calcite may indicate alow pressure during its mineralization. The high-salinity inclusions in cores of the primary diopside and the low-salinity inclusions in the rims of primary diopside and the secondary one indicate the decrease of the salinities as the mineralization progresses. Low salinities of the fluid inclusions in the other early minerals, garnet and apatite also imply that the salinity decreased during the early mineralization from diopside to garnet. Based on the above, the salinities of the rodingite-forming fluid(s) decreased during the early mineralization of rodingite. The rodingite-forming metasomatism progressed probably at the stable P–T conditions, while at the last stage of metasomatism where calcite mineralized, the pressure decreased.

References

Murzin V.V., Shanina S.N. Fluid regime and origin of gold-bearing rodingites from the Karabash alpine-type ultrabasic massif, Southern Ural //Geochemistry International, 2007. Vol. 45. No. 10. P. 998–1011.

D. Gregory[1], R. Large[1], S. Bull[1], J. Halpin[1], E. Lounejeva[1], V.V Maslennikov[2], P. Sack[3]
[1] *ARC Centre of Excellence in Ore Deposit Research, University of Tasmania, Hobart, Australia, ddg@utas.edu.au*
[2] *Institute of Mineralogy UB RAS, Miass, Russia*
[3] *Yukon Geological Survey Whitehorse, Yukon, Canada*

THE TRACE ELEMENT COMPOSITION OF SEDIMENTARY PYRITE AND VARIATIONS IN TRACE ELEMENT CONTENT WITH PYRITE TEXTURES

Изучение элементов-примесей в пирите осадочных толщ важно для понимания состава вод палеоокеана, особенностей соосаждения и диагенетического перераспределения металлов и полуметаллов в различных условиях. В статье обобщаются данные по составу примесей в пирите, полученные методом ЛА-ИСП-МС для 45 углеродистых сланцев от современных до архейского возраста. Показано, что примеси могут входить в структуру пирита и образовывать микровключения. Обычными примесями с содержаниями 100–1000 ppm являются As, Ni, Pb, Cu, Co; реже и в меньших количествах (10–100 ppm) встречаются Mo, Sb, Zn и Se; редко и в количествах до 10 ppm – Ag, Bi, Te, Cd, Au. Делается вывод о различии микропримесного состава диагенетических, метаморфогенных и гидротермальных пиритов в осадках.

The trace metal content of diagenetic pyrite is of interest for three main reasons: (1) it can be used to determine the chemical conditions of ancient oceans [Large et al., in prep.; Gregory et al., in prep.]; (2) it is a sink for metal and metalloid contamination in several environments [Huerta-Diaz and Morse, 1992; Lowers et al., 2007] and, (3) the trace metals within diagenetic pyrite can be remobilized to form ore deposits [Large et al., 2011; Large et al., 2009; Large et al., 2007; Thomas et al., 2011]. In this study diagenetic pyrite of several different textures was selected from 45 carbonaceous shale units of present to Archean age. These pyrites were then analyzed by LA-ICPMS to determine their trace metal content. The abundance of the trace metals can be split into 3 groups: most abundant, moderately abundant and least abundant. The most abundant elements are As, Ni, Pb, Cu and Co (median values ranging from 100 to 1000 ppm), the moderately abundant are Mo, Sb, Zn and Se (median values ranging from 10 to 100 ppm) and the least abundant are Ag, Bi, Te, Cd and Au (median values from 0.01 to 10 ppm) (Fig. 1). The data also showed that the trace metals are held within the pyrite in

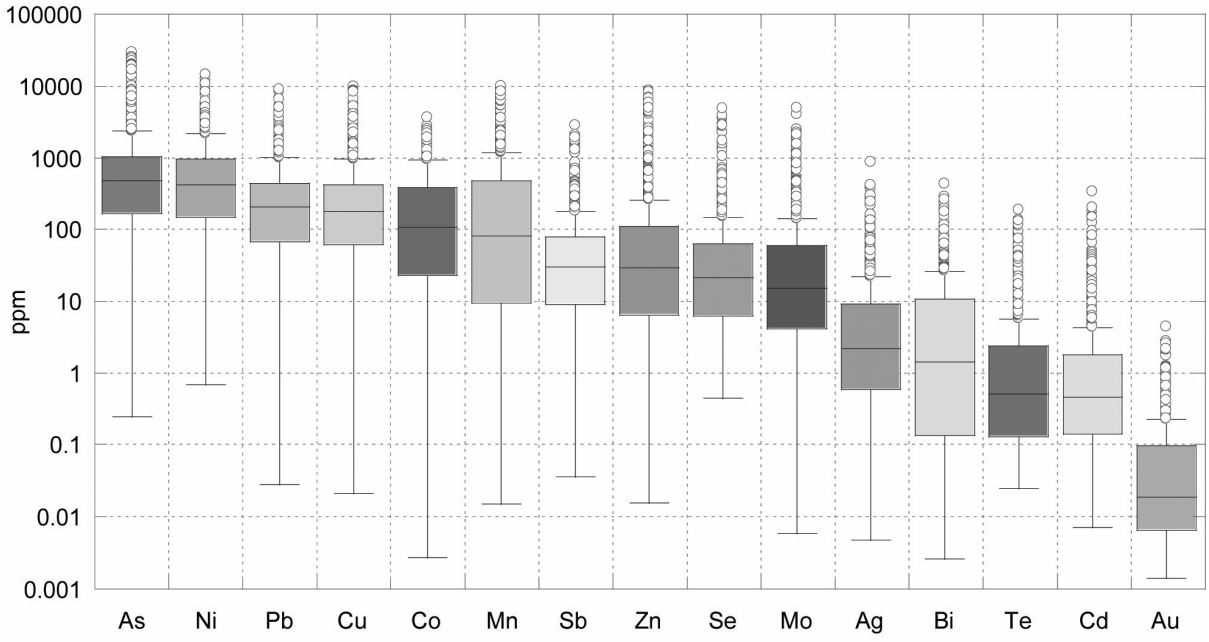

Fig. 1. Boxplot of trace metal content of pyrite in descending order of elemental abundance in pyrite: As ≥ Ni > Pb ≥ Cu ≥ Co ≥ Mn > Sb ≥ Zn ≥ Se ≥ Mo > Ag ≥ Bi > Te ≥ Cd > Au.

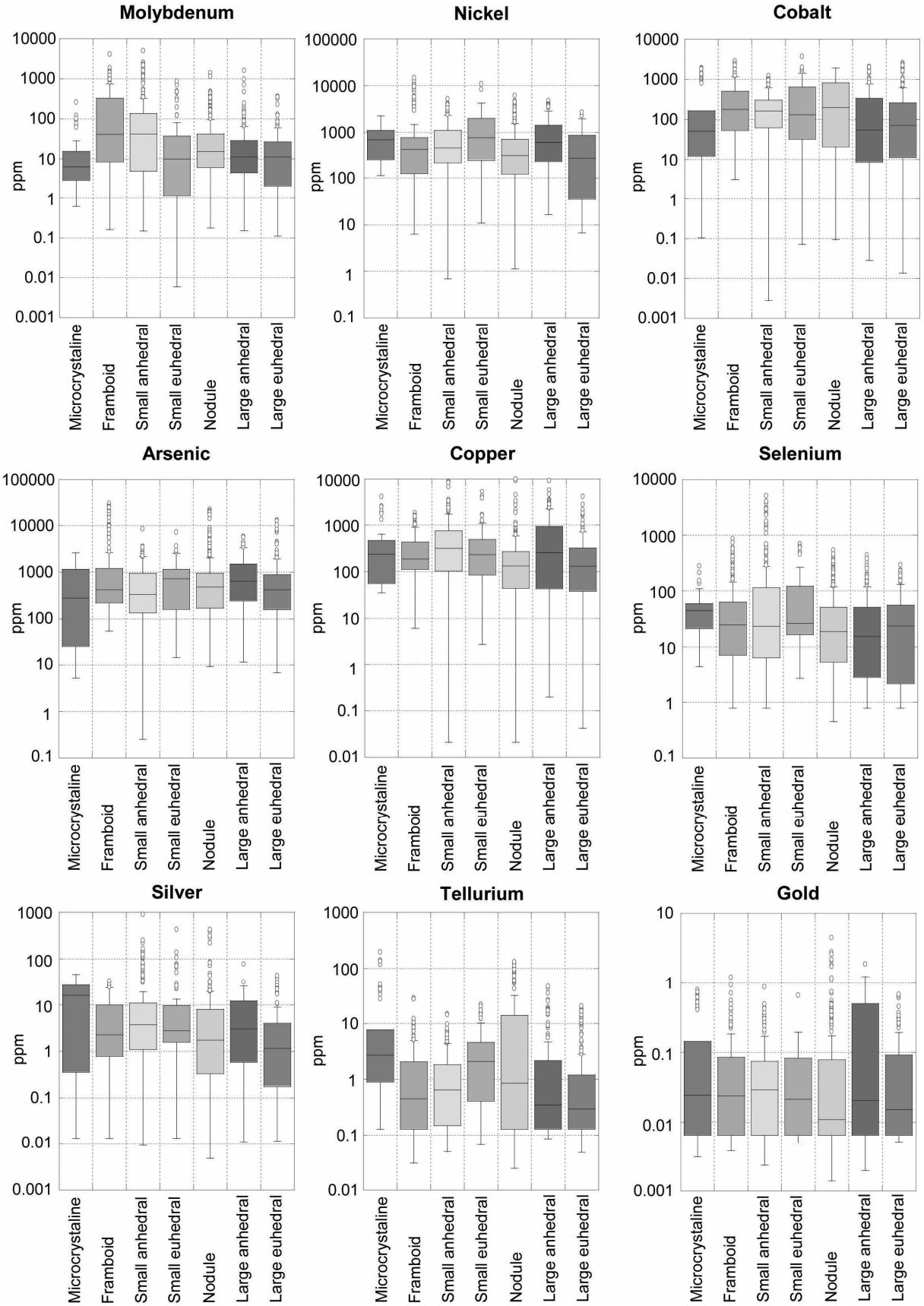

Fig. 2. Trace metal content of pyrite with groupings based on pyrite texture (microcrystalline, framboidal, small anhedral, small euhedral, nodule, large anhedral, large euhedral) for Mo, Ni, Co, As, Cu, Se, Ag, Te and Au.

Table

Mean geochemical values for pyrite of different textures but from the same sample

Mount	Texture	n	Formation	Co	Ni	Cu	Zn	As	Se	Mo	Ag	Sb	Te	Au
1	Microcrystalline	6	Jet Rock	75	401	103	122	328	9	100	2	7	1.5	0.04
1	Nodule	22	Jet Rock	48	238	61	51	272	7	108	1	3	1.2	0.02
2	Framboid	5	Que River Shale	297	511	252	128	764	77	20	17	85	–	0.20
2	Nodule	5	Que River Shale	100	287	221	46	304	118	1	8	43	0.7	0.10
3	Microcrystalline	14	McRea Formation	53	125	54	44	1194	21	8	0	18	0.9	0.03
3	Nodule	7	McRea Formation	2	21	212	3	338	3	1	1	22	0.7	0.04
4	Microcrystalline	5	McRea Formation	184	384	233	47	322	14	5	6	58	6.0	0.07
4	Small anhedral	3	McRea Formation	195	501	328	44	475	15	4	9	74	7.7	0.10
4	Large euhedral	10	McRea Formation	116	272	264	28	1111	17	4	3	36	4.3	0.05
5	Small euhedral	12	Alum Shale	137	2888	750	62	2204	205	332	55	123	3.0	0.08
5	Nodule	5	Alum Shale	88	2170	667	379	5696	405	200	323	228	5.8	0.43
6	Framboid	6	Canol Formation	77	1002	303	153	242	393	154	3	83	0.8	0.04
6	Nodule	8	Canol Formation	2	73	55	22	44	256	29	0	41	0.3	0.01
7	Small euhedral	6	Warrabarty	416	64	37	13	46	22	0	0	1	0.1	0.01
7	Nodule	10	Warrabarty	300	450	264	58	230	11	6	1	18	0.5	0.05
8	Small anhedral	9	Yul-12005	87	524	2066	1355	160	42	208	7	20	1.9	0.04
8	Large euhedral	12	Yul-12005	78	295	165	72	156	43	77	0	5	0.2	0.01

two ways; as micro-inclusions and incorporated into the structure of the pyrite. The different trace elements have thus been separated into 3 groups based on how the trace elements are incorporated into diagenetic pyrite. The first group consists of As, Ni, Co, Sb, Se and Mo and is held predominantly within the crystal structure of the pyrite. The second group consists of Ag, Au, Te and Cu, and is contained within the crystal structure of the pyrite at low concentrations but in micro-inclusions at high concentration. The final group is made up of Pb, Zn, Cd and Bi and is contained predominantly hosted in micro-inclusions within the pyrite.

Diagenetic pyrite generally contains enrichment in trace elements in the following order of abundance: As ≥ Ni > Pb ≥ Cu ≥ Co ≥ Mn > Sb ≥ Zn ≥ Se ≥ Mo > Ag ≥ Bi > Te ≥ Cd > Au. We have found that sedimentary pyrite has characteristic trace metal composition as follows: 0.01 < Co/Ni < 2, 0.01 < Cu/Ni < 10, 0.01 < Zn/Ni < 10, 0.1 < As/Ni < 10, Ag/Au > 2, 1 < Te/Au < 1000, Bi/Au > 1, Sb/Au > 100 and As/Au > 200. As hydrothermal and metamorphic pyrite have significantly different trace element compositions (Bajwah et al., 1987; Large et al., 2007) these chemical criteria can be used to determine whether pyrite is hydrothermal, metamorphic or sedimentary source when other methods to determining the pyrites origin are ambiguous.

The texture of diagenetic pyrite changes based on the local chemical conditions in which it forms, thus it is reasonable to expect that a difference in trace element concentrations in pyrite would also be observed. However, when the data set is taken as a whole this is not what is observed (Fig. 2). While there is some variation there is no systematic trend for higher or lower concentrations of pyrite within a given textural type. This suggests that other factors, such as depositional setting or age of pyrite, are more important controls in the trace element content of pyrite.

Although texture of diagenetic pyrite does not seem to be an important indicator of trace metal content over the entire data set it may be important in individual samples. Table shows the mean trace element content of pyrite of different textures for 8 samples that contain multiple pyrite textures. In the majority of the pyrite that was interpreted to have formed earlier (framboidal, microcrystalline, small anhedral and small euhedral) tends to have higher or equal trace metal content to the pyrite interpreted to have formed later. This is true for all textures except the fine euhedral. There are two possible reasons for this observation. First, the euhedral pyrite may have formed later than the nodules it is found with and the older pyrite (in this case the euhedral) contains fewer trace elements, which is similar to the rest of the data set. A second possibility is that the when the euhedral pyrite formed most of the trace elements were still adsorbed onto organic matter and other phases and were not free to be incorporated into the pyrite. Later during diagenesis the nodules formed by remobilizing sulphides in the surrounding shale [Ono et al., 2003]; trace elements were also remobilized and incorporated into the pyrite nodules.

This research was supported by the projects CODES (Tasmania University, Australia) and UB of RAS (no. 12-II-5-1003).

References

Bajwah, Z., Seccombe, P., and Offler, R. Trace element distribution, Co:Ni ratios and genesis of the big cadia iron-copper deposit, New South Wales, Australia // Mineralium Deposita, 1987. Vol. 22. P. 292–300.

Huerta-Diaz, M.A., Morse, J.W. Pyritization of trace metals in anoxic marine sediments // Geochimica et Cosmochimica Acta, 1992. Vol. 56. P. 2681–2702.

Large, R.R., Bull, S.W., and Maslennikov, V.V. A carbonaceous sedimentary source-rock model for Carlin-type and orogenic gold deposits // Economic Geology, 2011. Vol. 106. P. 331–358.

Large, R.R., Danyushevsky, L., Hollit, C., Maslennikov, V., Meffre, S., Gilbert, S., Bull, S., Scott, R., Emsbo, P., Thomas, H., Singh, B., and Foster, J. Gold and Trace Element Zonation in Pyrite Using a Laser Imaging Technique: Implications for the Timing of Gold in Orogenic and Carlin-Style Sediment-Hosted Deposits // Economic Geology, 2011. Vol. 104. P. 635–668.

Large, R.R., Maslennikov, V.V., Robert, F., Danyushevsky, L.V., and Chang, Z.S. Multistage sedimentary and metamorphic origin of pyrite and gold in the giant Sukhoi Log deposit, Lena gold province, Russia // Economic Geology, 2007. Vol. 102. P. 1233–1267.

Lowers, H.A., Breit, G.N., Foster, A.L., Whitney, J., Yount, J., Uddin, M.N., and Muneem, A.A. Arsenic incorporation into authigenic pyrite, Bengal Basin sediment, Bangladesh // Geochimica et cosmochimica acta, 2007. Vol. 71. P. 2699–2717.

Ono, S., Eigenbrode, J.L., Pavlov, A.A., Kharecha, P., Rumble, D., Kasting, J.F., and Freeman, K.H. New insights into Archean sulfur cycle from mass-independent sulfur isotope records from the Hamersley Basin, Australia // Earth and Planetary Science Letters, 2003, Vol. 213. P 15–30.

Thomas, H.V., Large, R.R., Bull, S.W., Maslennikov, V., Berry, R.F., Fraser, R., Froud, S., Moye, R. Pyrite and pyrrhotite textures and composition in sediments, laminated quartz veins, and reefs at Bendigo gold mine, Australia: insights for ore genesis // Economic Geology, 2011. Vol. 106. P. 1–31.

Q. Huang[1], Y. Zhu[2]
[1] CODES, School of Earth Science, University of Tasmania, Hobart, Australia, Qiuyue.huang@utas.edu.au
[2] Peking University, Pekin, China, yfzhu@pku.edu.cn

PETROLOGY AND GEOCHEMISTRY OF THE HALADALA PLUTON AND ASSOCIATED Au-BEARING HYDROTHERMAL VEINS IN SOUTHWESTERN TIAN SHAN, CHINA

Плутон Халадала (Юго-Западный Тянь-Шань) состоит преимущественно из троктолитов, оливинового габбро и габбро. Поведение РЗЭ и малых элементов свидетельствует о фракционировании первичной магмы. Наиболее поздними являются жилы магнетит-клинопироксенового габбро. Золотоносные кальцит-магнетитовые жилы являются результатом постмагматического эпитермального процесса.

The Haladala basic-ultrabasic pluton in Southwestern Tian Shan Mountains mainly consists of troctolite, olivine gabbro and gabbro [Zhang et al., 2000; Xue and Zhu., 2009]. After the fractional crystallization of olivine and plagioclase from the Haladala primary magma, the rest of the magma intruded and formed gabbro. The clinopyxene (Cpx-I) of the gabbro has the lowest concentration of Rare Earth Elements (REEs), and doesn't show Eu negative anomaly. The concentration of other trace elements (Sc, Cr etc.) of Cpx-I varies largely with a wide range of the Mg# (80–95). The magnetite-clinopyroxene vein intruded into the gabbro, and the composition of the clinopyxene (Cpx-II) in the vein is relatively consistent. Compared to Cpx-I, Cpx-II has a higher concentration of REEs with distinct Eu negative anomaly. At least two stages of heterogeneous magmas contributed to the formation of the Haladala pluton. Distinct from the rapid intrusion of the later-stage Fe-riched basic magma which formed the magnetite- clinopyxene vein, the early-stage magma went through a long period of evolution before it finally cooled down and formed the gabbro. Besides, exsolution texture can be found in both Cpx-I and Cpx-II, which implies that the Haladala pluton experienced rapid uplift or rapid cooling after the intrusion of the magnetite-clinopyroxene vein. Another auriferous calcite- magnetite vein came into being during the epithermal process after the magma process ended. The later vein ranges from 1mm–10cm in size, and the magnetite in it was cut by the calcite, which indicates that the magnetite formed earlier than the calcite in the same vein. There is also minor amount of pyrite in the vein, and it is surrounded by magnetite. It's worth noting that with the intrusion of the calcite-magnetite vein, Au-mineralization has also developed. There are three kinds of circumstances where native gold could be found: First, gold is located in the boundary of the calcite and magnetite; second, gold is in the calcite; third, gold is enveloped in the pyrites. The gold is usually about 10um in size Focus on this vein is of great significance to the gold exploration in this district.

References

Zhang, Y., Li X., Zhang, J. The Haladala Plutonic suite and its tectonic background. Xinjiang Geology, 2000. Vol. 18(3). P. 258–263.

Xue, Y,. Zhu, Y. Zircon SHRIMP chronology and geochemistry of the Haladala gabbro in southwestern Tianshan Mountains // Acta Petrologica Sinica, 2009. Vol. 25(6). P. 1353–1363.

E.A. Ivleva, N.T. Pak
Institute of geology NAS of the Kyrgyz Republic, Bishkek
paknikolay50@mail.ru

THE BIGGEST RARE-EARTH DEPOSITS IN TIEN SHAN

Приводятся данные о геологическом строении и минералогии крупнейших месторождений редкоземельных элементов Куттесай-II (80% добычи РЗЭ в Советском Союзе) и Сарасай. Месторождения представлены зонами гидротермально-метасоматической проработки, связан-

ной с магматизмом пермского возраста. Локализация месторождений определяется тектоническим строением. Основными концентраторами РЗЭ могут быть собственные минералы – ксенотим, монацит, бастнезит и др. карбонаты с определенной ролью в балансе РЗЭ флюорита и силикатов циркония и тория (Куттесай-II), на месторождении Сарысай главная роль принадлежит пирохлору с включениями собственных РЗЭ-минералов, а также гипергенных оксидов марганца с сорбированными РЗЭ.

The Tien Shan fold system is the largest rare earth and rare metal province in the Central Asia. A number of rare earths deposits and occurrences are concentrated in the territory of the Kyrgyz Republic. The most of them are related to the Permian intrusive magmatism.

The Kuttesai-II deposit. About 80 % of rare-earth elements in the Soviet Union were mined and extracted from this deposit, which has no analogues in the world. The deposit is composed of gneisses of the Early Proterozoic (?) Aktuz Formation and amphibole schists of the Middle Riphean (?) Kuperlisai Formation. The Riphean mafic and ultramafic rocks, Late Ordovician to Silurian granodiorites and leucocratic granites, Permian to Triassic monzodiorites, syenites, subalkali leucogranites, granophyres, lamprophyres, diorites, and diabase porphyrites intrude the metamorphic rocks.

The rare-earth mineralization from the Kuttesai deposit is a result of intense metasomatic processes associated with intrusion of the Permian granophyres (Fig. 1). The orebodies consist of me

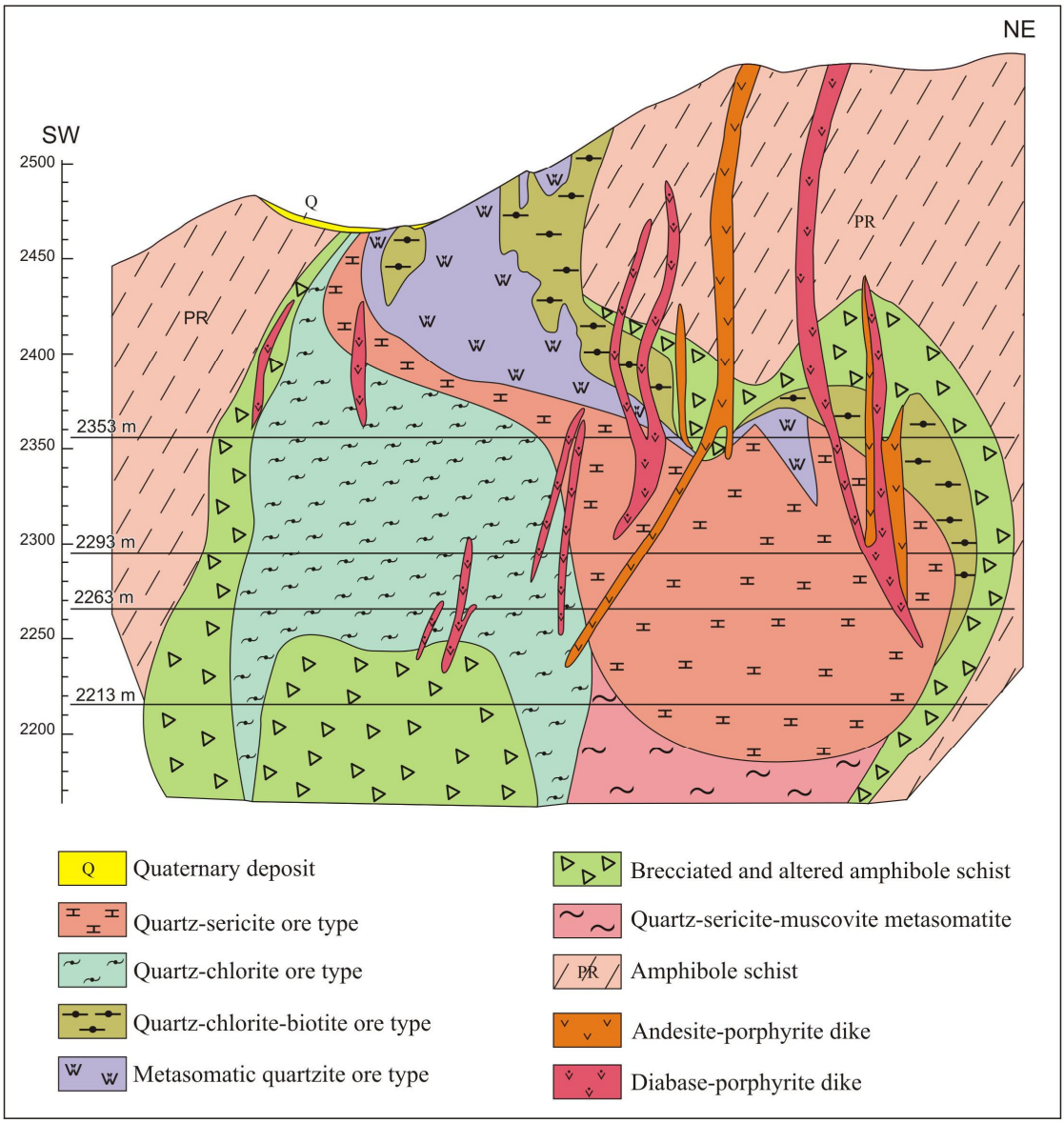

Fig. 1. Model of zoning for the Kutessai-II deposit.

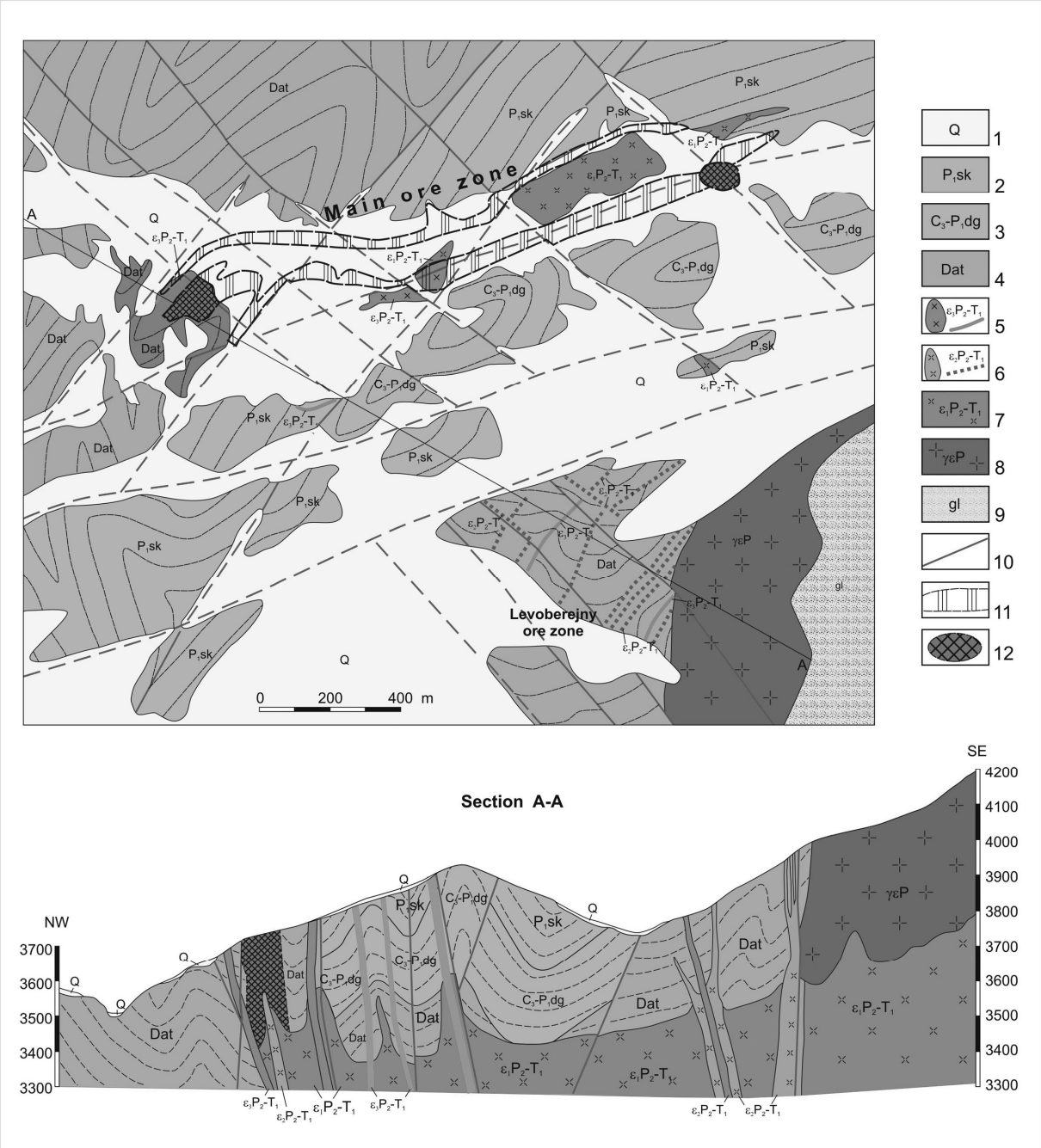

Fig. 2. The geologic map of the Sarysai deposit.

Quaternary sediments (1), Lower Permian shale, conglomerate, limestone, olistostromes (2), Upper Carboniferous to Lower Permian limestone, marble (3), Devonian siltstone, shale with interlayers of sandy limestone (4), Late Permian intrusive rocks of the Surteke complex (5–7): carbonatite of third phase (5), fine- to medium-grained alkali and nepheline syenite of the second phase (6), medium- and coarse-grained alkali syenite of the Kaichin pluton and its apophysises of the first phase (7), Early Permian rapakivi granite and syenite of the Dzhangar complex (8), glaciers (9), faults (10), ore zones (11), orebodies (12).

tasomatic rocks and eight zonal ore mineral types depend on metasomatic alterations: quartz-chlorite, quartz-sericite, altered granophyres, biotite hornfelns, altered amphibole schists, metasomatites after gneisses, and quartz-sericite-muscovite (greisen) and silicified rocks [Kim, 1965]. The carbonate-phosphate, carbonate-silicate, and silicate rare-earth ores are dominant at the upper, intermediate, and lower levels of the deposit, respectively.

Monazite, fluocerite, xenotime, yttroparisite, bastanaesite-(Y), cyrtolite, ferrithorite, and yttrofluorite, which are present in various proportions, are major minerals-concentrators of Y, La, Ce, Nd,

Pr, Dy, Sm, and Gd in all ore types. In spite of considerable amount of cyrtolite, ferrithorite, and yttrofluorite, they are of secondary importance.

The Sarysai tantalum-niobium-rare-earth deposit is an example of ore mineralization hosted in carbonatites related to syenites. The deposit is composed of the Devonian, Carboniferous, and Permian terrigenous-carbonate sedimentary rocks. The intrusive rocks include Early Permian granites, rapakivi granites, and Late Permian alkali rocks of the Kaichin intrusive pluton, whose satellite, the Sarysai intrusive body, hosts Ta-Ni and rare-earth mineralization (Fig. 2). The latter is composed of the rocks of three consecutive phases of alkali magmatism: lujavrites and pulaskites of the first phase, leucocratic alkali syenites of the second phase, and intrusive aegirine-calcite carbonatites of the third phase. The veins of metasomatic carbonatites branch from the Sarysai stock.

All three stages underwent ore-bearing metasomatism and autometasomatism, which led to formation of fenites, albitites, and carbonate metasomatic rocks. The ore metasomatites of all stages form the combined ore zones.

The content of rare earth elements in metasomatites are 0.01–0.05 % for Yb and about 0.05 % for each of Ce, La, Y, and Nb. The Nb/Ta, ΣREE/Y, and Y_2O_5/TR_2O_5 ratios in different ore bodies are approximately 10:1, 4:1, and up to 1:4, respectively.

The quartz-feldspar-aegirine ore veins are zonal: the central parts include leucocratic fenites, rarely with aegirine, and the marginal parts are composed of carbonatites with variable content of calcite. The aegirine-amphibole-feldspar metasomatites are the intermediate varieties. All of them are the products of metasomatic facies of the carbonatite process. The radioactive pyrochlore (hatchettolite), euxenite, xenotime, rare earth carbonates and products of their alteration, ilmenorutile, zircon, and thorite are economically valuable minerals. Sulfides include galena, pyrite, pyrrhotite, and molybdenite. Supergene minerals are iron and manganese hydroxides.

According to the geologic position, ore-bearing metasomatites, and ore mineralization, the closest analogues of the Sarysai deposit are the deposits of the carbonatite-related aegirine-albite type with hatchettolite and zircon [Solodov, 1987]. The high content of Y group elements is untypical of this type of the deposits. Probably, this is caused by involvement in ore formation both of carbonatites (intrusive and metasomatic), syenites, and derivatives of the granite magma.

References

Kim, V.F. Features of the internal structure, forming and distribution of rare-metallic mineralization at the Kutessai-II deposit // Candidate Dissertation in Geology. Frunze, 1965. [in Russian].

Solodov, N.A. etc. The geologic reference book for high-gravity lithophile rare metals. Moscow, Nedra, 1987. 121 p. [in Russian].

V.V. Maslennikov [1, 2], V.A. Simonov [3], N.S. Ankusheva [1,2], S.P. Maslennikova [1], C.T.S. Little [4], B. Buschmann [5], L.V. Danyushevskiy [6], B. Spiro [4]

[1]Institute of Mineralogy UB RAS, Miass, Russia, mas@mineralogy.ru
[2]National Research South Ural State University, Chelyabinsk, Russia
[3]Institute of Geology and Mineralogy SB RAS, Novosibirsk, Russia
[4] Natural History of Museum, London, UK
[5] TU Bergakademie Freiberg, Cermany
[6] CODES, University of Tasmania, Hobart, Australia

HYDROTHERMAL VENT FAUNA IN THE URALS VMS DEPOSITS: CRITERIA FOR OCCURRENCE

Рассмотрены критерии появления, фоссилизации и сохранности пригидротермальной фауны в рудах колчеданных месторождений Урала и других колчеданоносных регионов. Показано, что для появления фауны благоприятными являются колчеданообразующие системы черных курильщиков, формировавшихся на базальтовом и риолит-базальтовом основаниях. Установлено, что черные курильщики, обогащенные Fe, Sn, Te,Co являются спутниками сульфид-

ных тафоценозов. Менее перспективными являются гидротермальные системы серых курильщиков, формирующие колчеданно-полиметаллические месторождения на субстрате, сложенном кислыми вулканитами. Показано влияние подрудных черных сланцев на вероятность появления пригидротермальной фауны. Рассмотрены геохимические особенности пригидротермальной биоты, включающие данные ЛА-ИСП-МС и изотопного состава серы. Установлено, что вероятность сохранности оруденелой фауны уменьшается в ряду от сульфидных холмов к пластообразным продуктам их разрушения.

The finding of very well preserved sulfidized fauna was one of the numerous surprises in the Urals. Previously, the fauna was found in the Silurian Yaman-Kasy, Krasnogvardeyskoe and Middle Devonian Sibai, Yubileinoe and Saf'yanovka VMS deposits [Ivanov et al., 1949, 1960; Maslennikov, 1991; Zaykov, 1991]. This fauna represents the most ancient known taxonomical hydrothermal vent community [Buschmann, Maslennikov, 2006; Maslennikov, 2006; Zaykov, 2006; Maslennikov, 1991, 1999, 2006; Little et al., 1997, 1999]. The most samples of fossil hydrothermal fauna are stored in the depository of the Institute of Mineralogy UB RAS in Miass and some samples were presented by authors to the Vernadsky Geological Museum in Moscow, TU Bergakademie in Freiberg, and Natural History Museum in London. The recent recognition of potentially vast, unexplored biomineralization associated with modern and ancient VMS deposits yielded the new material for mineralogical and biogeographic investigation. In last years, the sulfidized vent fauna was revealed in the Blyava, Molodezhnoye, and Valentorka VMS deposits. The recent study of new samples has given a novel data on peculiarities of the unexplored sulfidized fauna from the Urals VMS deposits in comparison with fauna from the modern and other ancient vent sites. The ore facies mapping, analyses of mineral assemblages, LA-ICP-MS and sulfur isotope analyses, and fluid inclusion study are the main methods of the research.

The oldest known and most taxonomically diverse hydrothermal fauna has been recovered from the Early Paleozoic basalt-rhyolite-hosted Yaman-Kasy VMS deposit located in the central part of Orenburg district, South Urals, and confined to the Sakmara marginal paleobasin. The sulfide body has a mound shape. The vent chimney relics, sedimentary reworked sulfides, and ferruginous sediments (gossanites after Maslennikov et al., 2012) indicate a seafloor hydrothermal origin of massive sulfides [Zaykov et al., 1995]. The sulfidized fauna is covered with colloform pyrite and the inners walls of the moulds are incrusted with drusy marcasite, sphalerite, pyrite, chalcopyrite, quartz, and barite. The fragments of sulfidized fauna in clastic sulfides are the signatures of the seafloor fossilization processes similar to the modern vent sites [Avdonin, 1996, Maslennikov, 1999]. The pyrite tube moulds both of the large tube worm *Yamanlasia refeia*, which is similar to the modern vestimentifera *Riftia pschiptilla,* and small worm tube *Eoalvinellodes* annulatus display widespread entombment of fossil filamentous and rod-like microorganism [Little et al., 1997; Maslennikov, 1999; Buschmann, Maslennikov, 2006]. The most researchers have suggested that the trophic chain of the Yaman-Kasy paleocommunity was obviously established by chemoautolithotrophic bacteria, which are the primary producers in the modern hydrothermal vent community. The extremely large sizes of the thergomian mollusk *Termoconus shadlunae* and giant lingulate brachiopod *Pyrodiscus lorrainae* are indicative of more prolific nutritional source in ancient hydrothermal vent habitat [Little et al., 1999: Kuznetsov, Maslennikov, 2000; Buschmann, Maslennikov, 2006].

The Silurian vent fauna is widespread in other Urals VMS deposits. Small pyrite tube worms in clastic sulfides were found in the drill core from the Komsomolskoye VMS deposit located at the same district, as well as Yaman-Kasy deposit [Pshenichny, 1981]. Similar well preserved tube worms were found by authors in the damp of the Blyava VMS deposit and recently in the Valentorka VMS deposit, North Urals. The latter is referred to the Baimak VMS type or is considered as intermediate member in a range from the Baimak to the Urals type. Single sample of the pyrite tube worm was collected by Goroch A.V. in the Krasnogvardeiskoe VMS deposit in the Central Urals [Ivanov, 1959]. All deposits represent strongly degraded sulfide mounds and are similar to the Yaman-Kasy VMS deposit.

Diverse Devonian vent paleocommunity was found in the Sibai VMS deposit located in the inter-arc paleobasin. The deposit consists of four stacked massive sulfide lenses (mounds) enclosed in the bimodal mafic sequence. The fossils include the species of bivalvia (*Sibaya ivanovi* [Little et al., 1999]) and flanged worm tubes were formally described as *Tevidestus serriformos* [Shpanskaya et al., 1999], which are similar to the modern vestimentifera *Tevnia.* Much smaller annulated worm tubes resemble the modern near-vent polyhaetes. The same polyhaetes and other unexplored tube forms

were found in sulfide breccias around the sulfide mounds of the Molodezhnoe, Uzelga, and Talgan VMS deposits located in the East Magnitogorsk arc paleobasin. All of these VMS deposits are accompanied by ferruginous sediments, indicating oxidation conditions. In other hand, the sulfidized fauna in the Urals was also found in the Saf'yanovka deposit (East Uralian zone, Central Urals), which was formed under anoxic conditions expressed in the black shale and felsic sequence. Numerous worm tube samples were collected from the strongly destroyed sulfide mound and were formally described as vestimentiferas or polyhaetes [Maslennikov, 1999]. The problematic tube fossils were found at the Ishkinino, Oktyabr'skoe, Buribai, Barsuchiy Log, Levikha and other Urals VMS deposits, which merit further research.

Thus, the vent fauna is widespread at some VMS deposits in the Urals, Pontides, Cyprus, and California relative to other VMS districts in spite of the same degree of careful ore facies and mineralogical mapping. The petrologic, ore facies, mineralogical, and geochemical criteria of the vent fauna occurrences in the VMS deposits are reviewed herein.

The petrologic background includes the geological setting and composition of the host rocks. The most of the cast fossilized vent fauna occurs in the VMS deposits associated with mafic (Cyprus type) and bimodal mafic (Urals type) sequences. This is in agreement with an idea that hydrothermal systems developed in these sequences are characterized by the highest reduction potentials. The high reduction potential is a major factor for the development of the vent community based on chemosynthesis during bacterial consumption of the reduced gases such as H_2S, CH_4, and H_2 as a main source of energy. In the other hand, VMS deposits located in bimodal felsic and felsic sequences are commonly barren of sulfidized fauna. The most famous examples are Kuroko and Altai types of VMS deposits devoid of obvious sulfidized vent fauna. It is suggested that the hydrothermal systems from these deposits were depleted in reduced gases but enriched in SO_2 and CO_2, representing the higher state of fluid oxidation and, therefore, the lower potential for the bacterial chemosynthesis. One of the known exceptions is the Saf'yanovka VMS deposit, where oxidation of fluids was prevented by footwall organic-rich sediments.

The interrelationship of ore facies may be an indicator of occurrence and preservation of the vent fauna. Several ore facies (ore types) were recognized at the VMS deposits. The abundance of the well preserved hydrothermal black smoker chimneys and diffusers, indicating the hydrothermal activity, is the most important factor for the vent fauna occurrence. However, the chimneys from the Kuroko, Altai and Baimak types of VMS deposits are not commonly associated with vent fauna. The vent fauna is minor during the waning stage of the hydrothermal system, when the seafloor weathering and reworking of sulfide mounds are the main processes of the clastic ore formation. Thus, the vent fauna is unlikely to be preserved, where sulfide turbidites are the main ore facies. In addition to weathering of the sulfide mounds, the hydrothermal alteration of the mound above the feeder zone play important role in recrystallysation of biomorphic textures. The proportion of hydrothermal activity and alteration periods depends on volcanic intensity. At intense volcanism, the catastrophic entombment of sulfide mounds may be the main reason of preservation of primary vent fauna features.

The mineralogical criteria are also related to the assessment of the reduction potential of the hydrothermal system. The best proxies for this research are the vent chimneys and diffusers as the best mineralogical indicators of the hydrothermal physicochemical condition. The chimneys from most Cyprus VMS deposits comprises abundant pyrite, pyrrhotite, isocubanite, and chalcopyrite and display lack of tellurides, arsenides and other rare mineral assemblages. The reason for that is low-S and low-Te conditions, which led to substitution of metals (Au, Co, Ag, Ni) and semimetals (Te, As, Se, Sb) in the lattice of main sulfides. These attributive features of the high reduction potential seem to be favorable for the vent fauna occurrence in association with the modern and ancient black smokers. In the Urals types of VMS deposits, the chimneys and diffusers display specific composition suggestive of low-S (low S fugacity, $?S_2$) hydrothermal fluids. This means the low state of fluid oxidation or its high reduction potential. The mineral assemblages related to the low-S conditions include pyrrhotite or pseudomorphic pyrite after phyrrhotite, isocubanite, Fe-rich sphalerite, Fe-Co-arsenides, sulfoarsenides, and tellurides. The best indicator of low-S conditions is altaite (PbTe), which is widespread in chimneys associated with vent fauna. The chimneys and diffusers contain abundant colloform pyrite. In the other hand, the gray smoker chimneys from the Kuroko and Altai deposits include mostly barite, sphalerite, and stochiometric chalcopyrite or bornite and galena. Native gold, galena, and fahlores are most important rare indicative mineral of high-S conditions or high state of fluids oxidation. The low reduction potential of the hydrothermal systems of the Kuroko and Altai deposits may be an important reason of vent fauna defi-

ciency. The intermediate type between bimodal mafic and felsic types of VMS deposits are Pontide and Baimak type, which is associated with bimodal felsic sequences. The vent fauna in these deposits is absent or extremely poorly preserved owing to the deficiency in colloform pyrite coating because of the general lack of Fe-rich minerals. The best preserved samples of sulfidized vent fauna are commonly associated with colloform pyrite, which is abundant manly in the Cyprus and Urals types of VMS deposits.

The geochemical criteria are also consistent with maturation and reduction potential of the hydrothermal systems. The Se, Te, Co-, and Fe-rich massive sulfide ore are indicative of immature hydrothermal system with high reduction potentials. In opposite, the Zn-, Pb, Tl, Ba, and Sb-rich massive sulfide ores testify to the mature hydrothermal system with low reduction potential. The contents of trace elements in hydrothermal sulfides are most important indicators of physicochemical parameters of hydrothermal systems. The content of trace elements in sulfides may be high due to inclusions of rare minerals or substitution in lattice of sulfide structures. In the first case, the Pb/Te and Ag/Te ratios display telluride and fahlore-electrum-rich assemblages. The detection of second phenomena is most important instrument for physicochemical reconstructions. The chemical peculiarities of the hydrothermal chalcopyrite, which seals the conduits of the vent chimneys, are most interesting. The Se-, Te-, Co-, and Sn-rich chalcopyrite, which is typical of the black smokers in the Cyprus and Urals types of VMS deposits, is the best indicator of highly reduction potential. In the other hand, Se-poor chalcopyrite enriched in Ag is suggestive of high state of fluid oxidation unfavorable for the vent fauna occurrence. This chalcopyrite is characteristic of gray smokers in the Kuroko and Altai types of VMS deposits. The same situation is observed for the Fe-, Co-, and Sn-rich sphalerite associated with vent fauna. In contrast, Fe-, Co-, Sn-poor and Cd- and Mn-rich sphalerite is a constituent of the gray smokers, which are less favorable for association with plentiful vent community. It is less known on the relationship between vent fauna occurrence and substitution of trace elements in other sulfides. In general, Co-rich pyrite is most important for fertile vent ecosystems relative to Ni-rich varieties, because the first one is characteristic of low-S conditionsin contrast to the second one. The sulfur isotopic composition of biomorphic sulfides may be indirect criteria to distinguish fertile and barren VMS deposits in regard to vent fauna. The values of δS^{34} from –2 to +2 ‰ [Lein et al., 2004] are the most common for the vent chimneys and near vent fauna formed in the black smoker systems of the Urals VMS type. The δS^{34} for chimneys from the Kuroko deposits is somewhat higher (+2 to +6 ‰) that suggests involving of seawater sulfate into reduction of sulfur during sulfide formation. This process may decrease the reduction potential of the hydrothermal system. The diagenetic sulfidized fauna display much wider δS^{34} variation.

The promising data may be obtained by gas chromatography analyses of the fluid inclusions. The first results display CH_4 enrichment of quartz and barite in chimneys associated with vents fauna. However, we should be careful with these data, because influence of organic-rich sediments located in the footwall of the hydrothermal system on composition of the hydrothermal fluids and vent fauna occurrences is an unresolved problem.

Thus, petrologic, ore facies, mineralogical, and geochemical research has shown that Cyprus and Urals types of the VMS deposits display the highest reduction potential of the hydrothermal fluids, yielding abundant vent community and, therefore, plentiful sulfidized fauna versus Altai and Kuroko deposits. We suggest that VMS deposits of Pontides and Baimak types occupy intermediate position in a range of these bimodal mafic and bimodal felsic types of VMS deposits. The long-term research of VMS deposits allows exploration of linkages between formation conditions and near vent biosphere. Such approaches may provide significantly new information to resolve the problem of life origin.

The authors are grateful to Prof. V.V. Zaykov and Dr. R.J. Herrington for the prompt revision and advices. This work is supported by the Joint project of Urals and Siberian Branches of Russian Academy of Science (no. 12-C-5-1010) and CODES Visiting Program of Tasmania University.

References

Avdonin, V.V. Relics of "black smokers" in ores of massive sulfide deposits // Metallogeny fold systems from the perspective of plate tectonics. Ekaterinburg, Ural Branch of Russian Academy of Sciences, 1996. P. 148–152 [in Russian].

Buschmann, B., Maslennikov, V.V. The late Ordovician or earliest Sillurianhydrothermal vent fauna from Yaman-Kasy VMS deposit (South Uralides, Russia) // Paleontology, Stratigraphy , Facies, 2006. Vol. 14. P. 139–172.

Ivanov, S.N. Study experience of geology and mineralogy of the Sibay massive sulphide deposit // Akademia Nauk SSSR, Uralskiy Filial, 1947. Vol. 2. P. 1–109 [in Russian].

Ivanov, S.N. A discussion of some actual questions in formation of massive sulphide deposits in the Urals // Problems of geology and origin of massive sulfide deposits in the Urals. Sverdlovsk, 1959. P. 7–78 [in Russian].

Ivanov S.N., Kuritzyna G.A., Hodalevich N.A. New data about genesis of massive sulfide deposits of Urals // Genetic problems of ores. Moscow, 1960. P. 100–105 [in Russian].

Kuznetzov, A.P., Maslennikov, V.V. Hystory of the ocean hydrothermal fauna. Moscow, VNIRO, 2000. 118 p. [in Russian].

Lein, A.Yu., Maslennikov, V.V., Maslennikova, S.P., Spiro, B. Isotopes of carbon and sulfur in biomorphic ore facies from black smockers of the Uralian Paleoocean // *Geochemia*, 2004. No. 7. P. 770–785 [in Russian and English].

Little, C.T.S., Herrington, R.J., Maslennikov, V.V., Morris, N.J., Zaykov, V.V. Silurian high-temperature hydrothermal vent community from the Southern Urals, Russia // Nature, 1997. V. 385. №. 9. P. 146–148.

Little, C.T.S., Maslennikov, V.V., Morris, N.J., Gubanov, A.P. Two Palaeozoic hydrothermal vent communities from the Southern Ural mountains, Russia // Palaeontology, 1999. No. 6. P. 1043–1078.

Maslennikov V.V. Sedimentogenesis, Halmyrolysis and Ecology of massive sulphide-bearing vent fields. Miass, Geotur, 1999. 348 p. [in Russian].

Maslennikov, V.V. Lithogenesis and massive sulfide deposits forming processes. Miass, IMin UB RAS, 2006. 384 p. [in Russian].

Maslennikov, V.V. Lithological control of copper massive sulfide ores (after the example of Sibai and Oktyabrskoye deposits, Ural). Sverdlovsk, UB AN USSR, 1991. 139 p. [in Russian].

Maslennikov, V.V., Ayupova, N.R., Herrington, R.J., Danyushevskiy, L.V., Large, R.R. Ferruginous and manganiferous haloes around massive sulphide deposits of the Urals // Ore geology reviews, 2012. Vol. 47. P. 5–41.

Pshenichnyi, G.N. Texture and structure of the ore of VMS deposits of the Southern Urals. Moscow, Nauka, 1984. 207 p. [in Russian].

Shpanskaya A.Yu., Maslennikov V.V., Little, C.T.S. The tubes of Vestimentifera of early Silurian and middle Devonian hydrothermal biota of Ural paleoocean // journal of Paleontology, 1999. №. 3. P. 21–30.

Zaykov, V.V. Volcanism and sulfide mounds in paleooceanic margins. Moscow, Nauka, 1991. 206 p. [in Russian].

Zaykov, V.V. Volcanism and sulfide mounds in paleooceanic margins. Moscow, Nauka, 2006. 428 p. [in Russian].

Zaykov, V.V., Shadlun, T.N., Maslennikov, V.V., Bortnikov, N.S. Sulphide deposit of Yaman-Kasy – ancient black smockers of the Uralian paleoocean // *Geologia rudnich mestorogdeniy*, 1995. P. 511–529 [in Russian and in English].

S.P. Maslennikova[1], V.V. Maslennikov[1], R.R. Large[2], L.V. Danyushevsky[2], V.A. Kotlyarov[1], A.Yu. Lein[3], Yu.A. Bogdanov [3], R.J. Herrington[4], D. Ishiyama[5], T. Urabe[6], K. Revan[7], A.S. Tseluiko[1], B.Buschmann[8]

[1] Institute of Mineralogy UB RAS, Miass, Russia
[2] University of Tasmania, CODES, Hobart, Australia
[3] Institute of Oceanology RAS, Moscow, Russia
[4] Natural Hystory Museum, London, UK
[5] Akita University, Akita, Japan
[6] University of Tokio, Tokio, Japan
[7] Department of Mineral Research and Exploration, General Directorate of Mineral Research and Exploration (MTA), Ankara, Turkey
[8] Freiberg Mining Academy, Freiberg, Germany

MINERALOGY AND CHEMISTRY OF MODERN AND ANCIENT BLACK AND GRAY SMOKER CHIMNEYS AND DIFFUSERS

Показано минералогическое и геохимическое разнообразие сульфидных труб черных и серых курильщиков, формировавшихся в современных и древних колчеданоносных гидротермальных системах. Первые связаны с офиолитовыми и риолит-базальтовыми формациями, вто-

рые – с базальт-риолитовыми и андезит-риолитовыми. Выявлено, что в ряду от офиолитовых комплексов к риолитовым в сульфидах труб уменьшаются содержания Co, Ni, Se, Te и увеличиваются содержания Pb, Bi, Tl, Hg, Au и Ag. Установлены признаки гидротермально-осадочной дифференциации элементов-примесей при формировании минеральной зональности гидротермальных труб, свидетельствующие о единстве процессов формирования сульфидных труб современных и древних черных курильщиков. Показано влияние подрудных углеродистых отложений на появление черных курильщиков.

The study of rare mineral assemblages and trace elements in the hydrothermal chimneys yields a lot of information to resolve genetic problems of ore-forming processes in modern and ancient seafloor sulphide-bearing hydrothermal systems. Previous research has provided limited combined data on mineralogy and chemistry of modern and ancient black smoker chimneys. The first semi-quantitative data from Butler and Nesbitt (1999) illustrated the power of LA-ICPMS analysis by documenting the non-random distribution of V, Ag, In, Te, Ba, Au, and Pd within the chalcopyrite wall of an immature black smoker chimney from the Rainbow vent field (29° 10′N, MAR). In previous paper, we focused on mineralogy and the LA-ICPMS investigation of diverse Silurian-Devonian vent chimneys recently collected in the Urals VHMS deposit [Maslennikov et al., 2009; 2012]. Recently, we studied mineral assemblages and trace element concentrations in pyrite, chalcopyrite, and sphalerite of the chimneys from the Urals (Yaman-Kasy, Alexandrinskoye, Octyabrskoye, Tash-Tau, Yubileynoye, Saphyanovskoye, Molodezhnoye, Uzelga, Valentorskoye), Rudny Altai (Zarechenskoye, Nikolayevskoye, Artemyevskoye), Pontides (Lakhanos, Killik, Kutlular, Chaely, Kizilkaya, Kure), and Hokuroko (Mazumine, Mazuki, Ezury, Furutobe, Hanawa, Ainay, Kosaka Uchinotay and Kosaka Motoyama) VMS deposits in comparison with black, gray and white smoker chimneys from hydrothermal fields of Atlantic (Rainbow, Broken Spur, TAG, Lucky Strike, Menez Gwen, Snake Pit) and Pacific (EPR 9°N; Axial Seamount, Galapagos, North Manus, East Manus and Lau) oceans.

A preliminary mineralogical study of the chimneys was followed by scanning electron microscopy (REMMA-2M SEM equipped with energy dispersive X-ray detector and JEOL JXA 733) at the Institute of Mineralogy, Russian Academy of Sciences. Further mineral analyses were obtained in several laboratories equipped with CAMEBAX SX-50 and JEOL-JXL-8600 (Natural History Museum, London), Cameca SX-100 (University of Tasmania, Australia) and JEOL JXA 8900RL (Freiberg Mining Academy, Germany).

Laser ablation inductively coupled plasma mass spectrometry (LA-ICPMS) offers enormous potential in advancing trace element studies of sulfides through significantly improved detection limits for in situ analysis [Norman et al., 1998]. Many important innovations, including preparation of new glass standards, which enable improved quantitative LA-ICPMS analysis of sulfides, have been made over the last ten years at the Centre for Ore Deposit Research, University of Tasmania [Danyushevsky et al., 2003, 2010]. The LA-ICP MS is used for detection of trace elements substitution and rare mineral inclusions in sulfides.

In general, the chimneys show decreasing amount of Fe-rich sulfides and increment of barite-galena-sphalerite-fahlore assemblages in the range from ophiolite to rhyolite-rich associations. Abundant Ni-Co sulfides, rare Co-Fe arsenides and very rare tellurides are characteristic of mineral assemblages in modern black smokers formed on ultramafic basements. The deficient rare minerals are found in modern and ancient chimneys situated on basalt units (Cyprus, MOR). The heighest contents of Se and Te are substituted in chalcopyrite.

Tellurium-bearing minerals are generally rare in chimney material from mafic and bimodal felsic volcanic hosted massive sulfide (VMS) deposits, but are abundant in chimneys of the Urals VMS deposits located within Silurian and Devonian bimodal mafic sequences [Maslennikov et al., 2013]. High physico-chemical gradients during chimney growth result in a wide range of telluride and sulfoarsenide assemblages including a variety of Cu-Ag-Te-S and Ag-Pb-Bi-Te solid solution series and tellurium sulfosalts. A change in chimney types from Fe-Cu to Cu-Zn-Fe to Zn-Cu is accompanied by gradual replacement of abundant Fe-, Co-, Bi-, and Pb- tellurides by Hg-, Ag-, Au-Ag telluride and galena-fahlore with native gold assemblages. Decreasing amounts of pyrite, both colloform and pseudomorphic after pyrrhotite, isocubanite (ISS), and chalcopyrite in the chimneys is coupled with increasing amounts of sphalerite, quartz, barite or talc contents. This trend represents a transition from low to high sulfur conditions, and it is observed across a range of the Urals deposits from bi-

modal mafic- to bimodal felsic-hosted types: Yubileynoye → Yaman-Kasy → Molodezhnoye → Uzelga → Valentorskoye → Oktyabrskoye → Alexandrinskoye → Tash-Tau → Jusa. Ag-, Au-, Bi- tellurides are described in the rhyolite hosted chimneys from bimodal mafic sequences of Two Brothers seamount. Tellurobismutite has been found by our research in dacite hosted chimneys from bimodal mafic basement of Eastern Manus basin. In Pontides, chimneys contain rare inclusions of Ag-, Bi tellurides in association with native gold, galena and sulfosalts. This type can be considered as intermediate member in the range between bimodal mafic and bimodal felsic VMS deposits. Gold-barite-galena-tetrahedrite assemblages are typical of bimodal felsic and felsic series in Paleozoic (Rudniy Altay) and Cenozoic (Hokuroko, Okinawa) ensialic arc basins. In Hokuroko, the chimneys exhibit specific mineral and trace element zonation which is broadly comparable with those studied in modern black or gray smokers with exception lack of evidence for the former initial pyrrhotite, isocubanite and anhydrite. Several types of zoned chimneys are subdivided into three varieties by different outer wall composition: 1) sphalerite-galena-pyrite, 2) sphalerite-barite-galena and, 3) barite-hematite varieties. The inner walls of the chimneys are usually incrusted by drusy chalcopyrite or bornite, tennantite, galena which shows elongate dendritic or bladded growth features. The axial conduit zones of the chimneys are often filled with sphalerite, tennantite, galena and barite. Hokuroko chimneys show depletion in Fe-rich sulfides and elevation in barite, galena and fahlores in comparison with typical black smokers from MOR but they are very similar to black and gray smokers from the modern West Pacific, Paleozoic Uralian and Mesozoic Pontides ensimatic arc basins. The major differences are the lack of tellurides and sulphoarsenides and the predominance of fahlore-bornite-galena-electrum assemblage. This assemblage is typical of barite-rich chimneys from the Paleozoic Rudniy Altay ensialic arc. The laser-ablation ICPMS study has shown the systematic trace element distribution patterns across chimneys. In the outer wall, colloform and euhedral pyrite has elevated concentrations of Mn, Tl, Ni, Mo, Se and Te. Coarse-grained chalcopyrite layers in the central conduits are relatively low in most of trace elements with exception of Bi and Sn. Sphalerite is enriched in Au, Ag, As and Sb. In general, the grades of trace-elements in the Phanerozoic black smokers depend on composition of host suites: ultramafic – high Se, Sn, Co, Ni, Au, and U, mafic – high Co, Se and low Bi and Pb, bimodal mafic – high Te and Bi, Co, and moderate Se. The chimneys associated with bimodal felsic suites, like Hokuroko and Rudniy Altay, are characterized by elevated contents of As, Sb, Mo, Pb, Bi, Tl, Ag, W, and Hg and much lower grades of Co, Te, and Se.

The study has commonly shown systematic trace element distribution patterns across chimneys. Coarse-grained layers of chalcopyrite in the central conduits are relatively high in Se and Sn, but are low in other elements. Chalcopyrite at the margins of such layers is enriched in Bi, Co, Au, Ag, Pb, Mo, Te, and As which reside in microinclusions of tellurides and/or sulfoarsenides or sulphosalts galena and native gold. Sphalerite in the conduits and the outer chimney wall contains elevated Sb, As, Pb, Co, Mn, U, and V. Sb, As, and Pb reside in microinclusions of a galena-fahlore assemblage, whereas Co and Mn likely substitute for Zn^{2+} in the sphalerite structure. The highest concentrations of most trace elements are characteristic for colloform pyrite within the outer wall of the chimneys, and likely result from rapid precipitation in high temperature-gradient conditions. The trace element concentrations in the outer wall colloform pyrite decrease in the following order, from the outer wall inwards: Tl> Ag> Ni> Mn> Co> As> Mo> Pb> Ba> V> Te> Sb> U> Au> Se> Sn> Bi, governed by the strong temperature gradient. In contrast, pyrite in the high- to mid-temperature central conduits exhibits the concentration of Se, Sn, Bi, Te, and Au. The zone between the inner conduit and outer wall is characterised by recrystallization of colloform pyrite to euhedral pyrite, which becomes depleted in all trace elements except for Co, As, and Se. The iron hydrooxides covering outer wall of the chimneys have elevated contents of U, V, Ba, and Mn.

The mineralogical and trace element variations between chimneys are likely due to increasing fO_2 and decreasing temperature caused by mixing of hydrothermal fluids with cold oxygenated seawater. Average values of Se decrease in the order from black to gray and white smoker chimneys are in correlation with general increase of barite and sphalerite. The medium-temperature association (Te, Bi, Co, Mo, and Au) is typically present in the gray smoker chimneys. The Zn-rich chimneys are depleted in most elements except for Ag, Tl, Te, Sb and As, probably due to the dilution of the vent fluid by seawater which penetrates into deeper parts of the hydrothermal system. U and V are concentrated in the outer wall of most chimneys due to their extraction from seawater associated with the more reduced fluids of black and gray smokers.

The peculiarities in rare mineral assemblages and trace elements concentrations are consistent with a mineralogical type of the chimneys and also depend on general composition of host rocks. The hydrothermal chalcopyrite is the best subject for this research.

This study of trace element distribution in the chimneys has contributed to our understanding of the wide range of physico-chemical processes and conditions of seafloor sulfide mineralization. The trace element patterns described above are considered to result from temperature and redox gradients across the section of the chimneys, and the variation in temperature associated with black, gray and white smoker type chimneys.

The combination of data on chimneys from modern and ancient massive sulfide deposits allows to understand general peculiarities of trace elements changes in the range from ultramafic to basaltic and felsic sequences. In colloform pyrite, contents of As, Au, Sb, Tl, Pb, Bi, and Ni subsequently increase with growth of felsic volcanite amount. In euhedral pyrite, the contents of Co decrease, but the Ni and Se increase in the same range. In chimneys from felsic association, sphalerite has elevated contents of Hg, Ag, and lower contents of Co and Fe. In the same range, chalcopyrite loses Se and Co, Te with increase in Bi, Ag, As, Sb, and Pb. Maximum concentrations of Te, Bi, and Au have been detected in chalcopyrite of chimneys from ancient bimodal mafic sequences which occupy the middle part of the range. Nevertheless, the gold also displays concentration in chalcopyrite of chimney from ultramafic sequences and in sphalerite of chimney from felsic bimodal sequences. The high gold content is not typical of basalt hosted chimneys. However, in "mature" hydrothermal systems (TAG, Galapagos, Menez Gwen) gold can be occasionally found in concentration above 1–150 ppm. The gold is associated with barite- and bornite-rich chimneys similar to chimneys from felsic bimodal sequences. The influence either of composition of volcanic rocks, maturation of hydrothermal system or magmatic contribution of the trace element concentration is considered as a cause of trace elements concentrations.

The general trend encloses decreasing of Fe and Co and increasing of volatile elements such as Sb, As, Au, and Ag in the range of chimneys from ultramafic to felsic sequences. This is consistent with increasing of magmatic contribution in the hydrothermal system with increase in amount of felsic volcanic rocks. However, these data are not in contradiction with recycling seawater hydrothermal system in terms of increase in this "maturity" independently of primary composition of the host rocks. Some elements concentrations (Se and Te) are probably independent of composition of the host rocks, but reflect fluid oxidation state. The high concentration of Ni in pyrite of chimneys associated with felsic volcanic rocks depends on the fugacity of S_2 increase [Maslennikov, 2009].

Thus, the mineral and trace element patterns described herein are considered to result from temperature and redox gradients across the section of the chimney, and the variation in temperature associated with black, gray, and white smoker chimneys formed in different host rock environments. The grades of trace elements in chalcopyrite of the Phanerozoic vent chimneys depend on composition of host suites: ultramafic – high Se, Sn, Co, Ni, Au, and U, mafic – high Co, Se and low Bi, and Pb, bimodal mafic – high Te and Bi, Co, and moderate Se, bimodal felsic – high As, Sb, Mo, Pb, Bi, elevated Ag, W, and lower Co. In chalcopyrite of the chimneys studied, the contents of Ba, Bi, Pb, Ag, Sb, Mo, W versus Se and Co increase in the range from ultramafic and mafic to bimodal felsic series.

This research was supported by the Program of Presidium RAS no. 23 (project 09-П-5-1023 Urals Branch of RAS). The mineralogical research was supported by several collaborative projects with Natural History Museum (London) and Freiberg Academy, LA-ICPMS analyses were carried out during a visiting program (2006, 2009) funded by the ARC Centre of Excellence grant to CODES, University of Tasmania.

References

Butler, I.B., Nesbitt, R.W. Trace element distributions in the chalcopyrite wall of black smoker chimney: insights from laser ablation-inductively coupled plasma-mass spectrometry (LA–ICP–MS) // Earth and Planetary Science Letters, 1999. P. 335–345.

Danyushevsky, L.V., Robinson, P., Gilbert, S., Norman, M., Large, R., McGoldrick, P., Shelley, J.M.G. A technique for routine quantitative multi-element analysis of sulfide minerals by laser ablation ICP–MS // Geochemistry: Exploration, Environment, Analysis, 2010. Vol. 11. P. 5–60.

Danyushevsky, L., Robinson, P., McGoldrick, P., Large R., and Gilbert S. LA–ICP MS of sulfides: Evaluation of an XRF glass disc standard for analysis of different sulfide matrixes. Goldschmidt Conference, Japan // Geochimica et Cosmochimica Acta, 2003. Vol. 67 (18), A73 Suppl.

Maslennikov, V.V., Maslennikova, S.P., Large, R.R., Danyushevsky, L.V., Herrington, R.J., Stanley, C.J. Tellurium-bearing minerals in zoned sulfide chimneys from Cu-Zn massive sulfide deposits of the Urals, Russia // Mineralogy and Petrology, Special Issue: Ore deposits of the Urals, 2013. Vol. 107 (1). P. 67–99.

Maslennikov, V.V., Maslennikova, S.P., Large, R. R., Danyushevsky, L.V. Study of trace element zonation in vent chimneys from the Silurian Yaman-Kasy volcanic-hosted massive sulfide deposit (Southern Urals, Russia) using LA–ICP MS // Economic Geology., 2009. Vol. 104 (8). P. 1111–1141.

Norman, M.D., Griffin, W.L., Prearson, N.J., Garcia, M.O., O'Reilly, S.Y. Quantitative analysis of trace element abundances in glasses and minerals: a comparison of laser ablation inductively coupled plasma mass spectrometry, solution inductively coupled plasma mass spectrometry, proton microprobe and electron microprobe data // Journal of Analytical Atomic Spectrometry, 1998. Vol. 13. P. 477–483.

I.Yu Melekestseva[1], V.V. Maslennikov[1], S.P. Maslennikova[1], R.R. Large[2], L.V. Danyushevsky[2]
[1] Institute of mineralogy UB RAS, Miass, Russia, melekestseva-irina@yandex.ru
[2] CODES ARC Centre of Excellence in Ore Deposits, University of Tasmania, Hobart, Australia

TRACE ELEMENTS IN SULFIDES FROM THE SEMENOV HYDROTHERMAL CLUSTER, 13°30? N, MID-ATLANTIC RIDGE: LA-ICP-MS DATA

Установлен типохимизм сульфидов гидротермального узла Семенов (13?30´ с.ш., САХ). Ранние генерации пирита обогащены большинством элементов-примесей (в том числе, золотом) относительно поздних, что свидетельствует об истощении последних порций растворов микроэлементами. Дисульфиды железа, отлагавшиеся на поверхности морского дна, обогащены элементами-примесями по сравнению с метасоматическим пиритом, что говорит о более эффективной экстракции элементов-примесей в момент смешения гидротермального раствора с морской водой. Главным концентратором невидимого золота в Cu-Zn рудах поля Семенов-2 является ковеллин.

It is well known that ores from the continental massive sulfide deposits contain a series of economically important trace metals, including Au and Ag. Because of the future potential of the modern massive sulfide fields, it is necessary to understand the distribution of trace elements in sulfides. In this work, we examine the trace element composition of sulfide minerals from the Semenov hydrothermal cluster (13?31? N, MAR) using a LA-ICP-MS analysis, which became an effective instrument of mineral investigations during the recent years.

The Semenov hydrothermal cluster was discovered in 2007 by Russian R/V *Professor Logatchev* by Polar Marine Geosurvey Expedition and VNIIOkeangeologiya (St-Petersburg) [Beltenev et al., 2007]. It is situated in the western slope of the rift valley at the depths of 2400–2950 m on a seamount 10 km long and 4.5 km wide. The seamount is composed of basalts, gabbro, ultramafic rocks, and plagiogranites [Ivanov et al., 2008]. The hydrothermal cluster consists of five hydrothermal fields. Our study is based on the samples from the Semenov-1, -3, -2 and -4 fields directly obtained on board of the research vessel in 2007.

The massive sulfides from the Semenov-1 (13°30.87? N, st. 186 and 292) and Semenov-4 (13°30.24? N, st. 145) fields are the products of low-temperature (<250 °C) diffuse venting on the flanks of sulfide mounds and are characterized by fine-crystalline, nodule-like, porous, colloform, zonal, framboidal, and coarse-grained structures. Barite, pyrite, marcasite are major minerals, sphalerite, quartz and hematite are less abundant, and galena, chalcopyrite, pyrrhotite are minor. The fine-grained, porous, and massive sulfides from the Semenov-2 field (13°31.13? N, st. 287) are resulted from the high-temperature (>300 °C) venting inside the sulfide mound. Isocubanite, chalcopyrite, wurtzite, and opal are major minerals; sphalerite, marcasite, pyrite, covellite, and barite are widespread; and galena, pyrrhotite, native gold, and silver telluride are occasional. The clastic sulfides from the Semenov-3 field (13°30.70? N, st. 294) are composed of major marcasite, pyrite, barite, quartz, abundant chalcopyrite and hematite, and accessory sphalerite, pyrrhotite, bornite, covellite, jarosite. The stringer-disseminated massive sulfides in strongly altered basalts with major quartz and pyrite,

widespread hematite, and occasional sphalerite, chalcopyrite, pyrrhotite were dredged from the Semenov-4 field (13°30.24?N, st. 153).

LA-ICP-MS data demonstrate that sulfides from different hydrothermal fields or different generations in the same station accumulate various trace elements.

Semenov-1 field. The early disulfides are high in concentrations of most trace elements in contrast to the late disulfides. The fine-grained pyrite-1 from st. 186 is enriched in most elements and is depleted in Ti, Hg and Tl relative the crystalline pyrite-2. The early iron disulfides from st. 292 are also enriched in trace elements: framboidal pyrite-1 is enriched in Ti, V, Mn, As, Mo, Sb, Au, Hg and Tl relative pyrite-2 and in most elements, except for Pb, relative pyrite-3. In turn, pyrite-2 is enriched in Co, Cu, Cd, Sn, W, Pb and U relative framboidal pyrite and in most elements, except for Mn, Au, Hg and Tl, relative pyrite-3. The latter is depleted in most elements relative framboidal pyrite and pyrite-2. Marcasite is depleted in most elements, except for Mn, Hg and Pb relative pyFr and for Mn, Au, Hg and Tl relative pyrite-2 and is enriched in most elements in comparison to pyrite-3. All varieties of iron disulfides from st. 292, except for the late pyrite, are enriched in trace elements compared to those from st. 186.

Semenov-2 field. Sphalerite contains the higher amounts of Mn, Co, Se, and Cd, moderate contents of Ga, Sn, and Te, and minor to trace amounts of Ni, As, Mo, Ag, In, Sb, Tl, Pb, and Bi. Chalcopyrite is enriched in Co, As, Se, and Ag and has moderate amounts of Ni, Mo, Cd, Sn, Sb, Te, and Tl, and minor to trace contents of Mn, Ga, In, Pb and Bi. Isocubanite is characterized by negligible amounts of Ni, Ga, As, Mo, In, Sb, Tl, Pb, and Bi, moderate contents of Mn, Cd, Sn, and Te, and elevated contents of Co, Se, and Ag. In comparison to chalcopyrite, isocubanite is depleted in trace elements.

LA-ICP-MS analysis has shown that covellite developed after sphalerite and chalcopyrite is distinct in amount of trace elements similarly to Au contents. In the first case, covellite is strongly enriched in most trace elements relative to sphalerite, both in “high-temperature” (Se, Mo, Sn, Te, Au, Bi) and “low-temperature” (As, Ag, Sb, Tl, Pb) elements. Some elements (Ga, Ni, In) show no significant variations or are lower than in sphalerite (Mn, Co, Cd), being removed during the replacement. This covellite is also strongly enriched in all trace elements relative to covellite, which replaces chalcopyrite.

Covellite developed after chalcopyrite has lower contents of most trace elements in comparison to chalcopyrite but is enriched in Au and “low-temperature” elements (Ag, Cd, Sb, Pb) relative to chalcopyrite. No considerable variations are observed for Mn, Ga, Se, In, Sn, and Te and contents of Co, Ni, As, Mo, and Tl are lower in covellite relative to chalcopyrite.

Semenov-3 field. The pyrite-1 and pyrite-2 from the clasts in sulfide breccia are also enriched in most trace elements (excluding Ti, Co, Ni, As and Se) in comparison to pyrite-3. In contrast, pyrite-4 contains the higher amounts of most elements, excluding Co, Au and Hg, compared to pyrite-1 and -2 and Co, As and Se compared to pyrite-3. Similarly to the Semenov-1 field, marcasite is depleted in most elements (except for Ti, V, Cr, Mn, Mo, Sb, Tl and U) in comparison to the clastic pyrite-1 and -2 and is enriched in most elements relative to pyrite-3. The newly formed pyrite-4, in its turn, is enriched in most elements in comparison to the earlier marcasite and has the highest Cu and Zn contents in comparison to other varieties of iron disulfides.

Semenov-4 field. The tendencies of trace element enrichment or depletion in iron disulfides of the Semenov-4 field are generally very similar to those from Semenov-1 and -3 fields with some exceptions. The pyrite-1 from st. 286 is high in most trace elements except for the “high-temperature” Co, Cu and Se in comparison to pyrite-2. Marcasite is enriched in trace elements compared to both pyrites, excluding Co, Zn, As, Se and U for pyrite-1 and Co and Se for pyrite-2. The massive crystalline pyrite from st. 145 is enriched in V, Cu, Mo, Sn, Hg and Tl in comparison to pyrite-1 from st. 286 and is depleted only in Co, Cu and Se relative to pyrite-2. The veined crystalline pyrite from st. 153 is depleted in all trace elements relative to massive crystalline pyrite from st. 145 and pyrite-1 and -2 from st. 286. Slightly elevated average Co and Sn contents in pyrite from st. 153 relative to pyrite from st. 145 and Sn and Ti contents relative to pyrite from st. 286 are insufficient and fall into dispersion.

Conclusions. The same generations of pyrite from the different fields, which are formed under similar formation conditions, are similar in enrichment in most trace elements relative to late pyrite. This points to the input of most trace elements from the primary hydrothermal fluid. The late crystalline pyrite was crystallized from the fluid depleted in most trace elements. The crystalline py-

rite, which deposited from the new fluid portions closely to chalcopyrite and sphalerite, are enriched in Cu and Zn. The iron disulfides, which were formed on the seafloor, are strongly enriched in trace elements relative to the subseafloor crystalline pyrite that most likely is related to the effective accumulation of trace elements, when the high-temperature hydrothermal fluid meets the cold seawater. Gold is concentrated in the early generations of pyrite and marcasite.

The main carrier of the invisible gold in the Semenov-2 massive sulfides is covellite in contrast to traditional pyrite, chalcopyrite, bornite or isocubanite [e.g., Bortnikov et al., 2000]. Covellite from the Semenov-2 massive sulfides contains 22.51–226.64 ppm Au that is much higher than Au content in sphalerite (0.00–0.01 ppm), chalcopyrite (0.11–0.22 ppm), and isocubanite (0.03–0.06 ppm). Covellite, which replaces sphalerite, is characterized by the higher Au contents. We suggest that gold in covellite is chemically bound because each of 11 analyses has stable gold content and Au and Cu contents in covellite directly depend on each other.

Similarly to Au, all identified elements have more or less stable contents in all analyses that does not favor microinclusions of minerals. However, direct correlation between Bi and Te may probably indicate presence of microinclusions of Bi-telluride. The source of most trace elements in covellite, which replace sphalerite, is problematic and the mechanism of their incorporation is still unclear. Some of trace elements (Mn, Co, Ga, Cd) were inherited from the replaced sphalerite and were removed during the replacement. In case of covellite, which is developed after chalcopyrite, most trace elements (Mn, Co, Ni, Ga, As, Se, Mo, In, Sn, Te, Tl, and Bi) derive from the host chalcopyrite.

The study is supported by the Program of Presidium RAS no. 23 (project no. 12-П-5-1003).

References

Beltenev, V., Ivanov, V., Rozhdestvenskaya, I. et al. A new hydrothermal field at l3?30' N on the Mid-Atlantic Ridge. InterRidge News, 2007. Vol. 16. P. 9–10.

Bortnikov, N.S., Cabri, L., Vikent'ev, I.V. et al. Invisible gold in sulfides from recent submarine hydrothermal mounds. Dokl. Earth Sci., 2000. Vol. 372. No. 5. P. 863–866.

Ivanov, V., Beltenev, V., Stepanova, T.V. et al. Sulfide ores of the new hydrothermal cluster l3?31' N of MAR. In: Metallogeny of ancient and modern oceans-2008. Ore-bearing complexes and ore facies. Ed. by V.V. Zaykov. Miass, IMin UB RAS, 2008. P. 19–22 [in Russian].

I.Yu. Melekestseva[1], V.V. Zaykov[1, 2], N.N. Ankusheva[1,2]
[1] *Institute of Mineralogy UB RAS, Miass, Russia, melekestseva-irina@yandex.ru*
[2] *National Research South Ural State University, Chelyabinsk, Russia*

THE ALDAN-MAADYR ZONE, WESTERN TUVA, RUSSIA: FORMATION CONDITIONS OF GOLD-QUARTZ VEINS IN LISTVENITES, CONGLOMERATES, AND BERESITES

Установлено три стадии образования золото-кварцевых жил на месторождениях Алдан-Маадырской зоны в Западной Туве: высоко-, средне- и низкотемпературная (>350 °С, 270–180 °С и <180 °С). Отмечается понижение пробности золота от высоко- к низкотемпературной стадии. На основании близкого изотопного состава кислорода в кварце исследованных месторождений и валового состава флюидных включений сделан вывод о единой гидротермальной системе, образовавшей месторождения в лиственитах, конгломератах и березитах.

The gold-quartz deposits of the Aldan-Maadyr zone in the Western Tuva are worthy of interest because they are located in the common geological structure but are hosted in different kinds of rocks (listvenites, conglomerates, and beresites). Their formation is considered to be related to the Devonian granitic magmatism [Zaykov et al., 1981]. The aim of the present work was an identification of

Table 1

Homogenization temperatures, salinity, salt composition of fluid inclusions and composition of gold for the studied deposits

Deposit	Homogenization temperature, °C	Salinity, wt % NaCl-eq	Major salts	Statistical groups of values of Th and salinity	Statistical groups of composition of gold	Gold fineness
Khaak-Sair, vein 7	248–211 (n 42) 231 (10)	7.5–14.2 (n 42) 11.0 (2.0)	NaCl–KCl–H_2O	1) 248–233, 14.2–12.9 2) 248–214, 12.6–7.5 3) 230–211, 13.1–11.7 4) 229–214, 11.3–8.9	1) Au 96.84–99.87, Ag 0.00–2.74, Cu 0.00–0.57 2) Au 91.98–95.08, Ag 4.46–7.81, Cu 0.00–1.30 3) Au 87.59–90.24, Ag 8.73–11.88, Cu 0.32–2.51 4) Au 85.30–87.00, Ag 12.59–13.94, Cu 0.00–1.38	853–999 941 (39)
Khaak-Sair, vein 2	188–124 (n 83) 152 (17)	4.0–8.2 (n 83) 5.9 (1.1)	NaCl–H_2O ± NaCl–KCl–H_2O	1) 188–167, 7.5–4.9 2) 168–147, 5.5–4.0 3) 161–150, 7.8–7.3 4) 151–129, 8.0–4.4 5) 137–124, 8.2–6.0	1) Au 91.92–94.09, Ag 4.63–9.37, Cu 0.00–0.47 2) Au 90.03–91.94, Ag 5.61–9.64, Cu 0.00–0.61 3) Au 99.30–99.80, Ag 0.00–0.57	867–998 925 (31)
Khaak-Sair, vein 1	233–188 (n 31) 213 (12)	3.2–5.2 (n 31) 4.0 (0.6)	NaCl–KCl–H_2O	1) 233–200, 3.2–4.9 2) 231–210, 4.0–4.6 3) 232–188, 3.5–5.2	1) Au 86.04–90.58, Ag 8.97–13.15, Cu 0–0.65 2) Au 68.67–74.64, Ag 24.83–30.97	687–906 832 (76)
Ulug-Sair, vein 18	357–295 (n 37) 323 (15)	6.0–9.6 (n 37) 7.9 (1.1)	$MgCl_2$–H_2O + NaCl–KCl–H_2O	1) 357–299, 7.3–8.8 2) 344–314, 6.0–6.6 3) 351–295, 7.3–9.6	1) Au 93.82–96.44, Ag 3.31–5.33 2) Au 90.94–92.83, Ag 7.08–8.68	909–964 936(21)
Ulug-Sair, vein 4	237–200 (n 23) 220 (9)	4.5–6.8 (n 23) 5.4 (0.7)	NaCl–KCl–H_2O + $MgCl_2$–H_2O	1) 237–200, 4.5–5.1 2) 231–226, 6.4–6.8 3) 223–201, 5.4–6.0	1) Au 89.89–94.94, Ag 6.37–8.27 2) Au 86.96–91.27, 9.32–12.2, Cu 0.00–0.69, Fe 0.00–0.34 3) Au 64.2–78.45, Ag 21.87–35.35, Cu 0.00–0.52, Fe 0.00–0.61, Te 0.00–0.86	642–949 841(104)
Ulug-Sair, vein 33	168–114 (n 51) 135 (13)	3.5–9.3 (n 51) 5.9 (1.4)	NaCl–KCl–H_2O + $MgCl_2$–H_2O ± NaCl–$Na_2B_5O_8$–H_2O	1) 168–148, 3.5–5.4 2) 152–114, 7.8–9.3 3) 141–120, 6.5–7.4 4) 140–115, 4.3–6.3	1) Au 93.49–91.71, Ag 7.70–5.99, Cu 0.37–0.19 2) Au 85.76–82.83, Ag 16.96–14.13, Cu 0.30–0.08 3) Au 88.11–85.45, Ag 14.38–11.6, Cu 0.33–0.16 4) Au 94.5–94.01, Ag 5.76–5.3, Cu 0.26–0.19	828–945 893 (39)
Aryskan	272–201 (n 44) 237 (18)	3.8–8.2 (n 44) 5.8 (1.0)	NaCl–KCl–H_2O	1) 264–201, 5.4–6.8 2) 272–205, 3.8–4.8 3) 257–210, 6.5–8.2	1) Au 90.16–93.12, Ag 6.59–9.43, Cu 0.16–0.35 2) Au 88.63–92.44, Ag 7.21–10.89, Cu 0.26–0.40 3) Au 84.05–87.22, Ag 12.59–15.66, Cu 0.15–0.31	841–931 907(21)
Duushkunnug	158–116 (n 56) 139 (10)	4.1–7.5 (n 56) 5.5 (0.8)	NaCl–KCl–H_2O + $FeCl_2$–H_2O	1) 158–146, 5.7–6.5 2) 158–138, 4.1–5.4 3) 142–128, 4.8–6.0 4) 145–116, 6.3–7.5	1) Au 90.32–93.15, Ag 6.92–9.12, Cu 0.00–0.08, Hg 0.00–0.08, Te 0.00–0.04 2) Au 89.44–91.95, Ag 7.59–10.28, Cu 0.16–0.30 3) Au 88.16–89.95, Ag 9.79–10.79, Cu 0.00–0.04, Hg 0.00–0.11, Te 0.00–0.04 4) Au 86.64–88.67, Ag 11.09–12.90, Cu 0.18–0.28	866–932 904 (16)

The maximum and minimum values are given in the numerator and the average value and standard deviation are given in the denominator. Major salt composition based on eutectic tempertaures is estimated after the method of Borisenko [1977].

similar and distinct formation conditions of these deposits based on study of chemical composition of gold, fluid inclusions and O isotopic analysis of gold-bearing quartz.

The Aldan-Maadyr zone 5–6 km wide extends up to 20 km in the east-northeastern direction and is situated in a junction of the Western Sayan with Tuvinian trough [Zaykov et al., 1981]. The area is hosted in Silurian and Ordovician sediments rumpled into the linear isoclinal folds, the cores of which contain the wedges of Cambrian basalts and ultramafic rocks. The major gold-quartz deposits are hosted in listvenites (Khaak-Sair), conglomerates (Ulug-Sair), beresites (Aryskan), and beresitized rhyolites (Duushkunnug).

The composition and fineness of gold, homogenization temperatures, salinity, and major salt composition of the primary fluid inclusions in gold-bearing quartz from the studied deposits are shown in Table 1. The results of the gas chromatography and bulk (ICP MS) analysis of fluid inclusions are given in Table 2. The oxygen isotopic composition was analyzed for the gold-bearing quartz from the Khaak-Sair, Ulug-Sair, and Aryskan deposits. The δO^{18} values range from +17.0 to +17.7 ‰ (up to 18.5 ‰ in a single analysis).

Based on the correlation of homogenization temperatures and salinity, we may conclude that gold-quartz veins were formed in several stages. Their formation began from the crystallization of the Ulug-Sair vein 18 from most high-temperature (> 350 °C) moderately saline (6.0–9.0 wt % NaCl-eq) fluids and deposition of gold with the least dispersion of fineness. The following stage is characterized by medium-temperature (272–188 °C) and moderately saline (3.2–8.2 wt % NaCl-eq) fluids, which form gold-quartz veins at the Aryskan deposit, Ulug-Sair vein 4, and the Khaak-Sair vein 1. The homogenization temperatures of the fluid inclusions in quartz from the Khaak-Sair vein 7 may also belong to this stage but the fluid inclusions demonstrate the highest salinity among the studied veins (Table 1). The gold fineness from the medium-temperature veins is similar for the Khaak-Sair vein 7 and Aryskan deposits and for the Khaak-Sair vein 1 and Ulug-Sair vein 4. The low-temperature (188–114 °C) moderately saline (3.5–9.3 wt % NaCl-eq) stage of formation of gold-quartz veins was manifested at the Ulug-Sair vein 33, Khaak-Sair vein 2, and Duushkunnug deposit. The gold fineness of the low-temperature veins is similar (Table 1). As is seen from Table 1, in most cases, the number of statistical groups of gold composition and fluid inclusion data coincide that reflects the pulsating gold-quartz deposition while temperature decrease, which is also supported by gold grains zonal by Ag and Cu.

The higher (up to 14 wt % NaCl-eq) salinity of the fluids identified in the Khaak-Sair quartz and a wide development of tourmaline and auxinite both in the deposits and at the contacts with the nearest intrusive bodies may indicate magmatic contribution to the mineral formation. This is comparable to the Berezovskoe and Kochkar gold-quartz in the Urals associated with porphyry granites [Baksheev et al., 1998; Prokof'ev and Spiridonov, 2005]. These deposits also show higher saline (up 17 and 15.7 wt % NaCl-eq, respectively) fluids with dominant NaCl composition and admixture of $MgCl_2$ similar to the Tuvinian deposits.

The bulk composition of fluid inclusions has revealed the broad elements related to the ore-forming fluid (Table 2). Only Zn, Bi, Sn, Hg и Tl shows minor contents. Three groups of elements may be distinguished on the basis of the correlation analysis. The first group includes Cl and Na, which have strong positive correlation with H_2O content in quartz. The second group consists of B, As, and Sb, which are negatively correlated with Cl and Na, that may probably reflect the mixing of fluids of different composition. It is important all correlations are characteristic both of each deposit and the entire Aldan-Maadyr zone that supports an idea on the same type of the hydrothermal system for the reviewed deposits.

The third group includes K, Mg, Ca, and carbon-bearing gases. The contents of precious metals (Au and Ag) correlate precisely with elements of this group that may indicate their certain relation to the ore formation. The correlation between Au and CO_2/CH_4 ratio (a degree of the fluid oxidation) may testify to the fluid oxidation as one of the reasons of gold deposition.

The CO_2/H_2O ratio (relative content of the gaseous phase), which indirectly reflects the pressure and erosion level of the ore-forming system, respectively, increases towards the west and is maximum at the westward Khaak-Sair deposit, which geological structure is mostly eroded. This deposit is also distinct by elevated contents of As, B, Sb, Pb, Cd, W, Mo and presence of minor amounts of Bi, Zn, Hg. This is in accordance with occurrence of different kinds of fahlores, tourmaline, auxinite, galena, arsenopyrite, gersdorffite, bismuthinite, cinnabar, and sheelite in veins and listvenites. The high Cu contents in the fluid at the Ulug-Sair deposit may be correlated to the wide development

Table 2

Average contents of fluid components in quartz from the studied deposits

Component	KS (4)	US (4)	A (1)		Component	KS (4)	US (4)	A (1)
Major components, mg/kg quartz					Trace elements, mkg/kg quartz			
H_2O	871	1955	1544		Li	4.0	3.8	5.4
CO_2	127.0	114.3	37.0		Rb	1.2	1.0	1.2
CH_4	0.21	0.11	0.30		Cs	0.3	0.4	0.7
Cl	0.91	6.48	6.59		Sr	56.0	57.0	97.2
HCO_3^-	14.0	25.0	56.0		Sb	9352.7	18.2	0.0
Na	4.08	13.51	21.34		Ge	0.1	0.1	0.2
K	0.78	0.69	0.81		Cu	1.3	178.6	73.3
Ca	2.29	0.45	2.68		Cd	2.8	0.2	0.3
Mg	0.35	0.14	0.69		Pb	43.6	0.3	0.3
B	0.92	0.48	0.32		Au	0.08	0.07	0.16
Ba	1.13	0.37	0.54		Ag	2.8	0.1	4.8
As	0.69	0.16	0.16		Mo	8.2	3.1	4.5
Molar ratios					W	19.4	1.9	0.0
CO_2/H_2O	0.06	0.02	0.01		Co	0.2	0.1	0.7
CO_2/CH_4	223	370	44		Ni	2.9	7.6	2.2
Cl/HCO_3^-	0.11	0.45	0.21		Cr	0.5	0.0	1.4
B/Cl	3.22	0.24	0.15		Mn	9.5	16.9	54.2
Na/Cl	6.9	3.2	4.9		Fe	35.9	4.3	28.7

Gas chromatography and bulk analysis are carried out in TsNIGRI, Moscow, analyst Yu. V. Vasyuta. Deposits: KS (Khaak-Sair), US (Ulug-Sair), A (Aryskan). The number of analyses is given in brackets.

of chalcopyrite in the quartz veins. The higher concentrations of HCO_3^-, K, Ca, Mg, Mn, and Sr in quartz from the Aryskan deposit probably reflect beresite-type of alteration.

The narrow range of the oxygen isotopic composition in quartz from the studied deposit, which is similar to that from many world gold deposits, indicates (i) the common sources of the fluids, (ii) no isotopic exchange with host rocks, (iii) homogeneous isotopic system, and (iv) similar formation temperatures [Kerrich, 1987; Goldfarb et al., 1991; Jia and Kerrich, 2001]. The latter conclusion is well demonstrated by the overlapped homogenization temperatures at the studied deposits. The oxygen isotopic composition of quartz from the Tuvinian deposit is close to that from the metamorphic or sedimentary source [Taylor, 1974; Faure, 1989; Hoefs, 2009]. The $\delta^{18}O_{H2O}$ values of 10.02–11.51 ‰ calculated from the equation $1000 \ln \alpha = 3.38 (10^6 T^{-2}) - 3.40$ at 300 °C [Clayton et al., 1972] correspond to the metamorphic water. Similar $\delta^{18}O_{H2O}$ values of the fluids and their narrow variations are typical of many gold deposits in sedimentary sequences [Goldfarb et al., 1991]. The origin of the fluids at these deposits is considered to be related with progressive metamorphic dehydration and degassing of the host rocks. In case of Tuvinian deposit, we may suggest that the source of Si-O compounds in the fluids were the Precambrian metamorphic rocks presently occurred in the northern wall of the Sayan-Tuva fault.

The work is supported by the RFBR (project no. 11-05-00187-a).

References

Baksheev, I.A., Prokof'ev, V.Yu., Ustinov, V.I. Formation conditions of the vein quartz from the Berezovskoe gold field, Central Urals, based on study of fluid inclusions and isotopic data // In: Urals summer mineralogical school-98. Yekaterinburg, UGGGA, 1998. P. 41–49 [in Russian].

Borisenko, A.S. Study of salt composition of solutions of fluid inclusions in minerals with cryometry // Geologiya i Geofizika, 1977. Vol. 8. P. 16–27 [in Russian].

Prokof'ev, V.Yu., Spiridonov, E.M. Composition of metamorphic fluids and transformation conditions of the Kochkar gold deposit, South Urals // In: II All-Russ. Petrographic Conf. Syktyvkar, 2005. Vol. 3. P. 88–90 [in Russian].

Faure, G. Principles of isotope geology. 2nd edition. John Wiley and Sons, Inc., NY, 1986.

Clayton, R.N., O'Neil, J.R., Mayeda, T. Oxygen Isotope Exchange between Quartz and Water // J. Geophys. Res., 1972. Vol. 77. No. 17. P. 3057–3067.

Jia, Y., Li I., Kerrich, R. Stable isotope (O, H, S, C, and N) systematics of quartz vein systems in the turbidite-hosted central and north Deborah gold deposits of the Bendigo gold field, Central Victoria, Australia: constraints on the origin of ore-forming fluids // Economic. Geology, 2001. Vol. 96. P. 705–721.

Hoefs, J. Stable isotope geochemistry. Springer, 2009. 285 p.

Goldfarb, R.J., Newberry, R.J., Pickthorn, W.J., Gent, C.A. Oxygen, hydrogen, and sulfur isotope studies in the Juneau gold belt, Southeastern Alaska: constraints on the origin of hydrothermal fluids // Economic Geology, 1991. Vol. 86. P. 66–80.

Kerrich, R. The stable isotope geochemistry of Au-Ag vein deposits in metamorphic rocks // In: Mineralog. Assoc. Canada Short Course Handbook, 1987. Vol. 13. P. 287–336.

Taylor, H. P. The application of oxygen and hydrogen isotope studies to problems of hydrothermal alteration and ore deposition // Economic Geology, 1974. Vol. 60. P. 843–883.

Zaykov, V.V, Lebedev, V.I., Tyul'kin, V.G. et al. Ore complexes of Tuva. Novosibirsk, Nauka, 1981 [in Russian].

K. Novoselov[1], E. Belogub[1], A. Frolov[2], A. Mikhailov[3], P. Khvorov[1]
[1] *Institute of Mineralogy UB RAS, Miass, Russia, const@ilmeny.ac.ru*
[2] *Institute of Geology KRC RAS, Petrozavodsk, Russia*
[3] *Mineral Exploration Network Ltd., Tuupovaara, Finland*

GOLD MINERALISATION IN PIILOLA AREA (EAST FINLAND)

Рассмотрена геологическая позиция и минералогия рудопроявлений золота площади Пиилола (Восточная Финляндия). Площадь находится в пределах зеленокаменного пояса Кухмо в архейском домене Фенноскандинавского щита. Минералогия руд характеризуется преобладанием пирротина и арсенопирита; золото выявлено в самородной форме и в форме мальдонита. В ассоциации с золотом часто наблюдается самородный висмут.

Komatiite-hosted Ni, VMS, and orogenic gold are the most common metallogenic components in Archaean greenstone belts. Canadian shield, Western Australia and other Archaean areas have well-known examples of orogenic gold deposits.

The main Au provinces in Finland are the Archaean greenstones in the east of Finland, Palaeoproterozoic greenstone belts in Lapland, and the Palaeoproterozoic Svecofennian schist belts in central and southern Finland. About 200 hard-rock gold occurrences are presently known.

These are short results of investigations of the Piilola area which is located in the Kuhmo greenstone belt in Eastern Finland. Works are carried out by Mineral Exploration Network (Finland) Ltd. Geophysical, geochemical methods, and drilling have been used.

The Finnish part of the Fennoscandian shield comprises three major domains. There are the Archaean cratonic nucleus (Karelian domain) and the Paleoproterozoic mobile belts of Kola-Lapland and Svecofennia.

The Archaean bedrock can be subdivided into TTG-type complexes, and a few major supracrustal belts: Oijarvi, Kuhmo-Suomussalmi and Ilomantsi. The Kuhmo-Suomussalmi volcanosedimentary complex (Kuhmo, Suomussalmi and Tipasjarvi greenstone belts combined) was probably formed in an intra-plate, oceanic environment [Lahtinen et al., 2011]. Its central part (the Kuhmo greenstone belt) has a symmetrical syncline structure with a submeridional trend. The most voluminous rocks are mafic volcanic rocks [Papunen et al., 2009]. Several phases of the Archaean TTG granitoids have intruded the greenstone belt.

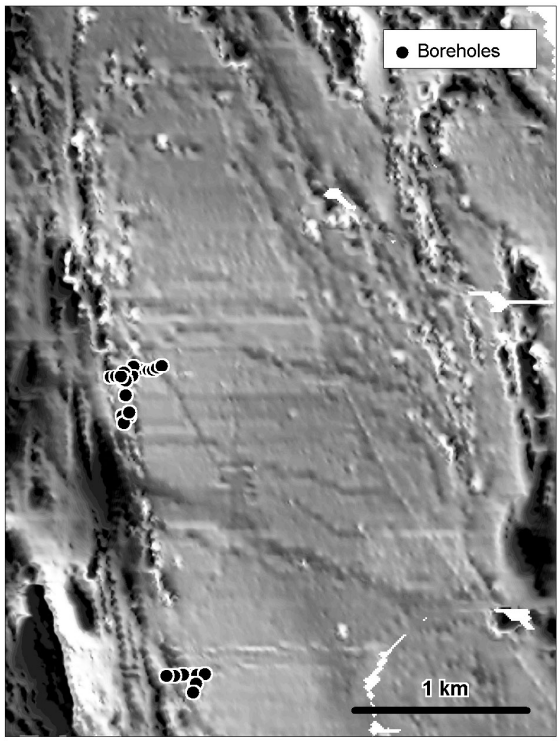

Fig. The map of magnetic field of studied area and boreholls position.

A number of drilling-indicated gold occurrences has been identified in the Kuhmo greenstone belt. On the basis of mineral assemblages in the gold occurrences and their host and adjacent rocks, the degree of regional metamorphism is from upper-greenschist to lower-amphibolites facies.

The Piilola area joins Piilola, Jousijarvi, Licasuo, Aittoranta, and some other occurrences.

Next greenstone rocks succession was observed in the Jousijarvi occurrence (from the west to the east):

1. Ultramafic rocks transformed to serpentinites, talk-carbonate, tremolite rocks. Aittoranta occurrence is hosted by these rocks.
2. Biotite schists with pyrrhotite dissemination.
3. Quartz-plagioclase schists.
4. Gneissic biotite-quartz-plagioclase rocks.
5. Biotite schists with pyrrhotite and arsenopyrite dissemination. These schists are ore-hosted for Piilola, Licasuo and Jousijarvi occurrences.
6. Gneissic biotite-quartz-plagioclase rocks.

Ore field structure has submeridional trend and subvertical dip. It is complicated by Palaeoproterozoic gabbro dykes with NW-trending. Magnetic and electric methods do show the structural features of the area, including those which control gold mineralisation (fig.).

The main ore minerals are, in a decreasing order of abundance, pyrrhotite, arsenopyrite, and pyrite. Only in a few locations, arsenopyrite forms visible grain aggregates. Chalcopyrite and pentlandite commonly occur as intergrowths together. Native gold has been observed at Piilola, Jousijarvi, and Mujesuo, and is predominantly associated with arsenopyrite. Native bismuth has been detected in the ore at Piilola, Mujesuo, and Jousijarvi. Native gold forms inclusions in arsenopyrite and silicate minerals. Inclusions in chalcopyrite or pyrrhotite are rare (e.g. Mujesuo). In spite of obvious structural relation between gold and arsenopyrite the Au-As correlation is not strong.

Till geochemistry shows an As and Au dispersion halo in the area.

It is suggested that Intrusion related gold system (IRGS) in combination with the previously applied orogenic shear zone hosted exploration model could be applied to the area of study.

References

Lahtinen R., Holtta P., Kontinen A., Niiranen T., Nironen M., Saalmann K., Sorjonen-Ward P. Tectonic and metallogenic evolution of the Fennoscandian shield: key questions within emphasis on Finland // Geol. Surv. Finland Spec. Pap. 49, 2011. P. 23–33.

Papunen H., Halkoaho T., Luukkonen E. Archaean evolution of the Tipasjarvi-Kuhmo-Suomussalmi greenstone complex, Finland // Geol. Surv. Finland Bull. 403, 2009. 68 p.

E.E. Palenova, E.V. Belogub, V.A. Kotlyarov, I.A. Blinov
Institute of Mineralogy, UB RAS, Miass, palenova@mineralogy.ru

FLORENCITE FROM KOPYLOVSKOE AND KAVKAZ GOLD DEPOSITS (BODAYBO ORE REGION, RUSSIA)

Флоренсит – главный минерал-концентратор РЗЭ на золоторудных месторождениях Копыловское и Кавказ (Бодайбинский район), локализованных в углеродистых терригенных породах. Образует идиоморфные кристаллы размером 0.1–1 мм, характеризуется оптической и химической зональностью, обусловленной главным образом примесью Ca и Fe. По составу РЗЭ флоренсит месторождения Копыловское отвечает схеме Ce>La>Nd, Кавказа – Ce>Nd>La. Наблюдаются вариации в содержании Th. Спектры распределения РЗЭ во флоренсите и вмещающих углеродистых породах сходны. Вероятно, флоренсит образовался в процессе катагенеза начальной стадии метаморфизма, при этом источником фосфора могло служить рассеянное органическое вещество, РЗЭ – глинистые минералы.

Introduction and geological setting. The Bodaibo ore region is located in the Patom highland and belongs to the northeastern part of Irkutsk administrative region, which is well-known as the largest gold placer province in Russia. The gold deposits in the Bodaibo ore region are confined to two main ore blocks: Kropotkin block with disseminated and veinlet deposits (e.g., Sukhoi Log deposit) and Artemovsky block with quartz vein deposits. The Kopylovskoe and Kavkaz deposits are located in the latter block and are confined to the near-latitudinal anticline fold composed of the rocks of the Dogaldyn Formation [Bendyuk et al., 1984; Ivanov, 2008].

The host rocks of both deposits include arkose and graywacke-arkose metasandstones, metasiltstones, and carbonaceous-clayey and clayey shales. The host rocks were metamorphosed under sericite-chlorite subfacies of green-schist facies and also are hydrothermally altered [Palenova et al., 2011]. Quartz, feldspar, muscovite, illite, chlorite, paragonite, and carbonates (breinerite, siderite, dolomite and rare calcite) are major minerals of the host rocks. Carbonates are observed as zonal euhedral crystals and concretions, which indicate their postsedimentary origin. Pyrite is a major ore mineral. Chalcopyrite, pyrrhotite, galena, and sphalerite are minor ore minerals. Gold forms free grains and inclusions in pyrite. Allotigenic tourmaline, apatite, zircon, monazite, and allanite form rounded or clastic grains. Florencite occurs in all types of host rocks but its maximal concentration is typical of the highly pyritized gold-bearing carbonaceous-clayey shales. In sandstones, florencite is found in clasts of carbonaceous shales.

Florencite was described as a typical accessory mineral of gold-bearing black shales of the Patom plateau [Buryak, 1998]. The placer gold from the Predpatom Mountains contains inclusions of florencite and monazite [Glushkova, Nikiforova, 2011]. However, in spite of numerous references, florencite from the Bodaibo region has not characterized yet.

Results. Florencite is observed as zonal and sectorial light yellow to brown (rarely greenish) sharp rhombohedral crystals 0.01–0.02 mm (up to 1 mm) in size or grains without crystal shape. The pores and inclusions of carbonaceous matter trace the boundaries between the growth sectors. Florencite hosts inclusions of monazite and zircon. Occasionally, goyazite $SrAl_3(PO_4)(HPO_4)(OH)_6$ epitaxially grows on florencite.

The chemical composition of florencite was studied using a SEM equipped with EDA. Florencite from both deposits have similar composition and belong to florensite $(Ce,La,Nd)Al_3(PO_4)_2(OH)_2$–crandallite $CaAl_3(PO_4)_2(OH)_2$ isomorphic series. The optical and chemical zoning in mineral coincide (Fig. 1). The zones enriched in Fe and Ca are porous. Florencite from the Kopylovskoe deposit is characterized by a Ce>La>Nd trend, admixtures of Th, Sr, rarely Pb and As, and inclusions of monazite in contrast to Ce>Nd>La trend and absence of Pb and As in florencite from the Kavkaz deposit.

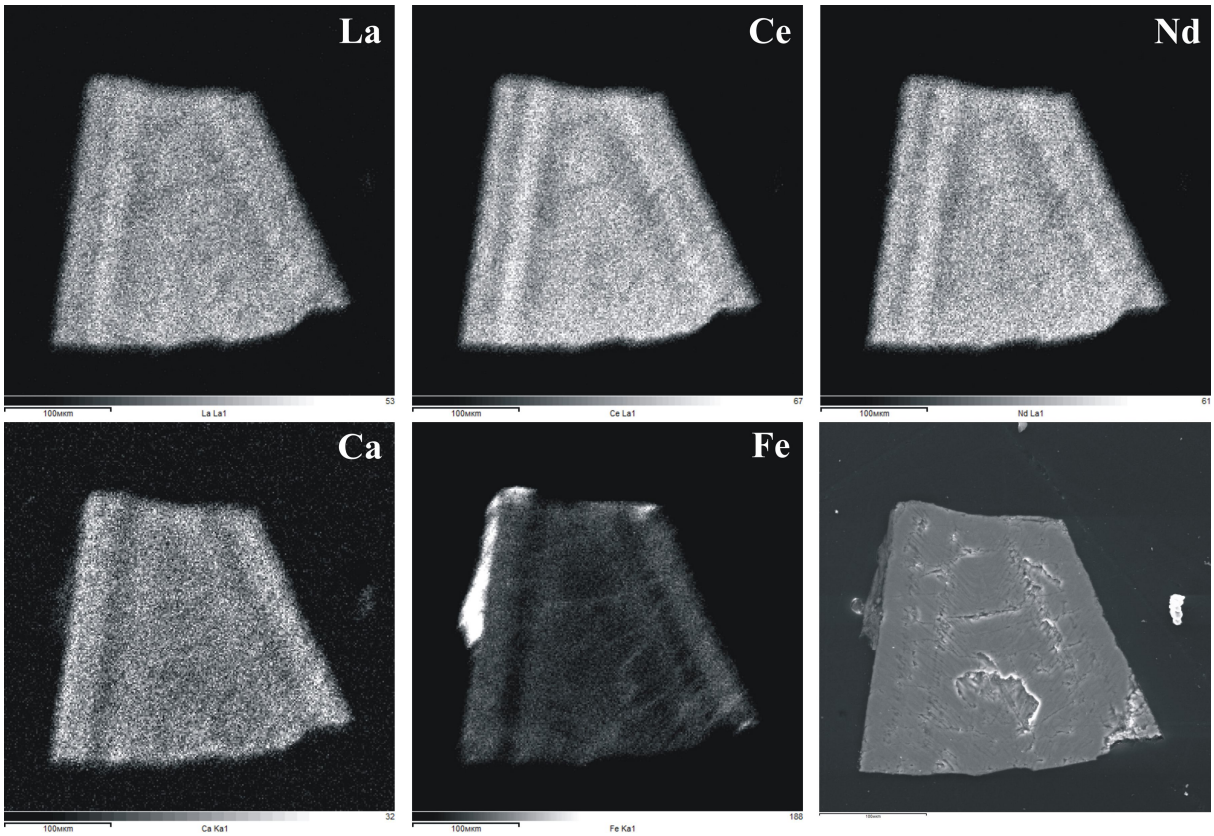

Fig. 1. Microgeochemical maps of florencite (SEM VEGA3 TESKAN, analyst I.A. Blinov).

The REE distribution in monazite (Ce>La>Nd>Pr) from the Kopylovskoe corresponds to those of florencite. Monazite also has Sr admixture.

The significant positive correlation for Ce–La, Ca–Th, Fe–Ca, and Fe–Th and negative correlation between Sr and REE (Ce, La, Pr) are typical of florencite from the Kopylovskoe deposit. Similar tendencies and negative correlation for Sm–Ce and Sm–La were found for florencite from the Kavkaz deposit.

The chondrite-normalized REE patterns of florencite from both deposits and monazite inclusion from florencite have similar configuration with a weak Pr maximum (Fig. 2). All rock types enriched in LREE. The maximum and minimum REE contents are characterized of the lamprophyre dikes and quartz veins, respectively. The lowest LREE and HREE fractionation is characterized of the clayey shales. The REE pattern of florencite is most similar with ones for the carbonaceous shales.

Discussion. Florencite is autigenic mineral in the carbonaceous shales that is evident from its crystal shape and absence of crushed clasts, cutting of zoning, and carbonaceous inclusions.

The host shales are the probable source of elements for florencite. The P content in the Dogaldyn Formation is ~0.05 %. All sedimentary rocks host apatite as the rolled grains and crystal fragments. Thus, the source of phosphorous for florencite was an organic matter, which released this element during transformation of carbonaceous shales. The exchange complex of clayey minerals is most likely source of REE: the enrichment of clays in REE is well known [Yudovich, Ketris, 1994]. The catagenesis and early metamorphism result in transformation of clayey minerals into mica and chlorite, involving of REE in porous solutions, and their further precipitation as proper minerals. The REE are located in the large XII-coordinated site that leads to the broad isomorphic ability. Similarity of LREE chemical features allows their joint occupation of the appropriate crystal site. The REE ratio in florencite completed correspond to the REE ratio of mineral-forming media.

Florencite contains Ca and Fe admixtures, which have negative correlation with REE. In general isomorphism scheme, the cation sublattice of florencite is as follows [after Silaev et al., 2001]:

$REE^{3+} \leftarrow Ca^{2+}$ ($\Delta r = 1 – 5$ %; $\Delta = 11$ %);

$REE^{3+} \leftarrow Sr^{2+}$ ($\Delta r = 14 – 18$ %; $\Delta = 20$ %);

$Al^{3+} \leftarrow Fe^{3+}$ ($\Delta r = 18$ %; $\Delta = 7$ %);

where Δr is the ion radius difference, and Δ is the difference of electronegativity.

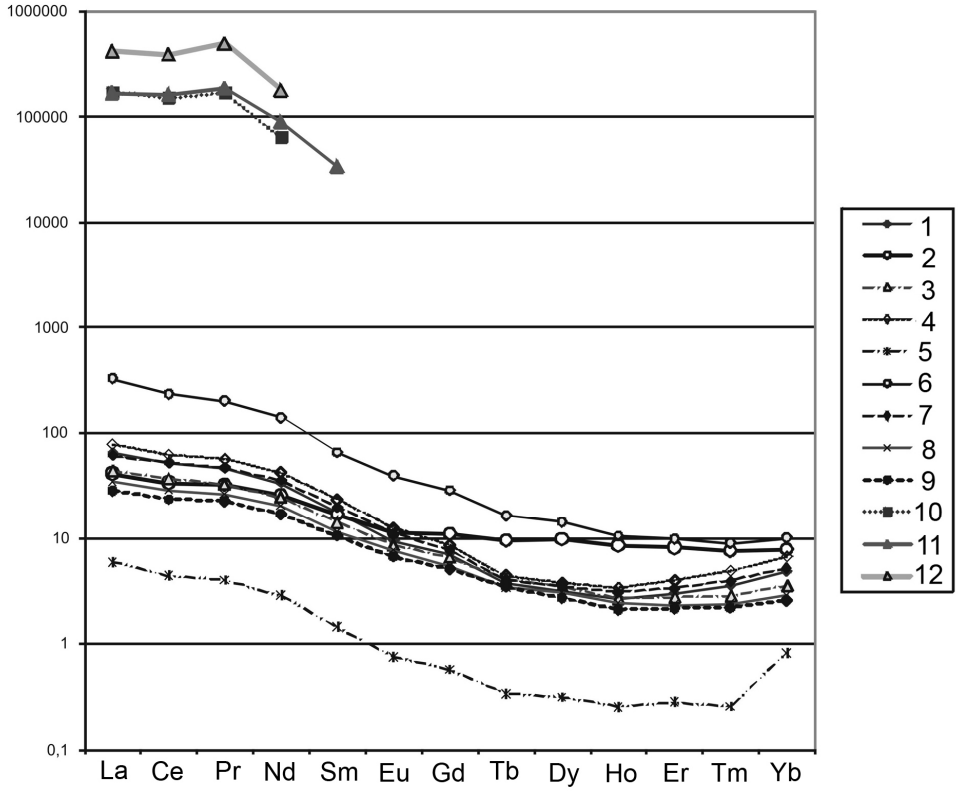

Fig. 2. REE spectra of various rocks from the studied region. Graphics are based on the chondrite-normalized average contents.

Kopylovskoye (1-6, 9-10, 12) and Kavkaz (7, 8, 11) deposits. Black shale (1, 7); clay shale (2); sandstones (3, 8); stockwork (4); quartz veins (5); lamprophyre (6); carboniferous sandstone (9); florencite-(Ce) (10, 11); monazite (12).

The substitution in the cation sublattice is accompanied by anion substitution according to $[PO_4]^{3-} \leftarrow [PO_3OH]^{2-}$ scheme [Somina, Bulakh, 1966].

Ca, Sr and Fe enter the florencite lattice jointly. This association compensates the geometrical deformation of the structure. Probably, the process begins owing to Al deficit in the mineral-forming medium. Al presence in the $2M_1$-mica structure (muscovite and paragonite). At the same time, the Fe content in the porous solution after sedimentation is enough to form the Fe-bearing carbonates (brennerite, siderite) and pyrite. So, some part of iron may represent Fe^{3+}, which may be included into florencite. Fe^{3+} comparatively expands the lattice, as well as Ca^{2+} and Sr^{2+}. The local structural heterometry between REE- and Ca-enriched zones leads to formation of pores.

The Th enrichment of florencite should also be noted. The Th and U content in carbonaceous clastic Dogaldyn Formation at the Kopylovskoe and Kavkaz deposits varies from 1.50 to 13.51 ppm (6.37 ppm, on average) and from 0.30 to 10.89 ppm (1.69 ppm, on average), respectively. The Th/U ratio is 0.70–8.82 (4.75, on average). Typically, the Th/U ratio for carbonaceous sediments (about 2.5) is lower because of the U sorption by organic matter [Yudovich, Ketris, 1994]. The chemical properties of Th are similar to LREE, in particular, to Ce. Thus, the clayey minerals adsorb Th together with REE [Yudovich, Ketris, 1994]. Th, as well as U, also forms water-insoluble complexes with organic acids [A review…, 2008]. During catagenesis, Th is included into florencite along with LREE. During metamorphism, U and Th are extracted from sediments, however, Th compounds are more stable than U ones at green-schist facies [Ermolaev, Sozinov, 1986]. The Th-Si positive correlation may be related to the inclusions of thorite.

We are not able now to distinguish the influence of crystal-chemical and geological factors on REE fractionation based on analysis of REE distribution in florencite and host rocks. However, we may state that the REE composition of catagenic and low-grade metamorphic florencite is inherited from that of primary sediments. Increase in temperature leads to the formation of anhydrous REE

phosphates such as monazite and xenotime, which concentrate LREE and HREE, respectively. Thus, no significant fractionation of LREE and HREE occur during initial metamorphism.

Conclusions. Florencite from the gold-enriched black shales of the Kopylovskoe and Kavkaz deposits in the Bodaibo region belongs to Ce variety with Ce>La>Nd and Ce>Nd>La trends for the Kopylovskoe and Kavkaz deposits, respectively. Florencite is enriched in Pr and Th. Florencite from the studied deposits is optically and chemically heterogeneous. Postsedimentary formation of florencite is confirmed by euhedral crystal shape and absence of cutting of zoning. The crystallization of florencite occurred during catagenesis and initial metamorphism of sediments. The dispersed organic matter was the source of phosphorous. The catagenic transformation of clayey minerals into mica and chlorite leads to extraction of REE into porous solution and further to formation of florencite that was expressed in similar REE spectrum of florencite and host rocks.

Acknowledgments. *The authors are sincerely grateful to M. Malyarenok, T. Semenova, and Yu. Melnova (IMin UB RAS) for chemical analyses and to S. Repina (IMin UB RAS) for useful advices. The field works were supported by OOO Kopylovskoe.*

References

Mernagh, T.P., Miezitis, Y. A review of the geochemical processes controlling the distribution of thorium in the earth's crust and Australia's thorium resources. Geoscience Australia, 2008. 48 p.

Benedyk, V.F., Zhukovich, M.A., Suslov, N.A. Report on exploration work in gold-bearing rocks in the Kavkaz area in 1982–1984. Irkutsk, 1984 [in Russian].

Buryak, V.A., Bakulin, Yu.I. Metallogeny of gold. Vladivostok, Dal'nauka, 1998. 369 p. [in Russian].

Ermolaev, N.P., Sozinov, N.A. Stratiform mineralization in black shales. Moscow, Nauka, 1986. 174 p. [in Russian].

Glushkova, E.G., Nikiforova, Z.S. Forecast of primary source of gold at the Urinsky anticline (Predpatom Mountains) // II Intern. Mining Geol. Forum. Magadan, 2011. P. 165–169 [in Russian].

Ivanov, A.I. The Ozherel'e deposit is a new kind of primary deposits in the Bodaibo ore region // Geology, search and prospection for ore deposits. Irkutsk, ISTU. Vol. 6 (32). 2008. P. 14–26 [in Russian].

Palenova, E.E., Belogub, E.V., Novoselov, K.A., Kotlyarov, V.A. The host rocks of the Kopylovskoe gold deposit (Bodaibo ore region) // Metallogeny of ancient and modern oceans–2011. Miass, IMin UB RAS, 2011. P. 169–173 [in Russian].

Silaev, V.I., Filippov, V.N., Sokerin, M. Yu. Solid solutions of woodhouseite-svanbergite-florencite in secondary quartzites // ZRMO, 2001. No. 1. P. 99–110 [in Russian].

Somina, M.Ya., Bulakh, A.G. Florencite from carbonatites of the East Sayans and some problems of chemical structure of the crandallite group // ZRMO, 1966. No. 5. P. 537–550 [in Russian].

Yudovich, Ya.E., Ketris, M.P. Trace elements in black shales. Yekaterinburg, UIF Nauka, 1994. 304 p. [in Russian].

J. Pique[1], J. Skarmeta[2]

[1] CODES, University of Tasmania, Hobart, Australia, Jose.PiquerRomo@utas.edu.au

[2] Gerencia de Exploraciones, CODELCO Chile, Santiago, Chile

STRUCTURAL GEOLOGY OF THE RIO BLANCO – LOS BRONCES DISTRICT, CENTRAL CHILE: CONTROLS ON STRATIGRAPHY, MAGMATISM AND MINERALIZATION

На основе геологического картирования в масштабе 1:25000 гигантского медно-порфирового узла Рио-Бланко–Лос Брончес, локализованного в Чилийском домене Высоких Анд, представленном эоценовыми и плиоценовыми вулканитами, воссоздана история геологического развития региона, включающая эволюцию внутридугового бассейна с переходом от режима растяжения к режиму сжатия. Приводятся результаты определения относительного и абсолютного возраста интрузивных пород, тектонических разломов и ассоциирующей с ними минерализации.

Introduction

The high Andes of central Chile and Argentina (32–35°S) can be divided into two major geological domains. The eastern domain exposed close to and to the east of the international border, is composed of strongly deformed marine and continental sedimentary rocks of Jurassic to Early Cretaceous age which constitutes the Aconcagua fold and trust belt [Ramos, 1996]. The western (Chilean) domain is composed of volcanic rocks of Eocene to Pliocene age which were erupted during the evolution and inversion of an intra-arc volcano-tectonic basin. They have been grouped in the syn-extensional Abanico Formation and the syn-inversion Farellones Formation [Charrier et al., 2002 and references therein]. Our study has focused on the evolution of the western domain, with an emphasis on the district of the giant Rio Blanco-Los Bronces porphyry Cu-Mo cluster, and is based on the results of a recently finished 1:25.000 geological mapping program [Piquer, 2010], which covers the entire Rio Blanco-Los Bronces district. This new district-scale geological map was used to prepare four E-W cross-sections, with the southernmost one passing through the mineral deposits. They provide the basis for a new model of the tectonic evolution of this part of the Andes that aims to clarify the first-order controls on stratigraphic changes, magmatic activity and associated mineralization.

Tectonic evolution

Upper Eocene – Lower Miocene extension. This period is associated with the development of an intra-arc volcanotectonic basin. The main basin-margin normal faults (Pocuro and Alto del Juncal – El Fierro faults) are N-oriented, and the area within them was completely covered by the products of the Abanico Formation, but our cross-sections show strong changes in thickness (from 2 to 5 km) and volcano-sedimentary facies, both factors indicative of the presence of various sub-basins and depocenters, which are bounded by NNW and NE-oriented internal normal faults. The associated stress field was that of an E-W extension and the ascent of magma to the surface was favoured by the existence of several deep-tapping extensional structures. From 34 to 22 Ma as much as 5 km of volcanic rocks were deposited in the basin, with no coeval plutonic bodies recognized.

Tectonic inversion and plutonism since the Lower Miocene. During this period, the high angle (~60–65°) NW-NNW and N-trending faults were reactivated in reverse-sinistral and reverse mode respectively, with associated folding of the nearby Abanico and sometimes Farellones Formation. This implies that, before their movement, supra-lithostatic pressures were achieved, as evidenced by abundant dilatational, sub-horizontal sills of Miocene age cropping out in the study area. Under this compressional tectonic regime, NE-trending faults were reactivated mainly as dextral strike-slip faults, with variable although generally minor dip-slip reverse movements. This selective reactivation of pre-existing normal faults with different orientations has produced the present-day structural architecture, whereby sub-basins are bounded by high-angle faults, each one with its own thickness of local volcano-sedimentary facies, intensity of folding and exhumation level. By correlating data from the Argentinean flank of the Andes [Ramos, 1996; Giambiagi, 2003] with earthquakes hypocenters and the inferred location of Mesozoic evaporites, the existence of three main Miocene detachment levels beneath the Rio Blanco-Los Bronces district is proposed. Tectonic inversion was coeval with the deposition of the Farellones Formation, which differs markedly from the Abanico Formation in that it is restricted to specific volcanic centres and reaches a maximum thickness of only 1.5 km. The basal units of the Farellones Formation were deposited in progressive unconformities over the Abanico Formation, and have been dated at 22.7±0.4 Ma (U-Pb SHRIMP age [Piquer, 2010]). Plutonic activity was contemporaneous with Farellones Formation volcanism. The main intrusive complex in the area, the Rio Blanco-San Francisco Batholith, was emplaced between 20.1 and 4.69 Ma [Deckart et al., 2005, 2013]. The units dated between 20.1 and 8.16 Ma are coarse equigranular plutonic rocks, while those with ages between 7.12 and 4.69 Ma are subvolcanic rocks directly associated with hydrothermal activity and mineralisation. The host rocks of these subvolcanic complexes are the older equigranular plutons. This implies that in the 1 Ma period between 8.16 and 7.12 Ma this area was affected by a violent exhumation event, unroofing the older, plutonic rocks and exposing them to the subvolcanic environment, with porphyries and breccias being fed by a deeper, unexposed magma chamber. Given the characteristics and erosion level of the Rio Blanco deposit, this magma chamber is inferred to have been localized between 5–7 km below the present surface [e.g., Proffett, 2009; Sillitoe, 2010]. This depth coincides well with the uppermost of the three detachment levels and also with a notable area of low Vp/Vs in seismic tomography, which we speculate correlates with the very young (<4 Ma) crystalline rocks of the deep magma chamber that solidified after volatile exsolution and formation of the Rio Blanco-Los Bronces deposit.

Intrusive contacts, porphyry dikes, hydrothermal breccias and mineralized veins, all show clear NNW and NE preferred orientations, indicating that pre-existing normal faults inherited from the extensional period channelled the ascent and emplacement of magma and hydrothermal fluids during the compressive stage. Statistically, there is an overwhelming predominance of NE and NNW-NW fault planes; N-trending faults, parallel to the orogen, are statistically insignificant and restricted to the eastern margin of the Abanico basin. The abundance of syn-tectonic hydrothermal minerals confirms that fault inversion occurred under high fluid pressures, as it can be inferred by the slip plane infilling of minerals such as epidote, chlorite, tourmaline, quartz, calcite and Cu-Fe sulphides. Given the high dip angle of the faults (60–0°), the compressive tectonic regime and the presence of hydrothermal fluids during faulting, the required conditions for reactivating severely disoriented faults, such as supralithostatic fluid pressures, are met [Sibson, 1985].

This study is based on research done by CODELCO through its subsidiary Exploraciones Mineras S.A. (EMSA), and both companies are thanked for allowing the dissemination of these results. Most of the hypocenter location data used in this work was captured during the Ring Project ACT N°18 carried out by the University of Chile and CODELCO.

References

Charrier, R., Baeza, O., Elgueta, S., Flynn, J.J., Gans, P., Kay, S.M., Munoz, N., Wyss, A.R. and Zurita, E. Evidence for Cenozoic extensional basin development and tectonic inversion south of the flat-slab segment, southern Central Andes, Chile (33 degrees-36 degrees SL) // Journal of South American Earth Sciences, 2002. Vol. 15. P. 117–139.

Deckart, K., Clark, A.H., Aguilar, C., Vargas, R., Bertens, A., Mortensen, J.K. and Fanning, M. Magmatic and hydrothermal chronology of the giant Rio Blanco porphyry copper deposit, central Chile: Implications of an integrated U-Pb and Ar-40/Ar-39 database // Economic Geology, 2005. Vol. 100. P. 905–934.

Deckart, K., Clark, A., Cuadra, P. and Fanning, M. Refinement of the time-space evolution of the giant Mio-Pliocene Rio Blanco-Los Bronces porphyry Cu-Mo cluster, Central Chile: new U-Pb (SHRIMP II) and Re-Os geochronology and 40Ar/39Ar thermochronology data // Mineralium Deposita, 2013. Vol. 48. P. 57–79.

Giambiagi, L.B., Ramos, V.A., Godoy, E., Alvarez, P.P. and Orts, S. Cenozoic deformation and tectonic style of the Andes, between 33 degrees and 34 degrees south latitude // Tectonics, 2003. Vol. 22. 1041. doi:10.1029/2001TC001354.

Piquer, J. Geologia del Distrito Andina, escala 1:25000 // Unpublished report. CODELCO Chile, 2010. 79 p (in Spanish).

Proffett, J.M. High Cu grades in porphyry Cu deposits and their relationship to emplacement depth of magmatic sources // Geology, 2009. Vol. 37 (8). P. 675–678.

Ramos, V.A. Evolucion Tectonica de la Alta Cordillera de San Juan y Mendoza // In: *Geologia de la Region del Aconcagua* (Ramos, V.A., editor), 1996. P. 447–460. Subsecretaria de Mineria de la Nacion, Buenos Aires.

Sibson, R. A note on fault reactivation // Journal of Structural Geology, 1985. Vol. 7. P. 751–754.

Sillitoe, R.H. Porphyry Copper Systems // Economic Geology, 2010. Vol. 105. P. 3–41.

M. Polgari

R*esearch Center for Astronomy and Geosciences, Geobiomineralization and Astrobiological Research Group, Institute for Geology and Geochemistry, Hungarian Academy of Sciences, Budapest, Hungary, rodokrozit@gmail.com*

TWO STEP MICROBIAL FORMATION MODEL OF BLACK SHALE-HOSTED MANGANESE CARBONATE DEPOSITS – CASE STUDY OF THE URKUT DEPOSIT, HUNGARY

Рассмотрено формирование низкотемпературных карбонатно-марганцевых месторождений, приуроченных к черносланцевым толщам, в окислительных условиях на стадии биогенного восстановления Mn^{3+} и Mn^{4+} при диагенезе. Приводятся данные о геологическом строении, минералогии и геохимии гигантского неметаморфизованного месторождения карбонатных марганцевых руд Уркут юрского возраста. Изотопный состав углерода карбонатов свидетельствует о его органогенном источнике, изотопный состав кислорода – о температурах

образования 17–23 °C. Источником металлов служили придонные гидротермальные флюиды, в результате деятельности которых формировались гидроксидно-марганцевые руды с преобладанием Mn^{3+}. Разнообразие оксидных минералов марганца в рудах объясняется с термодинамических позиций кислотно-основными свойствами растворов и наличием окислительно-восстановительного барьера. Бактериальное окисление органического углерода является необходимым условием для образования крупных залежей карбонатов марганца в черносланцевых толщах.

Introduction

To start any consideration concerning manganese we have to be aware of the sneaky (tricky) behavior of this element. Tracing the source of metals is very important, but enrichment effects, the way of accumulation of Mn (ore) are also important, and these two together let to propose a genetic picture.

The role of microorganisms in sedimentary and low temperature hydrothermal ore deposits is being increasingly appreciated, among them chemolithotrophs. Formation of black-shale hosted manganese-carbonate ores is an example of a low-temperature bacterial system characteristic of non-sulphidic, oxic environments.

Early diagenetic bacterially mediated Mn(IV) and Mn(III) reduction processes via organic matter oxidation and Mn-carbonate mineralization are well established [Polgari et al., 1991]. However, the fundamental processes of formation of these huge black-shale hosted accumulations of manganese was still poorly understood.

To address these issues, the well preserved, unmetamorphosed, black shale-hosted manganese-carbonate deposit of the Urkut Basin, Hungary offers an excellent case study for detailed petrographic, mineralogical, geochemical, and textural analyses. These early diagenetic Mn carbonates and primary Mn oxides are of Jurassic (Lias-Toarcian) age [Polgari et al. (eds.), 2000 and references therein]. This important deposit is among the 10 largest Mn deposits with current reserves of 80 million tons of Mn-carbonate ore (24 weight percent average Mn and 10 weight percent Fe).

Here, we review the main characteristics of the black shale-hosted Urkut Mn deposit, provide additional geochemical and geomicrobiological evidence for the chemolithoautothroph bacterial activity as a fundamental process of manganese-ore formation, discuss the importance of such deposits as paleoenvironmental indicators, provide a new general model for the origin of this type of deposits.

Geological setting and characteristics of the ore deposit at Urkut

The black shale-hosted Mn-carbonate ore bed is about 40 m thick. The ore deposit of economic importance now covers an area of 8 km^2. The ore deposit occurs in a limestone section and consists of three ore beds (10-, 3-, and 1 m thick), separated by a 20- and 4 m-thick black shale. The rhodochrosite ore is composed of laminated, alternating grey, green, brown, and black sections composed of mixtures of very fine-grained (1–2 μm) carbonate minerals and clay [Polgari et al., 2000].

The bulk XRD mineralogical composition of the Mn-carbonate ore beds shows rhodochrosite (Ca-, Mg-bearing), siderite, kutnohorite, 10A-phyllosilicate (celadonite), smectite (nontronite), goethite, quartz, Ca-apatite (phosphorite), and pyrite, with traces of chlorite, zeolite, feldspar, and manganite. The host black-shale consists of quartz, calcite, pyrite, smectite, 10A-phyllosilicate (illite, celadonite), goethite, and chlorite, with traces of zeolite, and feldspar. Manganite is the only Mn-oxide phase in the carbonate ore bed.

Mn-carbonate ore samples have average $\delta^{13}C$ value –16.8 ‰ PDB. These values reflect a significant input to the carbon reservoir from which the $MnCO_3$ formed from the degradation of organic matter via bacterially mediated early diagenetic processes [Polgari et al., 1991, second microbial cycle]. The $\delta^{18}O$ isotope values vary between –5.84 and +1.61 ‰ PDB, which reflect temperatures of precipitation between 17 and 23°C [Polgari et al., 2012].

Biomineralization – general aspect

Microbial geochemistry the development of research methods has allowed investigations of extant biogeochemical systems, which has produced considerable new insights into bacterially mediated Mn mineralization [Mandernack and Tebo, 1993; Mandernack et al., 1995; Moffett and Ho, 1996; Bargar et al., 2005; Webb et al., 2005]. Morgan [2005] provided a thermodynamic analysis of microbial Mn(II) oxidation in low temperature aquatic systems, giving a kinetic model of oxidation pathways for

Mn(II). Bacterial oxidation of Mn(II) to Mn(IV) is thought to drive the oxidative segment of the global biogeochemical Mn cycle [Krumbein, 1983; Ehrlich, 1990]. This important redox system is believed to be driven by an enzyme or enzyme complex involving a multicopper oxidase [Tebo et al., 1997].

Proximal environment

At Urkut-Csardahegy, a large Fe-Mn-oxide chimney system containing fluid-flow microchannels characterized the basin. Stromatolitic mounds grew at the sediment/water interface, which buried the chimneys. These prove the local hydrothermal metal source for mineralization. [Polgari et al., 2012].

Distal environment

It is difficult to decipher the original aerobic microbial cycle because the whole deposit was overprinted by anaerobic heterotrroph secondary microbial processes. But some remnants produced during the original processes are preserved in the Urkut Mn carbonate deposit, among which most importantly is the presence of manganite (MnO(OH)). To understand this so-called long-standing mineral phase, a detailed explanation is needed. During development of the Mn-oxide proto-ore, the first product of microbial Mn(II) oxidation probably was a bio-oxide based on the experimental studies of Villalobos et al. [2003], Bodeï et al. [2007], and others. This bio-oxide is an X-ray amorphous oxide similar to δ-MnO_2, which is thought to be a disordered thermodynamically unstable 7Å-vernadite (hexagonal phyllomanganate) containing Mn(IV) vacancy defects, having very small particle size (< 20 nm lateral dimensions), and having only two or three MnO_2 layers (Mn is in octahedral coordination) stacked along the c axis [Villalobos et al., 2003]. A structural model for the initial amorphous bio-oxides indicates that bacterial processes oxidize Mn(III) to (IV) via an enzymatic pathway [Bargar et al., 2005]. Based on the their results, it is assumed that Mn(IV) polymerization leads to sheet polymers or nanoparticles with a general structural formula of $Mn_xO_2^{(4x-4)}$ ($x \leq 1$) that exhibit the basic hexagonal phyllomanganate structure, but contain numerous vacancy defects and other structural defects [Bargar et al., 2005]. Reaction of Mn(II) with the primary biogenic oxide results in the production of abiotic secondary products, feitknechtite or a 10A Na-phyllomanganate [Bargar et al., 2005]. The identity of the secondary product depends upon the Mn(II) concentration as described by thermodynamic relations [Mandernack et al., 1995]. A decrease in the dissolved Mn(II) appears to act as a reductant for the biogenic oxide and to control the stability of secondary abiotic reaction products. The stability of Mn(III)-bearing phases such as MnO(OH) and Mn_3O_4 increases relative to that of Mn(IV)-bearing phases such as MnO_2 as pH and Mn(II) concentration increase. This behaviour can be seen from the reaction for MnO(OH) transformation to MnO_2 in aqueous solution: $2H^+ + 2MnO(OH) = MnO_2 + Mn^{2+} + 2H_2O$.

In ancient Mn-ore beds manganite is the common Mn(III) oxide phase and it is widely thought to reflect oxygen-deficient conditions [Roy, 1981]. Taking into consideration recent research, the existence of manganite may reflect high Mn(II) concentrations rather than an indicator of a suboxic environment. Giovanoli R. [1980] reported that the rate-determining step in γ-MnO(OH) (manganite) formation is the transformation of the rapidly formed initial products, such as feitnechtite, to manganite.

On the other hand, if the Mn(II) concentration is less than that in 7Å-vernadite, then 10Å (Na, Mg) phyllomanganate forms and during Mg^{2+} uptake Mg todorokite forms while the phyllomanganate transforms to tectomanganate. Interlayer Mg serves as a template for the transformation of 10Å-vernadite to todorokite. The abundance of Mg in seawater and its key role in converting phyllomanganate to tectomanganate explain why todorokite is common in marine diagenetic and hydrothermal ferromanganese oxides [Bodeï et al., 2007], but does not explain its near absence in marine hydrogenous deposits. Experimental studies showed that extracellular polymers from bacteria catalyze the adsorption of Mg on the surface of the cells [Mandernack et al., 1995]. The Mg uptake can be responsible for the elevated Mg content in black shale-hosted Mn-carbonate deposits. So the bacterial cells not only directly oxidize Mn(II) to Mn(IV) but also, in the early stages of oxidation, influence the cation composition of the Mn-oxide mineral being produced. Later chemical processes start to obscure the biological signal [Tebo et al., 1988].

The high Mg content of the black shale-hosted Mn-carbonate deposits might provide a geochemical proxy for early-stage aerobic chemolithoautotroph processes in the formation of huge Mn deposits. Previous chemical investigations showed high Mg contents in black shale-hosted Mn-carbonate deposits from Urkut (2.5–8 wt. % MgO). High Mg contents were reported without any ex-

planation for similar Mn deposits from Molango, Mexico [Okita et al., 1988] and Chinese deposits [Hein and Fan, 1999].

Microbial evidences and their palaeoenvironmental interpretation

Black shale-hosted manganese deposits contain a huge mass of mineralized bacteria that are at least in part responsible for major accumulations of metals in sediments by sequestering them from hydrothermal sources and seawater. Positive Ce anomalies are further evidence of oxidic conditions.

Aerobic chemolithoautotroph microbial model

Marine Mn-bearing deposits are generally classified as three types: hydrogenetic, diagenetic, and hydrothermal [Bolton et al., 1988; Hein et al., 1997]. The first type is represented by ferromanganese crusts, which slowly precipitate from seawater at the seafloor on to hard-rock substrate. Diagenetic deposits result from direct precipitation of Mn during early diagenesis at/or below the seafloor, which is usually related to changing redox conditions, where Mn-rich sediments accumulate where oxygenated water mixes with oxygen-deficient water (bath-tub-ring redox-interface model) [Force and Cannon, 1988; Frakes and Bolton, 1992]. These diagenitic deposits may be composed of Mn carbonates or oxides. Manganese deposits related to submarine hydrothermal system belong to the third type. It is evident that formation of huge black shale-hosted Mn-carbonate deposits cannot be explained solely by these three deep-ocean processes. For diagenetic-type redox-interface models into which these depsosits are placed, additional mechanisms are required. Mn-carbonate formation took place via bacterially mediated Mn(IV, III) reduction through C_{org} oxidation, and not from direct precipitation as carbonates from seawater. Under these circumstances, ore-deposit formation was the primary process that resulted from Mn (III, IV) oxide proto-ore accumulation. Thus, a fourth type of genetic model is required for these deposits, that is a model in which an aerobic, chemolithoautotroph microbial cycle (cycle I) are followed by an anaerobic heterotroph bacterial cycle (cycle II).

The study was supported by Hungarian Science Foundation (OTKA-NKTH No. K 68992).

References

Bargar, J.R., Tebo, B.M., Bergmann, U., Webb, S.M., Glatzel P., Chiu, V.Q., Villalobos, M. Biotic and abiotic products of Mn(II) oxidation by spores of the marine Bacillus sp. Strain SG-1 // American Mineralogist, 2005. Vol. 90. P. 143–154.

Bodei, S., Manceau, A., Geoffroy, N., Baronnet, A., Buatier, M. Formation of todorokite from vernadite in Ni-rich hemipelagic sediments // Geochimica et Cosmochimica Acta, 2007. Vol. 71. P. 5698–5716.

Bolton, B.R., Both, R., Exon, N.F., Hamilton, T.F., Ostwald, J., Smith, J.D. Geochemistry and mineralogy of seafloor hydrothermal and hydrogenetic Mn oxide deposits from the Manus Basin and Bismarck Archipelago region of the southwest Pacific Ocean // Marine Geology, 1988. Vol. 85. P. 65–87.

Ehrlich, H.L. Geomicrobiology. 2nd ed. New York (N.Y.): M. Dekker, 1990. 719 p.

Force, E.R, Cannon, W.F. Depositional model for shallow-marine manganese deposits around black shale basins // Economic Geology, 1988. Vol. 83. P. 93–117.

Frakes, L.A., Bolton, B.R. Effects of ocean chemistry, sea level and climate on the formation of primary sedimentary manganese ore deposits // Economic Geology, 1992. Vol. 87. P. 1207–1217.

Giovanoli, R. On natural and synthetic manganese nodules. In: Varentsov, I.M. es Grasselly, Gy. (Eds.) // Geology and Geochemistry of Manganese. Akademiai Kiado, 1980. Vol. 1. P. 159–203.

Hein, J.R., Fan, D. (Eds). Manganese and associated ore deposits of China // Ore Geology Reviews, 1999. Vol. 15. P. 1–3.

Hein, J.R., Koschinsky, A., Halbach, P., Manheim, F.T., Bau, M., Kang, J.-K., Lubick, N. Iron and manganese oxide mineralization in the Pacific // In: Nicholson, K., Hein, J.R., Buhn, B., Dasgupta, S. (Eds.), Manganese Mineralization: Geochemistry and Mineralogy of Terrestrial and Marine Deposits, Geological Society Special Publication, 1997. Vol. 119. P. 123–138.

Krumbein, W.E. Stromatolites – the challenge of a term in space and time // Precambrian Research, 1983. Vol. 20. No. 2–4. P. 493–531.

Mandernack, K.W., Tebo, B.M. Manganese scavenging and oxidation at hydrothermal vents in vent plumes // Geochimica et Cosmochimica Acta, 1993. Vol. 57. P. 3907–3923.

Mandernack, K. W., Post, J., Tebo, B.M. Manganese mineral formation by bacterial spores of the marine Bacillus, strain SG-1: Evidence for the direct oxidation of Mn(II) to Mn(IV) // Geochimica et Cosmochimica Acta, 1995. Vol. 59. P. 4393–4408.

Moffett, J.W., Ho, J. Oxidation of cobalt and manganese in seawater via a common microbially catalyzed pathway // Geochimica et Cosmochimica Acta, 1996. Vol. 60. P. 3415–3424.

Morgan, J.J. Kinetics of reaction between O_2 and Mn(II) species in aqueous solutions // Geochimica et Cosmochimica Acta, 2005. Vol. 69. P. 35–48.

Okita, P.M., Maynard, J.B., Spiker, E.C., Force, E.R. Isotopic evidence for organic matter oxidation by manganese reduction in the formation of stratiform manganese carbonate ore // Geochimica et Cosmochimica Acta, 1988. Vol. 52. P. 2679–2685.

Polgari, M., Okita, P.M., Hein, J.R. Stable Isotope Evidence for the Origin of the Urkut Manganese Ore Deposit, Hungary // Journal of Sedimentary Petrology, 1991. Vol. 61. No. 3. P. 384–393.

Polgari, M., Szabo, Z., Szederkenyi, T. (Eds.). Manganese Ores in Hungary – In commemoration of professor Gyula Grasselly – Hungarian Academy of Sciences. Szeged: Juhasz Publishing House, 2000. 675 p.

Polgari, M., Hein, J.R., Vigh, T., Szabo-Drubina, M., Forizs, I., Biro, L., Muller, A., Toth, A.L. Microbial processes and the origin of the Urkut manganese deposit, Hungary // Ore Geology Reviews, 2012. Vol. 47. P. 87–109.

Roy, S. Manganese deposits. London: Academic Press, 1981. 458 p.

Tebo, B. M, Nealson, K. H, Rosson, R. A. Occurrence and mechanisms of microbial oxidation of mangane // Advances in Applied Microbiology, 1988. Vol. 33. P. 279–318.

Tebo, B.M., Ghiorse, W.C., Van Waasbergen, I.G., Siering, P.L., Caspi, R. Bacterially Mediated Mineral Formation: Insights into Manganese(II) Oxidation from Molecular Genetic and Biochemical Studies // In: J.F. Banfield, K.H. Nealson, Eds. Geomicrobiology: Interactions Between Microbes and Minerals, 1997. Vol. 35. 448 p. (Reviews in Mineralogy Mineralogical Society of America).

Villalobos, M., Toner, B., Bargar, J., Sposito, G. Characterization of the manganese oxide produced by Pseudomonas putida MnB1 // Geochimica et Cosmochimica Acta, 2003. Vol. 67. P. 2649–2662.

Webb, S., Dick, G.J., Bargar, J.R., Tebo, B.M. Evidence for the presence of Mn (III) intermediates in the bacterial oxidation of Mn(II) // Microbiology, 2005. Vol. 102. P. 5558–5563.

M.K. Revan[1], Yu. Genc[2], V.V. Maslennikov[3], S.P Maslennikova[3], R.R. Large[4], V. Danyushevsky[4]

[1] Department of Mineral Research and Exploration, General Directorate of Mineral Research and Exploration (MTA), Ankara, Turkey, kemalrevan@gmail.com

[2] Department of Geological Engineering, Hacettepe, University, Ankara, Turkey

[3] Institute of Mineralogy, Urals Branch, Russian Academy of Sciences, Miass, Russia

[4] CODES, ARC Centre of Excellence in Ore Deposits, University of Tasmania, Hobart, Tasmania, Australia

UPPER CRETACEOUS HYDROTHERMAL CHIMNEY FRAGMENTS FROM THE EASTERN PONTIDE BELT, NE TURKEY: IMPLICATIONS FOR PONTIDE VMS DEPOSITS

Изучены трубы «черных курильщиков», обнаруженные в колчеданных месторождениях позднемелового возраста в западной части Понтид. Присутствие минерализованных фрагментов труб в колчеданных месторождениях западной части Понтид и содержания рассеянных элементов в них представляют собой значимые данные для понимания физико-химических условий и истории отложения колчеданной минерализации на океаническом дне.

Introduction

The fossil hydrothermal chimney fragments which have been documented to date in the volcanogenic massive sulfide (VMS) districts are quite limited and specific to very few districts (Urals, Cyprus and Japan). The relics of paleo-sulfide chimney fragments were first described in the Kuroko type VMS deposits of Japan, by Scott [1981]. Later, well preserved paleo-sulfide chimneys were described in the VMS deposits in Urals [Herrington et al., 1998; Maslennikov, 1991, 1999, 2006], Cy-

prus [Qudin and Constantinou, 1984] and recently in the eastern Pontide VMS deposits [Maslennikov et al., 2009; Revan, 2010]. The fossil chimney fragments in these regions were revealed in clastic sulfide ores. The Late Cretaceous VMS deposits in the eastern Pontides can be added to these limited chimney-bearing VMS districts with their well preserved chimney relics. The purpose of this study is to describe mineralogical and geochemical characteristics of paeo-hydrothermal chimneys of the Pontide VMS deposits and from this to make some interpretations on the environment in which the VMS deposits formed.

Geology of Pontide VMS deposits

The bimodal-felsic VMS deposits are located on the eastern Pontide belt which forms mountain range 500 km long by 100 km wide that lie in the eastern coast of Black Sea. The basement of the eastern Pontides is formed by the Paleozoic metamorphics and the granitoidic rocks that intersect these metamorphics. A thick volcano-sedimentary sequence ranging in ages from Paleozoic to Quaternary overlies these basement rocks. The Late Cretaceous volcanic rocks, in which the massive sulfide deposits occurred, lie along the eastern Black Sea coast. It is generally agreed that the Late Cretaceous to Paleocene volcanic rocks derived from a north-trending subduction zone which is closed today. The eastern Pontide belt is defined as one of the well preserved paleo-island arc samples formed on the ocean floor that has subducted to the north during the Senonian [Şengör and Yılmaz, 1981, Okay and Şahintürk, 1997].

The majority of the VMS deposits in the district relate to circular structures and fault-controlled subsidences (?) which developed on island-arc setting. These structural-controlled VMS deposits formed proximal to rhyolitic/dacitic domes. All known VMS deposits in the eastern Pontide belt occur in dacitic/rhyolitic rocks, not too thick (300–500 meters) and which comprise of lavas, hyaloclastites and sub-volcanic intrusions. They are overlain by a sequence comprising of dacite, andesite, basalt and volcano-sedimentary unit. Some of these are either deep marine cherts or chemical sediments (“exhalites” or “halmyrolytites”). The ore deposits are commonly located at the uppermost contact of the dacitic/rhyolitic pile or within the lowermost part of the overlying sequences [Revan, 2010].

Characteristics of paleo-hydrothermal vent chimneys

All of the fragments of paleo-hydrothermal chimneys in massive sulfide deposits (Cayeli, Killik, Lahanos, K?z?lkaya and Kutlular) are found in the clastic sulfide ores. The major constituents of clastic sulfide ores which includes chimney fragments compose mainly of pyrite, chalcopyrite, sphalerite, galena and bornite.The diameters of the well-preserved chimney fragments range from a few millimeters to ~6 cm, with one reaching ~10 cm. The well preserved chimney fragments typically have distinct concentric zones (Fig. 1). Numerous examples of what appeared to be chimney wall fragments have porous and laminated textures and some of which are displaying a thin alteration rim, indicative of oxidizing conditions on the sea floor. Chimney fragments are associated with vent-related fauna.

The presence of a zoning mostly consist of three layers from exterior to interior is clearly observed in chimney samples (Fig. 2). The zones of the chimney samples mainly comprise of sulfide and sulfate minerals. However, each zone is characterized with the predominant mineral abundance. Table 1 lists the minerals that were found in the chimney samples of the VMS deposits in the eastern Pontides. By using microprobe, some rare minerals such as kawazulite (Bi_2Te_2Se) mixed with chalcopyrite matrix, hessite (Ag_2Te) and wittichenite (Cu_3BiS_3) were detected (Fig. 3).

LA-ICP MS analysis

Two chimney samples collected from Cayeli ore body were analysed for their geochemical signatures. Each sample was analysed from the chimney interior to its exterior wall. Systematic trace element distribution across chimney zones is notable. As the result of the analysis performed using LA-ICP-MS, the chimney samples may be broadly divided into to three zones from external to internal considering the changes in the element values.

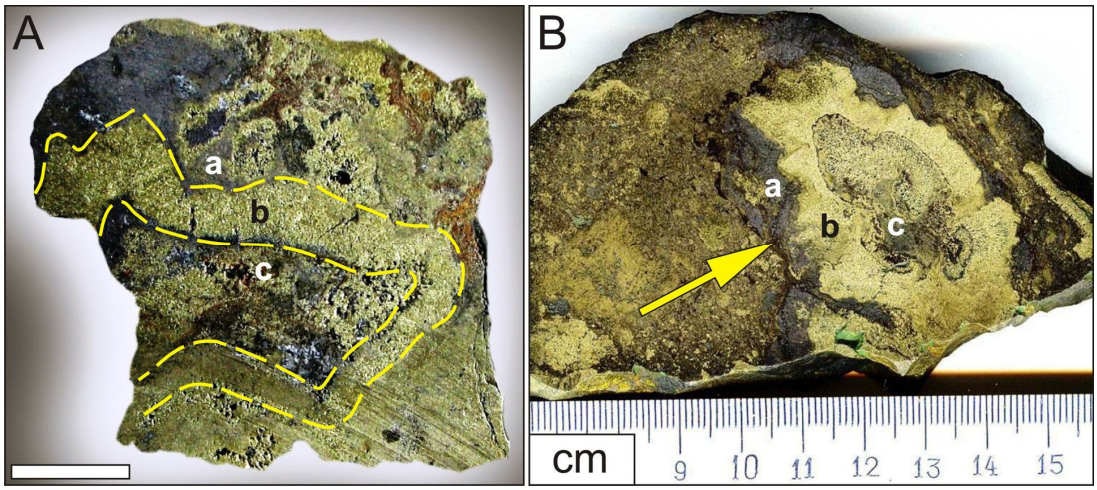

Fig.1. Photographs of paleo-chimney fragments. (A) The mineralogical zoning in the chimney sample of Killik mine. (B) Well preserved chimney from Lahanos mine. a – outer wall: b – inner zone: c – central zone. The scale bar is 2.0 cm.

Table.

The mineral associations in sulfides of chimney zones from the eastern Pontide VMS deposits

Mineral	Analytical Method			Deposit				
	TS	PS	MP	Cayeli	Kutlular	Lahanos	Killik	Kızılkaya
Barite ($BaSO_4$)	X	X		√	√	√	√	√
Bornite (Cu_5FeS_4),		X		√		√		√
Chalcopyrite ($FeCuS_2$)		X		√	√	√	√	√
Covellite (CuS)		X		√			√	√
Chalcocite (Cu_2S)				√				
Electrume		X						√
Fahlore		X					√	
Galena (PbS),		X		√	√	√	√	√
Gold (Au)		X		√	√	√		√
Hessite (Ag_2Te)		X	X			√		
Kawazulite $Bi_2(TeSeS)_3$			X			√		
Marcasite (FeS_2)		X		√			√	√
Pyrite (FeS_2)		X		√	√	√	√	√
Pyrrhotite (FeS)		X						√
Quartz (SiO_2)	X			√	√	√		√
Silver-sulfosalt		X					√	
Sphalerite (ZnS)		X		√	√	√	√	√
Tellurobismuthite (Bi_2Te_3)		X	X			√		
Tetrahedrite		X				√		
Tennantite		X		√		√		√
Wittichenite (Cu_3BiS_3)		X	X			√		

Analytical method being used to detect minerals are indicated. TS: thin section, PS: polished section, MP: microprobe.

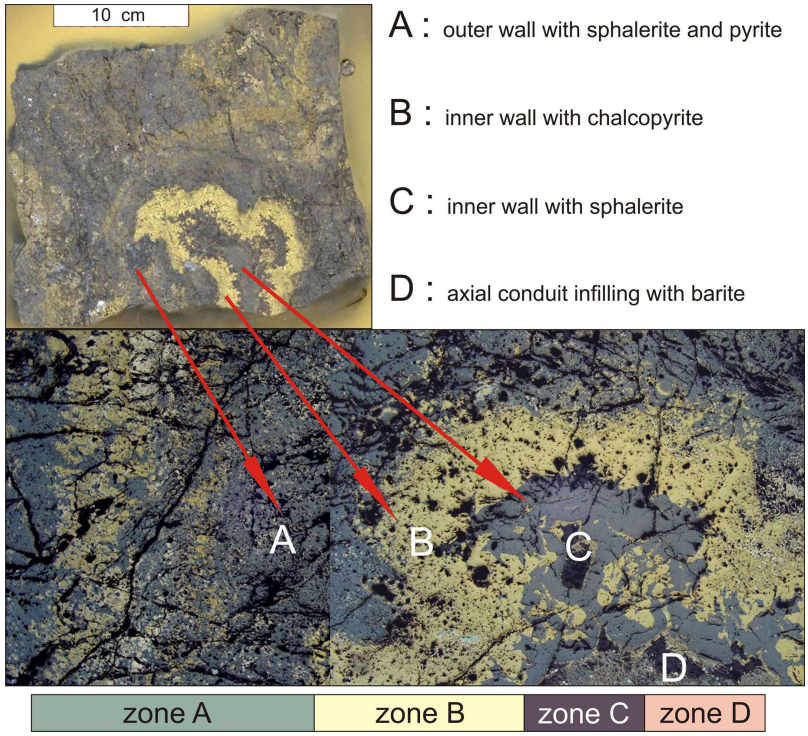

Fig.2. The mineralogical zoning in the chimney sample collected from Cayeli mine and their mineralogical contents (above). Close-up of the chimney walls shown above throught ore microscopy (below). See Fig. 1B for location of this chimney fragment.

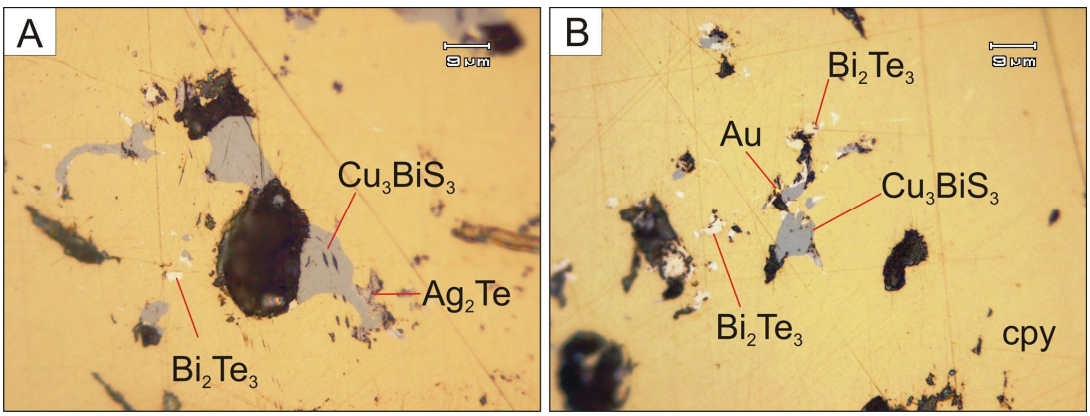

Fig.3. The rare minerals identified in the mineralized hydrothermal chimneys in Lahanos massive sulfide deposit. (A) Wittichenite (grey Cu_3BiS_3) – hessite (brown-grey Ag_2Te) in the inner zone. (B) Gold-wittichenite-tellurobismuthite (Bi_2Te_3) in chalcopyrite in the inner zone.

Some elements such as Ni, Co, Ag, Au, Mn, As, V and U are concentrated in the outer chimney wall (zone A). Co, Mn, Ag, V and U elements decrease through the zone B to the central zone C and Co, Ni and U elements remarkably decrease in the zone C. The high values of Sn (up to 760 ppm), Se (up to 407 ppm) and Te (up to 434 ppm) in the Zone B draw attention, especially where Cu concentrations exceed ~ 8 %. Gold is found in all chimney zones but has its highest concentrations (25 ppm) in zone A of chalcopyrite.

Se, Sn and Te elements enrich more than the other elements in the chalcopyrites in all zones. Average Se contents up to 39 ppm are present in the zone A, up to 236 ppm in the zone B, up to 188 ppm in the zone C. Average Te values up to 347 ppm are present in the zone A, up to 45 ppm in the zone B and up to 44 ppm in the zone C. When average Sn values are considered, it reaches up to 16 ppm in the zone A, to 48 ppm in the zone B and to 30 ppm in the zone C.

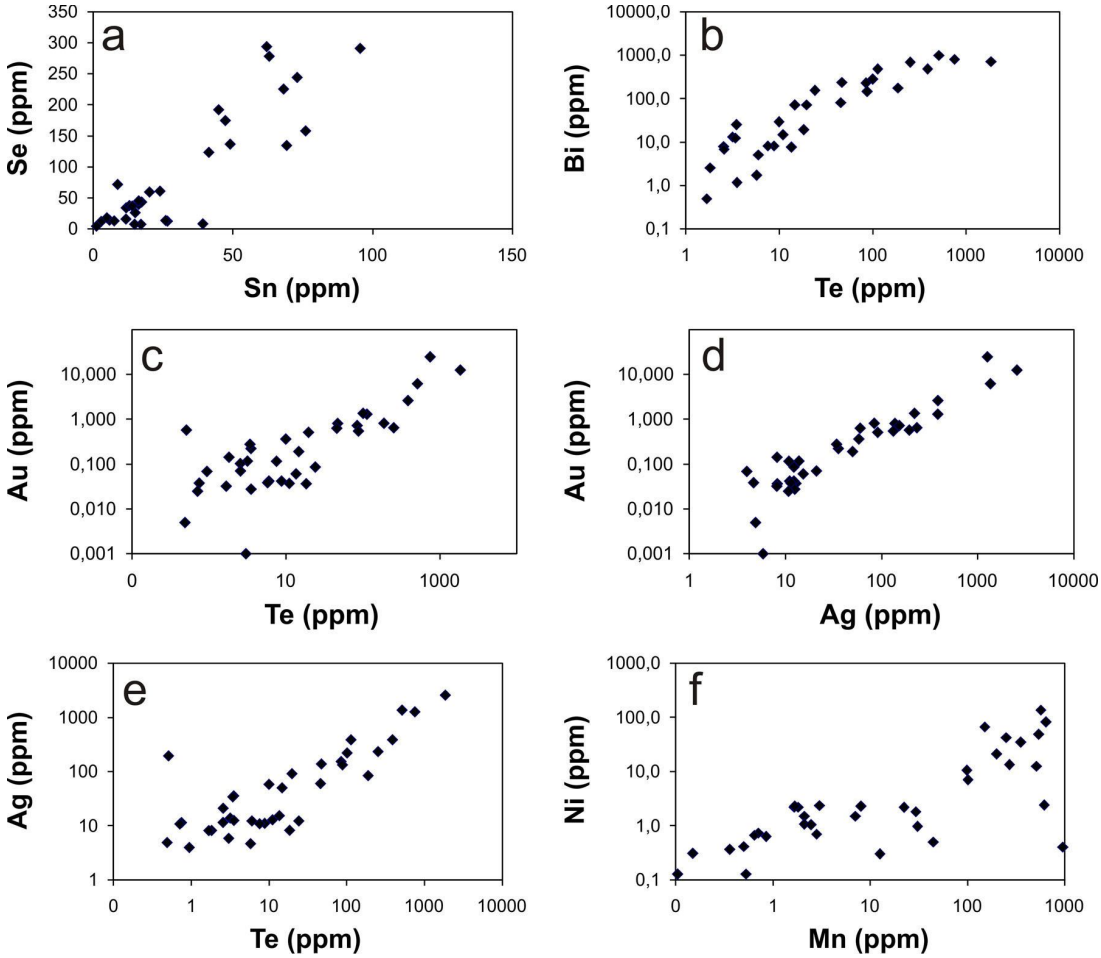

Fig.4. Chalcopyrite LA-ICPMS trace element correlations for Se-Sn, Bi-Te, Au-Te, Au-Ag, Ag-Te and Ni-Mn for the Cayeli chimney samples. Diamonds are analytical data points for chimneys.

Se contents reach up to 407 ppm in chalcopyrite. High level of Se in the inner zones of chimney supports the model of precipitation from a high temperature hydrothermal fluid. Tellurium contents (up to 1840 ppm) are also high in chalcopyrites from all zones, especially in zone A. Tin concentrations are high in chalcopyrite (Fig. 4a) and sphalerite compared with pyrite and reach 760 ppm in zone B. High Sn content is among the typical features of medium to high temperature sulfides from VMS deposits [Hannington et al., 1999].

The maximum Bi values, up to 1000 ppm, are noted in chalcopyrites of zone A. Elevated Bi concentrations also occur in sphalerite (up to 253 ppm) and pyrite (up to 729 ppm) of other zones. Bismuth is usually present in the high-temperature VMS assemblage while Te is typical in medium temperatures and Pb is common in the lower temperature assemblage [Hannington et al., 1999; Halbach et al., 2003]. Despite being characteristic of different temperature association there is a good correlation among these elements (Fig. 4b).

High Au and Ag concentrations occur in chalcopyrite and pyrite of zone A. It is observed that there is a positive correlation among Au, Ag and Te (Fig. 4c, 4d, 4e). This may be derived from the presence of hessite (Ag_2Te), electrum and other Ag-Te-Au bearing micro inclusions in chalcopyrites. When plotted of Mn against Ni, these element show positive correlations (Fig. 4f) and infer similar low-temperature and redox conditions [Maslennikov et al., 2009].

Discussion and conclusions

The sulfide chimney fragments exhibit a marked concentric mineral zoning. In the outer zone, main sulfides are pyrite and sphalerite with lesser amount of chalchopyrite. Sulfides within the inner zone consist predominantly of chalchopyrite with lesser pyrite and sphalerite. Axial conduit is commonly filled by barite gangue and with lesser amount of fahlore, sphalerite, chalchopyrite and galena. The chimney fragments are characterized by high metal content. Average Cu, Zn and Fe contents are

25.3 %, 20.7 % and 27.9 % respectively. Au concentrations in the zones of chimneys range from ~1 ppb to 25 ppm. Systematic trace element distribution across chimney zones is also notable. In general, Mn, Co, Ni, Tl, U and V are enriched in the outermost zones of chimneys and decrease towards interior zones. Elements indicative of high temperature conditions include Mo, Se, Sn and Cu and are generally enriched in the inner zones of chimneys.

Hydrothermal vent chimneys provide diagnostic evidence for sulfide accumulation at the sea floor and are of the products of rift (extensional) settings. They also provides strong evidence that VMS deposits formed on a deep-sea floor setting. Considering that present-day massive sulfides are situated near extentional zones [Francheteau et al., 1979; Hekinian et al., 1980; Haymon, 1983; Goldfarb et al., 1983; Qudin and Constantinou, 1984; Hannington et al., 2005] at depths >2500 m [Spiess et al., 1980; Qudin and Constantinou, 1984], it is essential that the depths in which hydrothermal black smoker chimneys formed should also be highly much. The same is true of ancient deposits. From this we may conclude that the VMS deposits of the eastern Pontide belt formed on a highly deep-sea floor and are attributed to extensional settings.

VMS deposits of the eastern Pontide belt are associated with rhyolitic to dacitic domes and show clear evidence of having formed on the seafloor. The presence of chimney fragments, fossil tube worms, sedimentary structures, exhalites and clastic nature of massive ores have provided distinctive evidence in support of a sea-floor origin for VMS deposits. Some chimney fragments display alteration rim indicating sea-floor oxidation. Alteration of these fragments implies that they laid on the sea floor for a long period and subjected to oxidation. Such an oxidation around chimney fragments and post-depositional modifications can be attributed to submarine alteration (halmyrolysis). It is clear that halmyrolitic processes such as oxidation, dissolution, hydration and resedimentation of disintegrated material [Maslennikov et al., 2012] were highly effective on Pontide paleo-oceans floor.

Acknowledgements

Financial and technical support for research was provided by Hacettepe University, General Directorate of Mineral Research and Exploration (MTA) and Urals Branch of Russian Academy of Science (no. 12-П-5-1003). The authors are grateful to S. Gilbert (University of Tasmania, Australia) for acces to LA-ICPMS analyses which were carried out during a visiting program to CODES, University of Tasmania.

References

Francheteau, J., Needham, H.D., Choukrone, P., Juteau, T., Seguret, M., Ballard, R.D., Fox, P.J., Normark, W.R., Carranza, A., Cordoba, D., Guerro, J., Rangin, C., Bougault, H., Cambon, P., Hekinian, R. Massive deep-sea sulfide ore deposits discovered on the East Pacific Rise // Nature, 1979. Vol. 277. P. 523–528.

Goldfarb, M.S., Converse, D.R., Holland, H.D., Edmond, J.M. The genesis of hot spring deposits on the East Pacific Rise, 21 ?N // Econ. Geol. Mon., 1983. Vol. 5. P. 184–97.

Halbach, P.E., Fouquet, Y., Herzig, P. Mineralization and compositional patterns in deep-sea hydrothermal systems // In: Halbach PE, Tunnicliffe V, Hein JR (eds) Energy and mass transfer in marine hydrothermal systems. Dahlem University Press, Berlin, 2003. P. 85–122.

Hannington, M.D., Bleeker, W., Kjarsgaard, I. Sulfide mineralogy, geochemistry, and ore genesis of the Kidd Creek deposit: Part I. North, Central and South orebodies // Econ. Geol. Mon., 1999. Vol. 10. P. 163–224.

Hannington, M.D., de Ronde, C.E.J., Petersen, S. Sea-floor tectonics and submarine hydrothermal systems // Econ. Geol. 100th Anniversary volume, 2005. P. 111–141.

Haymon, R. M. Growth history of hydrothermal black smoker // Nature, 1983. Vol. 301. P. 695–698.

Hekinian R., Fevrier M., Bischoff J.L., Picot, P., Shanks, W.C. Sulfide deposits from the East Pacific Rise near 21 ?N // Science, 1980. Vol. 207. P. 1433–1444.

Herrington, R.J., Maslennikov, V.V., Spiro, B., Zaykov, V.V., Little, C.T.S. Ancient vent chimney structures in the Silurian massive sulphides of the Urals // In: Mills, R.A., Harrison, K. (eds), Modern Ocean Floor Processes and the Geological Records. Geol Soc London, Special Publications, 1998. Vol. 148. P. 241–257.

Maslennikov, V.V. Lithological control of copper massive sulfide ores (after the example of Sibai and Oktyabrskoye deposits, Ural). Sverdlovsk, UB AS USSR, 1991. 139 p. [in Russian].

Maslennikov V.V. Sedimentogenesis, halmyrolysis, ecology of massive sulfide-bearing paleohydrothermal fields (after example of the Southern Urals). Miass, 1999. 348 p. [in Russian].

Maslennikov, V.V. Lithogenesis and massive sulfide deposits formation. Institute of mineralogy of UB RAS press. Miass, 2006. 384 p. [in Russian].

Maslennikov, V.V., Maslennikova, S.P., Large, R.R., Danyushevsky, L.V. Study of trace element zonation in vent chimneys from the Silurian Yaman-Kasy volcanic-hosted massive sulfide deposits (the southern Urals, Russia) using laser ablation inductively coupled plasma mass spectrometry (LA-ICP MS) // Econ. Geology, 2009. Vol. 104. P. 1111–1141.

Maslennikov, V.V., Ayupova, N.R., Herrington, R.J., Danyushevsky, L.V., Large, R.R. Ferruginous and manganiferous haloesaround the massive sulphide deposits of the Urals // Ore Geology Reviews, 2012. Vol. 47. P. 5–41.

Okay, A.İ., Şahintürk, Ö. Geology of the eastern Pontides. *In*: Robinson A.G. (ed.) Regional and Petroleum Geology of the Black Sea and Surrounding Regions // American Association of Petroleum Geologist Memoirs, 1997. Vol. 68. P. 291–311.

Qudin, E., Constantinou, G. Black smoker chimney fragments in Cyprus sulphide deposits // Nature, 1984. Vol. 308. P. 349–353.

Revan, M.K. Determination of the typical properties of volcanogenic massive sulfide deposits in the eastern black sea region // Unpub. Ph.D. thesis. Ankara, Hacettepe Univ., 2010. 320 p. [in Turkish].

Scott, S.D. Small chimneys from Japanese Kuroko deposits // In: Seminars on seafloor hydrothermal systems (eds. R.Goldie, T.J. Botrill). Geosci. Can., 1981. Vol. 8. P. 103–104.

Spiess, F.N., Mcdonald, K.C., Atwater, T., Ballard, R., et al. East Pacific Rise: Hot springs and geophysical experiments // Science, 1980. Vol. 207. P. 1421–1433.

Şengör, A.M.C., Yılmaz, Y. Tethyan evolution of Turkey: A plate tectonic approach // Tectonophysics, 1981. Vol. 75. P. 181–241.

M.K. Revan[1], Y. Genc[2], V.V. Maslennikov[3], T. Monecke[4], T. Unlu[5]

[1] Department of Mineral Research and Exploration, General Directorate of Mineral Research and Exploration (MTA), Ankara, Turkey, kemalrevan@gmail.com

[2] Department of Geological Engineering, Hacettepe University, Ankara, Turkey

[3] Institute of Mineralogy, Urals Branch, Russian Academy of Sciences, Miass, Russia

[4] Department of Geology and Geological Engineering, Colorado School of Mines, Golden, USA

[5] Department of Geological Engineering, Ankara University, Ankara, Turkey

FOSSIL FAUNA FINDINGS IN THE MASSIVE SULFIDE DEPOSITS OF THE EASTERN PONTIDE BELT, NORTHEAST TURKEY

В колчеданных месторождениях западной части Понтид изучены реликты придонных палеосообществ мелового возраста. Эти червеобразные формы организмов могут рассматриваться как предковые формы необычных придонных сообществ, обнаруженных в современных гидротермальных полях ВТП, Галапагоса и Хуан де Фука.

Introduction

Discovery of the communities living around the hydrothermal sulfur vents on the sea floor drew the interest of the researchers. Some of the most impressive of the unusual organisms are the tube worms which live in a symbiotic relationship with bacteria. Traces of these unique organisms living at present-day sea floor hydrothermal vents are rarely encountered in the massive sulfide paleohydrothermal fields. Since the discovery of hydrothermal venting along spreading centers, much has been learned about vent communites and associated sulfur deposits. But the findings and detailed studies on fossil fauna [Haymon et al. 1984; Banks, 1986; Kuznetzov et al. 1988; Little et al. 1997] are generally lacking. The possible ancient analogues of these fossil fauna living at present-day sea floor hydrothermal vents were described in the massive sulfide deposits in Cyprus, Urals, Oman and Ireland to date. Apart from above-mentioned VMS districs, Late Cretaceous Pontide massive sulfide deposits (Lahanos, Killik, Cayeli and Kutlular) are host to vent fossils (Fig. 1).

In the context of this study, VMS deposits in the eastern Black Sea region are included in massive sulfide districts in which findings of this unique fauna are found. The fossil fauna fragments (possibly fossil vestimentiferan tube worms) in the Pontide deposits are well-preserved in comparision to similar ones in the other massive sulfide districts.

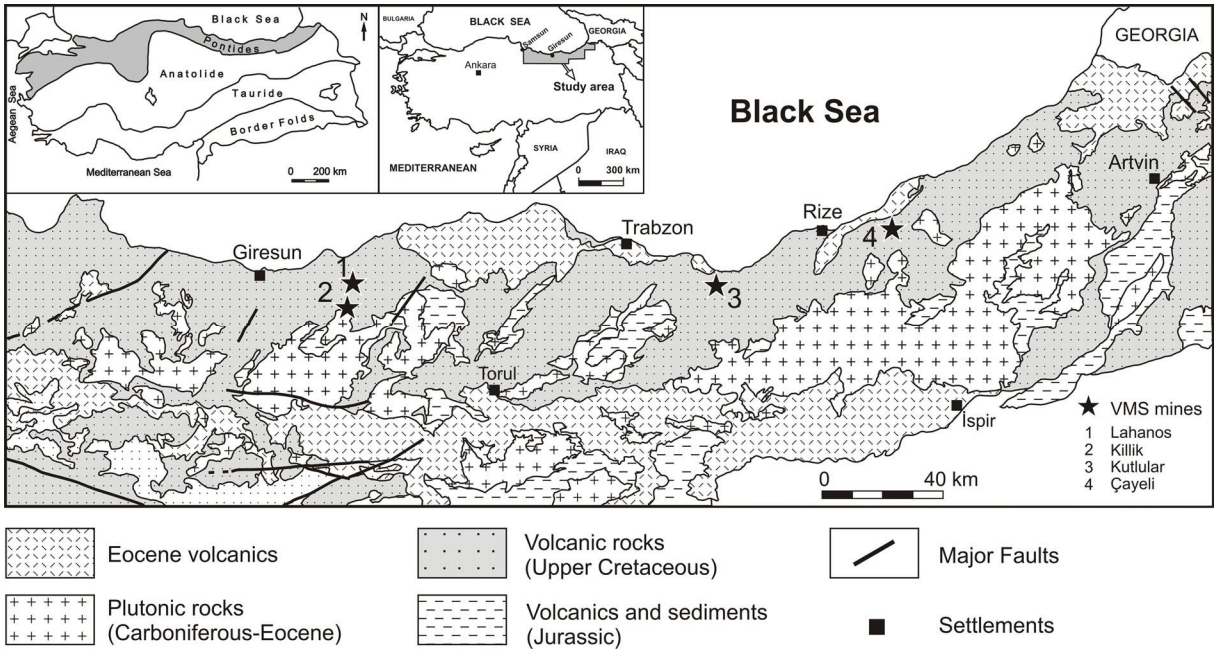

Fig. 1. Site location and simplified regional geologic maps of fossil fauna-bearing VMS deposits in the eastern Black Sea region.

Geologic features of VMS deposits

A large number of bimodal felsic VMS deposits and prospects are located in the northeastern part of the Pontide belt. The basement rocks of the Pontides consist of Devonian to Carboniferous metamorphic rocks such as gneiss and schist, and Paleozoic intrusive granitic rocks. The predominantly volcanic rocks with various age overlie the basement rocks. The coastal area of the eastern Black Sea is overwhelmingly composed of Upper Cretaceous to Paleocene volcanic and volcaniclastic rocks. Upper Cretaceous volcano-sedimentary sequences host volcanogenic massive sulfides, whereas Eocene volcanics host vein type deposits in the district.

Pontide VMS deposits are formed within volcanic-dominated sequences in deep seawater setting and hosted in a thick dacitic/rhylolite succession containing lavas, hyaloclastites and subintrusions. These deposits are commonly overlain by andesite, basalt, dacite and volcano-sedimentary sequence and located at the top contact of the dacitic/rhyolite successions or within the lower part of overlying sequence. Associated sediments are composed of deep seawater cherts, some of which are chemical sediments/exhalites and fossiliferous mudstones [Revan, 2010]. All the known VMS type deposit are hosted by Upper Cretaceous K?z?lkaya formation which is characterized by predominant dacitic volcanics.

Sample descriptions

All of the fossil fauna fragments described in massive sulfide deposits (Cayeli, Killik, Lahanos and Kutlular) are found in the clastic (brecciated) sulfide ores together with black smoker chimney fragments. The dimentions of the fossil tube worm traces defined in the Lahanos, Killik, Kutlular and Cayeli deposits reach up to 25 mm in diameter and 8 cm long (Fig. 2). The well preserved fossil fragments typically have distinct mineralogical zoning. Fossil tube worms were usually replaced by opaque and gang mineral (mostly barite) from the exterior to the interior while inside of which are filled with sulfide clasts such as pyrite, sphalerite, chalcopyrite and galena.

Mineralized fossil tubes are abundant in Lahanos mine and were preserved in a brecciated sulfide matrix consisting mainly of pyrite and sphalerite. In a sample from Lahanos, much of tube worm is infilled with barite (Fig. 3, Fig. 5a). Another sample contains only barite in the outer sections while the inner sides contain sulfide minerals (pyrite, chalcopyrite, covellite, sphalerite) as well as barite.

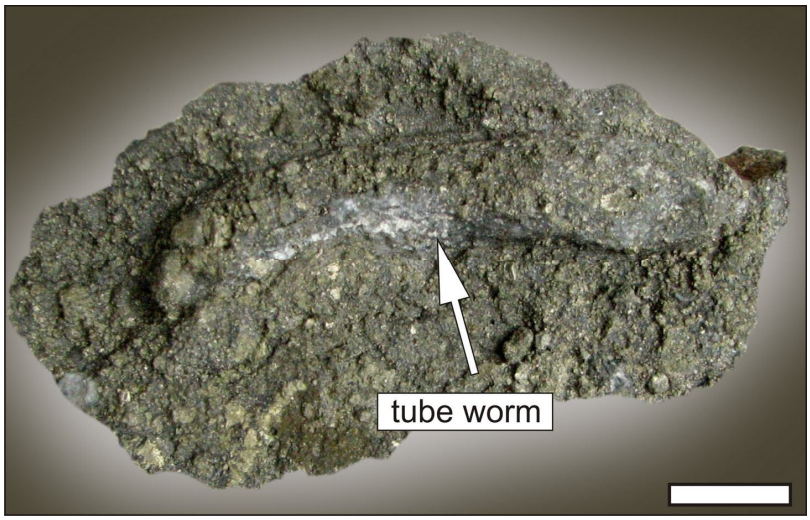

Fig. 2. A well preserved form of tube fossil in the eastern Pontide belt. Sample from the Killik deposit with clastic sulfide ore. Scale bar is 2 cm.

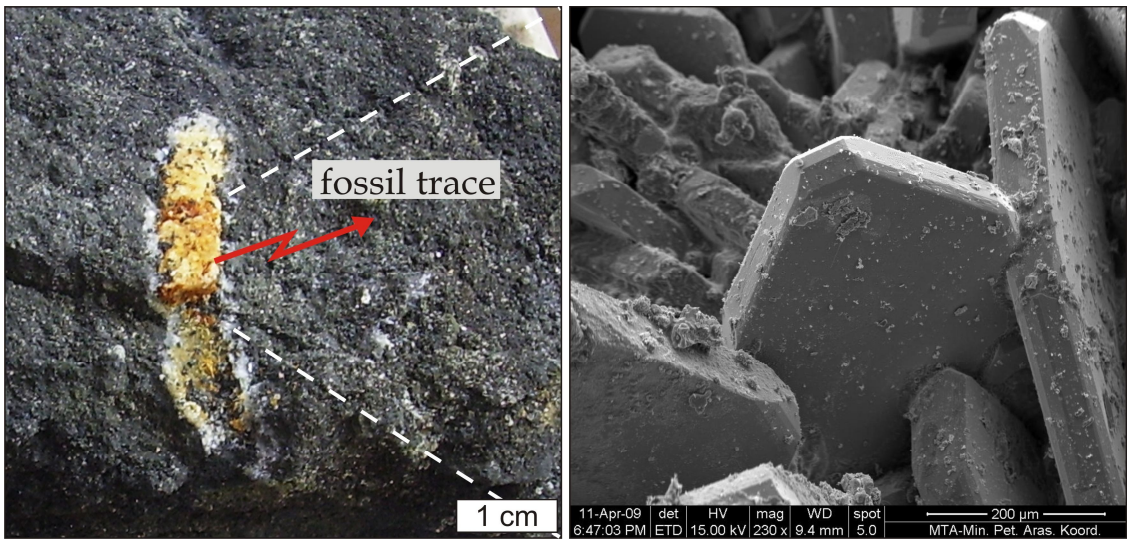

Fig. 3. SEM image of barite minerals from fossil tube worm replaced by sulfate and sulfide minerals. Sample is from clastic sulfide ore zone of Lahanos deposit.

In some samples from Lahanos mine, the existence of secondary minerals such as goethite [FeO(OH)], serpierite [$Ca(Cu,Zn)_4(SO4)_2(OH)_6.3(H_2O)$], native sulfur [S] and jarosite [$KFe_3(SO4)_2(OH)_6$] and dolomite [$CaMg(CO_3)$] in amounts that cannot be differentiated by microscope, has been detected by Raman Spectrometry.

In Killik mine, some tube walls are formed of predominantly silica and have infillings of barite and silica (Fig. 4, Fig. 5b). The restricted number of samples which appeared to be fossil fauna fragments were preserved in clastic sulfide ore of Kutlular and Cayeli deposits.

Discussion

Modern hydrothermal vent fields leading to massive sulfide accumulations are favorable sites for unusual vent faunas that depend on the vent fluid for their energy [Tunnicliffe et al. 1998]. In this complex environment, hydrosulfiric conditions which are inconvenient for the survival of many other organisms are dominant. The organisms that survive in such a environment have such special living conditions that is almost impossible for them to maintain their lives in other environments. Some of the unique fauna that survive in such a environment are tube worms which live in a symbiotic relationship with bacteria. The possible ancient analogues represented by tubular worm relics of this unique fauna living at present-day sea floor hydrothermal vents were discovered for the first time in the Sibay

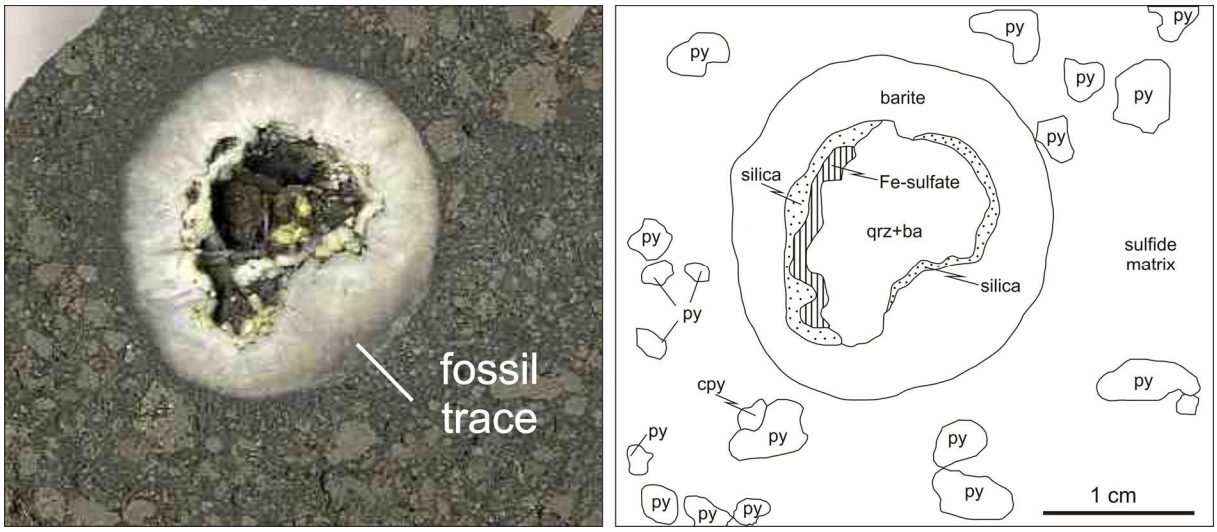

Fig. 4. A tube worm relic, having infillings of barite and silica in clastic sulfide ore of Killik deposit (py – pyrite; cpy – chalcopyrite; qrz – quartz; ba – barite).

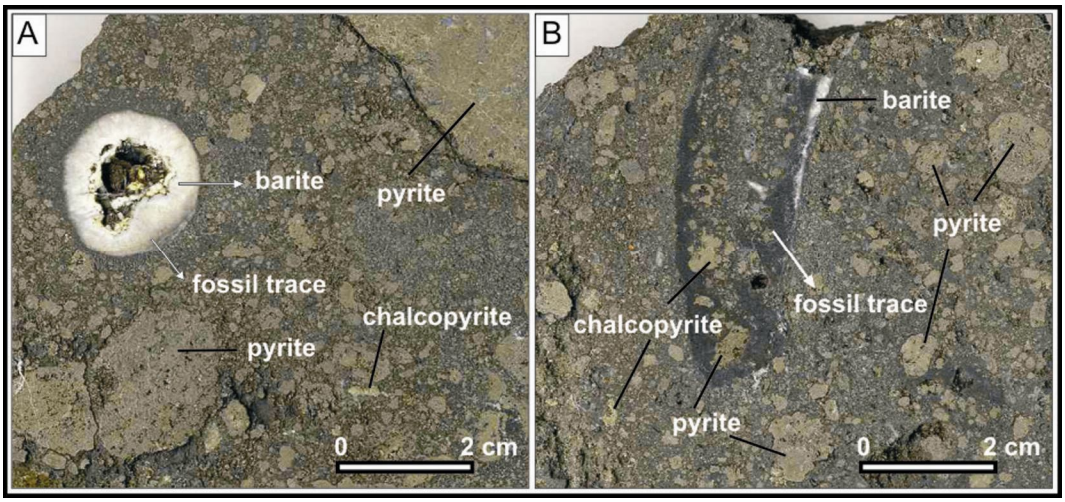

Fig. 5. Photographs representative of the various tube worm traces. Fossil tube worm trace replaced by the various sulfide minerals within the clastic sulfide ore of Killik deposit (A) and Lahanos mine (B).

deposit by Ivanov [1947]. Later, the similar fossil findings were defined in VMS deposits of Oman, Cyprus, Ireland, Alaska and Urals [Haymon et al., 1984; Qudin and Constantinou, 1984; Banks, 1985; Moore et al. 1986; Maslennikov, 1991; Kuznetzov et al., 1993; Zaykov et al., 1995]. Traces of fossil tube worms are also present in Late Cretaceous Pontide VMS deposits. The fossil fauna fragments described in Pontide deposits are well-preserved in comparision to similar ones in the other massive sulfide districts and associated with hydrothermal sulfide chimney fragments.

The fossil tube worms are diagnostic of sea-floor sulfide accumulation and their existence in sulfide ore bodies suggest that Pontide VMS deposits are remnants of Cretaceous sea-floor hydrothermal vent fields. The fossil fauna findings have not received systematic treatment because there are only 4 known fossilliferous VMS deposits in Pontide belt. The massive sulfide deposits probably host diverse fossil vent assembledge. Thus, much more detailed studies should be done in the belt.

This research was supported by the Joint projects Program of Uralian and Siberian Branches of Russian Academy of Science (no. 12-C-5-1010)

References

Banks, D.A. A fossil hydrothermal worm assemblage from the Tynagh lead-zinc deposit in Ireland // Nature, 1985. Vol. 313. P. 128–131.

Haymon, R.M., Koski, R.A., Sinclair, C. Fossils of hydrothermal vent forms discovered in Cretaceous sulfide ores of The Semail ophiolite, Oman // Science, 1984. Vol. 223. P. 1407–1409.

Ivanov, S.N. Study experience of geology and mineralogy of the Sibay massive sulphide deposit // Akademia Nauk SSSR, Uralskiy Filial, 1947. Vol. 2. P. 1–109 [in Russian].

Kuznetzov, A.P., Maslennikov, V.V., Zaikov, V.V., Sobetskii, V.A. Fosil fauna in the sulfide hydrothermal hills from the middle Devonian paleo-ocean of the Ural area // Doklady Akademii Nauk SSSR, 1988. Vol. 303. no. 6. P. 1477–1489 [in Russian].

Kuznetzov, A.P., Maslennikov, V.V., Zaikov, V.V. The near hydrothermal fauna of the Silurian paleoocean in the South Ural // Izvestia Akademii Nauk SSSR. Seria Biologicheskaya, 1993. no. 4. P. 525–534 [in Russian].

Little, C.T.S., Herrington R.J., Maslennikov, V.V., Morris, N.J., Zaykov, V.V. Silurian high temperature hydrothermal vent community from the Southern Urals, Russia // Nature, 1997. Vol. 385, no.9. P. 146–148.

Maslennikov, V.V. Lithological control of copper massive sulfide ores (after the example of Sibai and Oktyabrskoye deposits, Ural). Sverdlovsk, UB AN USSR, 1991. 139 p. [in Russian].

Moore, D.M., Young, L.E., Modene, J.S., Plahuta, J.T. Geological setting and genesis of the Red Dog zinc-lead-silver deposit, western Brooks Range, Alaska // Economic Geology, 1986. Vol. 81. P. 1696–1727.

Qudin, E., Constantinou, G. Black smoker chimney fragments in Cyprus sulphide deposits // Nature, 1984. Vol. 308. P. 349–353.

Revan, M.K. Determination of the typical properties of volcanogenic massive sulfide deposits in the eastern black sea region // Unpub. Ph.D. thesis. Ankara, Hacettepe Univ., 2010. 320 p [in Turkish].

Tunnicliffe, V., McArthur, A.G., McHugh, D. A biogeographical perspective of the deep-sea hydrothermal vent fauna // Advances in Marine Biology, 1998. Vol. 34. P. 353–442.

Zaykov, V.V., Shadlun, T.N., Maslennikov, V.V., Bortnikov, N.S. Yaman-Kasy sulfide deposits – ancient "black smoker" of Urals paleoocean // Geology of ore deposits, 1995. Vol. 37. P. 511–529.

S.A. Sadykov
Institute of Mineralogy UB RAS, Miass, Russia; sadykov1965@gmail.com

MAGNETIC FIELD EFFECT ON FRACTIONATION OF CARBON ISOTOPES IN THE REACTION OF $Ca(OH)_2$ WITH AIR CARBON DIOXIDE

Проведена серия экспериментов по изучению влияния магнитного поля на изотопный состав углерода в карбонате кальция, образующемся при взаимодействии $Ca(OH)_2$ с углекислотой воздуха. Изучение изотопного состава углерода образцов $CaCO_3$, синтезированных в магнитном поле и вне поля, показало, что под воздействием магнитного поля происходит обогащение карбоната кальция изотопом ^{13}C. Различия в величинах $\delta^{13}C$ достигает 14 ‰, PDB. Область максимального обогащения тяжелым изотопом углерода располагается там, где магнитное поле имеет максимальную напряженность. Вне зависимости от величины напряженности магнитного поля все изученные образцы имеют существенно облегченный изотопный состав по сравнению с изотопным составом углерода в углекислом газе атмосферы.

The nuclear spin (magnetic) isotope effect was discovered by A.L. Buchachenko and coworkers in 1976 [Buchachenko et al, 1976]. In the present work, we revealed for the first time the magnetic field effect on the carbon isotope composition in the course of formation of an inorganic compound, calcite $CaCO_3$. The experiments on studying the magnetic field effect on the carbon isotope fractionation during formation of calcite were carried out by the following scheme.

$$CaCO_3 \rightarrow CaO+CO_2\uparrow \rightarrow CaO+H_2O \rightarrow Ca(OH)_2+ CO_2(air) \rightarrow CaCO_3.$$

In all experiments, two plates with calcium hydroxide were used simultaneously. One of them was placed in the magnetic field, another, control one, was out of the field. The plates were disposed perpendicular to Earth's magnetic field.

In the first run, the plate with $Ca(OH)_2$ was placed in the field of a permanent magnet, which was located on the edge of the plate. The isotopic compositions at different distances from the magnet were determined in 500 h. The $\delta^{13}C$values at distances equal to 0.5, 1, and 2 cm from the magnet were –22, –26, and –27‰, respectively. The isotopic composition of $Ca(OH)_2$ on the control plate was $\delta^{13}C$ = – 26.65‰, PDB. A similar result was obtained when $Ca(OH)_2$ was applied to a steel plate not exposed to the magnetic field.

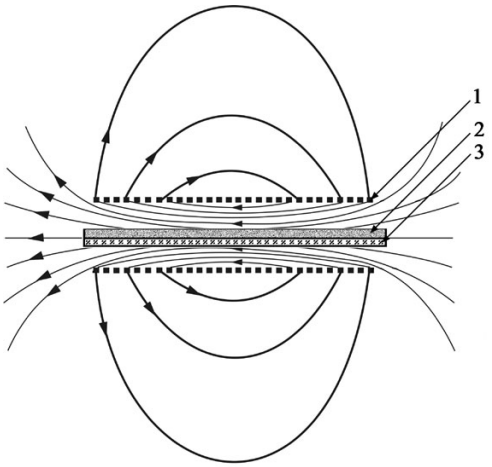

Fig. 1. The scheme of the experiment in the coil. Directions of the magnetic field strength are shown by arrows. Designations: (1) coil rings, (2) $Ca(OH)_2$ layer; (3) glassplate.

In the second run, a glass plate with dimensions of 90 ? 15 mm uniformly covered with $Ca(OH)_2$ obtained from the limestone was placed inside a DC coil 70 mm in length and 15 mm in inner diameter (Fig. 1). The plate with a sample was arranged along the coil axis and parallel to the solenoid magnetic field. The magnetic field strength inside the coil was 8700 A/m (110 Oe). The sample was kept in the solenoid field for 500 h. The isotopic composition of carbon on this plate was determined in 5 mm increments in the direction parallel to the coil magnetic field. The average values $\delta^{13}C$, PDB, obtained at the plate edge (coil south pole) and at a distance of 50–60 mm from the plate edge were –29.18 and –21.33 ‰, PDB, respectively; and the isotopic compositions at the points to the right and to the left from the latter point changed in favor of ^{12}C (Fig.2, curve 1). At the opposite edge (North Pole), $\delta^{13}C$ = –26.24‰, PDB. In the control experiment, at the plate without the magnetic field, $\delta^{13}C$ = –26.55‰, PDB.

To exclude the influence of admixtures, which can be present in limestone, all further experiments were carried out with calcium carbonate of reagent grade.

A sample of calcium hydroxide prepared from $CaCO_3$ of reagent grade was kept in the coil (the magnetic field strength of 8700A/m) for 500 h. The value of $\delta^{13}C$ for the control plate was –35.22 ‰, PDB. The isotopic compositions ($\delta^{13}C$) determined at the plate placed in the magnetic field were as follows: –28.47 and –28.73‰, PDB, at the edges of the plate, and –17.62 ‰, PDB, at a distance of 40 mm from the south pole of the coil. In the opposite directions from this point, an increase in the ^{12}C concentration was observed. The maximum difference between the ratios $^{13}C/^{12}C$ at the plate edge and at the points distant from the edges amounts to 11‰ at a distance of 50 mm. The carbon isotopic compositions along the profile of sampling are shown in Fig. 2, curve 1. The $\delta^{13}C$ value in the control experiment was –35.64 ‰, PDB.

In the third run, the sample was kept in the magnetic field with the magnetic field strength of 4350 A/m for 770 h. After this exposure, 18 probes 5?15 mm in size were sampled. The plate was arranged parallel to the solenoid axis. The carbon isotopic compositions along the profile of sampling are shown in Fig. 2, curve 2. The $\delta^{13}C$ value in the middle of the plate was –20.69 ‰, PDB. In the control run, in the absence of a magnetic field, the value was equal to – 35.61 ‰, PDB. The different $\delta^{13}C$ values in the second and third runs were due to different degrees of conversion of calcium hydroxide into $CaCO_3$ over the experiment time. The conversion was no more than 30% for experiment durations within 500–700 h.

The formation of calcite in all experiments is accompanied by an increase in the ^{12}C content compared with the isotopic composition of air carbon dioxide. However, the enrichment of $CaCO_3$ with ^{13}C isotope in the magnetic field is larger by 14% than in the runs without magnetic field.

In the fourth run, the sample was kept in the magnetic field with the magnetic field strength of 1750 A/m for 672 h. The carbon isotopic compositions along the profile of sampling are shown in Fig. 2. The $\delta^{13}C$ value have 2 minimum (– 29.60 and – 29.77 ‰; PDB). A distance is between minimums 45 mm (Fig. 2, curve 3). A deployment don't have well-marked from sampling points. The difference is between the values equal to 2.7 ‰; PDB. This is a heavy isotope ^{13}C enrichment is not located in the middle of the coil with a current. In this case, the magnetic field has a limit, at which there are noticeable changes in the isotopic composition of carbon. On further reduction of the strength of the current in the coil already practically there will be no nuclear isotope effect. But, and this value of the magnetic field there is still enrichment isotope ^{13}C of the newly formed $CaCO_3$. The $\delta^{13}C$ value in the control experiment was – 36.00 ‰, PDB.

In 5-th experiment study the formation of calcite occurred in the coil without input (0 A). The experiment was run for 1008 h. In the control experiment value is $\delta^{13}C$ = – 35.54 ‰; PDB. Control plate was located in another room. Profile isotopic composition is presented in Fig. 3, curve 4. This experiment was conducted to determine the additional factors that could change the isotopic composi-

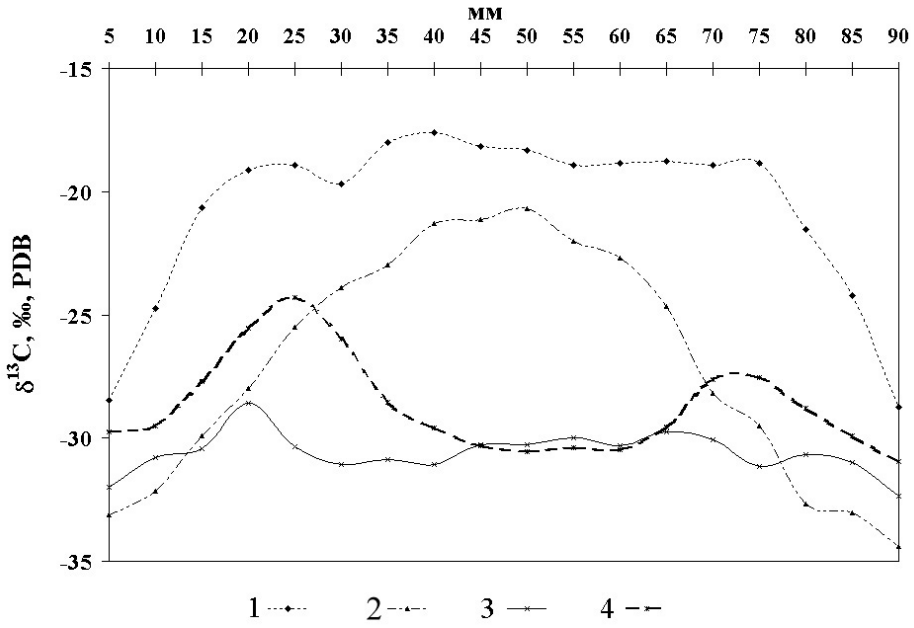

Fig. 2. Profiles of the isotopic composition of carbon in $CaCO_3$ formed in the solenoid magnetic field: 1 – the value of $\delta^{13}C$ in 2 experiment; 2 – value $\delta^{13}C$ in 3 experiment; 3 – the value $\delta^{13}C$ in 4 experiment; 4 – the value $\delta^{13}C$ in 5 experiment.

tion of carbon. There are two areas which were enriched with the heavy isotope ^{13}C, on the profile of the isotopic composition of carbon, as in previous experience. The distance between these points is equal to 50 mm, This distance is approximately equal to the length between the entries in the coil. Between are the terminals of the coil, the distance is 52 mm. They are made of steel, which is in the process of the electric current passing is magnetized. Accordingly, there is residual magnetic field, which affects the carbon isotope composition in 4 and 5 experiments. Where residual magnetic field has almost no effect, carbon isotopic compositions do not differ by more than 1 ‰; PDB.

The main difference is in the reaction of $CaCO_3$ at the interaction of $Ca(OH)_2$ with carbon dioxide air that no radical groups that are present in the photochemical reaction collapse of the dibenzylketone and subsequent recombination [Buchachenko, 2007; Galimov,1979]. It is known that two stable carbon isotope ^{12}C and ^{13}C have respectively zero and is half-integer spin. The oxygen isotopes ^{16}O and ^{18}O have zero spin, and isotope ^{17}O has spin equal to the 5/2 [Galimov,1979]. If to consider options for CO_2 molecule with different isotopes of carbon, the molecules $^{16}O^{13}C^{16}O$, $^{18}O^{13}C^{16}O$ and $^{18}O^{13}C^{18}O$ have is half-integer spin. In these molecules electrons are paired, and the electron spins are compensated, i.e. the total electronic spin is zero.

In the magnetic field of a molecule with half-integer spin behave as paramagnetic with the passage of the reaction, i.e. they have an additional component of the velocity in the thermal motion, which makes them move along the field lines. The direction of movement of molecules with half-integer spin along the lines of the magnetic field affects the probability of reaction of $CaCO_3$ with isotope ^{13}C. Maximum enrichment isotope ^{13}C is located in the middle of the coil with a current density of the magnetic field lines greatest experiments approximately.

Enrichment of the heavy isotope ^{13}C at the formation of $CaCO_3$ in a magnetic field is another factor that affects the isotopic composition of natural carbonates. In particular, in natural systems have magnetic minerals. Pyrrhotite and magnetite have its own magnetic field. Weakly magnetic minerals, acquire magnetic properties under the action of electric field. These minerals can change the isotopic composition of carbon in carbonates in sequential education. These changes will be localized around the magnetic minerals.

Another aspect of the manifestations of nuclear-magnetic effect may be holding paleomagnetic studies. You can imagine the Earth's magnetic field present in the form of a coil with electric shock. Proceeding from the above experiments, it is possible to change attitudes of stable isotopes of carbon $^{13}C/^{12}C$, spend paleomagnetic reconstructions. To conduct reconstruction requires a large amount of data on isotopic composition and careful selection of samples that should be strictly oriented.

References

Buchachenko, A.L., Galimov, E.M., Ershov, V.V., Nikiforov, G.A., Pershin, A.D. enrichment of isotopes, the induced magnetic interactions in chemical reactions // Doklady Akademii Nauk USSR, 1976. Vol. 228 (2). P. 379–381 [in Russian].

Buchachenko, A.L. New Isotopic in Chemistry and Biochemistry. Moscow, Nauka, 2007. 189 p. [in Russian].

Galimov, E.M. Nuclear spin isotope effect – a new type of isotope effect // Geochemistry International, 1979. No. 2. P. 274–284 [in Russian].

N.P. Safina[1, 2], I.Yu. Melekestseva[1], N.N. Ankusheva[1, 2], A.M. Yuminov[1, 2], P. Nimis[3], V.A. Kotlyarov[1]

[1] *Institute of Mineralogy UB RAS, Miass, Russia, safina@ilmeny.ac.ru*

[2] *National Research South Ural State University, Chelyabinsk, Russia*

[3] *Padova University, Padova, Italy*

BARITE FROM THE ANCIENT VMS-DEPOSIT AND MODERN HYDROTHERMAL SULFIDE FIELDS: A COMPARISON OF FORMATION CONDITIONS

В работе изложены результаты изучения минеральных ассоциаций, химического и изотопного составов, термобарогеохимических характеристик флюида, образовавшего барит из серноколчеданных колломорфных и обломочных руд палеозойского Сафьяновского месторождения (Средний Урал) и кайнозойских гидротермальных полей Семенов-1 и Семенов-3 (САХ).

В результате проведенных исследований установлены черты сходства и отличия процессов образования баритсодержащих минеральных ассоциаций в различных текстурных типах руд из разновозрастных колчеданных построек. В брекчиях, в отличие от колломорфных и тонкозернистых руд, отмечается сходство минеральных ассоциаций баритов. Отличия выявлены в содержании микропримесей, изотопном составе и параметрах флюида, образовавшего барит.

Barite is one of the widespread gangue minerals both in on-land volcanogenic-hosted massive sulfide deposits and submarine hydrothermal sulfide vent systems. The different formation conditions of barite are recorded in its morphology, chemical and isotopic composition, and fluid inclusions [Paytan et al., 2002], thus it may serve as an indicator of formation conditions of accompanying massive sulfides. This work presents the comparative study of barite from low-metamorphoused Devonian Saf'yanovka VMS-deposit in the Central Urals and Cenozoic Semenov-1 and Semenov-3 hydrothermal sulfide fields in the Mid-Atlantic Ridge. The mineral assemblage, chemical and isotopic composition, and fluid inclusions were analyzed in barite from colloform, fine-crystalline and clastic sulfides.

The barite-bearing ore samples from the Saf'yanovka deposit were collected from the main orebody in the operating open pit. The deposit hosted by rhyolitic–dacitic–andesitic–basaltic volcanic complex [Yazeva et al., 1991]. Based on the detail ore-facial mapping, the major subvertical triangle-shaped ore lens was reconstructed as a destroyed sulfide mound [Maslennikov, 2006]. The colloform pyrite ores with barite and quartz in the top of the sulfide body represent the fragments of seafloor hydrothermal slabs. The sulfide breccias and sandstones with clasts of massive and colloform ores and black smoker chimneys cemented by barite, quartz and, locally, by C-bearing silty sandstones are located in the southern flank of the main orebody.

Massive sulfides from the Semenov-1 and -3 hydrothermal fields were collected in the 30th cruise of the R/V *Professor Logachev* in 2007. The hydrothermal fields are the part of the large Semenov massive sulfide cluster [Beltenev et al., 2007]. The Semenov-1 field (13°30.87? N, 44°59.24? W) is situated near the seamount foot at a depth of 2570–2620 m. It represents a single mound or, more probably, a series of coalescent sulfide mounds and their destruction products [Ivanov et al., 2008]. The dredged samples included serpentinized ultramafic rocks, altered basalts, and massive sulfides, containing up to 20 vol % of barite. The Semenov-3 field (13°30.70? N, 44°55.00? W) is located on the northeastern slope of the seamount at a depth of 2400–2600 m and is associated with altered basalts [Beltenev et al., 2007]. Sulfide breccias with marcasite–pyrite clasts enclosed in the fine-grained sulfide–quartz cement were recovered from the seafloor.

The abundance of fine-crystalline, porous, nodular, banded, and colloform textures, predominant iron disulfides over Cu-Fe-Zn-sulfides and presence of barite and less abundant quartz bring together the Saf'yanovka and Semenov-1 colloform sulfides, indicating similar way of their formation. Barite crystals from both objects are large, tabular and form rosettes that is typical of hydrothermal barites [Paytan et al., 2002]. Barite from the Saf'yanovka colloform ores is associated with late quartz and was formed after major sulfides. The most part of barite from the Semenov-1 fine-crystalline massive sulfides is the earliest mineral precipitated before the sulfides. Less amount of barite was formed at the final stage of mineral deposition.

Barite from the Saf'yanovka and Semenov-3 pyrite breccias is a late mineral formed after destruction of the early colloform sulfides and their cementation by newly formed sulfides. Barite from the Saf'yanovka clastic ores is most likely postdiagenetic, because it develops after diagenetic pyrite framboids and metacrystals. Barite crystals, locally with stylilote boundaries, are deformed as a result of increasing pressure. The compact barite aggregates owing to the straitened crystallization conditions are similar in morphology with diagenetic barite from ocean sediments [Paytan et al., 2002]. Barite from the Semenov-3 field is a product of late hydrothermal input. It grew in the large cavities in clasts and cement, forming the typical radial aggregates of large tabular crystals and, locally, associating with late chalcopyrite.

Based on microprobe analysis, Sr is a major admixture in barite. Sr contents in barite from the Saf'yanovka deposit (0.00–0.83 wt %), Semenov-1 (0.31–4.45 wt %) and Semenov-3 (0.50–2.84 wt %) fields are typical of barite from many ancient VMS-deposits and modern hydrothermal sulfide fields. So, Sr content by itself could not be the reliable genetic indicator.

Different trace element distribution based on ICM-MS analysis is caused by different reasons. The increased Zn contents in barite from the Semenov-1 field and elevated Zn, Pb, As, Te, Hg and Bi contents in barite from the Saf'aynovka clastic ores reflect microinclusions of sphalerite (Semenov-1) and sphalerite, galena and various sulfosalts (Saf'aynovka). The elevated Co, Ni, Mn, and U contents in barite from the Semenov-1 field derived from seawater. The higher Cu, Ga, Ge, and Sb contents in barite from the Semenov-3 field may be attributed to the contribution of high-temperature hydrothermal fluid during coeval precipitation of barite and Cu-Fe-sulfides.

Increase in $\delta^{34}S$ values in barite from the Saf'yanovka colloform (+25.5 ‰) and clastic (+27.0 ‰) ores relative to the $\delta^{34}S$ values of the Silurian–Devonian seawater (+23...+24 ‰) [Claypool et al., 1980] is a result of bacterial activity that agrees with numerous relics of sulfidized near-hydrothermal fauna in colloform ores and their clasts in breccias. This fact also corroborates the presence of N_2, CO, and CH_4 in gaseous mixture from fluid inclusions. Sulfur isotopic composition of the Semenov-1 barite (+21.0 and +21.3 ‰) completely corresponds to that of the contemporary seawater (+21.2 ‰) [Rees et al., 1978]. Little decrease in $\delta^{34}S$ values in barite from the Semenov-3 breccia (+20.6 ‰) may indicate contribution of some portion of light sulfur isotope from the high-temperature hydrothermal fluid.

Barite in the Saf'yanovka colloform ores and Semenov-1 fine-crystalline sulfides was crystallized from relatively low- to medium-temperature and low-salinity fluids of compound composition: 182–204 °C, 1.5–4.5 wt % NaCl-eq., NaCl–Na_2SO_4–H_2O and NaCl—$NaHCO_3$–H_2O (Saf'yanovka) and 83–224 °C, 0.6–3.8 wt % NaCl-eq., Na_2SO_4–K_2SO_4–H_2O and Na_2SO_4–$NaHCO_3$–H_2O (Semenov-1). The hydrothermal fluid most likely underwent phase separation that is evident from low salinities. The presence of SO_2 and CO_2 in fluid inclusions in barite from the Semenov-1 field may indicate the magmatic contribution. Barite from clastic ores was formed from medium-temperature (150–190 °C), low-salinity (1.0–5.5 wt % NaCl-eq.) NaCl-dominant fluid at the Saf'yanovka deposit and high-temperature (270–340 °C), medium- to high-salinity (4.5–9.5 wt% NaCl-eq.) Na_2SO_4–NaCl–H_2O fluid at the Semenov-3 field.

The results of our study have revealed similar formation conditions of hydrothermal barite from the ancient massive sulfide deposit and modern hydrothermal sulfide fields. Barite from the colloform ores was formed from the low-temperature low-saline fluid of compound composition in contrast barite from clastic ores, which was crystallized from moderate- to high-temperature higher saline NaCl-dominant fluid. Phase separation of the fluids played important role in formation of barites from colloform ores that may be deduced from one- and two-phase fluid inclusions and low salinity relative that of seawater. Some discrepancies in chemical composition, sulfur isotopic composition or fluid inclusion data reflect specific geological-mineralogical environments of barite formation. The high-temperature barite from the Semenov-3 clastic ores could incorporate some portion of light sulfur isotopes from the high-temperature hydrothermal fluid that was resulted in slightly decreased $\delta^{34}S$ values. Increased sulfur

isotopic composition of barite from the Saf'yanovka ores is a consequence of bacterial reduction that is in accordance with abundant fauna relics in the deposit. Barite from the Saf'yanovka ores was formed under more reducing conditions that is evident from the higher CO and CH_4 contents in gaseous composition of fluid inclusions. High Cu content, higher homogenization temperatures of fluid inclusions and higher salinity of the fluid in barite from the Semenov-3 clastic ores are related to its precipitation from the high-temperature hydrothermal fluid in assemblage with late Cu-Fe-sulfides.

Authors thanks Dar'ya Kiseleva (IGG UB RAS, Yekaterinburg, Russia) for ICP-MS analysis, Raul Carampin (IGG-CNR Padova, Italy) for microprobe analyses, Tat'yana Nazarova (VSEGEI, St-Petersburg, Russia) for sulfur isotopic analyses, and Olga Mironova (GEOKHI RAS, Moscow, Russia) for gas chromatography of fluid inclusions.

This research is supported by Program of Presidium of the Russian Academy of Sciences No. 23 (project no. 12–P–5–1003) and Russian Federal Program of Ministry of Science and Education (project no. 14.740.11.1048).

References

Beltenev, V., Ivanov, V., Rozhdestvenskaya, I. et al. A new hydrothermal field at l3?30' N on the Mid-Atlantic Ridge // InterRidge News, 2007. Vol. 16. P. 9–10.

Beltenev, V., Ivanov, V., Rozhdestvenskaya, I. et al. New data about hydrothermal fields on the Mid-Atlantic Ridge between 11?–14? N: 32nd cruise of R/V Professor Logatchev // InterRidge News, 2009. Vol. 18. P. 14–18.

Claypool, G.E., Holser, W.T., Kaplan, I.R., Sakai, H., Zak, I. The age curves of sulphur and oxygen isotopes in marine sulphates and their mutual interpretation// Chem. Geol., 1980. Vol. 28. P. 199–260.

Ivanov, V.N., Beltenev, V.E., Stepanova, T.V. et al. Sulfide ores of the new hydrothermal fields at 13°31' N MAR // In: Metallogeny of ancient and modern oceans-2008. Ore-bearing complexes and ore facies. Miass, IMin UB RAS, 2008. P. 19–22 [in Russian].

Maslennikov, V.V. Lithogenesis and formation of massive sulfide deposits. Miass, IMin UB RAS, 2006. 383 p. [in Russian].

Paytan, A., Mearon, S., Cobb, K., Kastner, M. Origin of marine barite deposits: Sr and S isotope characterization // Geology, 2008. Vol. 30. No 8. P. 747–750.

Rees, C.E., Jenkins, W.J., Monster, J. The sulfur isotopic composition of ocean water sulfate // Geochim. Cosmochim Acta, 1978. Vol. 42. P. 377–381.

Yazeva, R.G., Moloshag, V.P., Bochkarev, V.V. Geology and ore parageneses of the Saf'yanovka massive sulfide deposit in the Central Urals back thrust // Geol. Ore Dep., 1991. Vol. 3

E.M. Sapargaliev, N.V. Polyansky, G.D. Ganzhenko
Altai Geological Environmental Institute, Ust-Kamenogorsk, Republic of Kazakhstan
sapar_vko@mail.ru, agei_vko@mail.ru

FORMATION CONDITIONS OF THE RIDDER-SOKOLNOE DEPOSIT, RUDNYI ALTAI, KAZAKHSTAN

Риддер-Сокольное золото-полиметаллическое месторождение является крупнейшим на Рудном Алтае. Формирование оруденения связано с раннедевонским (эмс) вулканизмом. Оруденение локализовано в депрессионной палеоструктуре, возникшей на склоне или подножье подводной вулканической гряды. Его размещение контролировалось зонами трещиноватости, служившими проводниками гидротермальных рудоносных растворов, отлагавших оруденение в придонной части морского бассейна и на путях их следования. Отчетливо проявлены признаки выноса рудного материала из подрудных пород месторождения.

The Ridder-Sokolnoe gold-polymetallic deposit is the largest deposit in the Rudny Altai. It is located in the Leninogorsk-Zyryanovsk subzone of the Rudny Altai metallogenic zone within the Leninogorsk graben bounded by the Ivanovsky (Obruchevsky) reversed fault in the south and Severny thrust in the west, north and northeast, which is alternated by the Bosyakovsky reversed fault in the southeast. The territory of the graben hosts the Leninogorsk ore field with Ridder-Sokolnoe and similar Kryukovskoe, Novo-Leninogorskoe, Obruchevskoe, and Dolinnoe deposits.

The polymetallic massive sulfide volcano-sedimentary deposits of the Rudny Altai are related to the Emsian-Frasnian basalt-rhyolite volcanism. The mineralization in the ore zones is concentrated at the different stratigraphic levels. In particularly, mineralization of the reviewed ore field is hosted in the Emsian rocks including Leninogorsk, Kryukovskaya, and Il'inskaya formations and Eifel Sokolnaya Formation.

The lower part of the volcanic-sedimentary Leninogorsk Formation consists of hydrothermally altered rhyolite and dacite lavas and lavabreccias and the upper part is composed of various kinds of tuffs, volcanomictic gravelstones, sandstones, and siltstones. The thickness of the formation is 50–350 m.

The Kryukovskaya Formation is subdivided into three members. In the northern part of the deposit, the lower member is composed of sedimentary breccias with angular and semirounded fragments of felsic volcanic rocks, rarely, sedimentary and metamorphic rocks and granites, which are cemented by aleuropelitic material. Occasional pyrite and pyrite-polymetallic ore clasts and interlayers of sandstones and siltstones may be found in the lower member. The thickness of the lower member reaches up to 350 m. These rocks facially transit to siltstones and silty sandstones with rare sandstones 120 m thick.

The intermediate member is composed of siliceous, carbonaceous-clayey, and calcareous claystones and siltstones with interlayers of sandstones. The siliceous rocks are often transformed into microquartzites and sericite microquartzites. The sericite-chlorite-quartz rocks are probably volcanic in origin. The thickness of members varies from 300–400 m in the western part of the ore field up to 50 m and complete pinching out at the northeastern part. In area of the Kryukovkoe orebody, this member is completely replaced by lava-extrusive bodies transformed into quartzites and sericite-quartz altered rocks. Some areas (Ridder, Central, and Northeastern orebodies) host andesitic sills.

The upper member with thickness varying from 10 m up to the first hundred meters includes calcareous siltstones (shists of the hanging wall). The member completely pinches out in the arches of some cupola structures and in these areas the rocks of the Il'inskaya Formation lie over this intermediate member of the Kruykovskaya Formation.

The boundary with Il'inskaya Formation is characterized by appearance of the mafic and intermediate volcanic rocks. The formation is composed of tuffs, tuffaceous and volcanomictic gravelstones and sandstones with interlayers of lavas of andesites, basaltic andesites, and basalts. The red and lilac colors of the rocks are the typical features of the Il'inskaya Formation. The thickness of the formation varies from 20–30 m in the northern part of the ore field up to 200–250 m in its southern part.

The Late Devonian dolerite dikes crosscut the entire Devonian structure of the deposit.

The Ridder-Sokolnoe deposit is located within the Severnaya (North) anticline, the near-latitudinal axis of which is close to the Severny thrust in the northern part of the deposit. Within the deposit, the Severnaya anticline is complicated by the Ridder-Sokolnaya and Kryukovskaya brachianticlines. The Ridder-Sokolnaya brachyanticline, hosting the major orebodies, is transversely oriented to the axis of the Severnaya anticline, is 2.5–3 km wide, and is traced for 50 m. The dip angles of its wings are usually 3–5? to 10–15?, locally, up to 60? in the western wing with flexural folds (the western flank of the Rudder orebody and Zavodskaya orebody). The wings are gradually flattened and beyond its limits become slightly inclined or horizontal. Uplifting again, the northeastern wing forms the Kryukovskaya brachianticline.

In addition to the above-mentioned Severny thrust and Ivanovsky (Obruchevsky) reversed faults, the ore field is cut through by NW- and NE-trending faults, which displace the structure for more than tens and hundreds of meters. These displacements probably reflect the weakened fracture zones resulted from the scattered spreading that is confirmed by the coinciding orientation of fractures developed in the rocks and above mentioned faults.

The polymetallic massive sulfide ores from the Ridder-Sokolnoe deposit are characterized by increased Au and Ag contents. Currently, it is accepted that formation of precious metal mineralization is closely related to that of polymetallic massive sulfide ores in contrast to the previous point of view.

The total area of sulfide mineralization exceeds 20 km^2. The mineralization occurs in the rocks from the upper member of the Kryukovskaya Formation up to the green shists of the Zavodskaya Formation and is traced for 800 m to the depth. It is subdivided into four horizons. The main volume of economic mineralization is concentrated in the intermediate member of the Kryukovskaya Formation.

Gold-polymetallic mineralization is related to the first horizon and concentrated in the intermediate member of the Kryukovskaya Formation under the hanging wall shists of the upper member. Below, in microquartzite, it is replaced by network stockwork, transiting into the vein bodies to the depth, which host gold-polymetallic mineralization in the transiting and upper parts and copper-zinc ores in the

deeper levels. The layered polymetallic ores of the second Ridder orebody are also related to the first horizon. These ores are hosted by the member of intercalating carbonaceous siltstones and claystones.

The second horizon includes the mineralization at the contact zone of intermediate siltstone and lower gravelite-agglomerate member of the Kryukovskaya Formation. The roots of the above mentioned veins with zinc-copper and copper ores are also related to this horizon. The boundary between the first and second horizons is either conditional or clear in different areas. For example, quartz-sulfide veins of the second horizon in the Central orebody forms subconformable body of copper ores, which are separated by the barren sericitized quartzites and sericite-quartz rocks from the overlying ores of the first horizon. In some areas, the mineralization of the second horizon is characterized by the absence of ores of the first horizon. The Au content of ores from the second horizon is lower in contrast to the first one.

The third ore horizon is confined to the contact of the Kryukovskaya and Leninogorsk formations and represents the pocket and stringer-disseminated polymetallic mineralization. It is possible that Zavodskaya orebody is located at this level.

The fourth ore horizon is hosted in the green shists of the Zavodskaya Formation at the contact with the Leninogorsk Formation. The mineralization represents the subconformable lens-shaped bodies of stringer-disseminated polymetallic and copper-zinc ores combined in the footwall with crosscutting bodies, intruding the green schists to the depth of 100 m and more. The content of precious metals is the lowest. At present, it is not mined. The relation of this mineralization and mineralization at other horizons is not identified. Probably, this mineralization is early, because ore clasts similar in composition were found in the clastic sediments of the lower member of the Kryukovskaya Formation.

On the basis of the above mentioned data, the generalized geological-genetic model of the formation of the deposit (mineralization of the first and second horizons) is as follows.

The Emsian depression on the slope or at the foot of the submarine volcanic ridge characterized by the high degree of fracturing of the seafloor was a place of discharge of the hydrothermal fluids, ascending through the fracture zones. The latters were probably related to the magma chamber, which has produced the volcanic rocks of the bottoms of the ore-bearing section. In the initial stages, the fluids were relatively low-temperature, depleted in metals, and enriched in Si. Mixing with cold bottom waters, they deposited siliceous hydrogel admixed with dispersed sulfides. The rate of accumulation of these sediments exceeded the rate of sedimentation outside the fracture zones that caused the formation of arched uplifts composed mostly of siliceous sediments along the fracture zones.

The main stage of ore formation is related to the high-temperature fluids enriched in metals, which were the products of the developed hydrothermal system affected deeper zones. At this stage, the hydrothermal vents were concentrated at the local areas of fracture zones, leading to the formation of the cupola structures.

The mineralization of the first and second horizons was deposited simultaneously that is evident from zonation typical of sulfide deposits. We suppose that copper and copper-zinc ores were deposited at the depth of 150–400 m from the seafloor surface and polymetallic veins were formed at the depth of 150 m under the boundary between the rocks and unlithified sediments. In initial stages, the polymetallic massive sulfide bodies were separated by areas of hydrothermal-sedimentary rocks with disseminated ore mineralization. In some areas, the formation of such orebodies is ended by formation of quartz-barite cupolas with size of 500 ? 200 m in the lower part of the cupola and more than 100 m along the vertical from the base. The basement and periphery of the cupolas contain individual massive sulfide bodies, locally, with clastic structure and cemented by quartz-barite or carbonate-quartz aggregates with disseminated sulfides. In the top areas of the cupolas, quartz-barite rocks may be alternated by hematite-barite-quartz rocks. The boulders and blocks of ores and quartz-barite rock buried in the sedimentary rocks of the hanging wall are often found in the cupola slopes. The quartz-barite bodies in the lower part of the cupolas transit into the underlying microquartzites through the stockwork zone, where the brecciated microquarzites are cemented by barite. The hematite-bearing rocks in the top of the cupolas indicate change of the reduced conditions into the oxidized ones.

At the final stages, the hydrothermal activity exhausted and orebodies were buried by the sediments. However, some areas show the traces of the late hydrothermal activity, manifesting in the small zones of hydrothermally altered rocks with stringer-disseminated polymetallic mineralization in the schists of the hanging wall.

I.B. Seravkin
Institute of Geology, Ufa Scientific Center, RAS, Ufa, Russia, seravkin@ufaras.ru

TYPES OF VHMS DEPOSITS OF THE URALS AND THEIR GEODYNAMIC SETTING

Рассмотрены колчеданные месторождения (КМ) Южного Урала в сравнении с мировыми типами и их геодинамическая позиция. Все типы КМ (ивановский (Ni)-Co-Cu, домбаровский (Co)-Cu, уральский Zn-Cu и Cu-Zn и баймакский Au-Ba-Pb-Cu-Zn) формировались в различных обстановках девонской островодужной системы. Локальные колчеданоносные пояса обладают поперечной и продольной зональностью. Последняя заключается в смене по простиранию пояса существенно медных руд медно-цинковыми и полиметаллическими.

The Urals is a classical province of the development of volcanogenic-hosted massive sulfide deposits. The South Urals VHMS deposits are less metamorphosed and retain the original features. The Magnitogorsk zone is most productive for sulfide mineralization in the South Urals and contains seven of eight large (100 000 t and more of ore) deposits in the Urals such as Uchaly, Novo-Uchaly, Uzelga, Sibai, Yubileinoe, Podolsk, and Gai [Prokin et al., 2011]. This gives a reason to examine in detail VHMS deposits from the Magnitogorsk zone as an example.

Based on the ore composition, the author distinguishes four main types of VHMS deposits: 1) Ivanovka (Ni)-Co-Cu, 2) Dombarovka (Co)-Cu, 3) Urals Cu-Zn and 4) Baimak Au-Ba-Pb-Cu-Zn. All types are characterized by certain correlations with ore-hosting complexes, such as basalt-ultramafic rocks, basalt, basalt-rhyolite, and basalt-andesite-rhyolite, which were formed in different geodynamic settings of the Devonian island arc system in the South Urals. The most common types were compared to the world known Noranda, Cyprus, and Kuroko types. The Zimnee deposit in the South Urals close to the other deposits of the Dombarovka ore region, however, may be referred to the Besshi type. The geological models of the VHMS deposits of the South Urals are shown in figure.

The Ivanovka type includes Ivanovka, Dergamysh, Ishkinino, South Voznesenka, and Yuldashevo deposits, which are hosted in the melange zone of the Main Ural Fault (MUF) in association with basalts and ultramafic rocks. Massive sulfide bodies occur at the top of ultramafic blocks and sheets in association with serpentinite conglobreccia. The ore clasts incorporated into serpentinite sandstones that overlap massive sulfide lenses indicate that sulfide ores were formed on a seafloor (Fig.). Later, the ores, serpentinites, and sandstones with ore clasts were probably overlain by basalts. Pyrrhotite is the major ore mineral of these deposits. The pyrite-pyrrhotite, chalcopyrite-pyrite-pyrrhotite, and cobaltite-arsenopyrite-chalcopyrite-pyrite-pyrrhotite ore types were recognized among massive ores [Melekestseva, 2007]. It is considered that the deposits were formed under conditions of the accretionary prism at the front of the Early Devonian island arc.

The Dombarovka type in the South Urals includes Letnee, Osennee, and Levoberezhnoe copper massive sulfide deposits in the same named ore district on the eastern limb of the Magnitogorsk zone. Mostly copper ore and host basalts are the specific features of these deposits. The sheetlike bodies of sulfide and magnetite ores are hosted in the Early Devonian pillow lavas and hyaloclastites of the Kiembaevo Formation (Fig). The magnetite, magnetite-chalcopyrite-pyrite, chalcopyrite-pyrite, and sphalerite-chalcopyrite-pyrite ore types were distinguished at the Letnee deposit [Ismagilov, 1978]. The magnetite ores also contain pyrite (~5%), rare chalcopyrite, sphalerite, molybdenite, hematite, and gangue minerals. This ore is localized at the basement and inside of sulfide bodies and also form individual bodies. The magnetite ores are often lenticular-banded. The host basalts at the Dombarovka type were formed in the inter-arc spreading basin, which was developed after the rift structure.

The well-known South Urals medium to large deposits (Uchaly, Sibai, Yubileinoe, Podolsk, etc.) and the giant Gai deposit belong to **the Urals type**. The Cu-Zn ores and host basalt-rhyolite and basalt-andesite-rhyolite complexes are their specific features. Based on the ore composition and geological setting, the deposits are subdivided into three subtypes: Urals I (copper massive sulfide ore with $Cu \geq Zn$ hosted in basalt of bimodal complex or at their top); Urals II (copper-zinc massive sul-

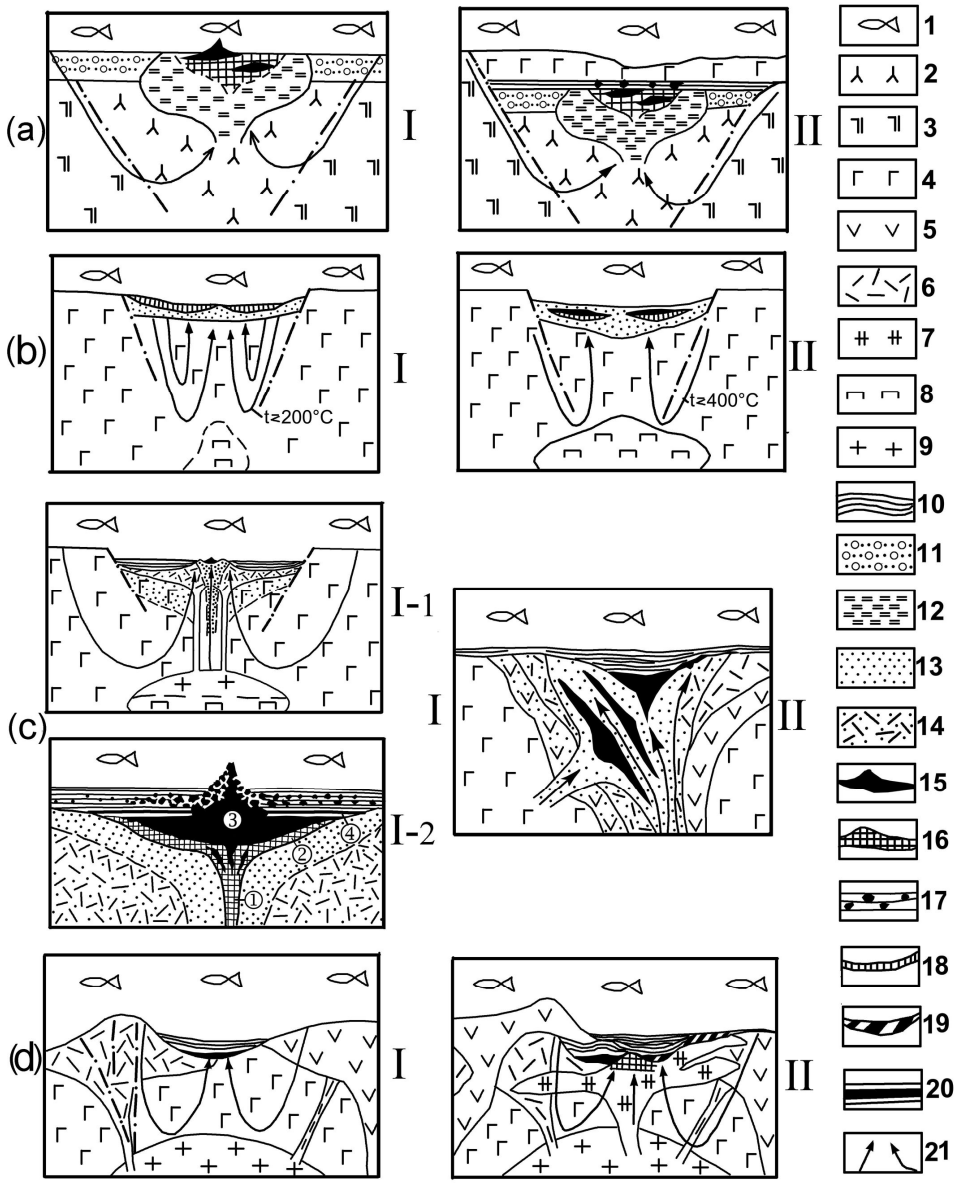

Fig. Geological models of different types of VHMS deposits in the South Urals [Seravkin, 2007]: a – Ivanovka, b – Dombarovka, c – Urals, d – Baimak types.

I – early stages of formation, II – late stages of formation; I-1, conceptual model of ore-generating volcanic edifice; I–2, model of Cu-Zn massive sulfide body of the Urals type; numerals in circles: 1, zone of feeder channels; (2–4) region of ore deposition: 2, zone of fractured volcanic rocks replaced by sulfides; 3, local depression of the sea floor filled with sulfide and terrigenous muds; 4, zone of deposition of bedded volcanosedimentary ore; (d) Baimak type: I, early Cu–Zn stage; II, late gold–barite–base-metal stage.

(1) Seawater; (2) serpentinite; (3) Ordovician–Silurian basalts; (4) Devonian basalts; (5) andesite and andesitic dacite; (6) felsic volcanics: dacite, rhyodacite, rhyolite; (7) late subvolcanic bodies of rhyodacite with quartz phenocrysts; (8, 9) magma chambers: (8) mafic and (9) felsic; (10) volcanosedimentary and sedimentary rocks; (11) serpentinite breccia, conglomerate, and sandstone; (12–14) metasomatic and partly altered rocks: (12) chlorite–talc, (13) chlorite–sericite–quartz and sericite–quartz; (14) chloritized, sericitized and propilitic rocks; (15–20) ores: (15) Cu and Cu-Zn massive, (16) impregnated, stringer–disseminated, and stockwork, (17) ore clasts in sedimentary rocks, (18) magnetite, (19) base-metal massive; (20) bedded volcanosedimentary sulfide; (21) paths of hydrothermal solutions.

fide ore with Cu ≤ Zn hosted in felsic rocks of bimodal complex or at their top); and Urals III (copper-zinc massive sulfide ore hosted in basalt-andesite-rhyolite complex).

The deposits of **the Urals I subtype** (Yubileinoe and Buribai) are hosted in the lower part of the Lower Devonian Baimak-Buribai Formation in the western part of the Buribai-Makan ore district. The deposits of the Urals I subtype are characterized by association of ore with pillow basalts. For ex-

ample, at the Yubileinoe deposit, the large lenticular orebodies occur at the top of volcanic structures composed of pillow-lavas and pinch out beyond them [Seravkin, 1986]. The copper (chalcopyrite-pyrite) ore is dominant, however, pyrite and sphalerite-chalcopyrite-pyrite ores are recorded as well. The deposits of the Urals I subtype were formed in a trough on the front of an embryonic island arc (D_1e).

The Urals II subtype includes the large and well explored Sibai, Uchaly, and New Uchaly deposits, which are situated in the Sibai and Uchaly ore districts. This subtype is distinguished by the prevalence of Zn over Cu (threefold at the Uchaly deposit) and by ore localization in felsic rocks or at their tops in bimodal complexes of the Eifelian Karamalytash Formation. The ore-bearing Karamalytash Formation was formed as a result of dispersed spreading in the inter-arc basin. The ore-bearing paleovolcanoes with increased volume of felsic igneous rocks such as Sibai and Uchaly were formed in the spreading centers.

The Urals III subtype includes the medium-sized Molodezhnoe, Imeni XIX Parts'ezda, and Oktyabr'skoe deposits, the large Uzelga and Podolsk deposits, and the giant Gai deposit. These deposits are hosted in basalt-andesite-dacite complex of the Lower Devonian Baimak-Buribai Formation (Makan ore field, Gai deposit), basalt–basaltic andesite-andesite-rhyodacite complex of the Lower-Middle Devonian Irendyk Formation (Podol deposit), and basalt-basaltic andesite-rhyodacite complex of the Eifelian Karamalytash Formation (deposits of the Verkhneuralsk ore district). The deposits of the Urals III subtype are characterized by stratiform orebodies at several closely located stratigraphic levels, for example, at three levels at the giant Gai deposit. The two lower levels consist, in turn, of several orebodies. The ore layers and lenses at each level end the local rhythms of felsic volcanics. The deposits of the Urals III subtype were formed under conditions of the early island arc on a thick basaltic basement, in the large volcanic centers that underwent caldera collapse [Seravkin, 1986, 2007].

The Baimak type of gold–barite–base metal massive sulfide deposits is widespread in the Baimak, Alexandrinka, and Terensai (Dzhusa and Barsuchii Log deposits) ore districts (Fig.). In the first district, the deposits are hosted in volcanic rocks of the Baimak-Buribai Formation, partly associated with its lower basalt-rhyolite complex but largely with the overlying continuous basalt–andesite–rhyolite complex. The early copper massive sulfide and late gold-barite-base metal stages of mineralization were distinguished in the Baimak district (Fig.). The second stage of mineralization followed emplacement of rhyodacite subvolcanic bodies with large quartz phenocrysts, which ends the continuous volcanic series. Most of numerous small base metal massive sulfide, gold-barite, and gold-pyrite deposits were formed at the late stage, emphasizing the zonal ore field structure. In addition to common sulfides, the ore minerals of the Baimak type deposits include barite, tennantite, galena, bornite, native gold, and silver minerals (argentite, stromeyerite, jalpaite). The sphalerite-galena and galena ores occur in the upper part of orebodies at the Bakr-Tau, Balta-Tau and other Baimak type deposits. The deposits of the Baimak type were formed under conditions of the young island arc with sialic basement, which caused a large amount of felsic volcanic rocks of different effusive, pyroclastic, extrusive and sub-volcanic facies.

The studied types of VHMS deposits consistently correspond to the Tubinsk-Gai, Uchaly-Alexandrinka and Dzhusa-Dombarovka local volcanic belts. The metallogenic zoning of these belts (cross and lateral) is manifested by change of copper ores by the copper-zinc and further by polymetallic ores. Lateral zoning is accompanied by the dispersed mineralization and decrease in ultimate reserves of ores and trace elements.

References

Ismagilov, M.I. Mineralogy and geochemistry of massive sulfide deposits, volcanic and sedimentary rocks of the Southern Urals, Ufa: Inst. Geol., Bashkir Branch USSR Acad. Sci., 1978. P. 34–47 [in Russian].

Melekestseva, I.Yu. Heterogeneous Co-Cu massive sulfide deposits in ultramafic paleoisland arc structures, Moscow: Nauka, 2007 [in Russian].

Prokin, V.A., Seravkin, I.B., Vinogradov, A.M. Geological conditions of localization and outlook for discovery of large copper VMS deposits in the Urals // Lithosphere, 2011. No. 6. P. 123–133 [in Russian].

Seravkin, I.B. Volcanism and VMS deposits of the Southern Urals, Moscow: Nauka, 1986 [in Russian].

Seravkin, I.B. Types of VMS deposits in the Southern Urals and sources of ore matter // In: Proc. Intern. Scie. Conf. Endogenic Mineralization in Mobile Belts. Yekaterinburg: IGG UB RAS, 2007. P. 58–62 [in Russian].

R.I. Shaybekov
Institute of Geology, Komi Science Center UB RAS, Syktyvkar, Russia, shaybekov@geo.komisc.ru

COLORADOITE FROM THE SILICIFICATION ZONES OF THE UCHASTOK KRUTOY GOLD OCURRENCE, PAY-KHOY, RUSSIA

Приводятся данные о колорадоите, который был впервые установлен (на основе электронно-микроскопических исследований) в областях окварцевания и кварцевых прожилках низко- среднетемпературного гидротермального рудопроявления «участок Крутой» в пределах хенгурского габбро-долеритового комплекса Пай-Хоя.

The Uchastok Krutoy ore occurrence is located in the central part of the Hengur [Zaborin, 1972] (Central Pay-Khoy [Ostaschenko, 1979; Yushkin et al., 1972]) complex, on the right bank of the Hengur-Yu River, 500 m southeast of the Krutoy stream mouth. It was distinguished in 1969 during the geological exploration of the Nyalpey geological party [Zhukov et al., 1969]. The occurrence represents a NW-elongated bedded gabbro-dolerite body concordant to the Middle Ordovician clay shales. The length of the deposits is about 1.5 km, in a plan the body is characterized by number of swells and pinches, so its visible thickness ranges from 60 to 200 m. The intrusion dips to the southeast at an angle of 60–70° and have a zonal structure. Its periphery is composed of crystalline pale-greenish-gray glomerogranular dolerites, which, toward to the central part, transits into the porphyry varieties replaced by coarse-grained quartz-amphibole gabbro-dolerites. The latter rocks are spatially and genetically related to a zone of evenly disseminated (1–2 mm) magmatic chalcopyrite-pyrite-pyrrhotite mineralization formed at the final stages of intrusion crystallization.

The vermiform sulfide ingrowths are associated with interstitial quartz-albite myrmekite aggregates between randomly distributed prismatic grains of plagioclase and, locally, form a discontinuous margin along their boundaries. An accessory apatite is often intergrown with sulfides; tourmaline and zircon are rare. The amount of sulfide varies from 5 to 20 vol % (7–10%, on average). Chalcopyrite is extremely rare (less than 0.5–1.0 vol %) and is locally associated with quartz in the thin cross-cutting veins.

As a result of mining activities, ore zone 2–20 m wide has been traced for 1.2 km by trenches at a distance from each other of about 80–120 m [Zhukov et al, 1969].

Previously, gold-telluride mineralization in the gabbro-dolerite bodies of the Hengur complex of the Pay-Khoy was observed only at the Pervyi and Savabey areas as a part of copper-nickel sulfide ores (Shaybekov, 2011). The Te mineralization has not been found yet at the Uchastok Krutoy occurrence [Yushkin et al., 2007] and its first description is given below.

Coloradoite as isometric inclusions up to 1 μm in size was found in a close assemblage with chalcopyrite for the fist time in the Pay-Khoy (Fig.). The composition of mineral is significantly distinct from the stoichiometry that is related to the admixtures of Ag (up to 25.35 wt %), Ni (up to 2.06 wt %), and Pb (up to 17.96 wt %) (Table). The Ag and Ni admixtures may be related to the specific regional mineralogy (copper-nickel ores, quartz veins and areas of silicification of mafic rocks, etc.).

The quartz veinlets also contains chalcopyrite, $Cu_{0.88}Fe_{1.00}S_2$, grains 1–4 mm to 2 cm in size, covellite, $(Cu_{0.64}Fe_{0.06})_{0.7}S$, grains 20?100 mm in size often replaced by native silver, rare wurtzite grain up to 1 mm in size associated with gold, and Ag-bearing (up to 17.60 wt %) gold 0.1–0.5 μm in size. Angular grains of native lead up to 1.5 μm in size (Sn up to 14.50 wt %) and native tin up to 3 μm in size are found in the cataclastic areas.

Table

Chemical composition of coloradoite (wt %)

Elements, wt%					Total	Formula
Ni	Ag	Te	Hg	Pb		
1.59	5.22	31.42	45.87	13.88	97.97	$Hg_{0.92}Pb_{0.27}Ag_{0.19}Te$
n/d	19.46	33.23	46.67	n/d	99.36	$Hg_{0.89}Ag_{0.69}Te$

n/d – not detected.

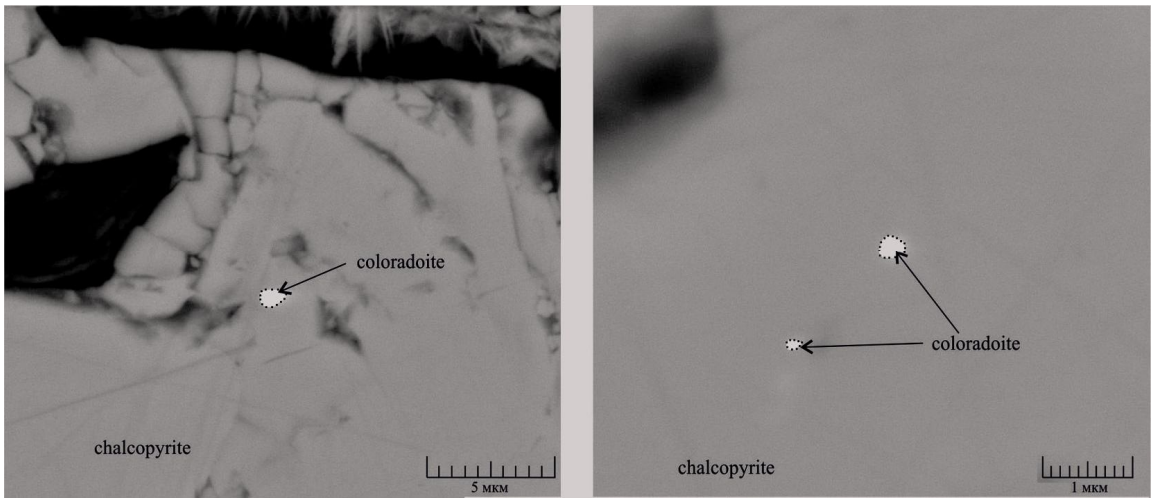

Fig. SEM image of coloradoite in chalcopyrite.

Thus, the chemical composition of coloradoite reflects the specific formation conditions under low- and medium-hydrothermal process in the quartz-chalcopyrite veinlets.

The author thanks I.S. Astakhova and S.S. Shevchuk for their consultations during the work. The work is supported by the program of Presidium of RAS no. 27 (project no. 12-P-5-1027), and project 12-5-6-016-ARCTIC.

References

Zaborin, O.V. Diabase formation Pay-Khoy // Magmatism, metamorphism and metallogeny of the North Urals and Pay-Khoy. Syktyvkar. 1972. P. 41–42 [in Russian].

Zhukov, Y.V., Zaborin, O.V., Kostyukova, L.A. e*t al* Geological structure sheets R-41-115-A, B; R-41-116-A,B. (Report Sopchinsk GPSP on the results of geological prospecting surveying at a scale of 1:50.000 for 1966–1968 yrs).. Vorkuta: Komi TGF, 1969. 261 p. [in Russian].

Ostaschenko, B.A. Petrology and ore tsentralnopaykhoysky basaltic complex. Leningrad: Nauka. 1979. 113 p. [in Russian].

Shaybekov, R.I. Mineral associations and genesis of platinum sulfide mineralization in the gabbro-dolerite Pay-Khoy (Russia, Nenets Autonomous District) // Notes RMO, 2011. No. 6. P. 70–86 [in Russian].

Yushkin, N.P., Davydov, V.P., Ostaschenko, B.A. Igneous rocks of the Central Pay-Khoy and their metallogenic features // Problems of Petrology of the Northern Urals and Timan. (Proceedings IG Komi SC UB AS of the USSR. Vol. 17). Syktyvkar. 1972. P. 3–34 [in Russian].

Yushkin, N.P., Kunz, A.F., Timonin, N.I. Minerageny Pay-Khoy. Yekaterinburg: UB RAS, 2007. 292 p. [in Russian].

A.G. Shevkunov

Kyrgyz Institute of Mineral Raw Materials, Bishkek, Kyrgyzstan, anatoly_shevkunov@mail.ru

FORMATION CONDITIONS AND DYNAMIC OF THE DEVELOPMENT OF THE OROGENIC ORE-FORMING SYSTEM OF THE KUMTOR GOLD DEPOSIT, CENTRAL TIEN SHAN

Месторождение Кумтор является одним из крупных золоторудных объектов Тянь-Шаня. Рудные зоны локализованы в породах черносланцевой формации в амагматичной пологозалегающей структуре. Отличительными особенностями месторождения в ряду золоторудных объектов, локализованных в черносланцевых толщах, являются преобладание руд пирит-(полевошпат)-карбонатного состава и практическое отсутствие в рудах мышьяка. Месторождение Кумтор – типичный представитель месторождений орогенного типа.

The Kumtor deposit situated in the Republic of Kyrgyzstan is one of the large gold deposits of the Tien Shan. The deposit is located in the Kumtor fold zone (flat (25°–45°) amagmatic tectonic structure) and is hosted in phyllites of the Vendian Dzhetymtau Group [Bogdetskiy et al., 1981]. The origin of gold mineralization of the Kumtor deposit is related to the metamorphic-hydrothermal-metasomatic activity occurred in the lens of metamorphic rocks (chlorite-sericite subfacies of the greenschist facies). The Kumtor deposit is an example of As-free gold deposits of the black shale type. Native gold, Au-Ag tellurides, scheelite, hematite and pyrite are typical ore minerals of the deposit. The main three groups of pyrite may be distinguished: sedimentary (PY1), metamorphic (PY2), and so called ore pyrite (PY3). Up to 90% of all Au-bearing minerals and mineral assemblages are related to PY3 [Anikin, 1992]. The sedimentary and metamorphic pyrite is broadly developed at the deposit without economic value.

The ore-bearing zones at the Kumtor deposit represent an alternation of intense stockwork zones in various phyllites and altered phyllites. The stockworks usually compose the peripheral parts of theorebodies. They consist of compact veinlets subconformable with foliation, crosscutting along the fracture cleavage system, and making the breccia-like structures. The various kinds of metasomatites compose the cores of orebodies.

The sericitolite haloes and quartz-potash-feldspar metasomatites were formed at the initial stage of the ore-forming process during alteration (bleaching) of phyllites, burning-out of the organic matter, and corrosion of primary pyrite. The pyrite-carbonate-albite stockworks and metasomatic bodies were formed after in more local zones. The pyrite-carbonate veinlets and microbrecciated-banded pyrite-carbonate (pyrite-dolomite or pyrite-ankerite-calcite) metasomatites (milonites, cataclasites) are overprinted on potassic-feldspar and albite metasomatites. The host rocks also bear the traces of dynamometamorphic transformations of the great depths with typical microtextures and structures of blastocataclasites, blastomilonites, and phyllonites. The thickness of pyrite-carbonate ores is up to 10 m and more. The orebodies usually have tectonic boundaries. Locally, they are banded pyrite-carbonate bodies similar to pyritized sedimentary calcarenites with fine dissemination of the rounded scheelite grains and metasomatic pyrite (Fig.). They are gradually replaced by carbonaceous carbonate phyllites and both form the mesofolds.

The ore-bearing zones are accompanied by Au, W, Te, Hg, Sb, Sr, Ag, Ba, and Pb endogenic haloes. As, Cu and Zn form the removal haloes. In the ore-bearing zones, Au has a significant positive correlation with Te, Ag, Cu, Hg, Sb, As, Sr and Zn, and weak correlation with Bi, Pb, and W. The Au + Te + Hg + Ag + W group is a root geochemical association of gold ores. All these elements form their proper minerals and occur as traces in other minerals. Arsenic forms no significant contents (<50 ppm) and occurs as admixture in tennantite and tetrahedrite or some pyrite types. The microinclusions of arsenopyrite rarely occur in grains of arsenic pyrite.

The ore pyrite (PY3) is characterized by anomalous contents of Au and is strongly distinct in geochemistry. It has high and intermediate contents of Au, Ag, Te, W, Cu, Zn, Sb, Hg, and Se. The broad dispersion of their contents and ore study indicate that these elements occurs as microinclusions of ore minerals, whereas Se is incorporated into a crystal lattice. The scanning of the PY3 surface has shown that Au, Ag, and Mn are evenly dispersed in the grains.

Among the sedimentary pyrite, the framboidal pyrite (PY1f) is characterized by the highest contents of Au, Ni, Co, As, Mn, Pb, Sb, Ba, Mo, Ag, Cu, Te, Se, Bi, Cd, Tl, and Hg. The formation of this pyrite was related, in a certain degree, to the biogenic sedimentation processes and we may suggest that the high content of these elements is a result of biochemical processes.

The subsequent transformation of the rocks leads to recrystallization of the primary pyrite, reconstruction of the internal structure, and strong decrease of the contents almost of all trace elements [Maslennikov et al., 2011].

The thick intervals (>100 m) of microcrystalline pyrrhotite-bearing schists of chlorite-biotite subfacies are found in the hanging wall of the ore-bearing Central area at the deposit. Pyrrhotite has replaced the early sedimentary, diagenetic and metamorphic pyrite that typically occurs at intensification of the metamorphic degree. At temperature higher than 400 °C, pyrrhotite replaces PY1 that is accompanied by release of S, As and other elements: $FeS_2 \rightarrow Fe_{1-x}S + S_{1+x}$.

The late metamorphic pyrite (PY2mt) is formed at the expense of the released sulfur in assemblage with pyrrhotite. The latter hosts the most part of Ni, while PY2mt contains almost all released As, which does not participate in the further migration. Thus, S, Au, Ag, Te, Pb, Sb, Mn, Mo, and Tl should easily migrate from the composition of PY1 owing to the intensification of the metamorphic

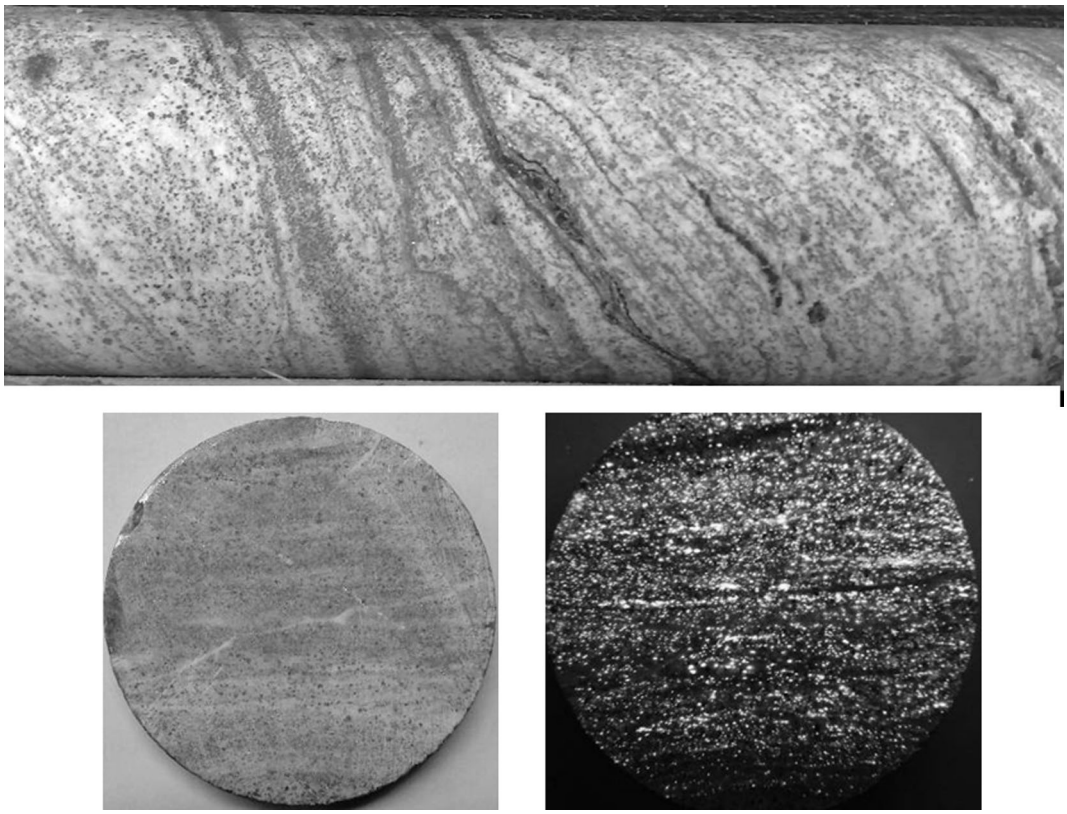

Fig. Banded calcite rock (limestone-calcarenite?) with interlayers of carbonaceous phyllite and dissemination of metasomatic pyrite (top photo, core fragment, actual size); transverse cross-section of this core fragment (bottom left photo) and the same under UV-rays (right photo; white is scheelite). Kumtor deposit, Central area, Stockwork ore body.

degree from the greenschist up to biotite facies. Most of these elements govern the ore geochemistry of the deposit.

However, this model characterizes only processes occurred in the rocks of the hanging wall, at a distance of 100–200 m and more from the ore-bearing structure. No pyrrhotite is observed closely to the ore-bearing structure. Two points of view on the pyrrhotite occurrence at the deposit are known: (i) continuous sequence of rocks in the overturned bedding and (ii) pinching out of the thrust sheet of more metamorphosed and pyrrhotitized rocks from the deeper parts of the deposit. At the current stage of research, both models are acceptable.

Two evolution ranges of metamorphic and hydrothermal-metasomatic alterations of the primary pyrite and position of ore pyrite are clearly evident from the geological evolution of the Kumtor structure. One of them is traced in the rocks of the hanging wall of the ore-bearing structure (I) and the second one is typical of the ore-bearing structure (II):

$$[(PY1s+PY1f+PY1sf) \rightarrow PY1sfp \rightarrow PY1mt] \leftrightarrow [POmt + PY2mt] \leftrightarrow [PY3] \quad (I)$$

$$[(PY1s+PY1f+PY1sf) \rightarrow PY1sfp \rightarrow PY1mt] \leftrightarrow [PY3] \quad (II)$$

The first range may serve as a part of the model of formation of the primary ore-bearing fluid composition because of the fragment of the deeper parts in the section of the deposit. The second range shows the model of the transformation of the primary pyrite in the major ore-bearing structure and probability of additional enrichment of the intruded fluid in ore trace elements from the primary pyrite.

The endogenic high-temperature fluid has gained CaO, MnO, SrO, CO_2, CO, S, Au, W, and Te from the ultra-metamorphic zone into the ore-locating structure. The main stages of ore deposition occurred under conditions of thrust stress deformations without visible intrusive rocks and are mostly related to the mobilization of water and rock-forming components (Na_2O, SiO_2, MgO, BaO, Fe^{2+}, Fe^{3+}) from the host rocks.

All above mentioned geological-structural features allow us to refer the Kumtor deposit to the orogenic gold deposits. The location of the Kumtor deposit well corresponds to the certain part of

formation model of the deposits during the convergence of the plate margins [Groves et al., 2007]. According to this model, the ore-forming structure of the Kumtor deposit is confined to a continent-continent collision zone and was formed in the Late Paleozoic (Upper Carboniferous to Early Permian) orogenic stage of the evolution of the region. That period was characterized by the renewal of the movements of the Ishim-Central Tien Shan microcontinent toward the Kyrgyz-Kazakh continent. At the same time, the crust of the Paleoturkestan Ocean was actively subducted under Ishim-Central Tien Shan microcontinent and the latter was compressed from the south.

This model assumes the ultra-metamorphic transformations of the rocks at the depth. Under conditions of the pressed wedge and bilateral pressure, the melting of the lithospheric fragments at the depth and uplift of the asthenospheric boundary in this place are suggested. All these may explain the peculiarities of ore composition of the Kumtor deposit, in particular, abundant newly formed carbonates. According to the model, ore-forming components originate from a zone of reworking of the lithosphere blocks and significant amounts of CaO and CO_2 are resulted from the thermal dissociation of sedimentary carbonates.

In accordance with a model of Groves et al. [2007], the small multiphase intrusive bodies were intruded at initial collision stage along the suture zone at the boundary of two continents. In our case, this is the Nikolaev Line and monzonite, monzogranite and monzogabbro intrusions of the Middle to Late Carboniferous Songkul-Kensoo complex. The skarn and porphyry Cu-Bi-Au-Mo-W occurrences and deposits (Kumbel, Kensu, etc.) are known to be related to these intrusions. They were described in a structure of the Au-Cu-Mo-W Songkel-Kensoo ore belt [Kudrin et al., 1990]. Many geologists relate the formation of the Kumtor deposit to the intrusions of this complex.

In our opinion, the Kumtor deposit was formed far southward this belt. The major ore-forming processes occurred at the depth in the central part of the Central Tien Shan structure under conditions of the Late Paleozoic thrusts system, dynamothermal metamorphism, and multistage hydrothermal activity. The close modern location of the deposit from the Nikolaev Line (~5 km) is related to the moving up of the ore-bearing zones along the thrusts to the north and northwest during the Alpine tectonic stage. The Alpine deformations have complicated the postorogenic structure of the region and, probably, significantly displaced it relative to the primary position.

References

Anikin, S.I. Geology and mineralogical-geochemical features of gold-tellurium rare-metal mineralization in the Vendian carbonaceous rock sequences at the Kumtor ore field (Central Tien Shan) // Extended abstract of PhD Thesis. Bishkek, BPI, 1992 [in Russian].

Bogdetskiy, V.N. et al. Geological position of gold-tungsten mineralization in carbonaceous schists on the example of one of the Tien Shan deposit // Stratiform deposits of non-ferrous and rear-earth metals in black slate formations. Frunze: FPI, 1981. P. 101–105 [in Russian].

Groves, D.I., Bierlein F.P. Geodynamic settings of mineral deposit systems // J. Geol. Soc., London. Vol. 164, 2007. P. 19–30.

Kudrin, V.S., Soloviev S.G., Stavinskiy V.A. et al. Gold-copper-molybdenum-tungsten ore belt of the Tien Shan // Geol. Ore Dep., 1990. No. 4. P. 13–26.

Maslennikov, V.V., Large R.R., Shevkunov A.G., Simonov V.A. Evolution of the Sukhoi Log and Kumtor gold ore giants // Abstract of CERCAMS14 & MDSG's34 Annual Meeting, 2011. Section XIII. P. 4–5.

V.A. Simonov[1], V.V. Maslennikov[2], A.V. Kotlyarov[1]

[1] Institute of Geology and Mineralogy SB RAS, Novosibirsk, Russia, simonov@igm.nsc.ru
[2] Institute of Mineralogy UB RAS, Miass, Russia

PHYSICO-CHEMICAL CONDITIONS OF MAGMATIC AND HYDROTHERMAL SYSTEMS OF THE PALEOZOIC "BLACK SMOKERS" FROM THE RUDNY ALTAI, NORTHEAST KAZAKHSTAN

Исследования расплавных и флюидных включений позволили выяснить физико-химические условия процессов минералообразования, связанных с магматизмом и постмагматическими флюидными и рудообразующими гидротермальными системами палеозойских

«черных курильщиков» Северо-Восточного Казахстана. Установлено, что кислые расплавы обладали повышенными содержаниями CuO (до 430 г/т) и воды (до 5.7 %). Выяснено, что постмагматические флюиды имели более высокие значения солености (до 8.8 %) и температур (до 288 °С) по сравнению с рудообразующими растворами – до 5.8 % и до 160 °С.

The representative samples of sulfide ores and host rocks from the massive sulfide deposits of the Rudny Altai (northeast Kazakhstan) were collected during the joint field works of specialists from the Urals and Siberian Branches of Russian Academy of Sciences. The analysis of morphology of orebodies and distribution and correlation of ore facies allowed construction of the morphogenetic range of the deposits from the sulfide mounds to the bedded massive sulfide deposits. A finding of fragments of the Paleozoic black smoker chimneys was the major achievement of the field works. This finding unequivocally indicates that deposits were formed in a similar manner to the modern black smokers with related abundant biota [Maslennikov et al., 2007; Maslennikov, Simonov, 2012].

Here, we report on new results of formation conditions of the Paleozoic black smokers in the northeast Kazakhstan based on melt and fluid inclusion study. The study of melt inclusions allows us to find out the features of the magmatic systems directly affected the hydrothermal ore-forming processes at the massive sulfide deposits from the Rudny Altai. The investigation of the fluid inclusions makes possible to identify the physical and chemical parameters of postmagmatic fluids and hydrothermal systems, which produced the sulfide mounds at the same deposits of the northeast Kazakhstan. The melt and fluid inclusions were studied on the specially designed devices at the Institute of Geology and Mineralogy SB RAS (Novosibirsk) [Simonov, 1993; Sobolev, Danyushevsky, 1994].

The melt inclusions, reflecting the magmatic system, were studied in quartz from the fine-grained quartz porphyric rocks of the Nikolaevskoe massive sulfide deposit. The samples were taken from the intrusive body 5–10 m thick at the bottom of the open pit in the immediate vicinity of the sulfide ore. The primary melt inclusions 10–50 μm in size are regularly distributed in the quartz phenocrysts. The one-phase inclusions filled with a pure homogeneous glass are dominant. Some inclusions contain the gas bubble, ore phases, and light crystals or a great amount of small dark phases in a glass. The majority of melt inclusions is depressurized during the high-temperature heating stage that indicates significant fluid pressure. The temperatures of homogenization of stable inclusions were ~1080 °C.

According to the chemical composition of glass, the melt inclusions (with alkali contents up to 5.3 wt %) correspond to the rocks of normal alkalinity and belong to the low-alkali rhyodacites. On the FeO/MgO–SiO_2 diagram, the data points of composition of melt inclusions fall to the area of the tholleiitic rocks. The decrease in TiO_2 (from 0.27 to 0.09 wt %), Al_2O_3 (from 11.8 to 9.9 wt %), Fe_2O_3 (from 2.1 to 1.6 wt %), and CaO (from 1.43 to 1.1 wt %) with simultaneous increase in Cl (from 0.11 to 0.23 wt %) is registered during the evolution of the acid melts (with increase of SiO_2 content). The characteristic decrease in Al_2O_3 content points to the fractionation of plagioclase during the differentiation of the magmatic systems.

Comparing these results with our data on melt inclusions in quartz from effusive rocks of other massive sulfide deposits, we can conclude that these melts are similar to acid magmas from the Yubileinoe deposit in the Rudny Altai and Yaman-Kasy deposit in the South Urals in TiO_2, Al_2O_3, MgO, CaO, and Na_2O contents. The content of the majority of oxides from our study also shows similarity with previously published data on melt inclusions in quartz of porphyry rocks from the Pamyatnik hill directly associated with the Nikolaevskoe deposit [Mergenov, 1987].

The microprobe analysis has shown the notable CuO content (up to 430 ppm and up to 640 ppm in single analyses) in melt inclusions from the Nikolaevskoe deposit. The copper accumulates during the fractionation of acid melts with increase in FeO/MgO ratio and chlorine content.

The ion microbe analyses of melt inclusion in quartz have revealed the increased H_2O contents (2.4–5.7 wt %) in magma of the Nikolaevskoe deposit comparable with those from the Yubileinoe (up to 4.30 wt %) and Yaman-Kasy (2.7–5.2 wt %) deposits. Based on ion microbe analyses, the REE distribution in the studied melt inclusions is similar to that from the felsic volcanic rocks of island arcs. In the LREE area, they coincide with data on melt inclusions from the Yubileinoe deposit and rhyolites of the Kuril-Kamchatka island arc. The acid melts from the Yaman-Kasy deposit with typically lower REE contents are obviously distinct. All REE spectra are characterized by the clear Eu minimum, which indicates the magma differentiation during the fractionation of plagioclase.

The physical and chemical parameters of postmagmatic fluids are based on the fluid inclusion study of melt-bearing quartz phenocrysts from quartz-feldspar porphyry rock closely associated with

sulfide ores of the Kamyshenskoe massive sulfide deposit. The fluid inclusions 3–15 μm in size are located as chains in quartz. The two-phase (light transparent liquid and gas bubble) inclusions are dominant.

The freezing temperature of the fluid inclusions is –35 – –40 °C. The eutectic temperatures vary from –23 to –26 °C, indicating dominant NaCl admixed with KCl. The final melting temperature includes two groups of values (–0.9 – –2.5 °C and –3.2 – –5.8 °C) that indicates two groups of salinity: 1.4–3.8 wt % and dominant 5.0–8.8 wt % NaCl-equiv. (up to 13 wt % in some cases). Three temperature ranges are typical of the studied fluid inclusions: 134–190, 204–250 and 272–288 °C.

The correlation of homogenization temperatures and salinity gives two groups of inclusions, which are overlapped with those from the Yaman-Kasy porphyry rocks. The low-temperature (to 190 °C) group is characterized by considerable salinity (up to 13 wt % NaCl-equiv.) that is comparable with data on quartz from the porphyry rocks of the Kyzyl-Tashtyg deposit. At the same time, inclusions with elevated temperature (up to 288 °C) are characterized by the lower salinity (up to 8.8 wt % NaCl-equiv.). It should be noted that homogenization temperature and salinity directly correlate in both groups of inclusions.

The formation conditions of the ore-forming hydrothermal system from the feeder channels to the top of the sulfide mound were studied in fluid inclusions in barite from sulfide ores of the Artem'evskoe massive sulfide deposit.

The fluid inclusions in barite from the feeder channels are 3–15 μm in size. They are mostly regular distributed in the crystals or confined to the numerous intercrossed healed fractures. Three types of co-existing fluid inclusions may be distinguished: (I) dominant one-phase liquid inclusions, (II) abundant two-phase inclusions with a light liquid and round gas bubble, and (III) vapor inclusions. This is similar to the fluid inclusions from the feeder channels of the Valentorka massive sulfide deposit in the North Urals.

The freezing temperature of the two-phase inclusions ranges from –35 to –40 °C. The eutectic temperatures vary from –24.5 to –26 °C that points to the presence of NaCl and KCl in the fluids. The final melting temperature of –0.15 – –3.7 °C corresponds to the salinity of 0.2–5.8 wt % NaCl-equiv. In most cases, the salinity is below that of seawater. The homogenization temperatures vary from 114 to 160 °C.

The homogenization temperatures and salinity of the studied fluid inclusions are similar to the low-temperature group of inclusions in barite from the Yaman-Kasy deposit. It should be noted that studied fluid inclusions are characterized by significant range of salinity at narrow temperature range. At the same time, fluid inclusions in barite from the Yaman-Kasy deposit and sulfide mounds from the Manus back-arc basin are characterized by the higher homogenization temperatures.

Thus, out studies of melt and fluid inclusions allowed us to identify the physical and chemical conditions of related processes of mineral formation at massive sulfide deposits of the Rudny Altai (northeast Kazakhstan) similar to the modern black smokers and to find the consecutive change of the magmatic systems by postmagmatic fluids and ore-forming hydrothermal systems. It was established that acid melts of normal alkalinity, corresponding to low-alkali rhyodacites in composition, have increased CuO (to 430 ppm) and H_2O (to 5.7 wt %) contents. The postmagmatic fluids are characterized by higher salinity (up to 8.8 wt % (rarely up to 13 wt %) NaCl-equiv) and elevated temperatures (up to 288 °C) in comparison with those of ore-forming hydrothermal solutions (up to 5.8 wt % NaCl-equiv and up to 160 °C).

The work is supported by the project of joint researches of the Siberian and Urals (no. 12-C-5-1010) Branches of the Russian Academy of Science.

References

Maslennikov, V.V., Simonov, V. A., Zhukov, I.G., Tretyakov, G. A., Herrington, P., Maslennikova, S.P., Kanygin, A.V. First findings of sulfide chimneys of the Paleozoic "black smokers" in the Central Asia // Geology of the seas and oceans: Materials of XVII International scientific conference (School) on the sea geology. Vol. II. M: GEOS, 2007. P. 47–49 [in Russian].

Maslennikov, V.V., Simonov, V.A. Some problems of near-hydrothermal fauna developed in the zones of activity of the Paleozoic "black smokers" of the Rudny Altai // Metallogeny of ancient and modern oceans-2012. Hydrothermal fields and ores. Miass: IMin UrB RAS, 2012. P. 65–68 [in Russian].

Mergenov, V.M. Physico-chemical features of formation of porphyry rocks and ores of the Nikolaevskoe deposit (Rudny Altai) // Geology of ore deposits, 1987. No 1. P. 59–65 [in Russian].

Simonov, V.A. Petrogenesis of ophiolites (thermobarogeochemical researches). Novosibirsk: UIGGM SB RAS, 1993. 247 p. [in Russian].

Sobolev, A.V., Danyushevsky, L.V. Petrology and Geochemistry of Boninites from the North Termination of the Tonga Trench: Constraints on the Generation Conditions of Primary High-Ca Boninite Magmas // J. Petrol., 1994. Vol. 35. P. 1183–1211.

I.V. Sinyakovskaya[1, 2], V.V. Zaykov[2, 1]
[1] *National Research South Ural State University, Chelyabinsk, Russia,*
sin@mineralogy.ru
[2] *Institute of Mineralogy, Urals Branch of RAS, Miass, Russia,*

GEODYNAMIC TYPES OF THE PYROPHYLLITE DEPOSITS

Пирофиллитовое сырье относится к сравнительно редким видам нерудных полезных ископаемых. По геологической позиции и условиям образования месторождения подразделены на 5 типов. Первые два связаны с гидротермально измененными породами в вулканогенных толщах кислого и среднего составов. К третьему типу относятся месторождения метаморфогенно-метасоматического генезиса. Проявления четвертого типа приурочены к низко- и среднетемпературным стадиям образования гидротермальных жил среди вулканических и метаморфических толщ. Пятый тип - это пирофиллитсодержащие коры выветривания по метаморфическим толщам и метасоматитам. Условия образования и размещения месторождений пирофиллитового сырья в складчатых поясах определяются геодинамической обстановкой формирования.

Pyrophyllite is a comparatively rare economic mineral. Basic consumers of raw pyrophyllite are ceramic and fire-resistant industries. It is also used for manufacture of fillers for paper, cardboard, rubbers, plastic, insecticides, technical ceramics, and in the electro technical industry. Monomineral pyrophyllite is used in high-pressure apparatus to manufacture synthetic diamonds and also as a material for stone culling (agalmatolite). Zaykov et al. [1988] proposed typification of the deposits. We adopt the scheme and relate it to a modern geodynamic scheme (table).

Deposits in metasomatic rocks of intra-continental and marginal-continental volcanic zones (Type I). Host rocks of this type deposit are typically calc-alkaline andesitic to rhyolitic lavas, which are enriched in potassium or sodium and potassium. The pyrophyllite deposits are associated with volcanogenic metasomatic rocks of the "secondary quartzites - pyrophyllites" series, and they are commonly found in ancient rifling zones on platforms and on active continental margins. Pyrophyllite deposits on Precambrian platforms are found in Ukraine, Sweden, South Africa, USA, Canada and Brazil. In contrast, pyrophyllite deposits in Middle Asia, Kazakhstan and Australia are distributed in Paleozoic active continental margins. Pyrophyllite deposits occur at Mesozoic-Cenozoic active continental margins in USA, Canada, Morocco, China, New Zealand, Korea, Japan, Vietnam, Georgia and Azerbaijan.

Pyrophyllite deposits in metasomatic rocks in island arcs and Paleozoic and Cenozoic marginal seas (Type II). In folded Paleozoic island-arc system there are pyrophyllite deposits, which occur in bimodal volcanogenic series. This type of deposit is widespread in the Ural folded Paleozoic island-arc system, where pyrophyllite-bearing metasomatic rocks of sericite-quatrz formations accompany massive sulfide mineralization [Udachin, Zaykov, I994]. Pyrophyllite mineralizalion in folded structures of Cenozoic age is known in "green tuff" region of Japan, the Bolnis area of Southeast Georgia and the Panagursko zone in Bulgaria.

Pyrophyllite deposits in metamorphosed terrigenous-argillaceous strata of Paleozoic and Mesozoic age, containing pyroclastic material and coals seams (Type III). Pyrophyllite deposits in Paleozoic beds in passive continental margins and interior seas and coal-bearing depressions occur in

Table

Types of pyrophyllite deposits [Sinyakovskaya et al., 2005]

Type, geodynamic situation	Ore-hosted formation age	Lode structure and parameters (thickness, m)	Mineralogy of raw material	Examples
I. Metasomatic rocks in intra-continental and continental margin volcanic zones	Trachyandesitic, trachyrhyolitic in Precambrian platforms	Linear zones, lens (n • 10) along faults at contacts with plutons; layers (n • 1) in tuffaceous-sedimentary packets	Pyrophyllite, pyrophyllite-quartz, sericite- pyrophyllite	East-Europe platform; North-American platform; South-American platform; African platform
	Dacite-rhyolite, rhyolite at Paleozoic continental margins	Lenses, strips (n • 10), bodies of irregular form in secondary quartzite massifs and in faults	Pyrophyllite, diaspore and kaolinite- pyrophyllite, chlorite- pyrophyllite	Ural-Mongolian belt; East-Australian belt, East-Atlantic belt
	Andesite-dacite-rhyolite in Mesozoic-Cenozoic continental margins	Bodies of stratal and lens-shaped form (n • 10), irregular form (30-60x300-800), steeply-dipping zones in tectonic dislocations (n • 10)	Quartz-pyrophyllite, diaspore- pyrophyllite, pyrophyllite, kaolinite- pyrophyllite, sericite- pyrophyllite	West-Pacific belt; East-Pacific belt, Mediterranean belt
I. Metasomatic rocks in island arcs and marginal seas	Massive sulphide-bearing rhyolite-basalt in Paleozoic continental margin	Strips (n • 10) extent up to 1500 m on strike of massive sulfide-bearing zones	Quartz-pyrophyllite, pyrophyllite-quartz, sericite- pyrophyllite-quartz, diaspore- pyrophyllite, pyrophyllite	Ural-Mongolian belt
	"Green tuffs" in Mesozoic island arcs	Irregular in form (l00-300 x 300-600), steeply-dipping zones along contact with plutons	Pyrophyllite- kaolinite- sericite-chlorite, pyrophyllite- quartz-sericite- diaspore-alunite	West-Pacific belt
III. Metamorphosed terrigenous- clay formations of platforms and folded belts	Terrigenous-clay in Paleozoic and Mesozoic passive continental margins, internal seas and coal hollows	Strata and intercalations (interlayers, interbeds) (10) among metamorphosed terrigenous and clay strata	Quartz-chlorite- pyrophyllite- sericite, kaolinite- pyrophyllite-illite, kaolinite- pyrophyllite	East-Europe platform; South-American platform, East-Australian belt, East-Pacific belt
IV. Hydrothermal veins in metasomatites in platforms and folded belts	Quartz veins in Precambrian granitoids and Paleozoic metamorphic rocks	Zones (0.01-1) parallel to contacts of veins	Pyrophyllite, muscovite-pyrophyllite, diaspore- pyrophyllite, kaolinite- pyrophyllite- muscovite	Indian platform; Ural-Mongolian belt
V. Weathering crusts metamorphites and metasomatites in folded belts	Weathering crusts in slates formed by metasomatism of Paleozoic and Mesozoic rocks	Linear weathering crusts (l5-20), extent n • 100	Illite-montmorillonite-pyrophyllite, kaolinite- pyrophyllite	East-Pacific belt; Ural-Mongolian belt

Germany, Argentina and Spain. Mesozoic terrigenous-argillaceous strata with pyrophyllite are known in Australia and the Carpathians.

Pyrophyllite occurrences in quartz veins in hydrothermal systems (Type IV). Pyrophyllite deposits in India at the margins of large vertical quartz bodies (so-called "quartz reefs") are connected with a Precambrian granitoid complex. In Russia pyrophyllite connected with hydrothermal veins is

found in Paleozoic metamorphic rocks. Pyrophyllite was identified as a mineral species in gold-quartz veins at Berezovsk (the Urals, in 1929).

Weathering crust containing pyrophyllite mineralization on the metamorphic and metasomatic rocks (Type V). Pyrophyllitic clays in weathering crusts formed by metasomatism of Paleozoic and Mesozoic rocks are found in the USA, Spain, Ural and Altai.

Analysis of formation conditions of raw pyrophyllite deposits shows that the geodynamic situation is a determining factor. Geodynamics influences composition of magma at depth of magmatic centers, character of volcanic structures, and their position in continental and oceanic crust, and in sea basins. These factors influence the composition of hydrothermal solutions, their dynamics, and the character of metasomatic reactions. At cessation of' volcanism, geodynamic situations govern the character of subsequent tectonic dislocations and fabrics, which then control the distribution of ore bodies.

The work is supported by the Russian Federal Program of Ministry of Science and Education (no. 14.740.11.1048).

References

Sinyakovskaya, I. V., Zaykov, V. V., Kitagawa, R. Types of pyrophyllite deposits in foldbelts // Resourse Geology, 2005. Vol. 55. no, 4. P. 405-418.

Zaykov, V. V., Udachin, V. N. Pyrophyllite and pyrophillite raw materials in the sulfide-bearing areas of the Urals // Applied Clay Science, 1994. Vol. 8. P.417-435.

Zaykov, V. V., Udachin, V. N., Sinyakovskaya, I. V. Pyrophyllite deposits // International Geology Review, 1988. Vol. 30. P. 90-103.

S. Tessalina[1], V.V. Maslennikov[2], V.V. Zaykov[2] R.J. Herrington[3], B. Spiro[3], J.-J. Orgeval[4]

[1] John de Laeter Centre for Isotopic Research, Curtin University, Australia

[2] Institute of Mineralogy of Russian Academy of Sciences, Miass, Russia

[3] Natural History Museum, London, United Kingdom

[4] Bureau de Recherche Geologiques et Minieres, Orleans, France

TIMING AND SOURCE OF METALS OF URALS VHMS DEPOSITS: BIOSTRATIGRAPHY VERSUS RADIOGENIC ISOTOPES

Формирование южно-уральских колчеданных месторождений считается связанным с внутриокеанической стадией развития Магнитогорской островной дуги [Herrington et al., 2001] в силуре-среднем девоне (444–385 Ma). В статье приводятся данные определения абсолютного возраста по соотношению Re-Os сульфидной минерализации колчеданных месторождений Яман-Касы и Куль-Юрт-Тау, которые сходны и составляют 362±9 Ma и 363±1 Ma. Эти данные согласуются с полученным ранее аналогичным методом абсолютным возрастом месторождений Дергамыш и Александринка. Верхнедевонский возраст несколько более поздний, чем возраст коллизии «Магнитогорская дуга – континент Лавруссия» [Brown et al., 2011]. Участие субдуцированного континента и/или осадков подтверждается также результатами изучения изотопного состава свинца 14-ти колчеданных месторождений Урала. Содержание древнего свинца понижается от преддуговой обстановки к дуговой и стремится к нулю на фронте субдукции. Повторяющийся «молодой» Re-Os возраст совместно с данными изотопии свинца позволяет предположить, что «закрытие» Re-Os радиогенных событий на Южном Урале произошло не позднее, чем в верхнем девоне (~360 Ma), несколько позже начала коллизии «Магнитогорская дуга – континент Лавруссия».

The tectonic setting and sampling

In the Southern Urals, the intra-oceanic subduction has triggered the volcanism leading to the Magnitogorsk island arc development starting from the Early Devonian time ~400 Ma ago (Fig. 1). The timing of collision of this volcanic arc with adjacent Laurussia continent was established at 380–372 Ma

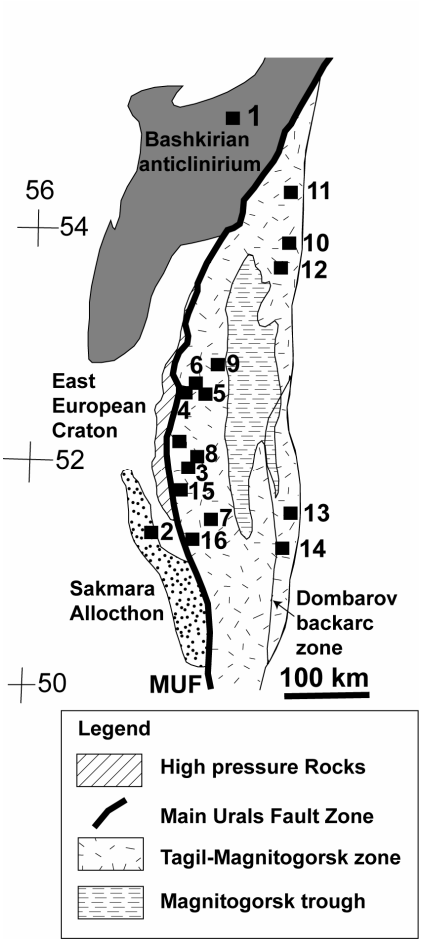

Fig. 1. Simplified geological map of the Southern Urals showing main regions of arc volcanic sequences and location of studied VMS deposits. The following subdivisions are shown: (1) Main Urals Fault (MUF) suture zone with relics of ophiolite in a tectonic melange containing blocks with ages ranging from Ordovician up to Late Devonian; (2) Magnitogorsk island arc zone, consisting of volcanics and sediments of Devonian age. An intermediate "intra-arc" basin, filled by Late Devonian-Lower Carboniferous volcanics and sediments, divides the Magnitogorsk structure into the West and East-Magnitogorsk zones; (3) Sakmara allochthon, whose origin is not clear. Massive sulphide deposits: 1 – Bakal, 2 – Yaman-Kasy, 3 – Oktyabrskoe, 4 – Bakr-Tau, 5 – Balta-Tau, 6 – Tash-Tau, 7 – Gay, 8 – Podolskoe, 9 – Sibay, 10 –Molodezhnoe, 11 – Uchaly, 12 – Alexandrinka and Babarik, 13 – Djusa, 14 – Barsuchi Log, 15 – Dergamish, 16 – 50 let October.

based on Ar-Ar, U-Pb and Sm-Nd dating of high-pressure metamorphic rocks and sediments belonging to the continental margin [Beane and Connelly, 2000]. The formation of Southern Urals Volcanogenic Massive Sulphide deposits was restricted to the intra-oceanic stage [Herrington et al., 2011], with the youngest age of 385 Ma, based on biostratigraphic studies of ore-hosting volcanic and sedimentary rocks [Artyuszkova and Maslov, 2008].

In this study, sulphide samples were collected from two VMS deposits occurring in distinct geodynamic settings. The studied Yaman-Kasy deposit [Maslennikov et al., 2009] is restricted to the Sakmara allochton and is hosted by an early Silurian volcano-sedimentary bimodal sequence. The mound-like Yaman-Kasy orebody consists of massive and clastic ore facies, with preserved fragments of sulphide chimneys and vent fauna. This is one of the best preserved Palaeozoic sulphide mound-like VMS deposits, analogous to the modern black-smoker VMS deposits. The hydrothermal chimney fragments were collected, including 4 pyrite-marcasite samples from the outer wall, 2 chalcopyrite samples from the inner wall, and 1 pyrite-marcasite-sphalerite sample from the chimney core.

The studied Kul-Yurt-Tau deposit is situated within West-Magnitogorsk island arc and restricted to the middle part of Baimak-Buribai formation. This mound-like ore body occurs on the flank of a rhyolite-dacite dome within the volcanoclastic horizon. The felsic volcanic host rocks at the top and flanks of ore body are transformed into sericite-pyrophyllite-quartz metasomatic rocks. The stud-

ied molybdenite samples form 0.1–2 mm thick coat-like aggregates in association with pyrophillite within these metasomatic rocks.

For Pb isotopic studies, we collected various types of galena samples from 14 VMS deposits across the Urals paleo-island arc system (Fig. 1), covering the range from fore-arc, arc and back-arc settings. Most galena samples were obtained from massive ores and footwall stockwork zones of the deposits.

The Results

Re-Os Systematics

The Rhenium-Osmium isotope systematics is used for accurate isotopic dating and fingerprinting the source of metals. Both the parent (^{187}Re) and daughter (^{187}Os) are chalcophile and siderophile in character, leading to their enrichment in sulphide minerals relative to silicates. This is a unique combination of chemical and isotopic features which allows the direct dating of sulphide mineralisation. The common sulphide mineral molybdenite is particularly useful in this regard, because it often contains high concentrations of Re, but virtually excludes Os during crystallisation. Thus, no correction is required for the presence of initial Os.

The plot of the isotope data for the Yaman-Kasy ores on the Re-Os isochron diagram (Fig. 2) defines a best-fit line with the age of 361.7 ± 9.0 Ma (MSWD = 3.4), which is much younger than the biostratigraphic Silurian age (*ca.* 443–419 Ma) of ore hosting rocks. In addition to that, the isotope data of the molybdenite samples from the Kul-Yurt-Tau deposit gave a model age of 363.4±1.1 Ma (Late Devonian) which is similar to the preceding dating of the Yaman-Kasy deposit, and it is ~40 Ma younger than the biostratigraphic Early Devonian age (*ca.* 400 Ma) of host rocks of the Kul-Yurt-Tau deposit [Artyuszkova and Maslov, 2008].

Source of metals defined by Pb-Pb isotope systematics

Galena is virtually free of U and records the initial composition of lead at the time of ore formation. For this reason, the lead isotopic composition in galena is an ideal indicator for the sources of lead and other metals.

The lead isotope data from 14 VMS deposits (Fig. 1) display a systematic increase in lead isotopic ratios across the Urals paleo-island arc zone, from fore-arc with the least radiogenic lead compositions to back-arc with the most radiogenic lead (Fig. 3). The latter shows Pb model ages close to the age of the arc volcanics (~400 Ma). The less radiogenic lead from fore-arc settings is indicative of a source older than the volcanics and implies a contribution of lead from older subducted material. The Pb isotopic composition of subducted Proterozoic rocks may be inferred from the analysis of lead occurrences from the Proterozoic rocks of Bashkirian anticlinorium (Bakal deposit). According to Fig. 3, the contribution of lead from these Proterozoic rocks can account for the composition of less radiogenic lead from VHMS deposits in fore-arc settings.

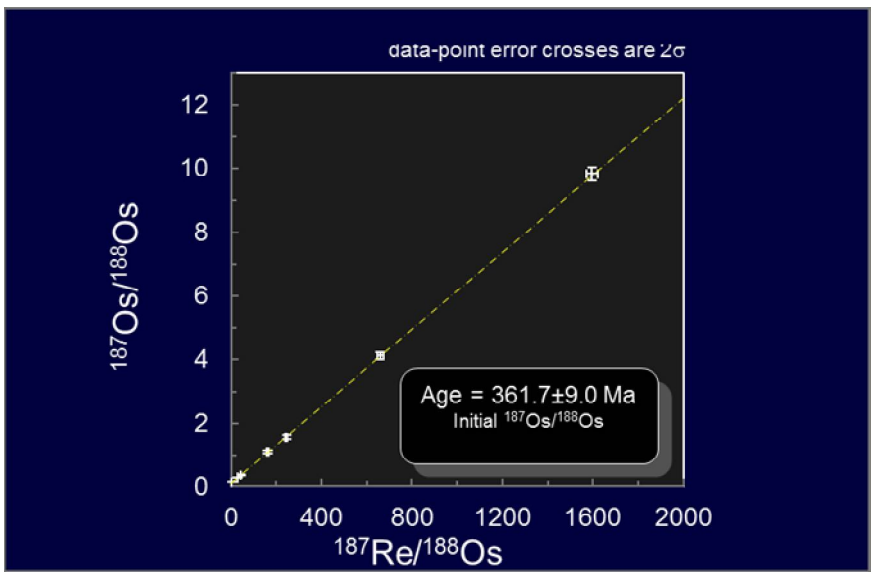

Fig. 2. Re-Os isochron diagram for Yaman-Kasy deposit.

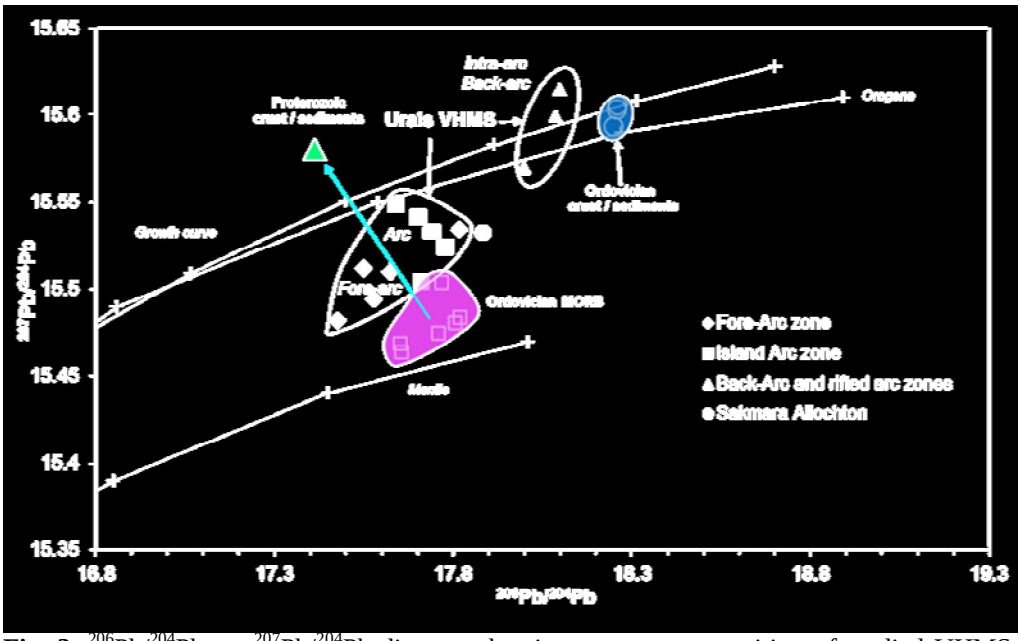

Fig. 3. $^{206}Pb/^{204}Pb$ vs. $^{207}Pb/^{204}Pb$ diagram showing average composition of studied VHMS deposits. Ordovician Mantle field was delineated using Ordovician MORB hosted VHMS deposits from the Caledonides of Norway (Bjorlykke et al. 1993). The Ordovician sediments field corresponds to the galena from the Ordovician sediments-hosted Saureyskoe Zn-Pb deposit, Polar Urals. The lead isotope composition of Precambrian sediments (*ca.* 1.3 Ga) from Bakal stratiform Pb-Zn deposit (Bashkirian anticlinorium) is shown.

Timing of VMS formation

Previously published Re-Os isotope data for two other Urals VMS deposits, namely Alexandrinka [Tessalina et al., 2008] and Dergamish [Gannoun et al., 2003], defines similar Late Devonian ages of 355±15 Ma and 366±2 Ma, respectively, post-dating the presumed biostratigraphic age of ore hosting volcanics.

The K-Ar ages for sericites from 8 Urals VMS deposits [Buslaev and Kaleganov, 1992] show the range from 390 to 301 Ma, with an average value of 348±27 Ma. The K-Ar ages in sericites often show a range spanning the whole life of a hydrothermal system. This range includes the age of the end of the hydrothermal activity, which can be few Ma younger than the age of the ore formation itself [Hu et al., 2012]. The average K-Ar age is consistent with the Sm-Nd and Rb-Sr ages of 347±12 Ma for the Berezovskoe Au deposit formation from the Middle Urals [Baksheev and Beliatsky, 2011], marking the end of intense hydrothermal activity.

The repetitive Late Devonian Re-Os model ages for sulphides for four studied Urals VMS deposits are younger than their respective host rocks and overlaying sediments based on biostratigraphy [Artyuszkova and Maslov, 2008]. Even though the additional chronological constraints for host volcanic rocks and sediments are needed to better constrain the geochronology of the Urals VMS deposits, the Re-Os model age would need to be much older to explain the formation of the Silurian Yaman-Kasy deposit, with perfectly preserved initial seafloor hydrothermal facies such as chimneys and fauna. However, this Late Devonian age may correspond to the later hydrothermal overprint for the Devonian Kul-Yurt-Tau deposit. In what follows, we examine several possible mechanisms for the Re-Os system re-setting.

Re-setting of the Re-Os isotopic system could occur under the following circumstances: (A) metamorphic overprint; (B) incomplete homogenisation of two or more components with different initial Os ratios during ore deposition; (C) open behaviour of hydrothermal system. These possibilities are examined in detail:

(A) In the history of the Urals development, the Late Devonian (385-359 Ma) corresponds to the ‘Arc-Continent’ collision, which was associated with exhumation of high-pressure metamorphic complexes [Beane and Connelly, 2000]. However, the good state of preservation of initial ore textures for the studied deposit Yaman-Kasy (colloform structures, relics of hydrothermal chimneys and fauna) does not favour the metamorphic overprint.

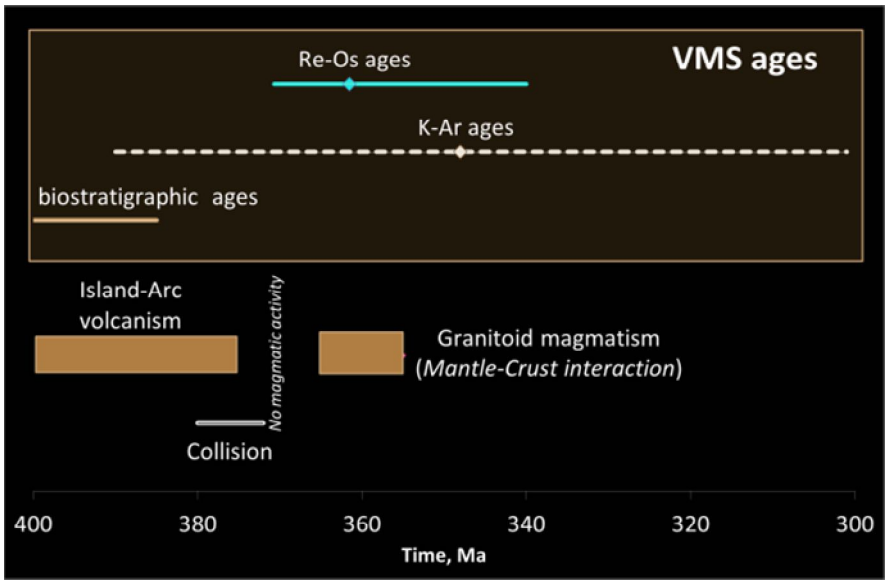

Fig. 4. Summary of available dating for Urals VMS using Re-Os and K-Ar systems (see references in the text), along with contemporaneous magmatic [Fershtater et al., 2007] and tectonic events [Beane and Connelly, 2000].

(B) The formation of VHMS deposits is due to the mixture of at least two components represented by seawater and hydrothermal fluid, which may have different isotopic composition at the time of ore formation, with osmium in the hydrothermal fluid coming mostly from the leaching of host volcanic and sedimentary rocks. Mixture of hydrothermal fluid with seawater during ore formation could produce mixed isotopic characteristics at the time of ore formation, which subsequently evolved to yield linear data arrays of questionable age significance. However, the similarity of model ages for the four deposits makes this possibility very unlikely.

(C) Open behaviour of the ore system is the most plausible scenario to explain the younger age of studied deposits. In this case, the gain of Re is the most possible explanation for the younger ages, which is estimated to be between 10 and 20%. The gain of Re could be related with interaction between sulphide ore and seawater, the latter having the Re/Os ratio of ~820. However we can argue that the closure of Re-Os systems for four studied Urals VMS deposits has happened no later than ~360 Ma.

Implication for tectonic setting

The evidence of continental crust/metals recycling from Proterozoic Laurussia craton into the mantle comes from the presence of zircons of crustal origin in subduction-related dunite-clinopyroxenite-gabbro massif of the Middle Urals [Bea et al., 2001]. These zircon ages of 370–350 Ma correspond to the beginning of Arc-Continent collision in the Southern Urals. Moreover, the presence of zircons of crustal origin in subduction-related mafic-ultramafic complexes suggest contribution of melt directly from melting of subducted crust/sediments of Laurussia craton, which entrained restitic zircons.

The Pb isotope data in galena from 14 Urals VMS deposits suggests that the contribution of fluids from subducted continental crust/sediments progressively diminish with increasing distance from the subduction front, becoming almost nil in some of the mature arc and back-arc settings.

This dataset is rather consistent with ensialic origin of the Northern part of the Uralian island arc structure, inferred from geophysical data of the basement (continental crust) and geochemistry of volcanics [Yazeva and Bochkarev, 1996; Smirnov et al., 2008].

In the Southern Urals, this stage of island arc development has been identified as hydrous suprasubduction melting during the mantle-crustal interaction [Fershtater et al., 2007] with large-scale granitoid magmatism. These intrusions provide necessary heat to promote the hydrothermal circulation along the existing tectonic faults.

Viewed on a larger scale, the Devonian episode of volcanic and hydrothermal activity corresponds to the beginning of the Pangea supercontinent assembly by amalgamation of Laurussia, Siberia

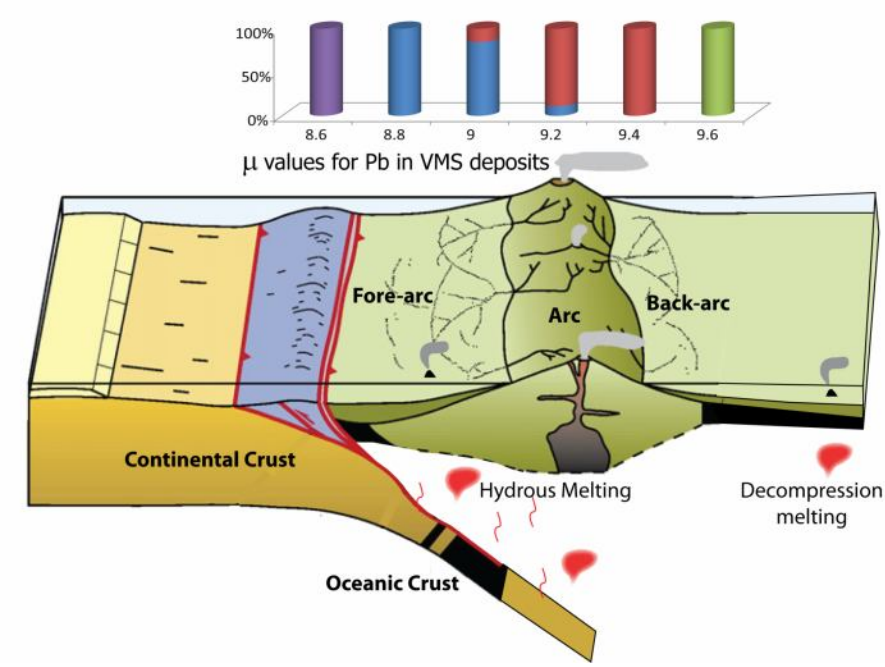

Fig. 5. Schematic model for arc-continent collision in Southern Urals (modified after Brown and Spadea, 1999). Entering of Proterozoic rocks into subduction zone caused high-pressure metamorphism accompanied by release of fluid. This fluid provoked hydrous melting in overlying mantle wedge. The lead isotopic composition of Proterozoic rocks is characterised by low μ-value of 8.8. In fore-arc setting, the μ-value of VMS deposits is close to that of Proterozoic rocks. Farther to the mature arc setting, the μ-value progressively increases, with maximum value of ~9.4. In back arc setting, the anhydrous decompressional melting of oceanic crust prevails, with highest μ-values corresponding to that of Ordovician crust (Fig. 3).

and China-Korea continental blocks. At that time, numerous microcontinents and volcanic arcs divided by basins of different character were present.

The fundamental plate boundary re-arrangements in Late Devonian, on a planetary scale, appear to be marked by intense magmatism under tectonic activation. This is manifested in island arc volcanism paired with episodic continental rifting, as well as hydrothermal activity on rifted or faulted outer continental margins, comprising large clusters of VHMS deposits in Spain, Portugal (Iberian Pyrite Belt province), Rudny Altai (Siberia), and the North American margin (Alaska). These deposits formed in local extensional volcanic basins within an overall contractional geodynamic environment during or after termination of convergence by accretion of an island arc or crustal block [Huston et al. 2010] throughout the Devonian until Early Carboniferous time.

Conclusions

Thus, these two radiogenic datasets (Re-Os and Pb-Pb), together with previous K-Ar dating, point out that the hydrothermal circulation was still active at the final stage of the island arc development after the collision initiation with an adjacent continent. The Re-Os model ages of hydrothermal system ‘closure’ correspond to the granitoid magmatism, initiated after the ‘Arc-Continent’ collision.

Acknowledgements

This work was carried out in the framework of the EU-funded MinUrals project INCO COPERNICUS ICA2 CT-2000-10011. Authors acknowledge the Program of the Russian Academy of Sciences (no. 12-П-5-1003) “Typochemistry of chalcophile elements from sulphide ores of modern and ancient oceans”

References

Artyuszkova, O.V., Maslov, V.A. Detailed correlation of the Devonian deposits in the South Urals and some aspects of their formation // Bulletin of Geosciences, 2008. Czech Geol Survey, Prague Vol. 83(4). P. 391–399.

Baksheev, I.A., Beliatsky, B.V. Sm-Nd and Rb-Sr isotopic systems of sheelite from Beresovskoe Au-bearing deposit (Middle Urals) // Lithosphere, 2011. No. 4. P. 110–118 [in Russian].

Bea, F. et al. Recycling of continental crust into the mantle as revealed by Kytlymdunite zircons, Ural Mts, Russia. Terra Nova, 2001. Vol. 13. P. 407–412.

Beane, R.J., Connelly, J.N. $^{40}Ar/^{39}Ar$, U-Pb, and Sm-Nd constraints on the timing of metamorphic events in the Maksyutov Complex, southern Ural Mountains // Journal of Geol. Society, 2000. Vol. 157. P. 811–822.

Bjorlykke, A., Vokes, F.M., Birkeland, A., Thorpe, R.I. Lead isotope systematics of strata-bound sulfide deposits in the Caledonides of Norway // Economic Geology, 1993. Vol. 88. P. 397–417.

Brown, D., Herrington, R.J., Alvarez-Marron, J. Processes of Arc-Continent Collision in the Uralides // In: Brown D and Ryan PD (eds) Arc-Continent collision. Springer-Verlag, Berlin Heidelberg, 2011. P. 311–340.

Buslaev, F.P., Kaleganov, B.A. The age of sulfide-ore formation according to the K/Ar method // In: Prokin VA and Buslaev FP (eds) Copper-sulfide deposits of the Urals: Conditions of formation. Russian Academy of Science, Ural Branch, Ekaterinburg, 1992. P. 186-199 [in Russian].

Fershtater, G.B., Krasnobaev, A.A., Bea, F., Montero, P., Borodina, N.S. Geodynamic settings and history of the Paleozoic intrusive magmatism of the Central and Southern Urals: Results of Zircon Dating // Geotectonics, 2007. Vol. 41. P. 465–486.

Gannoun, A. et al. Re–Os isotopic constraints on the genesis and evolution of the Dergamish and Ivanovka Cu (Co, Au) massive sulphide deposits, south Urals, Russia // Chem. Geol., 2003. Vol. 196. P. 193–207.

Herrington, R.J., Brown, D. The generation and preservation of mineral deposits in arc-continent collision environment // In: Brown D and Ryan PD (eds) Arc-Continent collision, Springer-Verlag, Berlin Heidelberg, 2011. P. 145–162.

Hu, R.-Z., Wei, W.-F., Bi, X.-W., Peng, J.-T., Qi, Y.-Q., Wu, L.-Y., Chen, Y.-W. Molybdenite Re-Os and muscovite 40Ar/ 39Ar dating of the Xihuashan tungsten deposit, central Nanling district, South China // Lithos, 2012. Vol. 150. P. 111–118.

Huston, D.L., Pehrsson, S., Eglington, B.M., Zaw, K. The Geology and Metallogeny of Volcanic-Hosted Massive Sulfide Deposits: Variations through Geologic Time and with Tectonic Setting // Econ. Geol., 2010. Vol. 105. P. 571–591.

Maslennikov, V.V., Maslennikova, S.P., Large, R.R., Danyushevsky, L.V. Study of Trace Element Zonation in Vent Chimneys from the Silurian Yaman-Kasy Volcanic-Hosted Massive Sulfide Deposit (Southern Urals, Russia) Using Laser Ablation-Inductively Coupled Plasma Mass Spectrometry (LA-ICPMS) // Econ. Geol., 2009. Vol. 104. P. 1111–1141.

Smirnov, V.N., Fadeicheva, I.F., Ivanov, K.S. Geochemistry of Volcanic Rocks in the Tagil Zone of the Urals as an Indicator of Geodynamic Environments of Their Formation // Doklady Earth Sciences, 2008. Vol. 423 (8). P. 1278–1281.

Tessalina, S.G. et al. Osmium isotope distribution within the Palaeozoic Alexandrinka seafloor hydrothermal system in the Southern Urals, Russia // Ore Geol. Rev., 2008. Vol. 33. P. 70–80.

Yazeva, R.G., Bochkarev, V.V. Silurian island arc of the Urals: structure, evolution and geodynamics // Geophysics, 1996. Vol. 29 (6). P. 478–489.

F.J. Testa, D.R. Cooke
CODES, University of Tasmania, Hobart, Australia, F.J.Testa@utas.edu.au

PRELIMINARY THERMODYNAMIC MODEL FOR Bi-MINERALS IN THE SAN FRANCISCO DE LOS ANDES Bi-Cu-Au BRECCIA PIPE, SAN JUAN, ARGENTINA

Комплексное месторождение Bi-Cu-Pb-Zn-Mo-As-Fe-Ag-Au Сан Франциско де Лос Андес располагается на восточном фланге Передового Хребта и представляет собой тело брекчий с турмалиновым цементом, возраст которого определяется пермским или более молодым магматизмом. Продуктивная минерализация представлена сульфидами, сульфосолями, теллуридами и самородными элементами и различается для разных участков месторождения, в основном содержаниями галенита и халькопирита и соответствующим уровнем примесей меди и свинца в висмутовых минералах, среди которых установлены висмутин, тетрадимит, промежуточные члены рядов висмутин-айкинит, крупкаит-паарит, зальцбурит-гледит. На основе термодинами-

ческого анализа делается вывод о том, что различия в минерализации на участках месторождения зависят в большей степени от активности растворенных Pb и Cu, чем от фугитивностей серы и теллура.

Introduction

San Francisco de los Andes mine (30?50?08??S – 69?35?58??W) is located on the eastern flank of the Cordillera Frontal, San Juan province, Argentina. The Cordillera Frontal is a geological province on the eastern flank of Cordillera de los Andes that extends from northern San Juan to southern Mendoza. The orebody is hosted by a tourmaline-cemented breccia pipe that has cut carboniferous sedimentary rocks [Llambias et al., 1969]. The sedimentary rocks have been intruded by the Tocota Pluton, a Permian intrusive complex that ranges from tonalite to granite in composition. Geochronological studies are currently being conducted in order to determine whether the breccia pipe is related to Permian or younger magmatism.

San Francisco de los Andes is characterized by complex Bi-Cu-Pb-Zn-Mo-As-Fe-Ag-Au mineralization, including native elements, sulfides, and sulfosalts. This article reports the occurrence of two different Bi-Cu-Pb mineral assemblages at opposite sides of the NW-SE trending elliptical breccias pipe. By means of detailed analytical studies and the available fluid inclusion data a preliminary thermodynamic model was developed for both assembles at a minimum temperature of 230 °C and a maximum temperature of 400 °C. It was aimed to constrain tentative fS_2 and fTe_2 values for the hydrothermal solutions using the previously determined sulfide and telluride assemblages.

Bi-Pb-(Cu) and Bi-Cu-(Pb) assemblages

Backscattered electron images (BSEI) were used to detect different mineral species, electron microprobe analyses (EMPA) to determine the major chemical compositions of each phase and laser ablation inductively coupled plasma mass spectrometry (LA-ICP-MS) to characterize their trace element geochemistry and mineral inclusion compositions.

Two apparently homogeneous bismuthinite crystals were chosen from each area. In both cases, a spot profile was drawn perpendicular to the main cleavage direction (010). Consecutive analyses were performed at 500 ?m intervals along the profile. The polished blocks were prepared from a sample of bismuthinite-cosalite cemented breccia (NW area) and bismuthinite-chalcopyrite cemented breccia (SE area).

Two distinct mineral species were identified from the 26 spots analyzed In the NW polished sample (Table). Fifteen out of the twenty six analyses correspond to bismuthinite ($Bi_{1.981}$ $Sb_{0.040}$) ($Pb_{0.025}$) ($Cu_{0.028}$ $Ag_{0.001}$) ($S_{2.986}$ $Se_{0.012}$ $Te_{0.002}$) No apparent chemical variations within the bismuthinite-aikinite solid solution series were detected. Bi contents are two orders of magnitude higher than Pb and Sb, three times higher than Cu and four orders of magnitude higher than Se and Te. Silver telluride inclusions are regularly spread within bismuthinite crystal. Argentocuprocosalite ($Pb_{1.663}$ $Cu_{0.326}$ $Ag_{0.240}$) ($Bi_{2.057}$ $Sb_{0.092}$) ($S_{4.976}$ $Se_{0.013}$ $Te_{0.011}$) was detected from nine EMPA analyses along the twenty-six-spot-profile. The term argentocuprocosalite is applied here to Ag- + Cu-bearing cosalite in order to explain the shift away from pure end-member cosalite as plotted on Fig. 1. The Bi and Pb signals from an LA-ICPMS analysis of argentocuprocosalite are two orders of magnitude higher than Ag, Sb and Cu and four to five times higher than Cd, Te, In, Se, Tl and Mn. No silver telluride inclusion was detected in this mineral. The two remaining analysis out of the 26 spots revealed two unclassified species.

Two recurrent mineral phases were found from the 35 spots analyzed In the SE polished sample (Table). Twenty four analyses determined that the species correspond to bismuthinite (Bi2.023 $Sb_{0.024}$) ($Pb_{0.022}$) ($Cu_{0.026}$ $Ag_{0.001}$) ($S_{2.972}$ $Se_{0.015}$ $Te_{0.012}$) No apparent chemical variations within the bismuthinite-aikinite solid solution series were detected. Seven out of thirty five EMPA analyses match with tetradymite inclusions ($Bi_{2.037}$ $Sb_{0.016}$) ($Pb_{0.001}$) ($Cu_{0.009}$ $Ag_{0.011}$) ($Te_{1.876}$ $S_{1.096}$ $Se_{0.028}$). The remaining four spots belong to four different members within the bismuthinite-aikinite solid solution series: Friedrichite ($Pb_{4.802}$) ($Cu_{4.939}$ $Ag_{0.032}$) ($Bi_{7.166}$ $Sb_{0.305}$) ($S1_{7.961}$ $Se_{0.026}$ $Te_{0.013}$), two species between the krupkaite-paarite members with the following chemical composition ($Pb_{0.911}$) ($Cu_{1.135}$ $Ag_{0.013}$) ($Bi_{3.094}$ $Sb_{0.012}$) ($S_{5.969}Se_{0.025}$ $Te_{0.006}$) and ($Pb_{0.891}$) ($Cu_{0.894}$ Ag_0) ($Bi_{3.121}$ $Sb_{0.045}$) ($S_{5.975}$ $Se_{0.019}$ Te0.006) and a mineral phase within salzburgite-gladite members ($Pb_{1.482}$) ($Cu_{1.475}$ Ag_0) ($Bi_{6.624}$ $Sb_{0.096}$) ($S_{11.945}$ $Se_{0.047}$ $Te_{0.008}$).

Table

EMPA mean chemical composition of each species

	NW Area				SE Area					
							Bismuthinite-aikinite solid solution series n=4			
	Bismuthinite n=15	Ag-Cu cosalite n=09	Unknown n=01	Unknown n=01	Bismuthinite n=24	Tetradymite n=07	Gladite-salzburgite member n=01	Paarite-krupkaite member n=01	n=01	Friedrichite n=01
Bi	79.31	43.33	47.56	40.49	79.46	60.81	63.04	59.63	58.52	43.62
Sb	0.93	1.13	0.55	1.68	0.55	0.27	0.53	0.50	0.14	1.08
Pb	0.99	34.74	20.95	26.09	0.84	0.03	13.98	16.88	17.09	28.98
Cu	0.34	2.09	6.71	7.53	0.31	0.08	4.27	5.20	6.53	9.14
Ag	0.01	2.61	7.58	6.56	0.02	0.17	0.00	0.00	0.13	0.10
S	18.34	16.08	16.74	16.62	17.91	5.02	17.44	17.52	17.32	16.78
Se	0.18	0.11	0.19	0.18	0.23	0.31	0.17	0.14	0.18	0.06
Te	0.06	0.14	0.18	0.21	0.30	34.18	0.04	0.07	0.07	0.05
∑	100.16	100.23	100.46	99.37	99.62	100.89	99.48	99.93	99.98	99.81

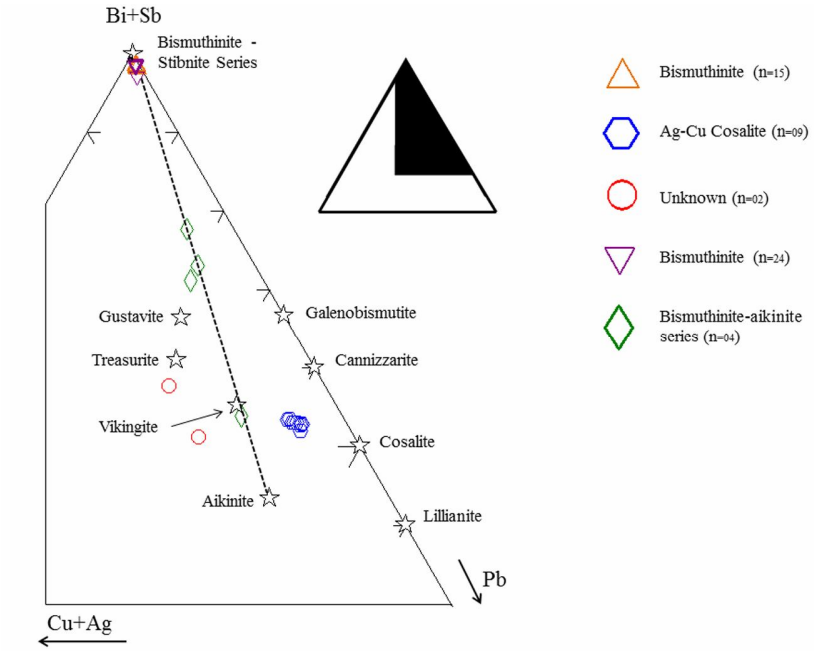

Fig. 1. (Cu+Ag)-(Bi+Sb)-Pb ternary diagram. Only sulfides and sulfosalts analyses are plotted.

Fluid inclusions

Little has been published on the conditions of formation of the San Francisco de los Andes deposit. The only data available are provided in a report by Cardo et. al [2008]. They estimated temperatures between 227 °C to 229 °C and a salinity of 14.6 wt % NaCl equiv for the two-phase, liquid-rich fluid inclusions found in quartz samples. Temperatures as high as 367 °C to 388 °C and salinities up to 45 wt % NaCl equiv were reported for the three–phase (liquid+vapor +halite) quartz-hosted fluid inclusions.

These temperatures are comparable with well documented tourmaline-breccia hosted Cu-Mo deposits such as Rio Blanco-Los Bronces [Frikken et al., 2005]. Measured homogenization temperature for Type ia (two-phase, liquid-rich fluid inclusions) and type iia (three-phases, salt saturated, halite-bearing fluid inclusions) range between less than 200 °C and more than 400 °C.

A thorough fluid inclusion study in the quartz and tourmaline hydrothermal cement from San Francisco de los Andes breccias will be conducted in the near future.

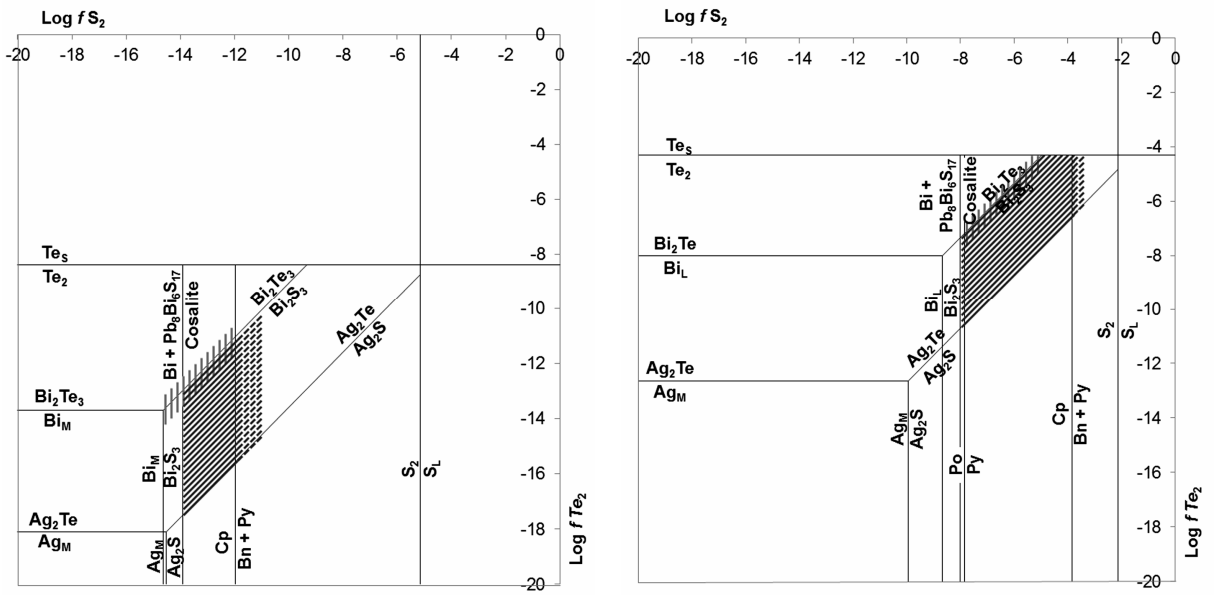

Fig. 2. fS_2-fTe_2 diagrams calculated at 230 °C (left) and 400 °C (right).

Preliminary thermodynamic model

Both mineral assemblages stability limits were calculated using thermochemical data from Afifi, Kelly and Essene [1988], Barton and Skinner [1967, 1979], Craig and Barton [1973], Garrels and Christ [1965], Krauskopf and Bird [1995] and Robie and Waldbaum [1968]. Each linear equation was calculated at two extreme temperatures (230 °C and 400 °C) and was plotted in fS_2-fTe_2 diagrams as it can be seen in Figure 2.

The stability field for the bismuthinite (Bi_2S_3) – hessite (Ag_2Te) – cosalite ($Pb_2Bi_2S_5$) assemblage is shown as diagonal lines. Given the fact that there is minor chalcopyrite and no bornite, as well as an uncertainty about the equilibrium of the Cu-minerals, we cannot precisely state an exact limit at higher values of fS_2. This is the reason why we continue the stability field with diagonal dashed lines further away.

Since there is no available thermochemical data for tetradymite (Bi_2Te_2S) we assumed that it could have formed from tellurobismuthite (Bi_2Te_3) according to the reaction: $2Bi_2Te_3 + S_2 = 2Bi_2Te_2S + Te_2$. Tetradymite could be formed at small fluctuations in fS_2 and fTe_2 as a slight S_2 fugacity increase or a subtle Te_2 fugacity decrease. It is our understanding that tetradymite stability space should be close to that of tellurobismuthite. According to previously made assumptions the stability field for the bismuthinite (Bi_2S_3) – tetradymite (Bi_2Te_2S) assemblage is approximately located along the following equilibrium line $Bi_2S_3 + 3/2Te_2 = Bi_2Te_3 + 3/2S_2$ and within pyrite chalcopyrite stability space.

Discussion and conclusions

At a minimum temperature of 230 °C, crystallization of bismuthinite, silver tellurides inclusions and argentocuprocosalite took place under minimum log fTe_2 = log fS_2 – 3.59 and maximum log fTe_2 = log fS_2 + 0.93 between log fS_2 values of –13.92 and –11.97. At higher temperatures (400 °C) the minimum Te_2 fugacity limit is given by the equation log fTe_2 = log fS_2 – 2.69 and the maximum boundary by log fTe_2 = log fS_2 + 0.68 between log fS_2 values of –8 and –3.86. Te_2 fugacity limits were constrained by the bismuthinite-hessite stability field. Although the lowest log fS_2 values are well define by cosalite appearance (–13.92 at 230 °C and –8 at 400 °C), the highest values are not. They are constrained by log fS_2 values of –11.97 at 230 °C and –3.86 at 400 °C.

The bismuthinite-tellurobismutite monovariant line has a fixed position and does not show significant changes with temperature variations. As a result, the bismuthinite-tradymite-chalcopyrite stability space is a straight forward function of the Po/Py and Cp/Bn+Py monovariant lines at high temperature and Bi_M/Bi_2S_3 and Cp/Bn+Py lines at low temperatures. Note that at 230 °C the stability field lower limit is given by the Bi_M /Bi_2S_3 line as Po/Py monovariant line would be drawn within the Bi_M space. At 230 °C and assuming that Bi-minerals crystallization took place within pyrite-chalcopyrite stability space, Bismuthinite and tellurobismutite (and probably tetradymite) log fS_2 val-

ues range between –14.63 and –11.97 while log fTe_2 values fluctuate between –13.70 and –11.04. At temperatures as high as 400 °C an increase in fS_2 (between –7.85 and –5.00) and an increase in Te_2 fugacity (between –7.17 and –4.31) is required.

The bismuth telluride inclusions trapped within bismuthinite may have formed in equilibrium with the Bi-sulfide. It is also possible that bismuthinite was the first mineral to crystallize followed by the bismuth telluride inclusions formation that may have been triggered by a slight S_2 fugacity decrease or even more likely by a Te_2 fugacity increase, possibly as a result of tellurium-rich magmatic vapor plumes.

The above data indicate that the stability fields for both mineral assemblages at a given temperature are rather similar, specially the log fS_2 values. The main difference between the NW area and SE area may not be a change in S_2 and Te_2 fugacity but a function of Pb and Cu concentration in the hydrothermal fluid. This hypothesis is consistent with the fact that galena was only found in the NW area along with cosalite but only minor chalcopyrite. On the other hand, chalcopyrite is abundant in the SE area while cosalite is rarely found and galena is absent.

It is necessary to conduct a detailed fluid inclusion study in order to constrain the temperature of formation and consequently improve the thermodynamic model. By the end of this project we hope to include all other minerals in order to make a detailed thermodynamic modeling for San Francisco de los Andes ore deposit.

References

Afifi A.M., Kelly, W.C., Essene E.J. Phase relations among tellurides, sulphides and oxides: I. Thermochemical data and calculated equilibria; II. Applications to telluride-bearing ore deposits // Economic Geology. 1988. Vol. 83. P. 377–404.

Barton, P., Skinner, B. Sulfide mineral stabilities // In: Barnes, H.L. (Eds.), Geochemistry of Hydrothermal Ore Deposits. New York, 1967. P. 236–333.

Barton, P., Skinner, B. Sulfide mineral stabilities // In: H.L. Barnes (Eds.), Geochemistry of Hydrothermal Ore Deposits. New York, John Wiley, 1979. P. 278–403.

Cardo, R., Segal S., Korzeniewski, L., Palacio, M., Chernicoff, C. Estudio metalogenetico de brechas hidrotermales portadoras de mineralizacion de Bi-Au-Cu en el ambito de la Cordillera Frontal, Provincia de San Juan // Serie de Contribuciones Tecnicas, Recursos Minerales N 31. SEGEMAR, 2008. P. 3–28 [in Spanish].

Craig, J., Barton, P. Thermochemical approximations for sulfosalts // Economic Geology, 1973. P. 493–506.

Frikken, P.H., Cooke, D.R., Walshe, J. L., Archibald, D., Skarmeta, J., Serrano, L. and Vargas, R. Mineralogical and Isotopic Zonation in the Sur-Sur Tourmaline Breccia, Rio Blanco-Los Bronces Cu-Mo Deposit, Chile: Implications for Ore Genesis // Economic Geology, 2005. Vol. 100. № 5. P. 935–961.

Garrals, R.M., Christ, C.L. Solutions, minerals, and equilibria. San Francisco. CA: Freeman, Cooper. New York, 1965. 450 p.

Krauskopf, K. B., Bird D.K. Introduction to geochemistry. 3rd edi. McGraw-Hill, New York, 1995. 647 p.

Llambias, E., Malvicini, L. The Geology and Genesis of the Bi-Cu Mineralized Breccia-Pipe, San Francisco de los Andes, San Juan, Argentina // Economic Geology, 1969. Vol. 64. P. 271–286.

Robie, R.A., Waldbaum D.R. Thermodynamic properties of minerals and related substances at 298.15 K (25.0 C) and one atmosphere (1.013 bars) pressure and at higher temperatures // US Government Printing Office, 1968. 256 p.

G.A. Tret'yakov
Institute of Mineralogy UB RAS, Miass, Russia, genatret@yandex.ru

EXTRACTION OF METALS FROM THE SEDIMENT BY THE HEATED SEAWATER: A PHYSICAL-CHEMICAL MODELING

Выполнено физико-химическое моделирование взаимодействия нагретой морской воды, осадка впадины Гуаймас и океанического габбро при соотношениях порода–морская вода (R/SW) от $1?10^{-5}$ до 10. Установлено, что максимальная экстракция железа из габбро происходит при минимальном pH и соотношении R/SW=0.007, а меди и никеля при 0.03. Кондуктивное

охлаждение раствора, отделившегося от габбро (R/SW=0.03), в зоне разгрузки приводит к осаждению руд, богатых халькопиритом, а прореагировавшего с осадком – пирротином. При R/SW=0.007 в осадочной системе отлагается пирит в этих условиях.

The physical-chemical and experimental modeling of the sediment-related hydrothermal systems is dedicated to the various problems of interaction of the heated seawater and organic-rich sediments. The interest to such studies is caused by discovery of the hot vents located on the sediment-covered ridges like Guayamas basin, Escanaba and Okinawa troughs or Middle Valley in Juan de Fuca ridge [Gieskes et al., 1988; Koski et al., 1988; et al.]. The massive sulfides from these systems are characterized by abundant pyrrhotite and hydrothermal vents contain oil distillates. However, the former works give the contradictory data on the extractive ability of the fluid and the metal source for the sediment-hosted sulfide edifices. Some researchers consider that metals were extracted from the sediments [Thornton and Seyfried, 1987; Seewald et al., 1990; Cruse, Seawald, 2001] in contrast to the metal extraction from the underlying basalts [Goodfellow and Franklin, 1993, Butterfield et al., 1994].

In order to estimate the extraction ability of the sediments, we model the interaction between the heated seawater, bottom diatomaceous sediments from the Guaymas basin in the Gulf of California, and oceanic gabbro, which average composition (n 250) was taken from the PetDB (http://www.petdb.org). The modeling was implemented in the Selector computer program and was based on a multisystem formed and debugged previously [Tret'yakov and Melekestseva, 2008]. The primary composition of sediment was taken from [Thornton and Seyfried, 1987, p. 1998, table 1] and seawater, from [Encyclopedia…, 2008].

Preliminary, Ba, Sr, and Cr contents in the composition of sediment were recalculated into oxides, Fe_2O_3 was converted to FeO (because the sediment is reduced), an organic carbon and a part of H_2O were recalculated into fulvic acid ($C_{135}H_{182}O_{95}N_5S_2$), O, N, and S were added in accordance to the formula, and contents of all elements were reduced to 1 kg. First, the gabbro-seawater interaction was modeled for the various rock-seawater (R/SW) ratios in order to reveal the maximum of extraction of Ba, Co, Cu, Fe, Ni, Pb, Si, and Zn (Fig. 1). Further, the mineral precipitation from the fluid was modeled at a temperature decrease based on the subsequent reactor method for the R/SW ratios of 0.007 and 0.03 (Fig. 2). The parameters of temperature and pressure for calculations were based on P-T-conditions of the hydrothermal systems from the Guaymas basin and Mid-Atlantic Ridge. Seawater reacted with gabbro or sediment at 350 °C and 250 bars and then the equilibriums were calculated with a step of 20 °C at decreasing temperature. The solution was separated from the solid phases at each step and moved into the following reservoir that corresponds to the conductive cooling of the fluid and mineral precipitation and imitates, with some assumptions, the growth of the sulfide mound on the sea floor.

It was found that R/SW interaction at 350 °C and 250 bars leads to the onset of mineral assemblages, which are similar to those from natural hydrothermally altered rocks. At low R/SW ratios (≤0.0001) under oxidized conditions, the solid phases include hematite, anhydrite, chlorite, chrysotile, and brucite in contrast to quartz, talc, montmorillonite, seladonite, amesite, pyrrhotite, cubanite, millerite, pyrite, and jaipurite under reduced conditions and R/SW ratio of >0.0001. Additionally, minerals typical of the altered sediments in the hydrothermal fields (clinoamphibole, actinolite, albite, illite, sphalerite, and galena) are formed at R/SW of ≥0.06.

It was established that cooling of the solutions produces the ore mineral assemblages. No mineral precipitation occurs at the gabbro/seawater ratio of 0.007 (maximum of Fe extraction from the seawater) in the high-temperature area (>250 °C, Fig. 2c). The quartz + pyrite + chalcopyrite + fahlore assemblage is deposited at temperature of <250 °C and chalcocite and barite, at temperature of <100 °C. In the sediment, pyrite and a few amount of vaesite precipitate at the same ratio and temperature of <250 °C (Fig. 2a) admixed by quartz, covellite, cattierite, barite, galena, and sphalerite at decreasing temperature. The greater diversity of minerals is observed at R/SW ratio of 0.03. At high temperature, gabbro contains chalcopyrite and small amount of minerals of the linnaeite-polydimite group; the decrease in temperature leads to the formation of major quartz and pyrite and occasional greenockite, vaesite, and chalcopyrite. Sphalerite, galena, and barite appear at low temperatures. Pyrrhotite is the major mineral of the sediment at high temperature and minerals of the linnaeite-polydimite group, chalcopyrite, and millerite are secondary in abundance. At lower temperatures, pyrite alternates pyr-

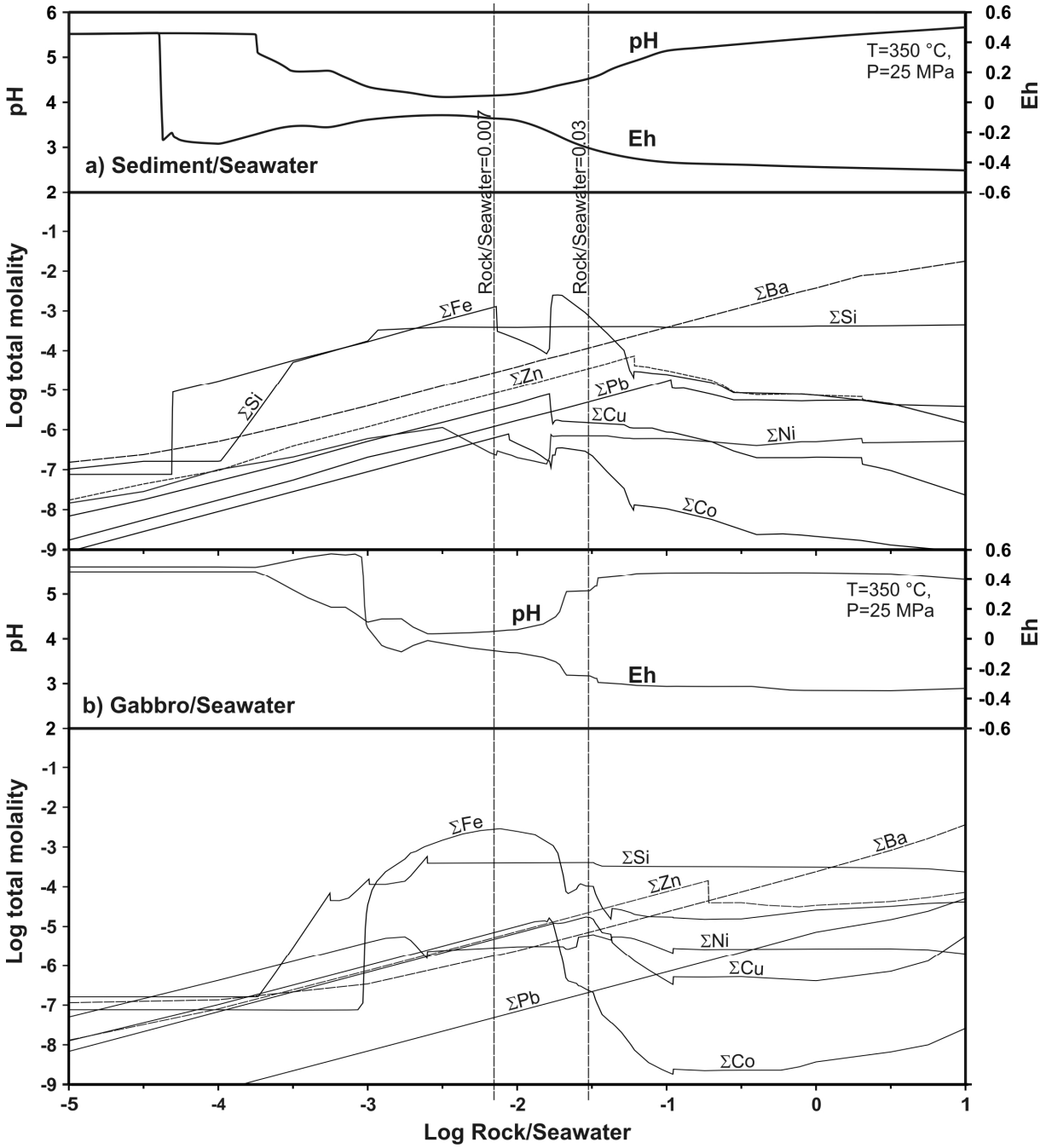

Fig. 1. Plots of Eh, pH, and total contents of metals extracted from the sediment (a) and gabbro (b) with the heated seawater at different R/SW ratios. The mineral assemblages precipitated from the fluid at decreasing temperature are calculated for the R/SW ratio of 0.007 and 0.03 (vertical dotted lines) (see Fig. 2).

rhotite and Ni-minerals disappear. Quartz with subordinate pyrite, sphalerite, and galena dominate in a range of 270–150 °C.

The modeling has shown that the maximum amount of Fe is extracted at minimum pH (see Fig. 1) that completely corresponds to the chemical direction of the R/SW interaction. Our estimations of R/SW ratios for the extractive fluid ability are somewhat lower than experimental sediment-seawater ratios of 0.25 [Seewald et al., 1990] and 0.625–1 [Cruse and Seewald, 2001].

Thus, our calculations are in agreement with suggestion that sediments, serving as a basement for the massive sulfide mounds on the seafloor, could be the source of metals. The composition of massive sulfides mostly depends on the rock-seawater ratio in the interaction zone and also on the style of discharge of the hydrothermal fluid on a seafloor.

The work is supported by the program of Presidium of Russian Academy of Science no. 23 (project no. 12-П-5-1003).

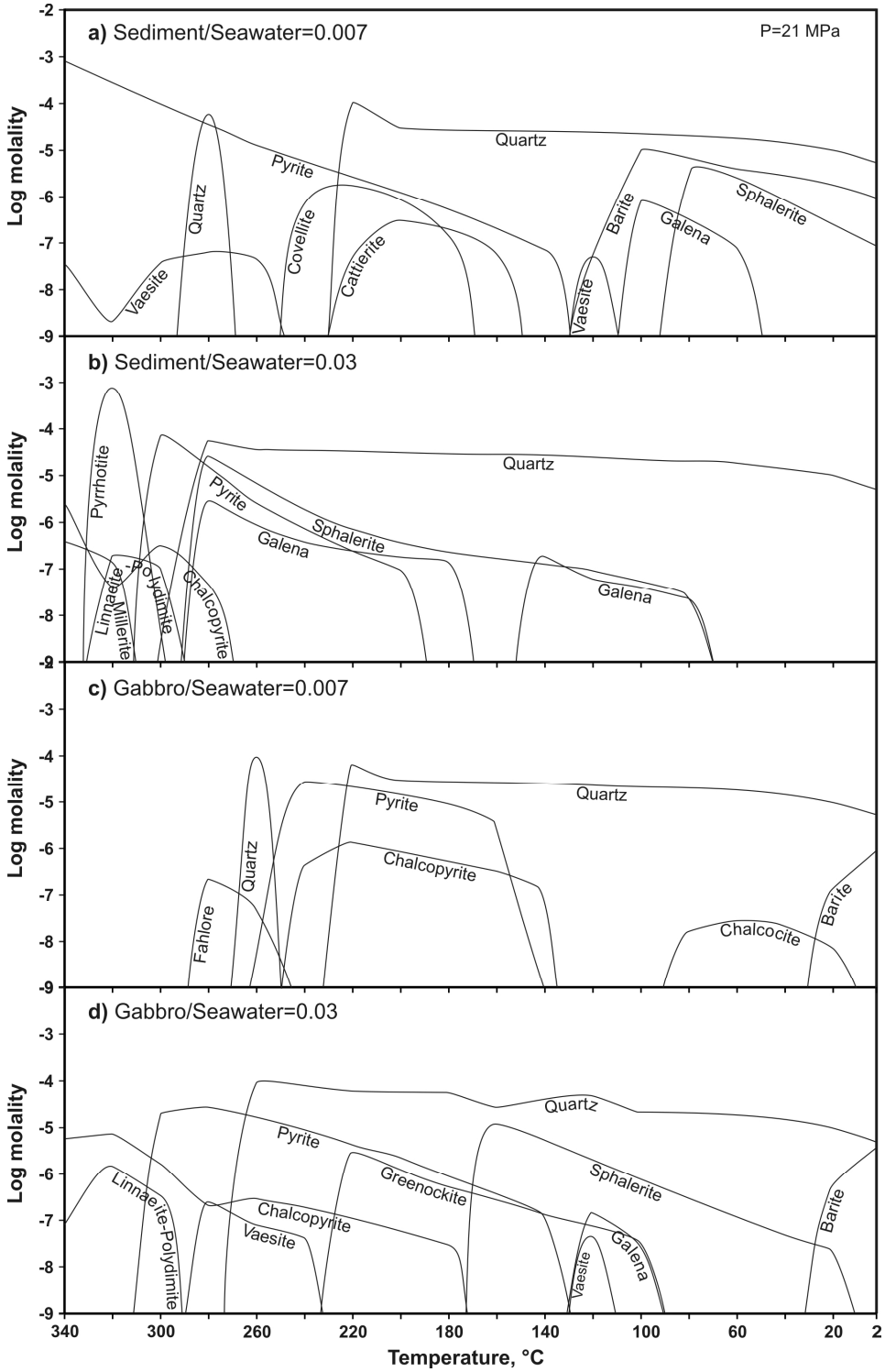

Fig. 2. Mineral assemblages precipitated from the fluid at its cooling from 350 to 2 °C at R/SW ratios of 0.007 and 0.03. These ratios were chosen owing to the maximum extraction of Fe (0.007), Cu, and Ni (0.03) at gabbro-seawater interaction (see Fig. 1).

References

Butterfield, D.A., McDuff, R.E., Franklin, J., Wheat, C.G. Geochemistry of hydrothermal vent fluids from Middle Valley, Juan de Fuca Ridge // Proc. of the ODP, Scie. Results. Eds. Mottle M.J., Davis E.E., Fisher A.T., Slack J.E. 1994. Vol. 139. P. 395–410.

Cruse, A.M., Seewald, J.S. Metal mobility in sediment-covered ridge-crest hydrothermal systems: Experimental and theoretical constraints // Geoch. et Cosmoch. Acta, 2001. Vol. 65. P. 3233–3247.

Gieskes, J.M., Simoneit, B.R.T., Brown, T., Shaw, T., Wang, Y.-C., Magenheim, A. Hydrothermal fluids and petroleum in surface sediments of Guaymas Basin. Gulf of California: a case study // Can. Min., 1988. Vol. 26. P. 589–602.

Goodfellow, W.D., Franklin, J.M. Geology, mineralogy, and chemistry of sediment-hosted clastic massive sulfides in shallow cores, Middle Valley, northern Juan de Fuca Ridge // Econ. Geol., 1993. Vol. 88. P. 2037–2068.

Encyclopedia of ocean sciences (second edition). Appendix 7. Estimated mean oceanic concentration of the elements // Editors: Steele, J.H., Turekian, K.K., Thorpe, S.A. 2008. P. 386–388.

Koski, R.A., Shanks, W.C.,III, Bohrson, W.N., Oscarson, R.L. The composition of massive sulfide deposits from the sediment-covered floor of Escanaba Trough, Gorda Ridge: implication for depositional processes // Can. Min., 1988. Vol. 26. P. 655–673.

Seewald, J.S., Seyfried, W.E., Thornton, E.C. Organic-rich sediment alteration: an theoretical study at elevated temperatures and pressures // Appl. Geoch., 1990. Vol. 5. P. 193–209.

Thornton, E.C., Seyfried, W.E. Jr. Reactivity of organic-rich sediment in seawater at 350°C, 500 bars: Experimental and theoretical constraints and implications for the Guaymas Basin hydrothermal system // Geoch. et Cosmoch. Acta, 1987. Vol. 51. P. 1997–2010.

Tret'yakov, G. A., Melekestseva, I.Yu. Serpentinization of ultramafic rocks and the source of metals for Co-bearing massive sulfide deposits // In: Metallogeny of ancient and modern oceans-2008. Ore-bearing complexes and ore facies. Ed. V.V. Zaykov and E.V. Belogub. Miass, Insitute of mineralogy UB RAS, 2008. P. 26–30.

Udachin V.N.[1,2], Weiss D.J.[3,4], Aminov P.G. [1,2], Spiro B.[4], Williamson B.J.[4,5]
[1] Institute of Mineralogy Urals Branch of RAS, Miass, Russia,
udachin@mineralogy.ru
[2] National Research South Ural State University, Chelyabinsk, Russia
[3] Department of Earth Science and Engineering, Imperial College, London, UK
[4] Department of Mineralogy, Natural History Museum, London, UK
[5] Camborne School of Mines, University of Exeter, Cornwall, UK

ISOTOPIC GEOCHEMISTRY OF TRACERS FOR MINING AND SMELTING ACTIVITIES IN LANDSCAPE ENVIRONMENT IN THE SOUTHERN URALS

Приведены результаты использования радиометрических трассеров для характеристики горнопромышленного техногенеза Южного Урала. С применением изотопов ^{210}Pb и ^{137}Cs оценены скорости озерной седиментации в условиях природных и природно-техногенных ландшафтов подзоны южной тайги. При пирометаллургии меди важным индикаторным признаком являются низкие отношения стабильных изотопов свинца ^{206}Pb/^{207}Pb для объектов окружающей среды (металлургические пыли, атмосферный аэрозоль, донные отложения озер доиндустриального периода и верхние интервалы гумусово-аккумулятивных горизонтов почв).

The South Ural area has been heavily affected by mining activities, which include mining, transportation, storage, beneficiation and smelting of metaliferous ores. These cause the atmospheric and aqueous transport accumulation, transformation and reactions of trace – toxic elements in this area. These cause a perturbation of the major environmental systems: atmosphere – soil, atmosphere – water surface, water – lake sediments. The most common effects of mining activity and ore processing of massive sulphide deposits are the dispersion and accumulation of chalcophile elements. In this areas, the technogenic industrial elements are added to the already high natural background levels of trace elements in rocks, soils and plants. This enrichment in technogenic constituent elements is largely caused by atmospheric transport of fine particles from the locations of exploitation, wastes, tailings and copper smelters, in particular of copper ores. Native landscapes are modified to natural-industrial landscapes with formation of geotechnogenic systems in and around the locations of mining and ore processing.

A series of geochemical isotopic methods was used to identify the effects of mining and processing. This series of methods includes the use ^{137}Cs and ^{210}Pb as chronological indicators for the dating of lake sediments and the determination of their sedimentation rate. It includes also the ^{206}Pb/^{207}Pb isotopic ratio for the evaluation of chalcophile elements transport and cycling in these

natural-industrial landscapes. One of the isotopic geochemical markers for the evaluation of sedimentation conditions and rate in continental lakes and costal areas is ^{210}Pb [Krishnaswami et al., 1971] during 55 years and ^{137}Cs [Pennington et al., 1973] during for 40 years. So far, to our knowledge, no such research was published. These methods have not been used for decoding of ecological processes in lake-ecosystems, that occur as a result of mining and ore processing. This seems to be the reason for the lack of information on geochronological reconstruction of changes in the landscape during the period of most intensive copper mining and smelting activity in the Southern Urals. Previous studies used palinological and radiocarbon methods for dating the effects on lake sediments at the South Urals. These studies showed the changes in the ecosystems in longer geological time scale of the Holocene.

Evaluation of ^{137}Cs in the sediments of 8 lakes makes it possible to identify two types of radionuclide distribution depending on the water surface area. The vertical distribution of radioactive cesium in the euthrophic lakes with the water surface area of approximately 1–2 km^2 has a natural character with a "stretched" peaks in the ranges of 0–22 cm and with the lack of a pronounced contrast of individual peak, which corresponds to the maximum of radiocesium deposition from the atmosphere or troposphere in 1963–1964.

At the same time two peaks of radiocesium can be identified in the oligothrophic lakes with the water surface area of 28–54 km^2: peaks of 1963 and 1986 were identified indicating the event of the Chernobyl disaster. The associated geochemical landscapes confirmed the picture of so-called primary mosaic ^{137}Cs distribution. This mosaic distribution depends on the sources features, fractionation processes during atmospheric radionuclide transport, relief conditions and the atmospheric the conditions.

The comparative analysis of sedimentation rates for ^{137}Cs and ^{210}Pb helped the assessment of sedimentation rates with a minimum of 1.5 mm/year (Lake Svetloe) and a maximum of 2.4 mm/ year (Lake Alabuga). The sedimentation rates of these two oligothrophic lakes are similar. These results are consistent with the data obtained for the lakes of the foothill-Siberian taiga landscapes: 1.5–2.0 mm/year. The sedimentation rate for the lakes near copper smelters increased 2–2.5 times and is 4.8 mm/year. This is due to high level of erosion in the catchment area, increase in terrigenous input and significant contribution of air dust components from copper smelters.

The application of Pb isotopic ratios was first proposed in the 1970-s to assess the antropogenic impact on the environment. Since then, nearly two hundred publications about Pb isotopic reported the data one human influence on atmosphere, hydrosphere, soil, and lakes sediments. The

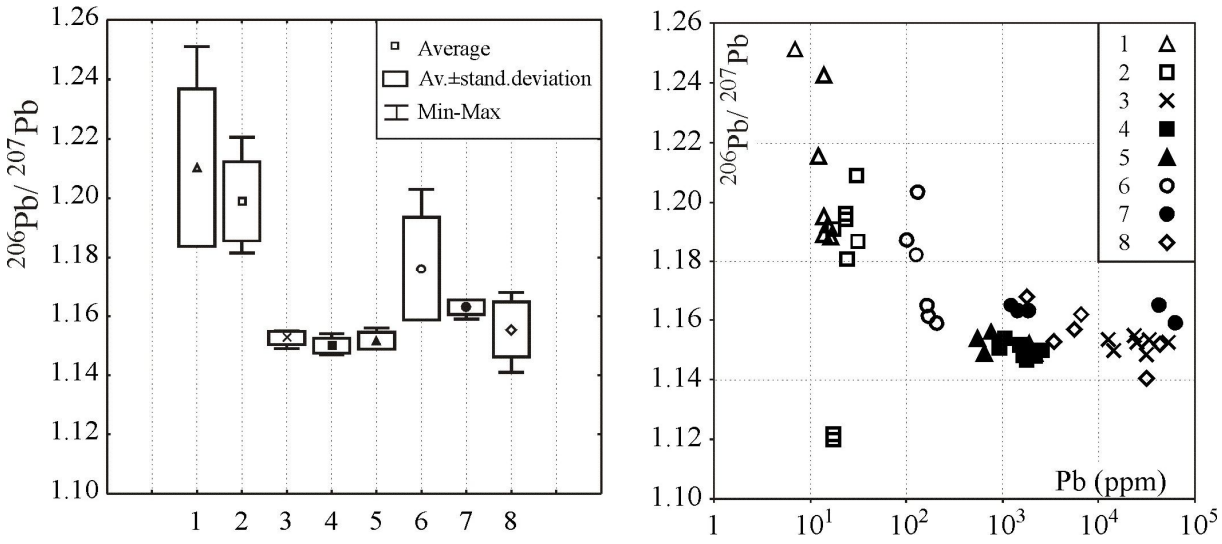

Fig. Isotopic ratio ^{206}Pb/^{207}Pb (left) and correlation rations from Pb concentration (right) in "background" environment and smelting area (1 – background lake sediments (depth 1 m), 2 – mineral horizons of soils (depth 30 cm), 3 – metallurgical dust, sulfide ores, slags, 4 – top soil horizons (0–8 cm), 5 – lake sediments smelting industry period (interval 0–20 cm), 6 – snow dust "background" environment, 7 – snow dust in smelting and mining area, 8 – atmospheric dust wet summer precipitation.

general observation is that the most contrast $^{206}Pb/^{207}Pb$ ratios for the background samples are at the level of 1.18–1.35, and reflects the original Pb isotope ratio. In contrast, alkyllead gasoline, atmospheric aerosoils, smelting dust have low $^{206}Pb/^{207}Pb$ in the range of 1.04–1.15. As the difference in isotopic ratios of $^{206}Pb/^{207}Pb$ is approximately 2%, it seems to be sufficient to distinguish between the natural and the anthropogenic components, and even to assess their relative contribution to the overall balance of the substances in the environment [Ettler et al., 2004]. Therefore the Pb isotope method is widely used in geochemical studies.

Figure 1 illustrates the Pb isotopic ratios of the major components in the natural environment of the Southern Urals. We can clearly see the contrast in $^{206}Pb/^{207}Pb$ isotope ratios for the two main components of the natural environment – lake sediments and soils of the pre-industrial period with average ratios of 1.210 and 1.198, respectively. In contrast industrial pollution has an $^{206}Pb/^{207}Pb$ average value of 1.152. The upper intervals, the humic part of soils and lake sediments under the influence of mining and smelting impact have similar relationships (Fig.). The Pb isotope ratio is a good indicator of anthropogenic impact on the snow dust composition, its "background" landscapes have an average ratio of 1.174 and atmospheric dust, which comes with rains in the summer has an average value of 1.154. These low values of isotopic ratios demonstrate regional scale of mining and smelting impact on the South Ural environment [Weiss et al., 2004; Spiro et al., 2013].

We thank to Martin Blunt, Andy Fleet and Terry Williams (ICL/NHM, London), Dariya Kiseleva (IGG UB RAS, Ekaterinburg) for access to analytical facilities. VU and PA gratefully acknowledges UB RAS Funds grant (projects no. 12-C-5-1037, 12-M-45-2051 and 12-M-45-2072). This study formed part of the 3 year European Union FP5 INCO-Copernicus 2, MINURALS Project (contract ICA2-CT-2000-10011). Follow-up work was funded by a 3 year (2010-2012) EU FP7 contract "Impact Monitoring of Mineral Resources Exploitation" (ImpactMin, Contract: 244166).

References

Ettler, V., Mihaljevič, M., Komarek, M. ICP-MS measurements of lead isotopic ratios in soils heavily contaminated by lead smelting: tracing the sources of pollution // Anal. Bioanal. Chem., 2004. Vol. 378. P. 311–317.

Krishnaswami, S., Lal, D., Martin, J.M., Meybeck, M. Geochronology of lake sediments // Earth Planet. Sci. Lett., 1971. Vol. 11. P. 407–414.

Pennington, W., Cambray, R.S., Fisher, E.M. Observations on lake sediments using fallout ^{137}Cs as a tracer // Nature, 1973. Vol. 242. P. 324–326.

Spiro, B., Udachin, V., Williamson, B.J., Purvis, O.W., Tessalin,a S.G., Weiss, D.J. Lacustrine sediments and lichen transplants: two contrasting and complimentary environmental archives of natural and anthropogenic lead in the South Urals, Russia // Aquat. Sci., 2013. Vol. 75. P. 185–198.

Weiss, D.J., Kobe,r B., Gallagher, K., Dolgopolova, A., Mason, T.F., Coles, B.J., Kylande,r M.E., LeRoux, G., Spiro, B. Accurate and precise Pb isotope measurements in environmental samples using MC-ICP-MS // Int. J. Mass Spectrom., 2004. Vol. 232. P. 205–215.

M.V. Zabotina[1], E.V. Belogub[1], A.M. Yuminov[1,2]
[1]Institute of Mineralogy UB RAS, Miass, Russia, mary_7-88@mail.ru
[2] National Research South Ural State University, Chelyabinsk, Russia

CHARACTERISTICS OF PRIMARY ORE AND FORMATION CONDITIONS OF KONTROL'NOE GOLD DEPOSIT (UCHALY REGION, RUSSIA)

Контрольное месторождение приурочено к серицит-кварцевым метасоматитам, образованным по вулканогенным породам карамалыташской свиты (D_2ef-zv*kr*). Для определения физико-химических параметров нами были изучены первичные флюидные включения из кварца и барита из сульфидсодержащих жил в рудной зоне. Измерения первичных флюидных включений показали следующие интервалы температур гомогенизации: для кварца 160–320 °С, для барита 160–250 °С. Температура эвтектики включений в барите варьирует в пределах от –20.5

до –22 °С и близка к солевой системе NaCl–H_2O. Температуры плавления последнего кристаллика составляют от –0.5 до –0.9 °С, что соответствует концентрациям солей в растворе 0.7–1.5 мас. %. Результаты исследований показали, что кварц в жилах Контрольного месторождения образовался в более высокотемпературную стадию, а барит – в более низкотемпературную. Температуры образования кварц-баритовых жил в рудах и вмещающих породах близки друг другу. Солевой состав флюида соответствует системе NaCl–H_2O и близок к составу, установленному на многих колчеданных месторождениях. Низкая концентрация солей во флюиде может быть связано с явлением фазовой сепарации.

Introduction

Our research is aimed to the determination of formation conditions of the Kontrol'noe gold deposit based on the fluid inclusions study. The deposit is hosted in the sericite-quartz metasomatic rocks, which were formed after basalts, andesibasalts, and dacites of the Middle Devonian Karamalytash Formation. The longitudinal steeply dipping structure of the deposit corresponds to the regional geological structure [Krylatov et al., 2006]. The ores include disseminated pyrite and rich stringer-disseminated and massive barite-polymetallic types. The quartz and quartz-barite veins devoid of ore minerals are widespread in host dacites and andesites. The sulfide-bearing quartz and quartz-barite veins occur in the axial part of the ore zone, which completely coincides with metasomatic rocks.

The major ore minerals are pyrite in pyrite ores and sphalerite, galena, and fahlore in polymetallic type. Chalcopyrite is a minor mineral in both ore types. Pyrite is observed as cubic euhedral crystals, framboids, and concretions. Sphalerite, galena, and fahlore form complicate aggregates. Gold 3–50 μm in size was found as inclusions in pyrite, sphalerite, galena, and fahlore and grains in fractures in quartz and barite. The composition of gold corresponds to $Au_{0.54–0.62}Ag_{0.36–0.42}Cu_{0.02–0.09}$ (inclusions in tennantite) and $Au_{0.46–0.67}Ag_{0.30–0.40}Cu_{0.01–0.14}$ (gold in fractures in quartz and barite) [Belogub, 2009].

Results

We have studied primary fluid inclusions in quartz and barite from sulfide-bearing veins from the ore zone. The two- and three-phase fluid inclusions are 3–10 μm in size. The homogenization temperatures of fluid inclusions vary from 320 to 160 °С in quartz (fig. a) and from 250 to 160°С in barite (fig. b). The eutectic temperatures determined for the fluid inclusions in barite range from –20.5 to –22 °С (fig. c) that correspond to NaCl–H_2O system [Borisenko, 1977]. The temperatures of the final ice melting (–0.5 to –0.9 °С) indicate the salinity of the fluids of 0.7–1.5 wt. % NaCl-equiv. (fig. d).

Discussion

The genesis of the gold-sulfide ores from the Kontrol'noe deposit is a matter of debate. From the one hand, the deposit is similar to the Baimak (Kuroko) type of VMS deposits by geological setting, mineral compositions of ores, and gold content. From the other hand, no typical lithologically controlled massive sulfide ores were found at the deposit. So, the deposit may be similar to the intrusion-related gold-sulfide-quartz deposits.

We have compared our results to the fluid inclusion data on the Balta-Tau, Tash-Tau, and Vishnevka VMS deposits from the Baimak ore region. The homogenization temperatures of fluid inclusions are as follows: 240–100 °С (barite, Balta-Tau deposit), 280–120 °С (quartz, Vishnevka and Tash-Tau deposits) [Holland et al., 2003; Zaykov et al., 2010]. The fluid salinity is 4.5–8 wt. % NaCl-equiv (quartz, Tash-Tau) and 2–8 wt. % NaCl-equiv [Zaykov et al., 2010]. At the same time, the fluid salinity and homogenization temperatures at the Degtyarskoe VMS deposit, Central Urals, are significantly higher relative to the Baimak type deposits (7.7–16.2 wt. % NaCl-equiv and 465–210 °С, respectively) [Vikent'ev, 2004].

The homogenization temperatures in quartz and barite from the Kontrol'noe deposit are similar to those from the Baimak type deposits. The homogenization temperatures of quart from the VMS deposits are higher in comparison with barite that is observed at the Kontrol'noe deposit.

The fluid salinity of at the Kontrol'noe deposit is significantly lower compared both to above mentioned VMS or typical gold-sulfide-quartz deposits [Baksheev et al., 1998]. The lower salinity (0.7–2.1 wt. % NaCl-equiv) was determined for barite from the Semenov hydrothermal field in the Mid-Atlantic Ridge [Melekestseva et al., 2010]. Similar lower salinity (0.2–4.5 wt. % NaCl-equiv) at medium temperatures of 290–170 °С was identified for the Lepanto epithermal gold-sulfide deposit,

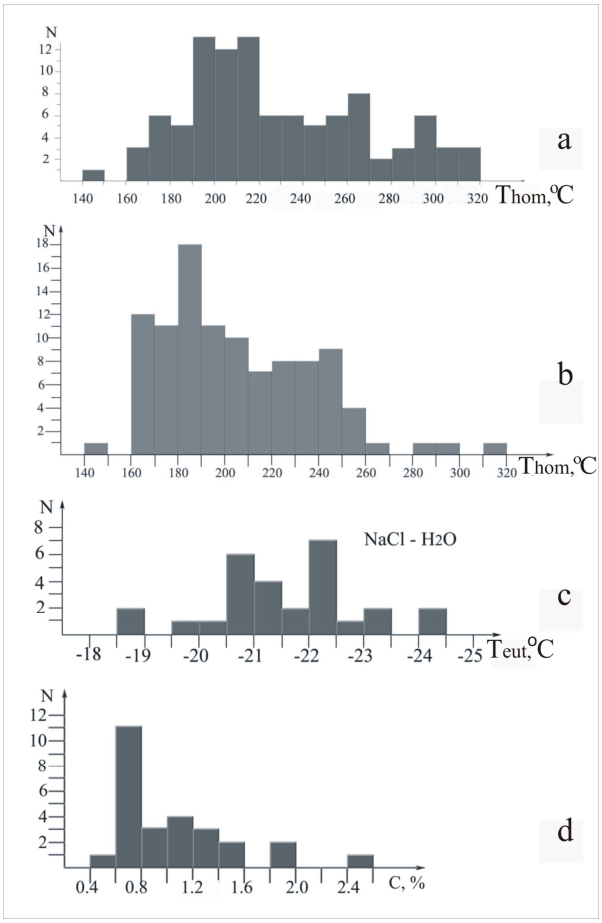

Fig. Histograms of homogenization temperatures of fluid inclusions in quartz (a) and barite (b), eutectic temperature of inclusions in barite (c), and salinity of fluid inclusions in barite (d).

Philippines. The low salinity of the fluid may be explained by phase separation of the homogenous fluid [Hedenquist, Arribas, 1999]. This is in accordance with presence of two- and three-phase fluid inclusions in gangue minerals from the Kontrol'noe deposit.

The one of the main differences between VMS and gold-sulfide-quartz deposits is different composition and salinity of the fluids: NaCl-dominated (± Na_2SO_4 and K_2SO_4) fluids with salinity similar to seawater at VMS deposits vs. compound and more saline fluids at intrusion-related gold-quartz deposits.

Conclusions

Thus, quartz from the veins of the Kontrol'noe deposit was formed slightly at higher temperatures relative to barite. The formation temperatures of quartz-barite veins in ore zone and host rocks are similar. The composition of salt ($NaCl–H_2O$) is similar to that observed at many VMS deposits. The salinity of the fluid is low (0.7–1.5 wt. % NaCl-equiv) that may indicate the phase separation of the fluid.

The authors are sincerely thankful to K. A. Novoselov and E. E. Palenova for useful advices. We also thank I. B. Fadina and G. N. Drokina for a chance to work at the deposit.

References

Baksheev, I.A., Prokop'ev, V.Yu., Ustinov, V.I. Formation conditions of quartz veins from the Berezovskoe gold ore field, Central Ural, based on fluid inclusions and isotope data // In: Urals summer mineralogical school-98. Yekaterinburg, 1998. P. 41–49. [in Russian].

Belogub, E.V. Hypergenesis of sulfide deposits of South Ural // Doctoral dissertation in Geology. Miass: IMin UB RAS, 2009. 536 p. [in Russian].

Borisenko, A.S. Study of salt composition of solutions of fluid inclusions in minerals with cryometry // Geologiya i Geofizika, 1977. Vol. 8. P. 16–27 [in Russian].

Vikent'ev, I.V. Formation conditions and metamorphism of massive sulfide ores. Moscow, Nauchny mir, 2004. 344 p. [in Russian].

Zaykov, V.V., Ankusheva, N.N., Melekestseva, I.Yu. Formation conditions of sulfide veins from the gold-massif-sulfide-polymetallic deposits of the Baimak ore region, South Urals // In: Metallogeny of ancient and modern oceans–2010. Miass: IMin UB RAS, 2010. P. 166 – 170. [in Russian].

Krylatov, V.A. et al. The working project "Searching of the gold deposits in the Kurpaly area for 2006–2009, 2006". [in Russian].

Melekestseva, I.Yu., Yuminov, A.M., Nimis, P. Sulfide ores from the Semenov-1 hydrothermal field (13°30,87' N, Mid-Atlantic Ridge): structures, mineralogy and formation conditions // In: Metallogeny of ancient and modern oceans–2010. Miass: IMin UB RAS, 2010. P. 56–61. [in Russian].

Hedenquist, J., Arribas, A. Epithermal gold deposits: I. Hydrothermal processes in intrusion-related systems. II. Characteristics, examples and origin of epithermal gold deposits // Epithermal mineralization of the Western Carpathians. Soc. Econ. Geol. Guidebook Ser., 1999. Vol. 31. P. 195–196.

Holland, N.G., Roberts, S.R., Herrington, R.J., Boyce, A.J. The Balta Tau VMS deposit: an ancient gold-rich white smoker? // In: Mineral Exploration and Sustainable Development (eds. D. Eliopoulos et al.), Rotterdam, Millpress, 2003. Vol. 1. P. 123–126.

V.V. Zaykov[1, 2], M.N. Ankushev[1], E.V. Zaykova[1], A.M. Yuminov[2]
[1] Institute of Mineralogy UB RAS, Miass, Russia, zaykov@mineralogy.ru
[2] National Research South Ural State University, Chelyabinsk, Russia

ORE GEOARCHAEOLOGY OF THE URALS METALLOGENIC ZONES

Рудная геоархеология исследует минерально-сырьевую базу древних обществ с помощью различных геологических дисциплин. Использованы данные по 3 металлогеническим зонам: Приуральской, Главного Уральского разлома и Магнитогорской. По составу хромитов определены источники сырья для ряда металлургических центров. Выявлены расплавные включения меди, халькозина и оловосодержащих фаз. Для определения источников золота важно изучение имеющихся в нем включений минералов группы осмия. Даны задачи дальнейших исследований.

The ore geoarchaeology studies the mineral base and metallurgical products (slags, bars, and metallic items) of ancient societies, using various geological disciplines and methods: economic geology, mining, ore mineralogy and petrography, geochemistry (including isotope geology), analytical researches, ore geophysics, and paleometallurgy. Our geoarchaeological research is based on proper geological and geoarchaeological data (slags, copper, bronze and gold items) from 30 archaeological monuments of the South Urals and those provided by colleagues from industrial and scientific organizations and universities.

The main objects (ancient mines) are located in the Cis-Urals, Main Urals Fault and Magnitogorsk metallogenic zones of the South Urals (Vorovskaya Yama, Ishkinino, Dergamish, and Ivanovka) and some of them were found by authors. The mines and ore-bearing areas were mapped and studied using geological, geochemical and micromagnetic surveys. We took part in excavations of the Arkaim, Alandskoye, Sintashta, and Kuysak ancient settlements and Bolshe-Karagansky, Alexandrovsky, and Kamenny Ambar burial mounds.

The mineral composition of the artifacts was studied on an Olympus BX-51 and Axiolab, Carl Zeiss optical microscopes and the chemical composition was analyzed on a REMMA 202M electron microscope and JEOL-733 microprobe, Perkin-Elmer 3110 atomic adsorption and INNOV-4000 X-ray fluorescent analyzers. The using of the compact non-destructive INNOV analyzer is very important for archaeological studies. The results of these works with descriptions of ancient mines, concentrating mills, and metallurgical kiln relics were included into geoarchaeological database. The composition of ores, mineral and melt inclusions in slags, and metallic items are shown in tables. These data show the distribution of the base metals in the ancient society at the studied territory.

Mining and extraction of copper ores. The ancient copper mines represent the open pits 80 m in diameter with vertical and inclined mines. The oxidized ores with malachite, azurite, bornite,

Table 1

Type of inclusions in slags and ores from the settlement the South Urals

Type	Malachite ores in ultramac rocks	Chalcocite ores in sulfide deposits	Sn-bearing ores
Mineral inclusions	Chromite in slags and clasts of ultramafic rock	Chalcocite and clasts of covellite	–
Melt inclusions	As- and Ni-bearing bronze regulus	Chalcocite-bearing regulus	Sn-bearing regulus
Compositions of ore	Azurite-malachite: Cu 3–8 %; Ni 0.1 %; Co 0.1%; As 1–3 %	Chalcocite Cu 5–20 %	Sn mixtures

tenorite and other minerals were mostly exploited. The sulfide ores were rare that is concluded from the compositions of the melt drops in the slags and mineral inclusions (covellite). Three main types of copper objects distinct in geological setting, structures of the orebodies, mineral and chemical composition, and mineral resources are distinguished in the South Urals:

1. Mines in the ultramafic rocks with Cu-, Ni-, Co- and As-bearing ores (Vorovskaya Yama, Ishkinino, Dergamish, Ivanovka);2. Mines in the rhyolite-basalt complexes of the VMS deposits and destroyed by the modern mining (e.g., Bakr-Usyak deposit); and

3. Mines at the contacts with granite intrusions (Elenovka tourmaline-malachite deposit).

Based on the composition of ore, mineral and melt inclusions, we can distinguish three main copper types, which were used during the Bronze Age at the South Urals: malachite ores in ultramafic rocks, chalcocite ores in sulfide deposits, and tin-bearing ores (table 1). The copper-tourmaline ores is a rare ore type.

The estimated resources of copper in the South Urals ancient mines are 70 thousand tons [Yuminov and Zaykov, 2010]. The Cu contents in ores (3–5 % for different mines) and coefficient of metallurgical extraction (min 50 %) are important for approximate estimation of the metal production [Kozlovsky, 1987]. Using these parameters, we may conclude that 1400 tons of copper were extracted from ores.

Ancient metallurgical slags and metallic items. We have studied the compositions of slags from 16 South Urals settlements. Several groups of slags are distinguished on the basis of composition, mineral and melt inclusions. According to XRF data, the main types are Cu-, Cr-, Co-, and Sn-bearing slags.

Chromite, chalcocite and covellite compose the major mineral inclusions in slags. A refractory mineral chromite (the melting temperature is 2180 °C) poorly reacts with a melting slag. The composition of chromite allows determination the source of the ore, which was used in different metallurgical centers. Chalcocite and covellite were found in slags from the Arkaim, Kamennyi Ambar and Konoplyanka settlements.

A few amounts of copper and As- and Sn-bronze melt inclusions were found. The first one is related to arsenide ores from the ultramafic-hosted Co-Cu-VMS and fahlore-bearing deposits (table 1). The Sn-bronze occurs as drops in the slags. Previously, these inclusions have not been revealed in the Urals metal-working products and their presence indicates exploitation of the Sn-bearing ores. According to geological data, Sn deposits of Kazakhstan could be the possible sources for Sn-bearing ores.

Mining of gold ores and jewel industry. The evidences for exploration of gold-quartz deposits and placers in the ancient mines are observed in the Kyzyl and Sakmara river basins in the Baymak ore region, Republic of Bashkortostan. The small ancient pits are characterized by the soot on walls. The stone stamps and mortars (stone plates 30 cm in diameter with a hollow in the centre) were found near the pits. The findings of the bronze and stone picks in the gold-bearing sands of the Miass, Kochkar and Berezovsk ore regions point to the exploration of placers.

The ancient jewelry was found in the Urals archaeological monuments in Orenburg and Chelyabinsk districts and Republic of Bashkortostan. The Filippovka, Perevolochan I, Magnitnyi, and Kichigino are the richest burial mounds. The gold deer and jewelry collection from the Filippovka burial mound, storing in the museums of Ufa and Orenburg, are most expressive [Yablonsky, 2008]. All

items were made with a “Siberian animal style”. Various jewelry pieces and wire balls were found in the Middle Age workshop at the Ufa II settlement.

The composition of the archaeological gold is different. Three groups of gold fineness (high 980–860 ‰, intermediate 840–600 ‰, and low 550–370 ‰) are distinguished that may indicates the

Table 2

Composition of inclusions of osmium minerals in ancient gold products (South Urals)

№	Place of sampling	No. of samples	No. of analyses	Artifacts	Average content (wt %)			Formula
					Os	Ir	Ru	
1.	Filippovka II, burial mound № 4	№ 7–1	6	Cover plates	45.76	36.10	17.45	$Os_{0.40}Ir_{0.31}Ru_{0.29}$
2.		№ 7–2	10		34.54	29.30	27.66	$Ru_{0.42}Os_{0.28}Ir_{0.24}Pt_{0.06}$
3.		№ 7–3	7		35.28	29.20	27.63	$Ru_{0.42}Os_{0.29}Ir_{0.23}Pt_{0.06}$
4.		№ 7–4	1		57.58	14.82	27.02	$Os_{0.47}Ru_{0.41}Ir_{0.12}$
5.		№ 7–5	8		56.88	17.04	25.57	$Os_{0.47}Ru_{0.39}Ir_{0.14}$
6.		№ 7–6	7		55.07	8.97	35.42	$Ru_{0.51}Os_{0.42}Ir_{0.07}$
7.		№ 7–7	5		32.67	53.85	3.43	$Ir_{0.53}Os_{0.32}Pt_{0.09}Ru_{0.06}$
8.		№ 7–8	6		45.03	20.56	33.93	$Ru_{0.49}Os_{0.35}Ir_{0.16}$
9.		№ 7–9	7		37.23	29.91	26.88	$Ru_{0.41}Os_{0.30}Ir_{0.24}Pt_{0.05}$
10.		№ 7–10	5		35.12	58.52	2.26	$Ir_{0.57}Os_{0.35}Ru_{0.04}Pt_{0.04}$
11.		№ 7–11	5		56.53	10.16	32.78	$Ru_{0.48}Os_{0.44}Ir_{0.08}$
12.		№ 7–12	5		37,74	56,05	5,87	$Ir_{0.55}Os_{0.37}\ Ru_{0.08}$
13.		№ 7–13	3		79.45	12.64	7.58	$Os_{0.75}Ru_{0.13}Ir_{0.12}$
14.		№ 7–14	2		73.36	16.17	10.09	$Os_{0.68}Ru_{0.17}Ir_{0.15}$
15.		№ 7–15	3		72.60	16.83	10.29	$Os_{0.67}Ru_{0.18}\ Ir_{0.15}$
16.		№ 7–16	6		40.32	38.13	17.28	$Os_{0.35}\ Ir_{0.33}\ Ru_{0.29}Pt_{0.03}$
17.		№ 7–17	5		35.83	53.34	2.85	$Ir_{0.52}\ Os_{0.36}\ Ru_{0.05}\ Pt_{0.07}$
18.		№ 7–18	8		38.99	42.80	17,71	$Ir_{0.37}Os_{0.34}Ru_{0.29}$
19.	Filippovka II, burial mound № 1	103ab	2	Cover plates	13.56	81.25	4.12	$Ir_{0.78}Os_{0.13}Ru_{0.07}Rh_{0.02}$
20.		103de	2		22.93	72.68	2.90	$Ir_{0.70}Os_{0.23}Ru_{0.05}Rh_{0.02}$
21.		103jk	2		58.65	35.02	5.45	$Os_{0.56}Ir_{0.33}Ru_{0.10}Rh_{0.01}$
22.		73	4		38.92	50.23	2.39	$Ir_{0.50}Os_{0.39}Pt_{0.06}Rh_{0.03}\ Ru_{0.02}$
23.	Perevolo-chan-I	11.5.8	4	Cover plate	71,86	21,15	6,81	$Os_{0.68}Ir_{0.20}Ru_{0.12}$
24.	Yakovlev-ka II	Я-3	6	Pendant	71,85	24,21	3,71	$Os_{0.70}Ir_{0.23}Ru_{0.07}$
25.	Magnitny, burial mound № 21	M2-1	2	Hemisphe-rical plaques	40.06	50.27	7.34	$Ir_{0.45}Os_{0.36}Ru_{0.12}Fe_{0.06}\ Rh_{0.01}$
26.		M2-1-1	4		32.89	30.06	29.87	$Ru_{.43}Os_{.26}Ir_{.23}Rh_{.05}Pt_{.02}Fe_{.01}$
27.		M2-A	5		46.55	39.29	12.26	$Os_{0.41}Ir_{0.34}Ru_{0.21}Fe_{0.03}\ Rh_{0.01}$
28.		M-II	5		73.62	14.47	10.41	$Os_{0.67}Ru_{0.18}Ir_{0.13}Rh_{0.02}$
29.		M3-1	5	Triangle plaques	59.86	37.05	2.39	$Os_{0.59}Ir_{0.36}Ru_{0.04}Fe_{0.01}$
30.		M3-1-1	5		42.74	13.01	37.80	$Ru_{0.52}Os_{0.32}Ir_{0.10}Rh_{0.04}\ Pt_{0.02}$
31.		M-III	6		28.82	60.97	5.68	$Ir_{0.53}Os_{0.25}Fe_{0.13}Ru_{0.09}$
32.	Ushkata, burial mound № 12	Ук7	3	Pendant	64.82	34.11	0.47	$Os_{0.65}Ir_{0.34}Ru_{0.01}$

Low contents of Rh, Pt, and Fe are shown only in formulas. The analyzes were carried out on a REMMA 202 M electron microscope (analyst V.A. Kotlyarov) at the South Urals Center for Collective Use (IMin UB RAS, Miass). The artifacts were provided by L.T. Yablonsky (1–22, Orenburg, temporary storage 419, under restoration in State NIIR), S.V. Sirotina (23, 24), A.D. Tairov (25–31), and V.V. Tkachev (32)

different metal sources. According to the chemical composition, the most gold items from Chelyabinsk and Orenburg districts and Republic of Bashkortostan contain 82–87 wt % Au (rare 61–67 wt %).

The wire with 97 wt % Au content was found in the jewel workshop of the Ufa II settlement. The Cu contents less than 3 wt % in the gold items is an alloying result. The items with higher (up to 9 wt %) Cu contents were produced with an artificial addition to the copper melt.

The finding of PGE minerals in the items from several archaeological monuments is the most important result of our study (table 2). The PGE minerals were identified in three groups of monuments: (i) Filippovka I and Ufa II mounds (western group of the South Urals), (ii) Perevolochan I and Yakovlevka II mounds (central group adjacent to the Main Urals Fault zone), and (iii) Kichigino I, Bolshoy Klimovsky, Stepnoy, and Ushkatta mounds (eastern group confined to the East Urals Fault zone in the area of the interfluves of the Ural and Tobol rivers). Three groups of chemical composition of 34 PGE mineral grains were distinguished on the basis of various contents of Os, Ru and Ir [Zaykov et al., 2011]. The most data points on the Os-Ru-Ir plot belong to the field of osmium from the Urals placers. Some compositions of PGE minerals from the studied mounds have no analogues in the corresponding deposits.

We have estimated the possible sources of gold and PGE minerals of the ancient jewelry. According to the round morphology and heterogeneous composition of the inclusions, they were extracted from the gold placers located in the Main Urals and East Urals Fault zones. These tectonic structures host Au-bearing ultramafic bodies with osmium mineralization and related placers. The composition of native osmium from the Urals placers and gold jewelry from all studied objects will be compared in order to identify the areas of extraction of gold for the jewelry.

Problems need to be solved in the future: (i) analysis of the metal resources of the ancient societies of various ages, (ii) study of structure of mines and ore composition from new mines; (iii) searching for the metallurgical workshops, which were operated in the Bronze and Early Iron Age; (iv) finding of mineral and geochemical indicators of sources of mineral deposits in the Urals and adjacent territories; and (v) identification of the boundaries of areas of mineral extraction, mining, and paleometallurgical production.

The work is supported by UB RAS project no. 12-M-456-2024, Russian Humanitarian Scientific Foundation (project no. 12-01-00293), and Russian Foundation for Basic Researches (project no. 13-06-12006). The authors are grateful to A.D. Tairov, D.G. Zdanovich, V.A. Kotlyarov, E.I. Churin, and E.V. Belogub for their assistance during the study.

References

Yuminov, A.M., Zaykov, V.V. The estimation of extraction of Cu ores in the Bronze Age at Southern Urals // XVIII Urals Archaeol. Symp.: Cultural areas, archaeological cultures, chronology. Ufa: BSPU, 2010. P. 183–184 (in Russian).

Kozlovsky, E.A. (Ed). Mining encyclopedia. Vol. 3. Moscow, Sov. Encyclopaedia, 1987. 550 p. [in Russian].

Yablonsky, L.T. Sarmates from the Southern Transurals // Treasures of sarmate leaders (Materials of Philippovka burial grounds excavations). Orenburg: Dimur, 2008. P. 17–32 [in Russian].

Zaykov, V.V., Yuminov, A.M., Zaykova, E.V., Tairov, A.D. Geoarchaeology. Chelyabinsk: SUSU, 2011. 263 p. [in Russian].

PARTICIPANT LIST

Adomako-Ansah K.	*Akita University, Akita, Japan*	*6, 28*
Aminov P.G.	*Institute of Mineralogy UB RAS, Miass, Russia* *National Research South Ural State University, Chelyabinsk, Russia*	*103*
Anfilogov V.N.	*Institute of Mineralogy UB RAS, Miass, Russia* *National Research South Ural State University, Chelyabinsk, Russia*	*10*
Anfimov A.L.	*Institute of Geology and Geochemistry UB RAS, Yekaterinburg, Russia*	*26*
Ankushev M.N.	*Institute of Mineralogy UB RAS, Miass, Russia*	*116*
Ankusheva N.N.	*Institute of Mineralogy UB RAS, Miass, Russia* *National Research South Ural State University, Chelyabinsk, Russia*	*42, 52, 80*
Apukhtina O.	*CODES ARC Centre of Excellence in Ore Deposit Research, University of Tasmania, Hobart, Australia*	*16*
Ayupova N.R.	*Institute of Mineralogy UB RAS, Miass, Russia;* *National Research South Ural State University, Chelyabinsk, Russia*	*17, 19*
Belogub E.V.	*Institute of Mineralogy UB RAS, Miass, Russia*	*22, 56, 58, 113*
Blinov I.A.	*Institute of Mineralogy UB RAS, Miass, Russia*	*24, 58*
Bogdanov Yu.A.	*Institute of Oceanology RAS, Moscow, Russia*	*46*
Bull S.	*CODES ARC Centre of Excellence in Ore Deposit Research, University of Tasmania, Hobart, Australia*	*35*
Buschmann B.	*Freiberg Mining Academy, Freiberg, Germany*	*42, 46*
Chuvashov B.I.	*Institute of Geology and Geochemistry UB RAS, Yekaterinburg, Russia*	*26*
Cooke D.R.	*CODES ARC Centre of Excellence in Ore Deposit Research, University of Tasmania, Hobart, Australia*	*103*
Danyushevsky L.V.	*CODES ARC Centre of Excellence in Ore Deposits, University of Tasmania, Hobart, Tasmania, Australia*	*19, 42, 46, 50, 67*
Ehrig K.	*BHP-Billiton, Adelaide, Australia*	*16*
Frolov A.	*Institute of Geology KRC RAS, Petrozavodsk, Russia*	*56*
Fujioka N.	*Taiheiyo Cement Corporation, Tokyo, Japan*	*28*
Ganzhenko G.D.	*Altai Geological Environmental Institute, Ust-Kamenogorsk, Republic of Kazakhstan*	*82*
Genc Y.	*Department of Geological Engineering, Hacettepe University, Ankara, Turkey*	*67, 73*
Gregory D.	*CODES ARC Centre of Excellence in Ore Deposit Research, University of Tasmania, Hobart, Australia*	*35*
Halpin J.	*CODES ARC Centre of Excellence in Ore Deposit Research, University of Tasmania, Hobart*	*35*
Hammond N.Q.	*Council for Geoscience, Pretoria, South Africa*	*6*
Herrington R.J.	*Natural History Museum, London, UK*	*46, 97*
Huang Q.	*CODES ARC Centre of Excellence in Ore Deposit Research, School of Earth Science, University of Tasmania, Hobart, Australia*	*39*
Hoshino K.	*Department of Earth and Planetary Systems Science, Hiroshima University, Hiroshima, Japan*	*32*
Ishiyama D.	*Akita University, Akita, Japan*	*6, 28, 46*
Ivleva E.A.	*Institute of geology NAS, Bishkek, Kyrgyzstan*	*39*
Kamenetsky V.S.	*CODES ARC Centre of Excellence in Ore Deposits, University of Tasmania, Hobart, Australia*	*16*
Kaneto F.	*Department of Earth and Planetary Systems Science, Hiroshima University, Hiroshima, Japan*	*32*

	insk, Russia *Institute of Mineralogy UB RAS, Miass, Russia;*	
Skarmeta J.	*Gerencia de Exploraciones, CODELCO Chile, Santiago, Chile*	*61*
Soroka E.I.	*Institute of Geology and Geochemistry UB RAS, Yekaterinburg, Russia*	*26*
Spiro B.	*Department of Mineralogy, Natural History Museum, London, UK*	*42, 97, 103*
Tessalina S.G.	*John de Laeter Centre for Isotopic Research, Curtin University, Perth, Australia*	*97*
Testa F.J	*CODES ARC Centre of Excellence in Ore Deposit Research, University of Tasmania, Hobart, Australia*	*103*
Tret'yakov G.A.	*Institute of Mineralogy UB RAS, Miass, Russia*	*107*
TseluikoA.S.	*National Research South Ural State University, Chelyabinsk, Russia*	*46*
Udachin V.N.	*Institute of Mineralogy UB RAS, Miass, Russia;* *National Research South Ural State University, Chelyabinsk, Russia*	*111*
Unlu T.	*Department of Geological Engineering, Ankara University, Ankara, Turkey*	*73*
Urabe T.	*University of Tokyo, Tokyo, Japan*	*46*
Weiss D.J.	*Department of Earth Science and Engineering, Imperial College, London, UK;* *Department of Mineralogy, Natural History Museum, London, UK*	*111*
Williamson B.J.	*Department of Mineralogy, Natural History Museum, London, UK;* *Camborne School of Mines, University of Exeter, Cornwall, UK*	*103*
Yamamoto M.	*Akita University, Akita, Japan*	*6*
Yuminov A.M.	*National Research South Ural State University, Chelyabinsk, Russia* *Institute of Mineralogy UB RAS, Miass, Russia*	*80, 113, 116*
Zabotina M.V.	*Institute of Mineralogy UB RAS, Miass, Russia*	*22, 113*
Zaykov V.V.	*Institute of Mineralogy UB RAS, Miass, Russia* *National Research South Ural State University, Chelyabinsk, Russia*	*52, 95, 97, 116*
Zaykova E.V.	*Institute of Mineralogy UB RAS, Miass, Russia*	*116*
Zhu Y.	*Peking University, Pekin, China*	*39*
Zhukov I.G.	*Institute of Mineralogy UB RAS, Miass, Russia;* *National Research South Ural State University, Chelyabinsk, Russia*	*17*

CONTENTS

Scientific publication

ORE GENESIS – 2013

PROCEEDING PAPERS of the International Conference
(August 7-9, 2013)

Recommended for publication by
the Academic Council of the Institute of Mineralogy UB RAS and
the educational-methodical commission of Faculty of Geology
of National Research South Ural State University, Chelyabinsk, Russia

Computer making: *Buslovskaya O.L.*
Correctors: *Sinyakovskaya I.V., Maslennikova A.V.*

Signed for printing 18.06.2013.
Printed in "Geotur" Ltd. Publishing House
Miass, Chelyabinsk district, Russia
Oktyabrya ave., 31, office 20.